NASA CONTRACTOR REPORT

NASA CR-1706

INVESTIGATION OF DC-8 NACELLE MODIFICATIONS TO REDUCE FAN-COMPRESSOR NOISE IN AIRPORT COMMUNITIES

Part II – Design Studies and Duct-Lining Investigations

by Alan H. Marsh, R. L. Frasca, D. K. Gordon, C. A. Henry, G. L. Laurie, and L. T. Kamei

Prepared by
MCDONNELL DOUGLAS CORPORATION
Long Beach, Calif. 90801
for Langley Research Center

NATIONAL AERONAUTICS AND SPACE ADMINISTRATION • WASHINGTON, D. C. • DECEMBER 1970

1. Report No. NASA CR-1706	2. Government Accession No.	3. Recipient's Catalog No.
4. Title and Subtitle Investigation of DC-8 Nacelle Modifications to Reduce Fan-Compressor Noise in Airport Communities. Part II – Design Studies and Duct-Lining Investigations		5. Report Date December 1970 6. Performing Organization Code
7. Author(s) Alan H. Marsh, R. L. Frasca, D. K. Gordon, C. A. Henry, G. L. Laurie, and L. T. Kamei		8. Performing Organization Report No. 10. Work Unit No.
9. Performing Organization Name and Address Douglas Aircraft Company McDonnell Douglas Corporation Long Beach, California 90801		11. Contract or Grant No. NAS1-7130 13. Type of Report and Period Covered Contractor Report for Period May 1967 to October 1969
12. Sponsoring Agency Name and Address National Aeronautics and Space Administration Langley Research Center Hampton, Virginia 23365		14. Sponsoring Agency Code

15. Supplementary Notes

Distribution of this report is provided in the interest of information exchange. Responsibility for the contents resides in the authors or organization that prepared it.

16. Abstract

Designs for two fan-exhaust ducts and eight inlet ducts applicable to the JT3D turbofan engines on DC-8-50/61 airplanes were studied. The designs were evaluated in terms of (1) their estimated ability to produce a 7 to 10 PNdB reduction in perceived noise level during landing approach and (2) their estimated impact on direct operating costs.

Two inlet-duct designs and one fan-exhaust-duct design were selected for ground static testing. One of the inlet designs incorporated acoustically absorptive linings on the walls of a revised inlet duct, two concentric ring vanes, and a lengthened centerbody. The other design had treatment on the walls of a lengthened inlet duct, one concentric ring vane, and an enlarged lightbulb-shaped centerbody. The fan-exhaust duct design provided acoustical linings in an exhaust duct 24 inches longer than the existing ducts, thus requiring a new fan thrust reverser but preserving the existing primary thrust reverser.

Acoustical duct-lining studies consisted of: flow resistance; acoustic absorption and impedance; duct transmission-loss; and sonic-fatigue tests. Structural duct-lining studies consisted of: determination of structural design criteria for duct linings; structural tests of bonded honeycomb sandwich structures; and development of fabrication procedures for duct linings. The result of these acoustical and structural studies was the selection of the materials and fabrication processes used in constructing the test articles for the ground static tests.

17. Key Words Suggested by Author(s)	18. Distribution Statement
McDonnell Douglas DC-8-50/61 airplanes JT3D turbofan engines Acoustically treated engine nacelles Flyover noise reduction Acoustically absorptive duct linings	Unclassified - Unlimited

19. Security Classification (of this report)	20. Security Classification (of this page)	21. No. of Pages	22. Price*
Unclassified	Unclassified	197	$3.00

*For sale by the National Technical Information Service, Springfield, Virginia 22151

CONTENTS

INVESTIGATION OF DC-8 NACELLE MODIFICATIONS TO REDUCE FAN-COMPRESSOR NOISE IN AIRPORT COMMUNITIES

PART II - DESIGN STUDIES AND DUCT-LINING INVESTIGATIONS

By Alan H. Marsh, R. L. Frasca, D. K. Gordon, C. A. Henry, G. L. Laurie, and L. T. Kamei

SUMMARY

In May 1967, the NASA initiated a program with the McDonnell Douglas Corporation to investigate turbofan-engine nacelle modifications designed to reduce fan-compressor noise from the JT3D engines on DC-8-50/61 aircraft. The program was directed at the definition of nacelle modifications that could reduce the landing-approach flyover perceived noise level by 7 to 10 PNdB with no increase in takeoff noise level. The program was conducted in five phases: (1) nacelle design studies and duct lining investigations, (2) ground static tests of noise-suppressor configurations, (3) flyover noise and cruise performance tests, (4) studies of the economic implications of retrofit, and (5) an evaluation of human response to the flyover noise of the modified nacelles. This document reports the results of the investigations of the first phase and the resultant selection of the articles tested in the succeeding ground static test phase of the program.

Eight inlet-duct and the two fan-exhaust-duct designs were studied and evaluated. Two inlet-duct designs and one fan-exhaust-duct design were selected for ground static testing. One of the selected inlet designs incorporated acoustically absorptive linings on the walls of a revised inlet duct, two concentric ring vanes, and a lengthened centerbody. The other design had treatment on the walls of a lengthened inlet duct, one concentric ring vane, and an enlarged lightbulb-shaped centerbody. The selected fan-exhaust duct design provided acoustical linings in an exhaust duct 24 inches longer than the existing ducts, thus requiring a new fan thrust reverser but preserving the existing primary thrust reverser. An alternate nacelle modification design using a variable-area primary nozzle to reduce the rotational speed of the fan stages during landing was also studied and recommended for ground static testing.

The duct-lining investigations included acoustical and structural studies. The acoustical studies consisted of: flow resistance; acoustic absorption and impedance; duct transmission-loss; and sonic-fatigue tests. The structural studies consisted of: determination of structural design criteria for duct linings; structural tests of bonded honeycomb sandwich structures; and development of fabrication procedures for duct linings. The result of these acoustical and structural studies was the selection of the materials and fabrication processes used in constructing the test articles for the ground static tests.

INTRODUCTION

The total human annoyance from operations of commercial jet transports has increased simultaneously with the growth of the air transportation industry and the number of people living in communities around airports. This increased annoyance has stimulated efforts to find means to alleviate the problem through reducing the level of the noise radiated from the aircraft, modifying aircraft operational procedures, and achieving compatible usage of the land around airports. The alleviation efforts have been conducted as part of a coordinated industry-government research program.

In 1965, the NASA extended its research programs to supplement those of industry in the development of practical nacelle modification concepts for reducing fan-compressor noise (ref. 1). In May 1967, the Langley Research Center of the NASA contracted with the McDonnell Douglas Corporation and The Boeing Company to investigate nacelle modifications for operational McDonnell Douglas and Boeing transports powered by four Pratt and Whitney Aircraft (P&WA) JT3D turbofan engines. The nacelle modifications were to achieve significant reductions in flyover noise levels in airport communities located under landing-approach flight paths.

During landing approach, the perceived noisiness and hence the annoyance of the sound from the JT3D engines is attributed principally to the discrete frequency tones radiated from the inlet and fan-exhaust ducts. Accordingly, the McDonnell Douglas and the Boeing investigations were directed at developing fan noise suppression methods.

The goal of the McDonnell Douglas program was to design, build and evaluate an economically viable nacelle modification using acoustically treated short fan-exhaust ducts and acoustically treated inlet ducts. The modification was to achieve a reduction of 7 to 10 PNdB in maximum perceived noise level (PNLM) outdoors under the landing approach path. Similarly, the goal of the Boeing program was to achieve a 15 PNdB noise reduction using acoustically treated long fan-exhaust ducts and a sonic-throat inlet duct. Both programs required that the nacelle modifications be designed to produce no increase in noise during takeoff or climbout. The results of the Boeing program are reported in references 2 through 7.

The scope of the Douglas investigation was limited to the study of nacelle modifications for the various models of the Series 50 DC-8 airplanes and Model 61 of the Series 60 airplanes. These airplanes are equipped with 24-inch long fan-exhaust ducts, considered to be short ducts.

The Douglas program is reported in six Parts: Part I, a summary of the major results of the program (ref. 8); Part II, a report of the nacelle modification design studies and duct lining investigations (presented in this document); Part III, a report of ground static tests of suppressor configurations (ref. 9); Part IV, a flight investigation of the acoustical and performance effects of the selected design of modified nacelles on a DC-8-55 airplane (ref. 10); Part V, a study of the economic implications of retrofit of the selected design (ref. 11); and Part VI, an evaluation of human response to the flyover noise of the modified nacelles (ref. 12).

This Part II of the report consists of three major sections: nacelle modification design studies, duct-lining acoustical investigations, and duct-lining structural investigations. The first section presents the goals and constraints of the program, discusses the preliminary considerations and the

requirements for treated area, and shows the development of the designs for fan-exhaust ducts, inlet ducts, and a variable-area primary exhaust nozzle. The second and third sections present the results of the acoustical and structural studies conducted to select the duct-lining design and the fabrication processes used in constructing the static-test inlet and fan-exhaust ducts.

Flexural-fatigue tests of samples of fibermetal sheets were conducted at the NASA's Langley Research Center. With the permission of the NASA, some of these results are presented in this document as part of the structural investigation of fibermetal surfaces.

SYMBOLS

A_{ns} area of noise source taken as the projected annular area of the fan inlet or fan exit, square feet

A_{tr} effective treated surface area, square feet

D_1 distance in standing-wave tube from face of sample to first node, centimeters (eq. 7)

D_2 distance in standing-wave tube between the first and second nodes, centimeters (eq. 7)

DOC direct operating cost

h distance between acoustically treated surfaces, feet

L/W for duct transmission-loss tests, the ratio of the axial length of treatment, L, to the width of the duct, W

n number of test locations for measuring flow resistance on a large sheet of porous material (eq. 14 in Appendix A)

NLF nonlinearity factor, the ratio of the flow resistance at 5.0 meters/second to the flow resistance at 0.2 meters/second

PNL instantaneous perceived noise level, perceived noise decibels (PNdB)

PNLM maximum value of the instantaneous PNL, PNdB

R resistive part of the acoustic impedance, dyne-second/cubic centimeters (eq. 8)

$\bar{R}$ arithmetic mean flow resistance of a sheet of porous material, cgs rayls (eq. 13 in Appendix A)

R_f flow resistance of a sample of porous material, cgs rayls (eq. 2)

R_i flow resistance of a sheet of porous material at a test location i, cgs rayls (eq. 13 in Appendix A)

S area used in flow resistance tests, square centimeters (eq. 2)

S_b/S_a ratio of root-mean-square (rms) stress at time of initial failure in test panel b to the corresponding rms stress in test panel a (eq. 12)

SFC specific fuel consumption, (pounds/hour)/pound

S/N ratio, in decibels, of the level of a signal, S, to the level of the background noise, N (eq. 9)

SPL sound pressure level, decibels (dB) re 0.0002 dynes/square centimeter

SWR standing-wave ratio in a standing-wave tube test (eq. 4)

TL transmission loss, decibels

U volume rate of airflow through a sample of porous material in a flow resistance test, cubic centimeters/second (eq. 2)

u linear velocity of airflow through a sample of porous material in a flow resistance test, centimeters/second (eq. 3)

v equivalent rms velocity of a particle of air moving through the porous surface of a duct lining, meters/second (eq. 1)

X reactive part of the acoustic impedance, dyne-second/cubic centimeters (eq. 8)

Z acoustic impedance, dyne-second/cubic centimeters (eq. 5)

a_n normal-incidence acoustic absorption coefficient (eq. 4)

Δp differential pressure through a sample of porous material, dynes/square centimeter (eq. 2)

λ wavelength of sound, feet

ρc characteristic impedance of air, cgs rayls (eq. 5)

σ standard deviation of the flow resistance measurements R_i from the arithmetic mean flow resistance $\overline{R}$, cgs rayls (eq. 14 in Appendix A)

NACELLE MODIFICATION DESIGN STUDIES

Existing Nacelles

All DC-8-50/61 airplanes are equipped with the same basic installation of the P&WA JT3D turbofan engine having short fan-exhaust ducts. Figure 1 illustrates the location of major nacelle components.

The inlet duct, figure 1(a), has a throat diameter of approximately 46 inches and is 45 inches long. At the engine inlet-guide-vane station, the diameter of the inlet duct is approximately 51.5 inches; the

diameter of the centerbody is approximately 18 inches. The inlet has a fixed geometry and has been designed with a relatively thick internal lip to provide the engine with airflow having high total pressure recovery at all engine operating conditions including takeoff. As a result, there is considerable volume between the inlet duct surface and the exterior nose-cowl surface. This area was utilized for the installation of engine-oil and pneumatic-system heat exchangers, the inlet-duct ice-protection system, and related piping, valves and ducting. The auxiliary inlet directly beneath the inlet lower lip admits cooling air to the oil and pneumatic-system heat exchangers.

Each fan-exhaust duct, figure 1(b), has an average radial duct cross-dimension of approximately 6.5 inches and a length of 24 inches. Four full-length flow splitters in each duct divide the duct into five separate flow channels. The thrust reverser for the fan exhaust directs the engine airflow through a cascade to provide reverse thrust at relatively high reversing efficiency. The hot primary engine airflow is exhausted through a nozzle at the rear of the engine. The reverser for the primary exhaust flow is also a cascade reverser similar to the reverser for the fan air. The cascade cover sleeve is translated aft to expose the cascade when the reverser is operated.

The noisiness of JT3D-powered aircraft is dominated by the discrete high-frequency tones radiating from the fan-exhaust and inlet ducts and by the lower-frequency broadband noise radiated from the primary jet exhaust. The discrete tones have frequencies equal to the blade-passage frequencies of the first and second fan-compressor rotor stages. The tones radiated from the unsuppressed fan-exhaust ducts determine the maximum value of the instantaneous perceived noise level (PNLM) during a landing approach. The jet-exhaust noise dominates the PNLM during takeoff when the distance to the airplane is more than 2000 feet. For distances less than 1000 feet, the PNLM during takeoff is dominated by fan noise.

Figure 2 shows a representative 1/3-octave band spectrum of the sound-pressure level (SPL) at the time of the PNLM during landing approach. The two discrete fan tones at the fundamental blade-passage frequencies are in the 2500-Hz band and the second harmonics are in the 5000-Hz band.

The SPLs in the 1000- and 1250-Hz bands contain additional discrete tones that are called combination tones or multiple pure tones. Combination tones occur at frequencies that are integral multiples of rotor speed and are caused by the series of weak shock waves propagated forward of those sections of the fan blades rotating at supersonic relative tip Mach numbers. The regular, periodic spacing between the shock waves changes to an irregular spacing as the waves propagate forward in the inlet duct. The most-intense combination tones have been noted to occur at frequencies that are 15 to 20 times the rotational speed of the low-pressure rotor.

The noise from the exhaust jets of the fan ducts and the primary nozzle is concentrated in the frequency band below 800 Hz. At the landing power setting shown in figure 2, the maximum value of the jet exhaust noise occurs in the 125-Hz band. The nacelle modification program was directed at reducing the amplitude of the SPLs at the fundamental blade-passage frequencies and their harmonics and not at the combination tone noise or jet-exhaust noise.

Design Goals

The goal of the program was to design nacelle modifications that could achieve a 7 to 10 PNdB reduction in PNLM during landing approach and that also could be installed on existing commercial

jet transports in such a way that resultant airline operations would be economically viable. Additionally, the designs were neither to compromise safety of flight nor to result in an increase in crew workload.

Because the intensity of the noise radiated from the inlet duct was less than that radiated from the fan-exhaust ducts, individual estimates were required for the amount of reduction needed for the noise radiated from the inlet and fan ducts. Information supplied by P&WA was used to determine that the PNLM from the inlet duct was about 3 PNdB less than the PNLM from the fan ducts. Therefore, to achieve a net reduction of 10 PNdB, a noise reduction requirement of 7 PNdB was selected for the inlet duct and 10 PNdB for the fan ducts. If these separate reductions could be obtained, the noisiness of the sounds from the inlet and the fan ducts would be approximately equal during a flyover.

Preliminary Considerations

To minimize the cost of incorporating noise suppression features within the nacelle, design solutions were sought that would require the fewest changes to, or relocation of, major existing nacelle components such as: the equipment between the fan-exhaust ducts and the engine case; the pylons that support the engines on the wings; and the mechanical and system interfaces between the engine nacelles and the pylons.

Preliminary design decisions concerning the acoustically absorptive duct linings were also made. It was decided that the porous facing surfaces would be supported by a honeycomb-core. The honeycomb-sandwich-construction decision was based on the recognition of the superior structural efficiency of the honeycomb-sandwich construction as well as the aerodynamic requirement to minimize losses because of air circulation in the backing cavities.

For the flyover noise tests conducted prior to program described in this report, acoustical treatment was installed in the 24-inch fan-exhaust ducts (ref. 13). No acoustical treatment was installed in the inlet ducts. The porous fibermetal surfaces were supported by a riveted rib-and-stringer structure; the cavities behind the porous surfaces were filled with fiberglass batting material in order to reduce circulation losses. Use of the fiberglass was undesirable because bulk fibrous materials are subject to erosion and would absorb and retain fluids; consequently they could cause corrosion and be a fire hazard. Bulk fibrous materials were, therefore, unsuitable for use in nacelles in airline services and were not considered in this program.

Sonic fatigue tests (refs. 13 and 14) had indicated that a well-bonded sandwich structure with honeycomb core was more efficient, in terms of its strength-to-weight ratio, in resisting acoustically induced fatigue than a riveted skin-and-rib structure. Honeycomb sandwich structure provides more uniform support for the porous surfaces and has smaller unsupported panels than the riveted rib-and-stringer structure.

It was decided that the acoustical sandwich structure for the duct linings should be designed as load-carrying structure and that the duct linings did not have to be easily removable. These decisions should result in the lightest, most efficient design of a retrofit installation.

The decision to not require easily removable duct linings was consistent with the results of contamination and cleaning tests (ref. 15). These tests indicated that it should be feasible to develop

an effective method for cleaning porous fibermetal sheets that were part of sandwich structures with honeycomb core and impervious metal backing sheets.

Approximate dimensions were also selected for the depth of the backing cavities and the thickness of the porous facing sheets. These selections were based on the results of the duct transmission-loss tests and flyover noise tests reported in references 1 and 13, and on the results of other independent studies conducted by the Contractor. The cavity depth was 1 inch on the walls of the inlet duct, centerbody, and the inner and outer walls of the fan ducts. Any splitters or vanes would have cavity depths of about 0.5 inch on either side of an impervious septum. The thickness of the porous facing surfaces was chosen to be between 0.03 and 0.05 inch.

Consistent with the goals and constraints of the program and with the preliminary decisions described above, the following approaches to the design of nacelle modifications were considered: (1) acoustically treated short fan-exhaust ducts; (2) acoustically treated fixed-geometry inlet ducts; (3) acoustically treated variable-geometry inlet ducts; and (4) a variable-area primary nozzle that could be operated during landing approach to reduce the rotational speed of the fan stages.

Treated Area Requirements

Estimates of the area of treatment needed in the inlet and fan-exhaust ducts to meet the design goals were required before the nacelle modification design studies could begin. Development of a means to make these estimates was hampered by the scarcity of information available on the acoustical effects of treated duct installations on jet aircraft. Six major acoustical design parameters that had been identified by previous duct-model transmission-loss tests (ref. 1) and flyover noise tests (ref. 13) were: (1) the area and the location of the acoustically absorptive duct-linings; (2) the height of the ducts through which the sound propagates; (3) the relative degree of acoustical effectiveness of the absorptive duct-lining surfaces; (4) the velocity of airflow over the absorptive lining surfaces; (5) the intensity and direction with which the sound in the ducts impinges on the absorptive linings; and (6) the effects, if any, that bends in the aerodynamic flow path have on the propagation of sound in the ducts because of the reduced line of sight to the noise source.

Figure 3(a) shows the design chart that was developed to relate some of the principal acoustical design parameters and to provide estimates of the amount of treated area required. The chart was developed from the results of: (a) duct transmission-loss tests reported in reference 1; (b) flyover noise tests reported in reference 13; and (c) duct transmission-loss tests conducted independently by the Contractor prior to the investigations reported in this Part.

Because of the nature of the assumptions used in developing the chart, an estimate for the value of the treated area required to achieve a given noise reduction should be considered only as approximate. The treated area determined from the chart was meant to be the effective treated area and not the gross treated area. The effective area was taken as the gross treated area less 25 percent. This 25-percent reduction accounted for losses in treated area caused by edge closeouts, vane or splitter support structure, access holes, splices between sheets of material, and blockage of the pores in the porous surface by the attachment method used to secure the porous surface to its support structure.

In addition, it should be noted that the chart does not specify the acoustical parameters of the duct-lining design. It was assumed that the duct lining would be nearly as effective as the 1-inch deep, single-layer fibermetal design, the basis for the chart. It was also assumed that any decrease in

attenuation, caused by changes in airflow velocity (over the duct Mach number range 0.2 to 0.6), would be as small as noted for the reference duct lining. If the duct-lining design chosen does not have these characteristics, an appropriate extra allowance for treated area should be made.

Figure 3(a) was only intended to be used for estimating the area required to reduce the amplitude of the tones at blade-passage frequencies because the acoustical energy in the inlet and fan ducts at these frequencies should be rather uniformly distributed owing to the large number of circumferential and radial modes excited by the fan-compressor stages. The chart does not apply to estimating the treated area required to reduce the amplitude of combination tones where the acoustical energy is concentrated near the walls of the inlet duct.

In figure 3(a), A_{tr} is the effective area of treatment required to achieve a reduction, ΔPNLM, in maximum PNL at low altitudes during landing approach. For the ordinate, the area, A_{tr}, was nondimensionalized by the area of the noise source, A_{ns}, which was assumed to be the projected annular area of the fan inlet or fan exit. The abscissa is the ratio of the duct height, h, to the sound wavelength λ. The height, h, was taken as the average perpendicular distance between two opposite, acoustically lined duct surfaces; if one surface was treated and the opposite one untreated, the value of h would be double.

In calculating λ for the JT3D installation with short fan-exhaust ducts, the temperature of the air in the ducts during a landing approach on a warm day was assumed to be 100°F and the speed of sound was 1160 ft/sec. At the 2500 Hz typical blade-passage frequency assumed for the landing approach, the value of λ was 0.46 ft (5.5 in.). The area of the noise source on the JT3D was 12.5 sq ft for the inlet duct and 5.8 sq ft for the fan ducts. The wavelength was assumed to be a constant in both the inlet and the fan-exhaust ducts at any specified engine power setting.

Figure 3(a) was used in designing candidate nacelles. However, it was difficult to use for evaluation of specific designs because of the requirement to interpolate between various noise reduction values. Figure 3(b) presents an alternate arrangement of the same information in a manner more suitable for design evaluations. The independent variable in figure 3(b) is a duct treatment parameter $(h/\lambda)/(A_{tr}/A_{ns})$. To use the chart, it is necessary to first calculate values for this parameter and then determine appropriate noise reduction estimates for separate portions of an inlet or fan duct corresponding to separate h/λ and A_{tr}/A_{ns} ratios. The separate estimates are then combined in a suitable manner to determine an estimate of total noise reduction.

Fan-Exhaust Ducts

24-inch-long ducts and supplementary treated panels. – The acoustically treated fan-exhaust ducts, considered in an earlier program and described in reference 13, had only 9.7 sq ft of gross acoustically treated area in each duct. The PNL reduction achieved during landing approach was approximately 2.5 PNdB at low altitudes.

The modification to the 24-inch fan-exhaust ducts considered for this program had 11.1 sq ft of treated area on the walls of each duct and 6.25 sq ft of treatment on the four flow splitters in each duct; i.e., a total of 17.35 sq ft of treated area in each duct. Henceforth, the convention will be used of describing the treated area by the gross area and not the effective area unless specified otherwise.

In keeping with the design constraints, the shape and location of the fan-exhaust nozzle exit were retained in order to preserve the fan thrust reversers and the external aerodynamic loft lines. Retention of the fan nozzle and inclusion of the thicker treated splitters required an expansion of the contours of the inner and outer duct walls. This expansion resulted in an increase in local wall curvature and an increase in duct channel height.

Using figure 3(b), it was estimated that the 17.35 sq ft of treatment in each duct would reduce the PNL by 6 to 7 PNdB, an amount insufficient to meet the 10 PNdB goal. Therefore, a design was studied that could provide additional treated area during landing approach through the use of retractable supplementary treated panels having 17.3 sq ft of treatment on the inboard surfaces of the panels as indicated in figure 4. The panels would normally be stowed flush with the nacelle's external contours in recesses on the sides of the nacelle forward of the fan-exhaust nozzle. During landing approach, the supplementary panels would be translated rearward on a track-and-roller system. It was estimated that the supplementary treated panels would provide 1 to 2 PNdB additional noise reduction.

As indicated in figure 4, the panels would have to be retracted before the fan thrust-reversers were actuated. An interlock system would be required to prevent inadvertent simultaneous extension of supplementary panels and fan reversers.

Although the 24-inch fan ducts with supplementary treated panels might have achieved 7 to 9 PNdB noise reduction and were compatible with the continued use of many of the existing nacelle components, they would have required the development of a new actuation and control subsystem to deploy and store the panels. In addition, the aerodynamic performance of the treated 24-inch ducts was not as good as that of the existing 24-inch ducts due to the expanded contours of the duct in the 24-inch length. For these reasons, an alternate design was studied wherein the ducts were lengthened to provide internally the required area of treatment without any external supplementary treatment.

48-inch-long fan-exhaust ducts. – The decision to study lengthened fan exhaust ducts resulted in a requirement to redesign the existing fan thrust reversers. The lengthened ducts, figure 5, would have revised internal duct contours and splitter locations, thereby providing more favorable flow area distributions and less wall curvature than the existing 24-inch fan ducts. The better area distribution and the reduced wall curvature would compensate to some extent for the increased duct wall friction expected from the absorptive duct linings.

The 48-inch duct length was selected as a compromise between treated area and nacelle weight. The internal contours of the ducts resulted in an average radial duct height of about 8.5 inches. By treating the inner and outer walls of the ducts and both sides of each flow splitter, it was possible to install a total treated area of 70.5 sq ft. The estimated noise reduction of this design was a satisfactory 9 to 11 PNdB.

Two designs for new fan-thrust reversers were examined: (1) a fixed-cascade and blocker-door reverser mounted within the fan duct, and (2) a target reverser with a single pivoted bucket on each side of the nacelle downstream of the fan-duct nozzle. The target reverser design was chosen because it had: (1) no loss in acoustically treated area; (2) no compromise of internal aerodynamic performance; and (3) it was a simpler and lighter design with lower cost and potentially superior reliability and maintainability. Although target reversers are not as effective in reversing airflow as

cascade reversers, it was considered that a target reverser, such as the one shown in figure 5, could be developed with effectiveness equal to those on existing airplanes known to have satisfactory reverse thrust effectiveness. The primary thrust reverser was unchanged by the design with the 48-inch fan ducts and new fan-thrust-reversers.

Evaluation of designs. – All nacelle modification designs were evaluated on the basis of their estimated capability for reducing flyover PNLM and on the basis of the estimated impact on direct operating costs (DOC). Changes were calculated relative to the PNLM and DOC of existing DC-8-50/61 airplanes.

Each of the fan-exhaust duct designs would affect the installed specific fuel consumption (SFC), drag, airplane empty weight, and depreciation-and-maintenance expenses, each to a different degree. The net effect of changes in these variables was accounted for by estimated increments in DOC. The calculated changes were considered valid for passenger operations on domestic routes where changes in the fuel load required for a trip can be accommodated without change in payload.

Incremental changes to DOC were based on simple change factors that related changes in DOC elements to independent changes in installed SFC, drag, and weight. The two principal DOC elements were trip fuel costs and depreciation-and-maintenance expenses. Depreciation expense was based on the estimated cost of a retrofit kit and its installation prorated over a 5-year period. No salvage value was assigned to the replaced parts because it was assumed they would be discarded. Maintenance costs were calculated by estimating the difference between the maintenance required by the modified and the existing fan-exhaust systems. For these studies, the additional elements in DOC of crew, oil and insurance costs were assumed to be constant.

Changes in trip fuel costs were based on changes in installed SFC owing to changes in total pressure loss in the ducts, nacelle drag, and nacelle weight. The addition of acoustical treatment to the fan-exhaust ducts would cause a decrease in fan-nozzle total pressure and hence a reduction in net thrust. Fuel flow would not be affected by the addition of the acoustical treatment. The method of calculating thrust loss was that provided by P&WA.

The increment in depreciation-and-maintenance costs was prorated on the basis of changes in nacelle weight relative to the weight of the existing nacelle. This cost increment was converted into a DOC increment using the following assumptions: (1) a five-year depreciation period for the cost of a retrofit kit and its installation; (2) an airplane utilization rate of 3800 flight hours per year; (3) no salvage value for replaced parts; (4) a value for spares of 20 percent; and (5) a base DOC of 1.15 cents per seat nautical mile. The base DOC corresponded to that of a DC-8-55 airplane operating over a range of 2000 nautical miles with a payload of 30 175 pounds consisting of 135 passengers, their baggage, and 2500 pounds of cargo.

The total impact on changes in DOC for the fan ducts was determined by combining the increment due to higher trip fuel costs with the increment due to the higher depreciation-and-maintenance costs. The cost of the retrofit kit and the cost of its depreciation-and-maintenance were the largest elements in the incremental changes in DOC.

The results of the acoustical and economic evaluations of the two fan duct designs are summarized in table I. After examination of these results, the 48-inch duct design was selected for the following reasons: (1) the higher probability of meeting the 10 PNdB goal for fan-exhaust noise reduction; (2)

the smaller increment in DOC; (3) the simpler mechanical design of the 48-inch ducts and target fan-thrust reversers; and (4) the lower technical risk and the better reliability compared to the design with the retractable supplementary treated panels and the existing cascade fan-thrust reversers.

Inlet Ducts

Fixed-geometry designs. – The goal of the inlet duct studies was to provide for installation of sufficient acoustical treatment in the inlet duct to yield 7 PNdB noise reduction. Studies of designs without movable surfaces were given first consideration. The designs were evaluated for their noise reduction possibilities by using figure 3(b).

Installation of treatment on only the walls of the existing inlet duct and centerbody would not have been feasible because of the prohibitive inlet length required. In the region ahead of the centerbody, the ratio h/λ was about 10 and the treated area required for 7 PNdB fan noise reduction would be about 850 square feet corresponding to an inlet duct length of about 67 feet. Therefore, designs were studied that could provide the required area of treatment within feasible duct lengths by using narrow channels with small h/λ ratios.

The three fixed-geometry inlet designs that were studied consisted of: (1) the existing inlet configuration with concentric ring vanes and support struts; (2) the existing inlet configuration with radial vanes; and (3) a lengthened inlet with an enlarged lightbulb-shaped centerbody and support struts.

Concentric ring vanes: Figure 6 illustrates two designs that used concentric ring vanes to achieve smaller duct channels than in the existing duct. Both designs preserved the existing inlet configuration, the existing centerbody, and the nacelle subsystems for pneumatics, oil, and anti-icing. The ring vanes would have treatment installed on both sides of an impervious septum and would be supported from the duct wall by untreated radial struts. The single ring-vane design, figure 6(a), used a short ring and required no change to the internal duct loft lines. Installation of two rings, figure 6(b), required a slight expansion of the internal duct loft lines to compensate for the flow area reduction caused by the ring vanes and support struts.

In studying these inlets having concentric ring vanes, consideration was given to ice protection requirements, in addition to the acoustical and aerodynamic requirements. Installation of acoustically treated surfaces with their supports in the inlet would require additional anti-icing, besides that supplied to the cowl lip and the tip of the centerbody in the existing inlet. Ice protection could be provided by hot engine-bleed air ducted through ring support struts of reasonable size.

Radial vanes: An inlet design having radial vanes to reduce the channel height (distance between treated surfaces) is shown in figure 7. Treatment would be installed on the inlet duct, both sides of the 16 vanes, and the centerbody. The duct was lengthened and its loft lines modified to accommodate the 1-inch-thick vanes. A possible advantage of this design over the concentric ring-vane design could be an ability to absorb more acoustical energy from spinning modes of sound propagating through the inlet.

Lightbulb centerbody: Figure 8 illustrates an alternate approach to the use of treated vanes. The difference between the two designs in figure 8 is the amount of treated area provided on the wall of the inlet duct.

The enlarged lightbulb-shaped centerbody not only reduced the channel height, but also provided line-of-sight blockage of the rotating fan blades. The term 47-percent refers to the ratio of the maximum cross-sectional area of the centerbody to the annular area of the inlet duct at the inlet-guide-vane station. Although a single ring vane was provided to reduce the channel height, the length of the duct had to be increased over that of the existing inlet duct because of aerodynamic considerations. The amount of blockage was selected on the basis of aerodynamic considerations.

Enlarging the centerbody required that the wall of the inlet duct be displaced outward to provide adequate flow area at the centerbody maximum-diameter station. The axial distances from this station to the inlet lip and to the fan inlet had to be large enough to prevent excessive curvature of the duct wall and of the centerbody downstream of this station.

Variable-geometry designs. – Because of the total pressure losses due to the friction of porous surfaces, as well as the various flow obstructions present in fixed geometry designs, three variable-geometry inlet designs were studied wherein the acoustically treated surfaces would be extended into the inlet airstream during landing approach. During takeoff, climb, cruise, and descent the treated surfaces would be held in a retracted position. In order to provide sufficient room for the various actuation and control mechanisims in each of the variable-geometry designs, it was necessary to modify the design constraints, move some of the nacelle subsystems, and change the cowl lines. It was assumed that the engine would operate satisfactorily while the treated surfaces were being deployed or stowed.

Retractable inlet flaps and retractable radial vanes: A retractable inlet flap design, figure 9(a), contained a number of segmented flaps located around the periphery of the inlet. The inlet was extended approximately 30 inches to provide sufficient length to meet aerodynamic requirements for satisfactory engine operation during a landing approach. The space available for the treated surfaces and their actuation and control devices, coupled with the requirements for engine airflow, precluded use of the narrow channels that would have been required to achieve the 7 PNdB goal with the amount of treated area that could be installed.

The retractable radial vane concept, figure 9(b), combined the potential acoustical advantage of the lightbulb centerbody with the ability to retract the treated surfaces. Pressure-actuated doors around the periphery of the cowl would permit sufficient supplementary airflow to allow satisfactory engine operation with the vanes extended. The supplementary airflow passageways would have some acoustical treatment on one surface.

Retractable curved vanes: A retractable-curved-vane design, figure 10, was studied in order to provide for retracting most of the acoustically treated surfaces without excessively increasing the length or diameter of the inlet. The vanes would be stowed against the inlet duct wall except during landing approach. Although this design did not remove all the acoustically treated surfaces from the inlet airstream during cruise (one of the treated sides of each vane would be exposed when stowed), it did reduce the amount of flow obstruction compared to the fixed-geometry designs.

Evaluation of designs. – A summary of several principal configuration changes, introduced by the eight inlet designs, is given in table II. The changes are given relative to the existing JT3D inlet on DC-8-50/61 airplanes. The increment in inlet weight is given relative to the 236-lb weight of the existing inlet. The total 426-lb weight of the existing inlet duct includes 190 lb of nacelle subsystems.

The results of the acoustical and economic evaluations of the eight inlet designs are given in table III. The evaluations of the inlet designs were conducted in the same manner as described for the fan-exhaust ducts. As noted in the evaluation of the fan-exhaust system, the depreciation-and-maintenance costs were much larger than the trip-fuel costs in the total change in DOC.

Based on these results, the two-concentric-ring design, Item 2, was selected as the most promising candidate to use with the 48-inch fan ducts for the nacelle modification because it was estimated that it could meet the 7 PNdB acoustical design goal and simultaneously had the smallest estimated increase in DOC.

Because the design of flyable, acoustically treated inlets to reduce landing noise by 7 PNdB had never been attempted before and because of the uncertainty of the acoustical and economic performance estimates, it was decided that a second treated inlet should be included in the ground static test program as added insurance toward meeting the design goal. Examination of the results in table III suggested the choice of the lightbulb inlet with maximum treatment, Item 5, for the backup inlet design, because of its greater noise reduction possibilities and because the differences in estimated DOC increment were not significant.

In summary, the nacelle modification designs selected for fabrication and ground static testing were the 48-inch fan exhaust ducts, the two-concentric-ring inlet with the existing inlet duct and centerbody, and the 47-percent lightbulb inlet with a lengthened inlet duct and single concentric ring vane. Assuming that the two-ring inlet would be designed so that the engine could be operated satisfactorily with one or both of the ring vanes removed, the selection of these two inlet designs provided a total of four acoustically treated inlet configurations for the static test program and permitted evaluation of a range of duct channel heights, treated surface areas, and inlet shapes.

Variable-Area Primary-Exhaust Nozzle

Although the basic approach of this JT3D nacelle modification program was the study of acoustically treated fan inlet and exhaust ducts, an alternate approach was investigated to determine its potential for noise reduction. This alternate approach provided control of the speed of the fan rotor during landing by in-flight reduction of the exhaust area of the primary nozzle, thereby reducing the pressure drop across the fan-drive turbine and hence the rotational speed of the low-pressure rotor. As a result, at any given level of landing thrust, the fundamental blade-passage frequency and the intensity of the fan tones should be reduced, while the primary jet exhaust velocity, and hence jet exhaust noise, would be increased. The possibility of a net reduction in PNLM would depend on the relative magnitudes of the reduction in discrete-frequency fan noise and the increase in broadband jet-exhaust noise.

An indication that the variable-area primary-nozzle approach might be feasible was provided by data obtained during development flight testing of the long-duct-pod thrust reverser for the Model 62 and 63 DC-8 airplanes. These flight tests, conducted prior to the contract effort reported in this Part, were performed with one engine fitted with a primary-exhaust nozzle having 50 percent of the exhaust area of a standard primary nozzle. At 6000 lb net thrust (an approach power setting for a heavy landing weight), the referred low-pressure rotor speed was reduced from approximately 4400 to 3600 rpm while the high-pressure rotor speed was slightly decreased. However, the tailpipe temperature and engine pressure ratio were both considerably increased by the 50-percent nozzle; in fact, the engine pressure ratio increased from 1.20 to 1.56 at the 6000-lb thrust setting.

Based on the flight test indications and on the potential fan noise reduction, it was decided to evaluate the concept of a primary nozzle having a variable area in the ground static tests. No estimates were made of changes in flyover PNLM for this concept because there was no adequate method to assess the noise reduction other than by test. Tests were planned using conical nozzles with 50, 60, and 80 percent of the normal JT3D primary exhaust area. The acoustical and engine performance results of the tests are presented in reference 9.

DUCT-LINING ACOUSTICAL INVESTIGATIONS

Because of the Contractor's previous duct-lining acoustical investigation (ref. 1), and because of the design decisions discussed previously, there were four major acoustical parameters of the duct lining remaining to be specified for the static test articles. These parameters were: (a) the type of porous material to be used and its nominal acoustic flow resistance; (b) the number of porous layers to be included in the design of the lining; (c) the depth of the backing cavities; and (d) the size of the cells in the honeycomb support. The duct-lining acoustical investigations were aimed at selecting values for these four parameters appropriate to the inlet and fan-exhaust ducts.

Selection of candidate materials for the porous facing surfaces of the duct lining was based on structural and economic considerations as well as acoustical criteria. Using the guidelines of Appendix B of reference 1, candidate materials were selected from among commercially available metallic products. The materials were of two different classes. One class consisted of sintered stainless-steel fibermetals reinforced by one or two layers of stainless-steel wire screens sintered to the fibermetal mat. The other class consisted of sintered layers of woven stainless-steel wire-screens. Variations in the acoustical properties of the fibermetal materials were obtained by using wire fibers of differing diameters, by changing the surface density of the material, and by varying the thickness of the material. Variations in the acoustical properties of the woven wire-screen materials were made by using different diameter wires, weave patterns, thicknesses, and surface densities.

Four types of acoustical tests were used to evaluate duct lining designs. Flow resistance tests with airflow through the material determined (a) the nominal flow resistance and the magnitude of the nonlinear increase in nominal flow resistance of sample pieces of candidate porous materials, and (b) the uniformity of the nominal flow resistance over the surface of a sheet of material. From normal-incidence standing-wave-tube tests, acoustic absorption coefficients and the components of acoustic impedance were determined as a function of the SPL incident on the porous surface. Duct transmission-loss tests, with and without airflow through the duct, provided a means for rank ordering the attenuation of various duct linings and also provided the design information required to specify the acoustical parameters of the duct linings for the static test articles. Sonic-fatigue tests established the relative resistance to acoustically induced fatigue of selected duct linings and verified that the choice of the structural design of the duct lining could withstand the acoustical environment of the inlet and fan-exhaust ducts on the JT3D engine for a length of time sufficient for the flight-test program.

The honeycomb core used to support the porous facing sheets was made from phenolic-resin-coated fiberglass cloth. Fiberglass honeycomb with a sine-wave ribbon pattern was chosen because it was readily available with a range of cell sizes that could provide adequate noise reduction and strength-to-weight ratios.

The fibermetal samples consisted of either random arrays of long wire-fibers with diameters between 0.0004 and 0.001 inches or random arrays of comparably shorter wire-fibers with diameters of 0.003 or 0.004 inches. The reinforcing screens provided extra strength without changing the acoustical characteristics.

Flow Resistance

Background. – Flow resistance is a basic acoustical characteristic of any porous material. It is a measure of the resistance to a steady flow of air through a material. Theoretical studies (ref. 17) and previous tests (ref. 1) had indicated that there was a relationship between the flow resistance of the material and the real part of the acoustic impedance of a duct lining. Because the impedance of a duct lining is one of the factors that determines the attenuation achieved, flow resistance measurements provided an easy means of determining the potential usefulness of various candidate materials for duct linings.

When the airflow velocity through a porous material is low, the flow resistance is due principally to the viscosity of the air in the interstices of the material. In this low-flow region, the flow resistance is constant and independent of velocity. As the velocity through the material increases, additional energy losses occur owing to turbulent airflow through the pores and to acoustic streaming (ref. 18); consequently, the flow resistance increases. The velocity at which the flow resistance begins to increase and the rate of increase in flow resistance depend on the size and arrangement of the wires, interstices, and voids in the material, as well as its thickness and surface density.

When a porous material is installed as part of a duct lining in the environment of a jet engine, the material is exposed both to airflows over the surface and to high SPLs. Because the high airflows and SPLs affect the impedance and hence the attenuation, it was necessary to determine the flow resistance over a wide range of velocities in order to study the nonlinear behavior of porous materials. A non-linearity factor (NLF) was developed to assist in rank ordering the non-linearity of porous materials. The NLF was defined as the ratio of the flow resistance at a velocity of 5.0 m/sec to the flow resistance at 0.2 m/sec.

This factor was developed based on an assumed correlation between the steady airflow velocity through a porous material in a flow-resistance test and the equivalent rms velocity of a particle of air moving through the porous surface of a lining installed in an inlet or fan-exhaust duct. The equivalent velocity has components due to the sound field impinging on the lining and to the turbulence from the air flowing over the lining.

Because there were data available on the SPLs in the ducts but there was no way to account for the turbulence component of the airflow, the equivalent velocity v was estimated using eq. (8) of reference 1. Thus, with velocity v in m/sec,

$$v = 10^{[(SPL-146.4)/20]} \qquad (1)$$

with SPL in dB re 2×10^{-5} newtons/sq m.

Previous tests (ref. 1) had shown that narrow-band SPLs on the order of 160 dB at blade-passage frequencies were incident on the walls of the inlet and fan-exhaust ducts on the JT3D engine. From eq. (15), a SPL of 160 dB would correspond to an equivalent velocity of 5 m/sec.

By agreement with the suppliers of the porous materials and other investigators of acoustical duct linings, the system of units to be used for the airflow velocity, when plotting flow resistance data, was the internationally preferred mks system. However, because of the wide usage of the cgs system of units for flow resistance, the cgs rayl unit was retained for flow resistance. (In the mks system, the flow resistance unit, in mks rayls, is ten times larger than the unit in the cgs system.) Again by agreement, the nominal flow resistance of a porous material was defined to be that at a velocity of 0.2 m/sec. This velocity was chosen because it is in the low-flow region for materials suitable for duct linings in jet engines.

Sample materials. – The nominal flow resistance and NLF were determined for 93 samples of porous material. Table IV summarizes the results of these flow-resistance tests and also lists the thickness and surface density of the samples. Table IV (a) presents the results for fibermetal samples made from 0.0004-, 0.0005-, and 0.001-inch-diameter wire fibers; table IV (b) presents the results for fibermetal having 0.003- and 0.004-inch-diameter wire fibers. Most of the fibermetal samples were reinforced by a coarse-weave wire screen sintered to the mat of wire fibers to provide additional strength with no change in flow resistance. With the exception of Item 20 in table IV (a), the 0.001-inch-diameter wire-fiber samples did not have reinforcing screens.

Table IV (c) presents results for woven-wire-screen samples made from combinations of 1 to 5 layers of wire screens with various weave patterns and wire diameters. The wires in each layer of screen were sintered together and the various layers were bonded to each other by sintering. The diameters of the wires in the woven-wire screens were not available, although some information was available on the number of wires per inch for some of the weave patterns. Variations in thickness and density were obtained by a rolling process known as calendering.

Test procedures. – The flow resistance of a material was determined as the ratio of the pressure differential through the material to the linear velocity of airflow through the material. Linear velocities were determined from measurements of volume flow rate.

Flow resistance was therefore determined as

$$R_f = \Delta p/(U/S), \text{ or} \tag{2}$$

$$= \Delta p/u. \tag{3}$$

With the differential pressure, Δp, in dynes/sq cm, volume flow rate, U, in cu cm/sec, test area, S, in sq cm, and linear velocity, u, in cm/sec, the flow resistance has units of (dyne-sec)/cu cm. This unit is termed the cgs rayl.

The apparatus illustrated in figure 11 was used to determine the flow-resistance of various porous materials. The apparatus used high-pressure air from a central compressed-air system. The air was filtered to remove oil and water vapors and solid particles such as rust and scale that were present in the system. The large plenum tank acted as a settling chamber to ensure uniform and steady airflow

through the sample. The pneumatic cylinder was used to hold a 10-cm-diameter test fixture down onto the surface of the porous sample. Edge airflow leakage, between the bottom of the test fixture and the surface of the porous sample, was minimized by a rubber gasket located on a 1-inch-wide flange on the bottom of the test fixture.

Differential pressures up to 20 inches of water through the sample were measured on a micromanometer that used water as a working fluid. The accuracy of these pressure measurements was ±0.0005 inch of water. The micromanometer was capable of measuring pressures as low as 0.001 inch of water. Differential pressures greater than 20 inches of water could be measured on a mercury manometer in the manometer bank. Flow resistance tests were conducted over the range of velocities from 0.07 to 14 m/sec to investigate the behavior of materials over as wide a velocity range as possible with the flow-resistance test apparatus.

Results. – Selected results of the flow-resistance tests are presented in figures 12, 13, and 14. The accuracy of the flow-resistance measurements was to within ±0.2 cgs rayls.

Porous materials in each of the two classes that were tested can be produced in a variety of ways. Because of this and because of continuing product improvements made by the suppliers, the results presented here should be considered only as representative of those that can be obtained. Inspection of the data in table IV will show that materials can be made by any of the three manufacturing processes with equal nominal flow resistance, though they may differ in other respects.

Figure 12 shows the effect of increasing the surface weight density (weight per unit area) of four fibermetal samples having a nominal thickness of 0.048 inches; figure 13 presents the effect of calendering samples of woven wire-screen to decrease their thickness. In figure 12, small increases in surface density resulted in significant increases in nominal flow resistance. In figure 13, small reductions in thickness resulted in significant increases in nominal flow resistance. These observations suggested that careful control of thickness and density would be required to ensure that a large sheet of porous material would have a nominal flow resistance that was uniform over the sheet. A set of flow-resistance uniformity requirements was developed and used in purchasing large sheets of porous materials. These requirements are given in Appendix A.

Another observation from the results presented in figures 12 and 13 is the differences in NLFs. The NLF for the fibermetal in figure 12 is two to three times smaller than the NLF for the woven-wire-screen material in figure 13. This result suggested the conclusion that material made from small diameter wires would have smaller NLFs than material made from larger diameter wires.

Further information on the nonlinear characteristics of porous material is given in figure 14. Figure 14(a) presents results for nominal 40 cgs rayl material; figure 14(b) presents results for nominal 10 cgs rayl material. For both nominal flow resistances, the NLF decreased as the fiber diameter decreased. However, the NLF also decreased with decreasing thickness and surface density. Therefore, the data available are not sufficient to determine the best combination of parameters to obtain the lowest NLF for the materials tested.

In summary, flow resistance tests showed that (1) any of the three types of porous materials investigated can be manufactured in a wide range of nominal flow resistance; (2) by keeping all parameters constant, the material with the smallest NLF was the thinnest, had the smallest surface

density, and was made with the smallest diameter wires; (3) significant changes in the nominal flow resistance occurred with small changes in thickness and density of the material. A quality control procedure based on flow resistance testing was developed and used to ensure that the nominal flow resistance of a large sheet of porous material would be acceptably uniform over the sheet.

Acoustic Absorption and Impedance

Background. – To supplement the acoustic flow resistance studies, investigations of various candidate porous materials and duct lining concepts were conducted using a standing-wave-tube (SWT) apparatus. These investigations determined the normal-incidence acoustic absorption coefficients and the real and reactive components of the complex acoustic impedance as a function of frequency, SPL, and cavity depth behind the porous facing sheet.

Although there were some fundamental limitations on the usefulness of absorption coefficients or acoustic impedances for selecting duct-lining designs for the acoustically treated inlets and fan-exhaust ducts, the SWT tests did provide valuable information on the change in the acoustical characteristics of a duct lining when exposed to high SPLs. Two fundamental limitations of the SWT tests were: (a) sound propagating through the inlet and fan-exhaust ducts impinges on the walls of the ducts at angles not necessarily normal to the surface, and (b) the high-speed flow of air over the duct lining in the duct has an important bearing on the effective acoustic impedance of the lining. These absorption coefficient and impedance tests did not account for the effects of non-normal incidence or airflow.

Sample materials. – Three samples of screen-reinforced, 0.040-in.-thick fibermetal, having nominal flow resistances of 8, 10, and 40-cgs rayls, were used for the tests. The samples were made from nominal 0.004-inch-diameter wire fibers. For the SWT tests, no honeycomb support structure was used. The cavity behind the samples was a single cavity without cells or partitions.

Apparatus. – The diagram in figure 15 shows the experimental arrangement of the components of the SWT apparatus. Three cylindrical tubes with different diameters and lengths were used. The dimensions of the tubes were chosen to cover the frequency region between 400 and 8000 Hz in three overlapping ranges. For a given range of frequencies, the upper limit of the range determined the diameter of a tube while the lower limit of the range determined the length. The criterion for choosing the diameter was based on maintaining plane waves in the tube. The length was chosen to permit measurements of the level and location of the first and second antinode of the standing-wave pattern.

The diagram in figure 16 shows the sample holder section of the SWT. The end plate was made from steel to approximate a rigid termination. Cork gaskets were used to minimize sound energy losses due to leakage. The depth of the cavity behind the sample was determined by the thickness of the cavity spacer rings. Four rings for each SWT were used to obtain four different cavity depths.

Test procedure. – The samples were tested at the fourteen geometric-mean center-frequencies of the 1/3-octave bands between 400 and 8000 Hz. The cavity depths used for the tests were: 0.25, 0.50, 0.75, and 1.0-inch. At each frequency and cavity depth, the porous surfaces were exposed to SPLs of 125, 135, 145, and 155 dB.

The standing-wave pattern in a tube was established with a loudspeaker mounted on the end of the tube opposite the sample holder. A small-diameter probe tube attached to a capacitor microphone was used to detect the SPLs at the antinodes and nodes of the standing wave pattern. The signal from the microphone was passed through a 1/3-octave-band filter to remove spurious electronic system noise.

Determination of acoustic absorption coefficient and impedance. – Acoustic absorption coefficients (a_n) were determined from the SPL measurements; i.e., from the standing wave ratio (SWR) of the sound pressures. The SWR was determined from the ratio of the mean-square sound pressure at the node closest to the sample and the mean-square sound pressure at the immediately following antinode. The following relation (ref. 19) was used to calculate absorption coefficients

$$a_n = 1 - \left[(\mathrm{SWR} - 1)/(\mathrm{SWR} + 1)\right]^2. \tag{4}$$

The acoustic impedance, Z, of a porous material was determined from measurements of: (1) SWR, (2) the distance D_1, from the face of the sample to the node in the standing wave pattern closest to the sample, and (3) the distance D_2 from the first to the second node in the standing wave pattern. The impedance was normalized by ρc, the characteristic acoustic impedance of free air and was calculated from

$$Z/\rho c = \coth (A + jB), \tag{5}$$

where

$$A = \coth^{-1} (\mathrm{SWR}), \tag{6}$$

$$B = \pi\left[0.5 - (D_1/D_2)\right], \tag{7}$$

and ρc = 41.5 cgs rayls at standard temperature and pressure.

The normalized resistive ($R/\rho c$) and reactive ($X/\rho c$) components of the impedance were determined from,

$$Z/\rho c = (R/\rho c) + j\,(X/\rho c). \tag{8}$$

Results. – Selected results of the SWT tests are presented to show the effect of high SPL on absorption coefficient and impedance. Although tests were conducted for various cavity depths, all the results presented here are for a single cavity depth of 0.75 inch. Increasing the depth of the cavity behind the porous surface increased the volume of the cavity and hence lowered the frequency at which maximum absorption occurred.

Figure 17 shows the effect of increasing the SPL incident on the 10- and 40-cgs rayl samples. For the 10-cgs rayl sample, the absorptivity was greater at 155 than at 125 dB. However, for the 40-cgs

rayl sample, the absorptivity at 155 dB was less than at 125 dB. Note that the frequency at which maximum absorption occurred decreased somewhat as the nominal flow resistance increased from 10- to 40-cgs rayls.

Figure 18 shows the effect of SPL on the maximum absorption coefficient of the 10- and 40-cgs rayl samples. The curves corroborate the trends noted in figure 17 in that the absorptivity of the 10-cgs rayl material increased as the SPL increased, while that of the 40-rayl material decreased as the SPL increased.

The decrease in the absorption coefficient for the 40-cgs rayl sample at high SPLs was due to the increase in the resistive component of the acoustical impedance of the material. The effect of SPL on the resistive component, $R/\rho c$, is illustrated in figure 19. For the 40-cgs rayl sample, $R/\rho c$, which was approximately equal to 1.0 at 125 dB, was considerably greater than 1.0 at 155 dB.

Duct Transmission-Loss Tests

Background. – Although tests using small samples of porous material to determine basic acoustical properties yield information which is useful in designing actual duct linings, additional experiments are required to assess the behavior of larger samples of various duct-lining designs with air flowing over the treatment. The type of experiment selected to make these assessments was duct transmission-loss (TL) tests. These tests were run at the Pratt & Whitney Aircraft Co., at a facility in East Hartford, Connecticut. This facility permitted the rapid determination of the TL of sound propagating through a duct with various rates of airflow. SPLs were measured inside two reverberant enclosures, one upstream and one downstream of a test duct. These enclosures served as source and receiver rooms for the sound waves transmitted down the duct. The direction of sound propagation could be chosen to be either with or against the direction of the airflow to simulate an exhaust or inlet duct.

Duct-model TL tests conducted in the past used various models to simulate full-scale sections of fan exhaust or inlet ducts as might be installed on the JT3D turbofan engine. The models all had very specific geometries and were run to provide answers for specific configurations. These past tests consisted of three series which began in November 1965 (ref. 1). A summary of the range of parameters investigated is presented in table V.

The tests that were planned for the test program described in this document utilized a straight duct with a simple rectangular cross section to determine the effects of a wide range of parametric variables on the attenuation of sound propagating in a duct. The basic fixture for the sides and frame of the test duct incorporated special quick-release clamps to hold the top and bottom panels in place. This feature permitted rapid configuration changes and made the best use of the limited amount of vacuum-pump time available for these tests.

Test description. – This section describes the test articles, variables, facility, and procedures used for the duct TL tests.

Test articles: A 45-inch-long rectangular duct with a 5 x 20-inch cross-section was built using 0.093-inch-thick sheet aluminum for the 5 x 45-inch sides. The 45-inch length was selected to duplicate the length of the existing inlet duct of the JT3D engines on DC-8 aircraft. Figure 20 shows

the test duct with two panels clamped in place by the special quick-release clamps. The criterion for selecting the duct cross sectional area, and thus the duct width, was based on the available airflow capability of the P&WA vacuum-pump air-supply system to simulate the airflow velocities in the JT3D inlet and fan-exhaust ducts during landing approach.

Test panels used nominal 0.040-inch-thick fibermetal and 0.063-inch-thick solid aluminum backing sheets bonded to fiberglass-honeycomb core enclosing air-filled cavities. Screen-reinforced fibermetal made from 0.003 and 0.004-inch-diameter stainless-steel wire fibers was used because of the experience gained with this product in previous test programs (refs. 1 and 13) and because information on alternate porous metallic products was not available in time to affect the decision of which material to use for these test panels. (The honeycomb core was not slotted to provide drainage of liquids. Provisions for liquid drainage would be required in a flight design.)

The procedure used to bond the panels is described in Appendix B. All panels, with the exception of two which were acoustically treated along the entire 45-inch length, were treated along only a 22.5-inch length but across the full 20-inch width as shown in figure 21(a). Figure 21(b) shows the honeycomb core bonded to the fibermetal (right) and sheet aluminum (left) of a typical panel partially removed from the duct. One-, two-, three-, and four-layer structures were tested but only the one-layer structures were completely bonded. All multi-layer structures were tested by superimposing two or more panels together. The sandwich assembly was held in place with screws around the perimeter of the panels and then clamped tightly in place. When the outermost panel was not one of the completely bonded one-layer panels, an 0.063-inch-thick aluminum sheet was laid over the outermost honeycomb core to provide an impervious backing sheet.

A total of five duct airflow splitters, each 5 x 45 inches and 1 inch thick, were fabricated. One of these splitters had hard aluminum walls along the full 45-inch length and the other four were acoustically treated with nominal 0.040-inch-thick fibermetal over air-filled cavities. A cross-section diagram of the four acoustically treated splitters is given in figure 22. Although the amount of fibermetal area exposed to the airflow in figures 22(c) and 22(d) was the same, the two-layer structure had twice the amount of fibermetal. The support structure used for fabricating each splitter was fiberglass honeycomb, with the exception of the corrugated design which used 0.040-inch-thick aluminum. All splitters, except the aluminum corrugated design which was riveted together, were bonded using a procedure similar to that used to bond the one-layer duct wall panels together. The corrugated riveted-aluminum splitter is shown installed in the test duct in figure 23.

Test variables and configurations: Systematic parametric investigations of a large number of test variables and configurations were possible with the 5 x 20 x 45-inch test duct. With this thought in mind, a detailed test program was developed to fulfill the general goals of the program described above. The following six items were common to the tests:

- Rectangular test duct with dimensions of 5 x 20 x 45 inches.
- Exhaust and inlet tests conducted by moving the sound source from the upstream to the downstream chamber.
- Airflow velocities of 0, 300, and 500 ft/sec.

- Test data analyzed at the following one-third octave-band center frequencies: 1600, 2000, 2500, 3150, 4000, 5000, and 6300 Hz.

- Test panels consisting of fibermetal sheets bonded to fiberglass-honeycomb core material in a sandwich construction.

- Air-filled backing cavities.

One-, two-, three-, and four-layer duct lining concepts were investigated. The test variables and their ranges for the one- and two-layer structures were as follows:

One-layer structures

- Nominal flow resistance (10 to 160 cgs rayls)

- Cavity depth (0.25 to 1 inch)

- Honeycomb cell size (0.375 to 3 inch)

- Ratio of treated-duct-length to duct-width (L/W) (2.25 to 9.0)

- Treated area (450 to 1800 square inches with no splitter and 225 to 2250 square inches with splitter)

- Area location (two sides vs one side) and (upstream vs downstream)

- Four splitter designs (all 1 inch thick), see figure 22

Two-layer structures with combinations of backing depth and flow resistance within the limits shown below:

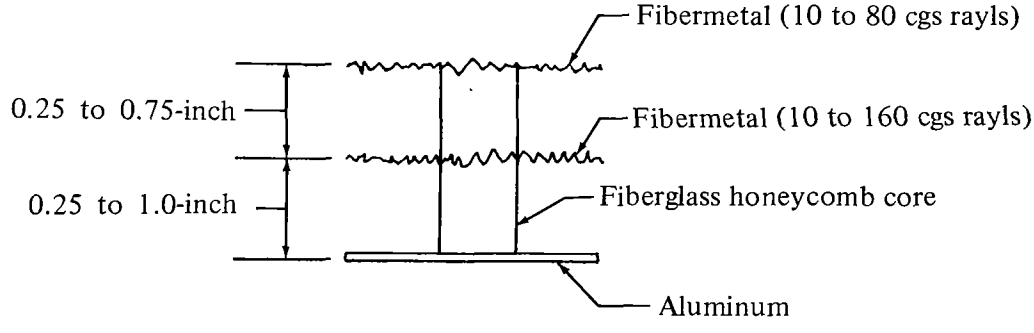

A detailed description of the tests to be conducted was developed before the start of the test program and is given in table VI. With the large number of parameters that were to be studied, the number of configurations that could be tested was very great. The table indicates the selection of configurations for which materials were ordered and for which test panels were built. The table also gives a listing of the combinations of the above configurations selected for testing. Each combination of duct lining concepts that was selected for testing was given a configuration code. The grand total of the configuration codes listed in table VI is 159. However, it was not the intention of the test

program to test each of these configurations. As the tests proceeded, various judgments were made to keep the total scope of the test program within reasonable limits. The tests actually performed included all of those outlined in table VI with the exception of those with an asterisk next to the configuration code.

Test facility: The test facility consisted primarily of a dual reverberant chamber system, five vacuum pumps each capable of inducing a volume flow of air of 11 200 cu ft/min under standard pressure and temperature (56 000 SCFM total), a source of high intensity sound, and an instrumented control room.

With the acoustically treated duct installed between the two reverberant chambers and a source of high-intensity sound located in one of the enclosures, the SPLs in the source and receiver rooms were measured. These measurements were made both with and without air flowing through the duct. The sound source was located in the upstream chamber when performing exhaust tests (sound propagating with the direction of airflow), and in the downstream chamber when performing inlet tests (sound propagating against the direction of airflow). Figure 24 shows the major components of the duct TL facility.

The two reverberant chambers with no parallel walls were identical in internal volume and shape. The internal volume was 268 cu ft and the internal surface area was 325 sq ft. The upstream chamber is constructed of 0.25-inch-thick steel plates covered on the outside by a 2-inch-thick layer of vibration-damping material. The downstream chamber was constructed of 0.5-inch-thick steel plates welded together and braced with steel I-beams. Additional description of the reverberant chambers is given in reference 1.

Figure 25 shows the two types of sound sources that were used. The pulse jet used in the upstream chamber for exhaust tests produced intense sound with acoustical energy at the firing frequency (about 220 Hz) and harmonics thereof. Because of the reverberant nature of the room in which the source was installed, the number of room modes excited by the source was large and the modal density (per unit frequency) was such that above 1500 Hz the spectrum of the sound in the chamber had almost constant SPL when analyzed in 1/3-octave bands. Excitation of a great many duct modes at once was believed to give the best simulation of the behavior of a duct-lining treatment in an actual engine installation where the rotating pressure field can excite many radial and circumferential modes.

A burner-can was used for inlet tests because it was nearly impossible to make the pulse jet work in the downstream chamber because of the partial vacuum with air flowing through the chamber. A description of the features of this novel sound source is given in Appendix C.

Figure 26 compares the 1/3-octave band SPLs in the downstream chamber produced by the pulse jet to those produced by the burner. The duct airflow velocity was 500 ft/sec. The three burner spectra are characterized by the fuel-flow rating (in gal/hr or gph) of the three burner tips that were used. The highest SPLs were produced at the highest fuel-flow rate. The SPLs produced when the 19.5-gph tip was used were about the same at 1600 Hz and about 5 dB higher between 2000 and 6300 Hz than those produced when the pulse jet was used. When a 10-gph burner tip was used, the SPLs were considerably lower, by about 10 dB between 1600 and 6300 Hz, than those produced when a 19.5-gph burner tip was used.

Figure 27 shows typical spectra measured in the downstream chamber with the pulse jet, and with the burner having a 17.5-gph burner tip. These spectra were obtained with a 1/3-octave band filter swept through the frequency range of 50 to 20 000 Hz. With the burner sound-source, the fluctuations in the overall SPL were only about ±0.5 dB compared to about ±1.5 dB with the pulse jet. In addition, each curve shows the variation with time of the overall SPL for a 124-second sample. The overall SPL was that indicated on the level recorder when no filter is used.

Test procedures: The term TL is defined herein as the difference in decibels (for a given frequency) between the SPL in the source chamber and the SPL in the receiver chamber when a sound source was activated. Figure 28 shows a schematic arrangement of the instrumentation and equipment used in these tests. Single-point SPL measurements in the source and receiver rooms were made. This procedure simplified the testing compared to duct-probing tests or to measurements of the radiated noise field from a duct exhausting into the atmosphere.

For each test, data were recorded for approximately 90 seconds in order to avoid making tape loops or rewinding the tape when reducing data. SPLs were read at the following seven 1/3-octave band center-frequencies: 1600, 2000, 2500, 3150, 4000, 5000, and 6300 Hz. Test data repeatability (for TL and thus attenuation values) was, for the most part, within ±1 dB.

The 5 x 20 x 45-inch test duct was installed between a two-dimensional bellmouth-shaped inlet attached to the upstream chamber and a tapered diffuser attached to the downstream chamber. The purpose of the bellmouth-shaped inlet and the downstream-diffuser sections was to provide aerodynamically smooth flow through the test duct, thereby keeping the background (airflow) noise levels as low as possible. Low background noise levels meant higher signal-to-noise (S/N) ratios. With higher S/N ratios, tests could be conducted at higher duct airflow velocities. Because the available S/N ratio effectively determined the maximum attenuation that could reliably be measured, it was necessary to measure the S/N ratio in the receiver chambers, with various airflow velocities through the duct, before conducting TL tests.

The S/N ratio in the receiver chamber with the air flowing through the system is the difference in the SPL with the sound source on and the sound source off. The ratio is defined only for hardwall tests because this was the reference or baseline case. The procedure used to establish desired duct velocities was similar to that used in reference 1.

The maximum TL and the maximum attenuation that could be measured were determined from receiver chamber S/N ratio measurements by analogy to panel sound-transmission-loss tests. The maximum TL for the hardwall ducts was

$$(\text{Maximum TL})_{\text{hardwall}} = (\text{TL})_{\text{hardwall}} + (\text{S/N})_{\text{hardwall}} \qquad (9)$$

at any frequency and duct velocity. This quantity is a direct measure of the limitation of a facility for duct TL measurements.

The measure of the ability of a duct-lining treatment to reduce the intensity of sound propagating along a duct is defined in this document as attenuation. Attenuation was determined by comparing

the TL obtained with a treated duct to that obtained with a hardwall, untreated duct.

Thus,

$$\text{Attenuation} = (\text{TL})_{\text{treatment}} - (\text{TL})_{\text{hardwall}} \qquad (10)$$

The maximum attenuation that could reliably be measured with a treated duct was determined, assuming a 3 dB margin, from

$$\text{Maximum attenuation} = (\text{S/N})_{\text{hardwall}} - 3 \text{ dB}. \qquad (11)$$

Hardwall S/N ratio measurements were made at the start of this test program in the exhaust mode using two different diffusers located between the test duct and downstream chamber. The first diffuser was one that was available and was used in the past for other duct TL test programs. This diffuser was 84 inches long and had a cross sectional area that varied from 132.25 sq in. (11.5 x 11.5 inches) to 676 sq in. (26 x 26 inches). In addition, a 24-inch-long transition section, varying in cross-sectional area from 100 sq in. (5 x 20 inches) to 132.25 sq in. (11.5 x 11.5 inches) was installed between the test duct and diffuser. The second diffuser was 46 inches long with a cross-sectional area which varied from 100 sq in. (5 x 20 inches) to 200 sq in. (10 x 20 inches).

The S/N ratios with the new 46-inch-long diffuser were expected to be higher than measured with the 84-inch-long diffuser because of the more gradual expansion of the shorter diffuser and the smaller exit area of the diffuser (200 compared to 676 sq in.). Figure 29 compares the exhaust mode S/N ratios obtained using the 46-inch-long diffuser to those obtained using the 84-inch-long diffuser for airflow rates of 300 and 600 ft/sec. Based on the results of these S/N ratio measurements, it was decided that the remainder of the test program, with the treated surfaces installed in the rectangular duct, would be conducted with the 46-inch diffuser, rather than the 84-inch diffuser, installed between the exit plane of the test duct and the downstream chamber.

Figures 30(a) and 30(b) illustrate typical S/N ratio values, using the 46-inch-long diffuser, as a function of frequency for duct velocities between 100 and 600 ft/sec. Figure 30(a) shows values for the downstream chamber for exhaust tests. Figure 30(b) shows values for the upstream chamber for inlet tests. At any given frequency and duct velocity, the S/N ratios were always highest in the upstream chamber, permitting inlet testing at higher duct velocities than exhaust testing. This result was attributed to (1) the higher signal strength generated by the burner-can over that produced by the pulse jet and (2) the lower background noise levels in the upstream chamber. As the air flowed through the test duct and transition sections into the downstream chamber, the turbulence level increased and the background SPLs in the downstream chamber were correspondingly increased.

Each configuration was tested at duct velocities of 0, 300, and 500 ft/sec in both the exhaust and inlet mode. Some configurations were also tested at other velocities. The maximum velocity was selected as 500 ft/sec based on the results of exhaust-mode hardwall S/N measurements [figure 30(a)] and measurements of exhaust-mode attenuation of a selected treated configuration. The criterion for selecting the maximum velocity was to pick the highest velocity that satisfied equation (11). The maximum velocity was selected based on exhaust rather than inlet measurements primarily because the S/N ratios were larger for exhaust than for inlet tests. The treated configuration selected to

determine the maximum duct velocity had nominal 40-cgs rayl fibermetal overlaying 1.0-inch-deep backing cavities. The honeycomb core had 0.75-inch cells. The treatment extended halfway along the length of the duct and was located on both the top and bottom of the 20 x 45-inch duct walls, see configuration code R15 in table VI. Figure 31 shows how attenuation varied with velocity for the exhaust tests for this configuration. The 900 sq in. of treated area for configuration R15 was the same as that used for all other configurations with the exception of a few which had less area and six (R19, R20, R33, R34, R35, and R36) which had more area. For those configurations which had more area, and thus produced higher attenuation values, the maximum test velocity for which valid data could be obtained was 300 ft/sec.

A total of 100 different treatment configurations were tested. These included 37 one-layer structures, 58 two-layer structures, 4 three-layer structures, and 1 four-layer structure. A description of the configurations tested is presented in table VI.

In general, systematic efforts were made to vary one parameter at a time. However, in view of the great number of possible combinations of acoustical treatment, treatment orientation, and duct velocity, it was not feasible to conduct a complete study. Therefore, evaluation of the results, during the course of testing, guided the selection of the combination of variables that were tested.

Results of exhaust-duct tests. – The results are discussed in the order in which the tests were performed: exhaust and then inlet. Because of the large quantity of data obtained, discussion of the results is limited to tests at 500 ft/sec, unless otherwise mentioned. In general, the duct TL tests showed that increasing the duct velocity reduced the attenuation for these fibermetal duct linings. Appendix D presents a series of charts showing the effect on attenuation of duct velocity. Chart series Nos. 1 through 25 shows how attenuation varies with duct velocity for exhaust tests, chart series Nos. 26 through 49, for inlet tests.

Unless mentioned otherwise, the acoustical treatment was installed along half the length and across the entire width of the two 20 x 45-inch duct walls, providing 900 sq in. of treated area. The treatment began at the inlet plane of the duct. Also, unless mentioned, the size of the honeycomb cells was 0.75 inch. Although the discussion concentrates on the results obtained with the one-layer duct-lining designs, some results of tests with multi-layer designs are also described. The discussion of the results of the two-layer designs is limited because the difference in attenuation produced using the two-layer designs to that produced using the more practical one-layer designs was relatively small.

The results presented in this section describe the effects of the following seven test parameters: flow resistance, cavity depth, honeycomb cell size, multilayer designs, flow splitters, treated area, and location of treatment.

Flow resistance: The effect of flow resistance on attenuation, as shown in figure 32, was primarily a function of cavity depth. For cavity depths of 0.5, 0.75, and 1 inch, the attenuation values were highest for the linings with the lowest flow resistance values. For a 0.25-inch cavity [figure 32(a) where results are presented for 10, 40, and 80-cgs rayls], the 40-cgs rayl material produced slightly higher attenuation values than the 80-cgs rayl material and considerably higher (5.5 dB at 5000 Hz) attenuation values than 10-cgs rayl material. For a 0.5-inch-deep cavity, figure 32(b), the attenuation produced with 10-cgs rayl material was 8 dB higher, between 3150 and 4000 Hz, than that produced using 160-cgs rayl material. The acoustical flow resistances tested in conjunction with a 0.75-inch-deep cavity were 10, 40 and 80-cgs rayls. The maximum variation in attenuation between

the 10- and 80-cgs rayl duct linings was 4.5 dB at 3150 Hz, with the 10-cgs rayl lining producing the highest values, figure 32(c). Figure 32(d) shows that for those configurations comprised of 1-inch cavity depths, the attenuations produced using 10- and 20-cgs rayl linings appeared about equal with both configurations producing about 10 dB more attenuation at 2000 and 2500 Hz than the 160-cgs rayl lining configurations.

Cavity depth: The results obtained with various cavity depths are presented in figure 33 for duct linings with nominal flow resistances of 10 and 160 rayls. The cavity depth primarily controlled the frequency at which the maximum attenuation occurred; i.e., the resonance frequency. For those configurations with duct linings having high flow resistance values (80 and 160 cgs rayls), the spectrum was broad and no resonance frequency was apparent. The resonance frequencies were much more distinct at duct velocities of 0 and 300 ft/sec than at 500 ft/sec. For 10-cgs rayl fibermetal, figure 33(a) shows that the resonance frequency increased from between 2000 and 2500 Hz for a cavity of 1 inch to between 4000 and 5000 Hz for a 0.25-inch-deep cavity. The increase in resonance frequency was approximately proportional to the inverse of the square root of the cavity depth, in accordance with a simplified Helmholtz-resonator analysis. The spectrum produced when a 160-cgs rayl lining was used over a 0.75-inch-deep cavity had no resonance frequency, figure 33(b).

Honeycomb cell size: Figure 34 shows that, for configurations using 40-cgs rayl fibermetal over 1-inch-deep cavities, the largest attenuations were achieved using 0.75- and 1.125-inch cells with the variation in attenuation between 0.75- and 3-inch cells being about 4 dB at 1600 and 2500 Hz. Above 2500 Hz, the difference was less, although the 0.75-inch cells always produced more attenuation than the 3.0-inch cells. The 0.75-inch cells also produced more attenuation than the smaller 0.375-inch cells, but only by 1 to 2 dB.

Multi-layer designs: A total of 63 multi-layer duct-lining configurations were tested. Because of the large quantity of data obtained, it was not possible to adequately describe the variation of attenuation and resonance frequency in accordance with the parametric variations tested. However, the following generalized trend was observed from the tests with the two-layer designs. Depending on the flow resistance of the inner and outer lining materials, the distance separating the porous sheets and the total thickness of the configuration, in the frequency range analyzed, the attenuation spectrum produced can be either one with a broad resonance peak (with the resonance frequency depending on the construction details described above) or a broadband spectrum with no resonance peak.

Figure 35 shows a comparison between a one-layer and a two-layer configuration for a duct velocity of 500 ft/sec. These two configurations were representative of the best designs of the two types of configurations. The one-layer configuration (R13) had 1-inch-deep cavities with a 10-cgs rayl fibermetal lining. The two-layer configuration (R131) was a total of 1-inch-thick with a 10-cgs rayl fibermetal lining located against the airflow. The second layer also had a flow resistance of 10-cgs rayls and was positioned 0.5 inch outboard of the first layer. The attenuation produced with the one-layer configuration was about 4 dB higher, between 1600 and 2000 Hz, than that produced with the two-layer configuration and about 3 dB lower between 4000 and 6300 Hz.

Flow splitters: Figure 36 shows that the largest attenuation values were achieved using the splitter which had treatment installed on both sides and an aluminum septum dividing the 1-inch-thick splitter into two 0.5-inch-deep sections. [See figure 22(b).] This configuration was superior, by about 4 dB, to the splitter with 1-inch-deep cavities and treatment on one side only and also superior to the

two-layer splitter. The amount by which the design with 0.5-inch-deep cavities and septum was superior to the corrugated splitter design was about 2 dB.

Treated area: Increasing the amount of treated area from 450 sq in. to 1800 sq in. correspondingly increased the attenuation values for duct velocities of 0 and 300 ft/sec, as shown in figures 37(a) and 37(b) respectively. Test results are not shown for the 500 ft/sec duct velocity because the S/N ratios at this velocity were inadequate for treatment areas of 1350 and 1800 sq in. However, as noted in figure 37(b) for a duct velocity of 300 ft/sec, the attenuation produced for 1800 sq in. of treatment was, on the average, about the same as that produced when the duct was lined with 1350 sq in. of treatment. This phenomenon may be associated with the L/W ratio. The amount of additional acoustical effectiveness obtained by increasing the L/W ratio may become asymptotic to some finite limit at high values of L/W.

Four configurations were tested which had treatment on the duct walls as well as treated splitters installed on the duct. The total treated area varied from 900 sq in. to 2250 sq in. The splitter used for all tests remained the same; i.e., 40-cgs rayl fibermetal linings installed on both sides of an aluminum septum dividing the 1-inch-thick splitter into two 0.5-inch thicknesses. The total treated area of the splitter was 450 sq in. The duct wall treatment used was also 40-cgs rayl fibermetal but the cavity depth was 1 inch rather than 0.5 inch, because full-length panels with 40-cgs rayl linings and 0.5-inch-deep cavities were not available.

Increasing the treated area from 900 sq in. to 2250 sq in. correspondingly increased the attenuation values for duct velocities of 0 and 300 ft/sec. However, for a duct velocity of 300 ft/sec, the attenuation produced for 2250 sq in. of treatment was about the same as produced when the duct was treated with 1800 sq in. of treatment. This same trend occurred when no splitter was installed, figure 37(b). The negligible increase in attenuation with increasing amounts of treated area may again have been associated with the L/W ratio. On the other hand, the explanation may also be associated with the growth of the boundary layer over the acoustical lining material. The boundary layer may have affected the propagation of sound through the duct and the subsequent diffraction of sound into the absorbent lining. The boundary layer may also have modified the impedance of the lining in such a way as to reduce its absorptivity.

The TL values obtained with a hardwall duct with a hardwall splitter installed in the duct were higher than those obtained with a hardwall duct with no splitter installed by 0 to 3 dB in the frequency range between 1600 and 6300 Hz for duct velocities of 0, 300 and 500 ft/sec.

Location of treatment: Figure 38 shows how the attenuation was affected by varying the location of the treated area. In one case, the full 45-inch length of one wall was treated, and the opposite parallel wall was left hard with sheet aluminum. In the second case, half the length of both top and bottom walls was treated, with the treatment being on the downstream half of the duct. In both cases described above, the treatment was 1 inch deep with 40-cgs rayl fibermetal surfaces. The treated area was 900 sq in. in each case. The configuration with treatment on both walls was superior to the configuration with the treatment installed along the entire length of one wall by about 3 dB in the frequency range between 2000 and 6300 Hz. For zero airflow, the attenuation produced with two walls treated was considerably higher (by 10 dB at 2000 Hz) than that produced when the full length of one wall was treated.

Another test was performed to determine the effect of varying the location of treated area. In one case, the area of treatment began at the inlet plane of the duct near the source chamber while in the

other case the treatment started at the exit plane of the duct away from the source chamber. In both cases, treatment was installed along half the length of the duct on the two 20 x 45-inch duct walls. The treatment used was 40-cgs rayl fibermetal over 1.0-inch-deep cavities. The attenuation values produced for both treatment orientations were the same within ±1 dB.

Results of inlet-duct tests. – The results presented in this section describe the effects of six of the seven test variables from the exhaust-duct tests. The multi-layer designs did not yield substantially more attenuation than the single-layer designs in these inlet-duct tests. Because of this result and because of the more complex nature of the multi-layer design compared to the single-layer design, presentation of the results of the multi-layer inlet-duct tests was not warranted.

Flow resistance: In contrast to the results of the exhaust tests, the effect of flow resistance on attenuation for cavity depths of 0.25 inch, 0.5 inch, and 0.75 inch was essentially negligible. For a cavity depth of 1 inch, however, the attenuation values produced did vary with the flow resistance of the surface material. At a velocity of 0 ft/sec, figure 39(a) shows that, for the frequency at which maximum attenuation occurred (i.e., 1600 Hz for the 1-inch cavity depth) the highest attenuations were achieved with the lowest flow resistances, with a 13-dB difference in the attenuation produced by 10- and 160-cgs rayl material. At 6300 Hz, the maximum attenuation was produced with the larger flow resistances. The trends described above for a duct velocity of 0 ft/sec were also evident at 500 ft/sec, figure 39(b). It is interesting to compare the attenuation spectra in figure 39(b) produced for 1.0-inch-deep cavities at 500 ft/sec for the inlet tests to those in figure 32(d) produced for the exhaust tests.

Cavity depth: The cavity depth primarily controlled the frequency at which the peak attenuation occurred, i.e., the resonance frequency. (This observation was also made in exhaust tests.) The resonance frequency was much more pronounced with low flow resistances and low duct velocities. Figure 40(a) shows how the resonance frequency varied with cavity depth for a 10-cgs rayl lining at zero airflow. For this configuration, the resonance frequency changed from 2000 Hz to 2500 Hz to 3150 Hz when the cavity depth was changed from 1 inch to 0.75 inch to 0.5 inch. No resonance frequency was observed with a 0.25-inch-deep cavity. Although the results for an 80-cgs rayl fibermetal lining exposed to an airflow of 500 ft/sec, figure 40(b), show no resonance frequency in the range between 1600 and 6300 Hz for backing depths between 0.25 inch and 1 inch, the attenuation values produced were highest for the largest cavity depths. The variation in attenuation at 1600 Hz between 1-inch-deep and 0.25-inch-deep cavities was 14.5 dB.

Honeycomb cell size: Figure 41 shows that for configurations using 40-cgs rayl fibermetal over 1-inch-deep cavities, the attenuation achieved by the 0.375-, 0.75-, and 1.125-inch cells was approximately the same, but larger than that achieved with the 1.5- or the 3.0-inch cells. The variation in attenuation between 0.375-inch and 3.0-inch cells was about 8.5 dB at 1600 and 2000 Hz. The trend described above also held true for exhaust duct configurations, although, as observed in figure 34, there did seem to be a 1 to 2 dB advantage to the 0.75-inch honeycomb cells.

Flow splitters: The largest attenuation values were achieved using the splitter which had treatment installed on both sides of an aluminum septum dividing the 1-inch-thick splitter into two 0.5-inch thicknesses. This configuration was superior to the 1-inch-deep corrugated splitter with treatment on only one side by 1 to 4 dB in the test frequency range between 1600 and 6300 Hz. The same trend also occurred for exhaust duct configurations.

The TL values obtained with a hardwall duct with a hardwall splitter installed in the duct were higher than those obtained with a hardwall duct with no splitter installed by 0 to 3 dB in the frequency range between 1600 and 6300 Hz for duct velocities of 0, 300, and 500 ft/sec. This same trend was also noted in the exhaust tests.

Treated area: A range of treated areas was tested with the result that increasing the amount of treated area from 450 sq in. to 1800 sq in. correspondingly increased the attenuation values for 0 and 300 ft/sec as shown in figures 42(a) and 42(b). For exhaust duct tests at 300 ft/sec, the results in figure 37(b) showed that the attenuation produced for 1800 sq in. of treatment was, on the average, about the same as that produced when the duct was lined with 1350 sq in. of treatment. This phenomenon was not apparent for inlet tests.

Location of treatment: Figure 43 shows how the attenuation was affected by varying the location of the treated area. In one case, the full 45-inch length of one wall was treated and the opposite parallel wall had a sheet aluminum surface. In the second case, half the length of both top and bottom walls was treated, with the treatment being on the downstream half of the duct closest to the noise source. In both of the cases described above, the treatment was a single-layer design, with 1-inch-deep cavities and a 40-cgs rayl fibermatal surface. The treated area was 900 sq in. in each case. The configuration with the treatment installed along the entire length of one wall was superior to the configuration with treatment on both walls by 3.5 dB at 2000 and 2500 Hz. The attenuation produced for the two configurations described above, for all test frequencies other than 2000 and 2500 Hz, was essentially the same. These inlet results were completely reversed from the exhaust results presented in figure 38 for a duct velocity of 500 ft/sec.

The effect on attenuation of varying the location of the treated area relative to the sound source was also determined for the inlet tests. In one case, the treated area began at the inlet plane of the duct and extended halfway along the top and bottom walls of the duct. In the second case, the treatment was also installed along half the length of the duct on the top and bottom walls but began at the exit plane of the duct. In both cases the treatment was the same as that used to determine the effect of area location. The attenuation values produced when the treatment was installed upstream and away from the sound source were about the same as those produced when the treatment was installed downstream and close to the sound source for duct velocities of 0, 300, and 500 ft/sec. These inlet trends were also true for the exhaust tests.

Selection of duct-lining designs for JT3D nacelle modifications. – The selection of the acoustical parameters of the duct-lining design for the treated inlet and fan exhaust ducts was based on the results of the duct TL tests conducted in this program and those conducted in a similar program by Boeing, reference 3. The selection was limited to designs with one layer of porous material because both test programs had shown that there was no significant acoustical advantage, for the JT3D landing noise problem, to be gained by the use of the complicated multi-layer designs compared to the simpler and lighter single-layer design.

At the start of the program, allowance had been made for 1-inch-deep cavities on the walls of the inlet duct, inlet centerbody, and fan-exhaust duct. The test results that have been presented indicated that the nominal flow resistance should be on the order of 10 to 20 cgs rayls for maximum noise reduction. With this flow resistance, the cavity depth should be 1 inch to produce maximum attenuation around the 2500-Hz fundamental blade-passage frequency.

The results presented in this document were obtained with a 5-inch duct-height where the h/λ ratio was about 1.0 at 2500 Hz. The aerodynamic design of the two-ring inlet, the 47-percent lightbulb inlet, and the 48-inch fan-exhaust ducts resulted in distances between treated surfaces greater than 5 inches. The results shown in reference 3 indicated that the choice of nominal flow resistance for maximum attenuation and the choice of cavity depth for maximum attenuation in the desired frequency range depended on the distance between treated surfaces as well as on the parameters investigated in this program. The effect of the separation distance on the choice of flow resistance and cavity depth, in turn, depended on whether the duct lining was installed in an inlet or exhaust duct. The effective bandwidth of high attenuation was also shown to be increased by use of different cavity depths on opposite walls. The results of the duct TL tests presented here were combined with those presented in reference 3 in determining the design for the static test articles.

- Fan-exhaust ducts: It was recommended that the walls of the 48-inch fan-exhaust ducts be treated with nominal 8-cgs rayl fibermetal overlaying honeycomb with 0.75-inch cells. The cavity depths were recommended to be 0.5 inch on the inboard walls and 0.75 inch on the outboard walls. The duct airflow splitters were treated with nominal 8-cgs rayl fibermetal overlaying honeycomb with 0.75-inch cells. The recommended cavity depth was 0.5 inch on each side of an impervious septum.

- Inlet ducts: It was recommended that the walls of the inlet duct and centerbody be treated with nominal 10-cgs rayl fibermetal overlaying honeycomb with 0.75-inch cells; the recommended cavity depth was 0.75 inch. The circumferential rings were treated with nominal 10-cgs rayl fibermetal over honeycomb with 0.75-inch cells; the recommended cavity depth was 0.5 inch on each side of an impervious septum.

- Porous material: Screen-reinforced fibermetal made from 0.004-inch-diameter stainless-steel wire fibers was selected for the full-scale acoustically treated ducts. This material was available and could be obtained with the desired nominal flow resistance and with desirable low NLFs. All the treated duct-TL test panels had used this type of material. The information developed from the flow-resistance and impedance-tube tests on other types of porous metallic products was not completely available at the time required by the program schedule for selecting the type of porous material. Therefore, it was decided to use the material that had demonstrated good acoustical performance, though it is recognized at the end of the program that equivalent acoustical performance can be obtained with alternate types of material.

Sonic Fatigue

Background. – Duct-linings installed in inlet and fan-exhaust ducts are exposed to high-intensity sound. The linings must be designed to withstand long-term exposure to this acoustical environment without failure. Sonic-fatigue tests were run at a Douglas facility capable of generating acoustic power levels that were intense enough (in the frequency range between 50 and 800 Hz) to make it possible to simulate the noise environment at the surface of aircraft structure susceptible to sonic fatigue.

An empirical procedure developed by Douglas is used to design various types of aircraft structure to prevent acoustically induced fatigue (refs. 20 and 21). However, because of the heterogeneous, non-uniform nature of the porous surfaces, this design procedure cannot be used to design duct-lining structures to resist acoustically induced fatigue. The design procedure requires that a random, reverse-bending S-N curve (stress S versus the number of cycles to failure N) be available for the

surface material. The nonuniformities in the porous surface material are the cause of non-repeatable, wide variations in the S-N data obtained from reverse-bending tests, making it difficult to obtain a valid S-N curve.

If it were possible to develop a random reverse-bending S-N curve, this curve, together with test data of the type reported herein, could be used to determine whether or not various designs would be free of acoustically induced fatigue for a given design life.

Sonic-fatigue tests of the type conducted in this test program, however, provided valuable information on the relative fatigue strength of various panel designs. The fatigue resistance of the acoustically treated panel designs was evaluated by comparing the test conditions which caused the panels to fail, i.e., by comparing the overall SPL of the excitation that caused the initial failure, the approximate length of time the panel was exposed to that overall SPL, and the type and extent of damage incurred.

In describing results of sonic-fatigue tests of conventional aircraft structure, it is customary to use a relationship between differences in the overall level of the acoustic excitation (for a given test spectrum) and the rms stresses in the structure. Thus,

$$S_b/S_a = 10^{[\Delta \text{ overall SPL}]/20} \qquad (12)$$

where [Δ overall SPL] is the difference, in dB, between the overall SPL noted at the time of initial failure on two different test panels and S_b and S_a are the rms stresses at the time of initial failure on panels b and a. Equation (12) assumes that the mean-square overall stress produced in the test panels is proportional to the mean-square overall sound pressure. The stress ratio given by equation (12), though approximate, is indicative of the different stress levels which exist in the various acoustically treated test panels at the time of the initial failure.

SPL measurements, reported in reference 1, at the walls of the inlet and fan-exhaust ducts on the JT3D engine for various engine operating conditions were used to establish a baseline spectrum and overall SPL. The baseline overall SPL was 150 dB for the frequency range from 35 to 1120 Hz. The Douglas sonic-fatigue facility not only could simulate the overall level and shape of the baseline spectrum, it also could produce levels higher than the baseline overall SPL and therefore was capable of being used for accelerated tests.

Sonic-fatigue tests reported in reference 14 had evaluated the ability of several nacelle acoustical-treatment designs to resist acoustically induced fatigue. These designs included riveted skin-and-rib structure as well as bonded honeycomb-core structure. A summary of the parameters investigated in these previous tests and results obtained is presented in table VII. Some of the conclusions from these tests were presented in reference 13. The experience gained in these previous test programs aided in establishing the test procedures used in conducting the tests described in this document.

One of the principal lessons learned from these previous test programs was that careful attention had to be paid to the design of the perimeter of the test panels in order to produce failures in the structure of the panel and not in the structure of the panel support. As a result, all of the test panels in this test program had doublers around the perimeter to increase the strength of the perimeter relative to that of the panel.

Test panels. – A total of four flat panels each with dimensions of 20 x 26.75 inches were fabricated and tested. One panel had a solid-aluminum riveted skin-and-rib construction to provide baseline information. Three panels were acoustically treated with fibermetal surfaces bonded to fiberglass honeycomb core. A description of the panels is given in table VIII. Some special features of the panels are described below.

Test Panel No. I: Figure 44 shows the front and back sides of Test Panel No. I in its pre-test condition. The honeycomb had 1.125-inch cells. The method used to bond the porous fibermetal surface and the solid aluminum backing sheet to the fiberglass honeycomb core was basically the same as that used to bond the acoustically treated single-layer panels built for the duct TL tests. The only difference was in the adhesive used to bond the fibermetal to the honeycomb core. Details of the bonding procedure are given in Appendix B.

Test Panel No. II: The second acoustically treated panel tested was identical to Test Panel No. I except for the following:

- A honeycomb core with nominal 0.75-inch cells was used rather than one with nominal 1.125-inch cells. This cell size was chosen because the duct TL tests had indicated that there would be no significant loss in noise reduction if the smaller cells were used and because of the improved strength of the smaller cells.

- The technique of bonding the fibermetal and aluminum surfaces to the honeycomb core was changed to increase the strength of the bond. For Test Panel No. II, both fibermetal and aluminum surfaces were bonded to the honeycomb core using a modified film-epoxy adhesive. Heat applied to the film from a heat gun caused the film to shrink back and collect around the perimeters of the cell walls. Use of the film epoxy produced larger fillets of adhesive between the fibermetal surface and the honeycomb core than had been possible to achieve with the roller coating technique used for Test Panel No. I. Both Test Panels I and II were vacuum bagged, placed in a circulating oven, and cured under a vacuum pressure of 8 to 10 inches of Hg at 350^{o}F for approximately 1 hour.

Test Panel No. III: The baseline skin-and-rib panel simulated the rigidity, skin gage and construction of the existing DC-8 short fan-exhaust ducts. Figure 45 shows the front and back sides of the baseline panel in its pre-test condition.

Test Panel No. IV: The third and last of the acoustically treated panels tested was 1.1 inch thick and simulated the design chosen for the flow splitters in the 48-inch fan-exhaust duct and for the concentric ring vanes in the two-ring and lightbulb inlet ducts. The bonding technique was that used for Test Panel No. II. In fabricating Test Panel No. IV, the 0.040 x 2-inch stainless-steel doubler was bonded to the outside of the fibermetal rather than between the fibermetal and fiberglass honeycomb core, as it was for Test Panels No. I and II. The reason why the doubler was bonded to the outside of the fibermetal was because the 0.5-inch depth of the honeycomb core was too thin to attempt to shave off a 0.040-inch-thick by 2-inch-wide strip around the panel perimeter.

Test description. – The test facility consisted primarily of a progressive wave tube (PWT), a bank of ten electropneumatic transducers coupled to 72-inch-long exponential horns with 7 x 7-inch mouths, a motor-driven air compressor and an instrumented control room. The PWT was constructed with a double-wall technique using 0.5-inch-thick steel plates separated by 4 inches. The 4-inch space between the walls was filled with sand to damp wall resonances and increase the noise reduction

through the wall. The interior dimensions of the PWT were 6 x 60 inches. Test panels as large as 5 x 10 ft could be mounted on the side of the PWT. An overall view of the PWT and associated equipment is shown in figure 46.

Panel mounting: A 48 x 72-inch panel-holding fixture was fabricated from 0.5-inch-thick sheet steel to accommodate the 20 x 26.75-inch test panels and to function as a wall section of the PWT. Figure 47 shows Test Panel No. I installed in the PWT. All panels were installed with the 26.75-inch dimensions parallel to the floor of the PWT.

Noise generation: High-intensity broadband random noise was produced using electropneumatic transducers rated at 2000 or 4000 acoustic watts. Panel I was tested using four of the 2000-watt transducers plus four of the 4000-watt transducers. Panels II, III and IV were tested using ten of the 4000-watt transducers.

Each electropneumatic transducer was supplied with 300 SCFM of air at a gage pressure of 40 psi. High-intensity sound was generated by modulating the static pressure in the air as it flowed through the transducer. The spectrum of the sound incident on a test-panel in the PWT was determined by the electrical signal applied to the voice coils. All the tests reported here used random noise with a spectrum shaped in octave-bands. The insertion-loss of each of the octave-band filters was variable.

Noise measurement: Three microphones were used to monitor the SPLs over the surface of the test panels. The variation in overall SPL (a frequency range of either 40 to 1000 Hz or 2 to 40 000 Hz) was approximately ±1 dB among the three microphones. Figure 48 shows typical microphone locations along the horizontal panel centerline and spaced 6.75 inches apart. The middle microphone was at the geometric center of the panel. Each microphone was positioned 0.5 inch from the panel surface and oriented to obtain grazing incidence.

The noise detected by the microphones was filtered in 1/3-octave bands. A typical 1/3-octave-band spectrum is shown in figure 49. In order to insure that all of the instrumentation functioned properly during each test, 1/3-octave-band analyses were made during each test as often as four recordings per test-hour per microphone location. A diagram of the instrumentation and equipment used for noise generation and measurement is given in figure 50.

Test specification: A test specification was defined for each panel. The specification included the spectrum of the SPL used to excite the test panels. The spectrum simulated, for the most part within ±2 dB from 50 to 800 Hz, that existing at the walls of the inlet and fan-discharge ducts of a JT3D engine operating at takeoff power. Figure 51 shows the 1/3-octave-band SPLs for the specification test spectrum compared to an actual test spectrum averaged over the face of a typical test panel. The average spectrum was determined from measurements at 5 microphone locations. It was not possible to alter the level of the 80-Hz peak and the 125-Hz dip to produce better compliance with the specification without significantly changing the entire spectrum.

Each panel, with the exception of Test Panel No. IV, was subjected to an overall SPL of 150 dB, using the test spectrum shown in figure 51, for a period of 2 hours and thereafter to a series of one-hour exposures to overall SPLs varying from 153 dB to the 165-to-166 dB maximum output capability of the test facility. The overall SPLs were increased in 3 dB increments until a failure occurred or until a total of 10 hours of sonic-fatigue-free time (including the initial 2 hours of exposure to 150 dB) had been accumulated. Periodically, the tests were stopped and the panels were

visually inspected for signs of fatigue. Failure-inspection-time intervals varied from 30 minutes during tests when the panels were exposed to overall SPLs of 150 and 153 dB, to 15 minutes for overall SPLs higher than 153 dB. This test specification was selected to be compatible with previous sonic-fatigue tests of acoustically treated panels and to be able to compare the relative sonic-fatigue strength of the panel designs tested in the program with those tested in the past.

The test specification recommended for the third acoustically treated panel tested (i.e., Test Panel No. IV) was essentially the same as that used for Test Panel Nos. I, II and III except that the overall SPL was varied in the following manner: 159 dB or 1 hour, followed by 162 dB for 1 hour followed by 165 dB for 8 hours. The reason for this change to the panel loading was to give the panel a more severe test by exposing it to the maximum loading for a longer period of time; i.e., 8 hours compared to 4 hours at 165 dB. The inspection time intervals remained at 15 minutes throughout the entire test.

Results. – The results of testing the four test panels are given below in the order in which the panels were tested. Results are presented separately for each panel.

Test Panel No. I: The first observed failure was an unbonding of a 9 x 9-inch piece of the fibermetal surface of the panel near the mid-upstream edge during the second 15-minute interval after exposure to an overall SPL of 165 dB. This unbonded area increased to about 75 percent of the total panel area during the following 8 minutes of testing at the same overall SPL. After 45 minutes of exposure to 165 dB, a 1-inch piece of fibermetal separated from the honeycomb core at the same location where the initial unbonding of the fibermetal from the honeycomb core occurred. The test was continued for an additional 4.5 minutes during which time several small pieces of fibermetal, located adjacent to where the initial separation occurred, separated from the honeycomb core. Figure 52 shows the area where the fibermetal unbonded and separated from the honeycomb core. The cause of failure of Test Panel No. I was inadequate bonding strength between the 0.040-inch-thick 10-cgs rayl fibermetal surface and the fiberglass-honeycomb core with its 1.125-inch cells. The next step in the development of a panel design with adequate fatigue strength was to improve the bond between the fibermetal surface and the honeycomb core.

Test Panel No. II: Comparing the results of testing Panel No. II, with its smaller honeycomb cells and its improved bonding strength, with those from Panel No. I, revealed that Panel No. II was superior to Panel No. I in its ability to resist acoustically induced fatigue. Test Panel No. II withstood, without failure, the entire 10 hour program of stepwise increases in acoustic loads specified, including 4 hours of exposure to an OASPL of 165 dB. This panel was the first fibermetal panel tested (including the 9 fibermetal panels described in table I) which endured, without failure, the specified series of tests and demonstrated conclusively that the failure of Panel No. I (and also the failure of the 5 other bonded fibermetal-honeycomb panels tested) was due to poor bonding and not to inadequate strength of the fibermetal.

Test Panel No. III: The first observed failures in panel No. III were small 0.5-inch vertical cracks in two of the frames. The cracks occurred during the first 15-minute exposure to an overall SPL of 165 dB. One of the two vertical cracks was in the bottom portion of frame No. 1 (the frame farthest upstream) and the other in the upper portion of frame No. 5 (the frame farthest downstream). Both cracks were oriented along the 0.125-inch bend radius outboard from the panel skin beginning at the end of the frame where the edge of the shear clip butted against the curved portion of the frame.

The test was continued at the same overall SPL of 165 dB for an additional 105 minutes to conclude 8 hours of stepwise increases in acoustic loads as specified above. After the initial failures, additional damage was confined to the shear clips or to the ends of the frames either at their outboard bend radius, or at a location slightly inboard from this bend radius. The shear clip failures were primarily at the bend radius of the rivets. The shear-clip cracks were in the bottom four shear clips and in shear clip Nos. 2, 3, and 5 at the top. The only one of the four shear-clip failures that did not occur at the bend radius was in shear clip No. 2 at the bottom where the failure was in the rivets fastening the clip to the side of the panel.

The accelerated sonic-fatigue test of this stiffened aluminum hardwall baseline panel provided data for use in evaluating the sonic-fatigue resistance of acoustically treated panels. Because the aluminum baseline panel, designed to simulate the construction of existing fan-exhaust duct structure, did have an acoustical fatigue failure, it was now possible to determine which of the previously tested panel designs possessed equal or greater resistance to acoustically induced fatigue. For equal fatigue life, acoustically treated panels must be at least as strong as the baseline reference panel and therefore should be able to withstand without failure the first six hours of the programmed exposure to sound with overall SPLs of 150, 153, 156, 159, and 163 dB.

Test Panel No. IV: During the second 15-minute interval of exposure to an overall SPL of 159 dB, the downstream vertical aluminum doubler became unbonded along a 2-inch length at the bottom and bent out away from the panel in a tapering fashion to a maximum of about 1/16 inch. During the following 15-minute exposure to the same 159 dB level, the 2-inch unbonded length expanded to a 4-inch unbonded length. The unbonded portion of the panel was then bolted together in order to prevent a premature and unrepresentative failure of the fibermetal-honeycomb sandwich.

During the first 15-minute exposure to an overall SPL of 165 dB the upstream vertical aluminum doubler became unbonded along a 3.5-inch length at the bottom and bent out away from the panel surface in a tapering fashion to a maximum distance of about 1/32 inch. In addition, a 1-inch-long vertical crack developed in the fibermetal underneath the unbonded portion of the upstream doubler. The unbonded portion of the upstream doubler was then bolted together. Figure 53 shows the test panel mounted in the PWT. The two sets of three bolts tying the panel together indicate where the two doublers unbonded from the fibermetal sheet.

Apart from the two premature edge-support failures that are believed to be a result of inadequate bonding of the outer doubler to the fibermetal panel, test panel No. IV endured without failure the entire 10-hour exposure to the high-intensity noise field in the PWT. This was the second failure-free fibermetal panel tested (including the nine fibermetal panels of table VII), and the only panel tested which endured an overall SPL of 165 dB for as long as 8 hours. The other failure-free fibermetal panel (No. II) was exposed to 165 dB for only four hours.

Recommendations for duct-lining fabrication. – To insure that adhesive-bonded honeycomb structure is free of acoustically induced fatigue, the adhesive and bonding method must be carefully chosen to provide a strong and reliable bond.

DUCT-LINING STRUCTURAL INVESTIGATIONS

The nacelle-modifications design studies had assumed that an acoustically absorptive duct-lining system could be developed with adequate strength for retrofit aircraft and the flight-test airplane. Before constructing any full-scale test parts, it was necessary to specify certain items to insure the structural integrity of the duct linings. These items were considered in making estimates of the structural weight allowances for the nacelle-modification design studies. In construction of the full-scale test articles, these items were defined to the extent needed to ensure that the test programs could be safely conducted.

The duct TL tests had selected a duct-lining design with a single layer of screen-reinforced porous fibermetal made from 0.004-inch-dia stainless steel wire fibers. The nominal flow resistance of the fibermetal was either 8 or 10 cgs rayls. The fibermetal surface was to be adhesively bonded to fiberglass honeycomb core. The principal goal of the structural investigations was the development of an acoustically acceptable and structurally adequate adhesive-bonding procedure. Sonic-fatigue test panels II and IV used the bonding procedure that was developed and indicated that this type of construction should have adequate sonic-fatigue strength for use in the acoustic environment of the treated inlet and fan-exhaust environment.

Structural tests of the components of the bonded fibermetal-honeycomb sandwich and of the composite fibermetal-honeycomb sandwich were conducted to provide the structural design information used in the detail design of the full-scale static and flight-test inlet and fan-exhaust ducts, references 9 and 10. The structural tests included studies of the effect of exposing the components of the sandwich duct lining to various environments. Figure 54 shows the major components of a duct lining with one or two porous layers.

Design Criteria

In developing structural design criteria it was not possible to use directly any of the conventional structural analyses that have been developed for symmetrical or asymmetrical sandwich structures because fibermetal is anisotropic with different properties in different directions. Figure 55 shows a micrographic section of fibermetal and indicates the numerous voids between the various wire fibers.

As explained earlier, it had been decided during the preliminary duct-lining design consideration that the duct linings were to be designed as load-carrying structure that did not have to be easily removable. In determining whether components of a duct-lining design were to be considered as structural or nonstructural items, it was necessary to clarify the meaning of structural and nonstructural.

Federal Civil Air Regulations (ref. 22) require that aircraft structure be capable of supporting limit loads without suffering detrimental permanent deformations or without deformations which would interfere with the safe operation of an airplane. The aircraft industry, for purposes of airworthiness certification by stress analysis, has further defined aircraft structure in three categories as follows:

- Primary structure: those parts or elements the failure of which alone, without requiring a further unusual sequence or combination of events to render the failure serious, would endanger the airworthiness of the airplane or the safety of its occupants or ground crew.

- Secondary structure: those parts or elements the failure of which alone would not directly endanger the airplane or its personnel, although such failure would tend to impair the structural or mechanical airworthiness of the airplane.

- Nonstructural parts: those parts or elements which are provided primarily for functional purposes not related to the airworthiness of the airplane or the safety of its personnel, the failure of which might cause inconvenience, but which would not necessitate delay of flight pending its repair or replacement.

Within the context of those definitions, a structural design was defined as any design, which by the nature of its mechanical attachment, was capable of transmitting structural loads between elements of primary and secondary structure. Nonstructural designs were defined as those which were only required to maintain geometric shape when held in place by primary or secondary structure. A design which was attached to primary structure by weld, adhesive bond, or numerous mechanical fasteners was defined as fixed, whereas designs attached by quick disconnect methods were defined as nonfixed or removable. The duct-lining design for the test airplane installation was to be a fixed, structural design.

Structural design criteria for a retrofit design and for a test airplane installation are not identical. There would be definite differences in the strength and rigidity of the acoustically treated nacelle components. Although it was outside the scope of this program to define structural design criteria for a retrofit installation, it was necessary to determine the items that would have to be specified. For the test airplane, it was required to specify structural criteria in order to conduct the stress analysis needed to obtain permission from the FAA to fly the acoustically treated nacelles. The items that were considered are described in the following sections.

Retrofit. – Four general types of structural designs were considered for the retrofit-airplane installation as indicated in the table below.

STRUCTURAL TYPE	DESIGN	INSTALLATION
I	Nonstructural	Removable
II	Structural	Removable
III	Nonstructural	Fixed
IV	Structural	Fixed

The items that would need to be defined for a retrofit installation are:

1. The type of structural design chosen from the table above.

2. Minimum fatigue-free life based on the total number of flight hours and the number of flights per day.

3. Maximum and minimum thermal environment including considerations for anti-icing, firewalls, or fuel fires within the acoustical sandwich.

4. Pressure and thermal environments which determine the aging or corrosion life of structure.

5. Maximum and minimum differential pressures acting across the plane of the sandwich panel.

6. Maximum and minimum in-plane loads to be applied to the sandwich, including spectrum of loads for fatigue.

7. Maximum out-of-plane deflection to be allowed.

8. Spectrum and intensity of acoustical environment incident on the duct linings.

9. Method and minimum rate of draining liquids from the honeycomb cells.

10. Method of cleaning contaminated surfaces.

11. Corrosion, erosion, and contamination environments.

12. Repairability of damaged duct linings.

Test airplane. – The structural design criteria for the modified nacelles to be installed on the test airplane were based on a philosophy of maximum structural integrity with an emphasis on providing an adequate structural stiffness without disruption of the geometric envelope required for the acoustical treatment. To achieve adequate stiffness, it was determined by structural tests and stress analyses that the individual elements of the basic acoustical sandwich should have the following minimum effective strengths and rigidity:

- Sandwich flatwise tensile strength . . . . . 300 psi
- Sandwich flatwise compressive strength . . . . . 75 psi at 350°F
- Adhesive lap shear strength . . . . . 1000 psi
- Slotted-core stabilized shear strength . . . . . 120 psi
- Sheet tensile strength for the nominal 0.040-inch-thick fibermetal . . . . . 320 lb/in.
- Sandwich flexural rigidity . . . . . 32 000 psi/in.

In conjunction with these criteria, the flight test nacelles were designed for 1000 flight hours or one year, whichever occurred first, with the major components designed to withstand the following load and environmental conditions:

- The concentric ring vane was designed to withstand a differential ultimate pressure of 2.5 psi. In addition each support strut was designed to withstand a thrust or drag shear of 1000 pounds.

- The interior wall of the inlet duct was designed to withstand an imploding ultimate pressure of 5

psi (static takeoff condition) and an exploding ultimate pressure of 40 psi (violent engine surge condition).

- The inlet centerbody was required to withstand a differential ultimate pressure of 15 psi and the mounting flange and bolt were required to withstand the thrust load created by a 15 psi exploding ultimate pressure.

- The fan duct walls were designed to withstand an 18-psi ultimate exploding pressure. The duct walls were further required to resist a 2000°F flame for a sufficient length of time to allow the flight crew to recognize a fire situation and actuate the fire extinguishers.

- The fan-duct flow splitters were designed to withstand a differential ultimate pressure of 5 psi and were required to withstand a 300 lb per linear inch tensile load in order to constrain the exploding pressure to within the fan ducts.

- All of the acoustically treated assemblies were designed for a maximum out of plane deflection of ±0.125 inch and a thermal environment of −80°F to 250°F.

- Although the design of the inlet installation had provisions for anti-icing, the inlet structure was not designed to be flown in icing conditions.

Adhesive-Bonding Technique

The acoustical and structural requirements for the fibermetal-honeycomb duct-lining design required development of a new adhesive-bonding technique. The fillet of adhesive between the honeycomb core and the fibermetal surface was required to have a minimum of 300 psi flatwise tensile strength and yet not produce unreasonable blockage of the pores of the fibermetal. Figure 56 shows a micrographic section through a typical juncture between a fibermetal surface and the honeycomb core and illustrates the magnitude of adhesive migration that had to be controlled.

As explained in Appendix B, the bonding technique for the duct TL test panels used a roller coating process to apply adhesive material to the honeycomb core. This technique was not suitable for use in constructing the full-scale test articles because it was not possible to control the amount of adhesive applied to the honeycomb. The strength of the bond between the fibermetal and the honeycomb was therefore not uniform over the surface of the duct lining. An acceptable adhesive was obtained by adapting a carrier-supported, aluminum-filled, modified-epoxy film. The use of film adhesive eliminated the scrim cloth carrier and the roller-coating application procedure.

The materials used in the bonding process and the steps involved are shown in figure 57. This bonding process was used for the fabrication of all mechanical property test specimens and all full-scale treated ducts described in references 9 and 10.

1. Two sheets of adhesive film were spread over the surface of the honeycomb core.

2. The adhesive was coagulated at the core ribbon by application of localized heat with a heat gun or heat lamp. (In step 2 of figure 57, note the thick coagulations due to the double layer of adhesive.)

3. The adhesive-core subassembly was then inverted into the impervious facing sheet, vacuum bagged, and cured for one hour at 350°F in an autoclave at 25 psi differential pressure.

4. When the sheet-adhesive-core subassembly had cooled, one layer of adhesive film was spread on the exposed surface of the core, coagulated to the core ribbon, and allowed to cure.

5. The porous acoustic facing sheet was then positioned. This operation was not critical because the adhesive hardened after cooling, was not tacky, and did not smear.

6. The final assembly was vacuum bagged and cured for one hour at 350°F in an autoclave at a differential pressure of 25 psi as shown in figure 57, the pattern of the bondline was usually visible on the exterior surface of the porous facing material after completion of the bonding process.

Structural Tests

Structural tests were conducted to determine mechanical properties of acoustically treated structures and components. The results of the mechanical property tests were used to determine the structural integrity of the acoustically treated components of the nacelles on the test airplane. In addition, the materials were tested in a salt-spray and a high-temperature environment to assess the effect of these environments on the mechanical properties of a composite acoustical sandwich. In the tests described here, each component of the sandwich was evaluated individually. Tests were then conducted to determine composite sandwich properties utilizing all of the components. The separate components of the sandwich were the porous facing sheets, the honeycomb core, the impervious backing sheets, and the adhesive system.

Fibermetal surfaces. – The specimens of the fibermetal sheets that were selected had nominal flow resistances of 8- and 10-cgs rayls and a nominal thickness of 0.040 inch. Fibermetal has a randomly interlocked structure of metallic fibers sintered to produce microscopic welds at the fiber intersections to form an orthotropic three-dimensional truss of fibers within the felted sheet. All samples were reinforced on both sides with an open-weave wire screen made from 0.009-inch-diameter wires. All fibermetal samples were made from stainless steel designated type 347 by the American Iron and Steel Institute. A close-up view of a sample of fibermetal is shown in figure 58.

The strength of the fibermetal specimens was defined in terms of the gross cross-sectional area of the specimen, i.e., in terms of the product of the nominal thickness and the width of the specimen. For design purposes, an effective stress was defined in terms of the load in pounds per unit gross-cross-sectional-area in square inches (i.e., lb/sq in. or psi).

Because of the nature of fibermetal, it was necessary to perform tensile tests along three axes in the plane of a sheet to completely define the tensile properties of the material. Two of the axes were mutually perpendicular and the third was diagonal to the first two.

The tensile tests determined the effective ultimate tensile strength and the effective modulus of elasticity of the fibermetal specimens. Interlaminar-shear and flexural-fatigue tests were also conducted. The interlaminar-shear tests determined the interconnecting shear strength between the sintered fibers. The flexural-fatigue tests determined the endurance limit of specimens of fibermetal sheets.

Tensile tests: Ultimate tensile strength tests were conducted using test procedures derived from the standard procedures given in reference 23. Test specimens used available fibermetal made from 0.003-inch-diameter wires. A typical specimen failure is shown in figure 59. The 8- and 10-cgs rayl material selected for the static- and flight-test inlet and fan ducts was to be made from 0.004-inch-diameter wire fibers.

The results obtained with the 0.003-inch-diameter wire fibers are representative of those that would have been obtained with 0.004-inch-diameter wire fibers. It is believed that the trends would have been similar but the absolute tensile and interlaminar-shear strengths would have been greater with material made from the larger diameter wires and having the same nominal sheet thickness, screen reinforcing, and flow resistance. Reference 15 contains additional information on the mechanical properties of various fibermetals.

The polar orientation of the effective ultimate tensile strength is shown in figure 60 for three different materials. Figure 61 shows the effective modulus of elasticity for two load orientations because, as shown in figure 60, the ultimate tensile strengths obtained at 0° were approximately the same as those obtained at 90°. The effective modulus of elasticity of 10-cgs rayl fibermetal ranged from 0.333×10^6 to 0.488×10^6 psi; that of 8-cgs rayl material ranged from 0.348×10^6 to 0.521×10^6 psi.

Interlaminar-shear tests: Interlaminar-shear tests were conducted using procedures specified in method 1042 of reference 24. Examples of failed specimens are shown in figure 62. The average minimum effective interlaminar-shear stress was 630 psi. However, the results were influenced by the thickness of the test specimen and the method of fabricating the specimens and therefore no additional results can be presented.

Flexural fatigue tests: Unpublished results of flexural-fatigue tests conducted by the NASA using procedures given in reference 25 are presented in this section. These tests used fibermetal with relative densities of 40, 55, and 70 percent. These densities encompassed the range of densities for materials suitable for duct linings. The 10-cgs rayl material chosen for the inlet ducts was 53.5 percent dense; the 8-cgs rayl material for the fan-exhaust ducts was 45 percent dense. These flexural-fatigue tests determined flexural-strength and endurance. A test specimen mounted on an electrodynamic shaker is shown in figure 63.

The endurance limit was defined as the limiting value of peak effective stress below which the material could presumably endure an infinite number of bending cycles. Figure 64 shows that the endurance limit of 40-percent dense material was 1500 psi, that of 55-percent dense material was 2600 psi, and that of 70-percent dense material was 7600 psi. It should be noted that these effective S-N curves are not the random reverse-bending S-N curves needed for sonic-fatigue analyses of porous duct-lining structure.

Honeycomb core. – Structural tests of 0.5- and 0.75-inch-thick specimens of fiberglass-honeycomb-core material included flatwise-compression and core-shear strength tests and liquid-drainage tests. No flatwise tensile strength tests are reported because all failures of this type were in the adhesive and are described under the adhesive-bonding tests. A photograph of a section of honeycomb core is shown in figure 65. The inscribed cylinder whose diameter defines the cell size is shown in phantom view.

Flatwise-compression tests: Flatwise-compression tests were conducted in accordance with section 5.1.4 of reference 26. The honeycomb-core specimens were tested with and without drainage slots.

Because the 0.75-inch cells were larger than those specified in reference 26, the test specimen size was increased from 2 x 2 inches to 6 x 6 inches to reduce the effect of cell size on the test results. Tests were run at room temperature and also at 350°F. The elevated temperature simulated the curing temperature used in the adhesive-bonding process. Figure 66 shows a typical compression test specimen.

The results of the compression tests at room temperature were failures of the walls of the honeycomb cells due to instability buckling. In tests using 1.9 lb/cu ft material and no liquid drainage slots, the 0.5-inch-thick specimens failed at an average pressure of 145.7 psi; the 0.75-inch-thick specimens failed at an average pressure of 125.0 psi.

The compression tests conducted at 350°F used fiberglass honeycomb that had been slotted to provide for drainage. The slots were 0.125-inch wide and 0.187-inch deep in the edge of the core adjacent to the impervious backing sheet. To make up for the reduction in strength due to the slots, the fiberglass was coated with an additional layer of phenolic resin and the density was increased to 2.1 lb/cu ft. All compression failures of slotted honeycomb occurred at a pressure between 75 and 95 psi while exposed to 350°F. This pressure was well above the 25 psi differential pressure used in the autoclave during the curing cycle.

Compression strength was also determined for the hard points used for mounting attachments for the fan-duct splitters and the struts for the concentric ring-vanes. One method of creating a hardpoint was to densify the core by pressing two pieces of core into each other. The compression strength at room temperature of densified core with nominal 0.75-inch cells was 178 psi for a sample that was 1-inch thick. Additional study of this procedure for providing a hardpoint mount was abandoned in favor of the use of phenolic compression inserts for which no tests were required.

Core-shear tests: Core-shear tests were conducted in accordance with the procedures of reference 26. A typical core-shear test specimen is shown in figure 67.

Core-shear tests were conducted on both unslotted and slotted specimens. The specimens were sheared along the longitudinal and the transverse ribbon directions. A typical failure of a core-shear test specimen is shown in figure 68.

Maximum core-shear stress in the longitudinal ribbon direction for a specimen with drainage slots was 137.3 psi; the corresponding average shear modulus was 1887 psi. For specimens tested along the transverse ribbon direction, the maximum shear stress and shear modulus with drainage slots were 67 and 1172 psi; without drainage slots, they were 71 and 1329 psi.

Drainage tests: Honeycomb-drainage tests were required because liquids could collect within the cells of linings installed on the bottom of a duct. It was calculated that as much as 100 lb of water might be trapped within each nacelle if no drainage system were provided. It was therefore decided that an overboard drainage system should be provided in both the retrofit airplane nacelle and the test-airplane nacelle. This decision was based on concern for corrosion, freezing of water, loss of acoustical absorptivity, and the added weight of trapped liquids.

Tests were conducted to determine the effectiveness of the proposed drainage method. A cylindrical drainage test-fixture, figure 69, was built with a fibermetal surface bonded to 0.75-inch-thick honeycomb core. The 0.75-inch cells were grooved with circumferential slots so that the water would drain downwards. (Note that in figure 69 the porous surface is shown with openings to illustrate the path that the water would follow.) Longitudinal interconnections between the honeycomb cells were not allowed because they would lead to circulation losses if installed this way in the inlet and fan ducts. A manifold at the bottom of the fixture collected and drained away the water.

Under simulated rain conditions, the proposed drainage system emptied approximately 65 percent of the water in the cells. Failure to achieve complete drainage was because the drainage slots were not located at the lowest physical level in each cell. In a retrofit design, drainage slots would be located so as to completely drain liquids from the cells.

Impervious facing sheets. – No tests were conducted of any impervious facing sheets because the maximum allowable design stress for any of the proposed materials (sheet aluminum, sheet stainless-steel, and epoxy-fiberglass-laminates) was available in references 27, 28, and 29. Impervious sheets on the walls of the ducts were required to be able to withstand a bursting pressure of 40 psig and a collapsing pressure of 5 psig. For the splitters and ring vanes, the impervious septum was required to withstand a differential pressure of 5 psi.

Adhesive-bonding tests. – Flatwise tensile strength tests of bonded sandwich structures were conducted using the procedures of section 5.1.6 of reference 26. Figure 70 shows a typical flatwise tensile-test-specimen. A typical failure of a flatwise-tensile-test-specimen is shown in figure 71.

All failures occurred in the adhesive system and were above the minimum ultimate tensile stress of 300 psi. The average results were 318 psi for specimens with drainage slots and 331 psi for specimens without drainage slots.

Composite fibermetal-honeycomb sandwich structures. – Five types of tests were conducted with composite sandwich structures. These tests were bending-beam tests, flexural-fatigue tests, fan-duct-wall–to–flow-splitter attachment-tests, freeze tests, and burn-through tests. Bending-beam tests were conducted using specimens that were exposed to the normal room environment and specimens that had been exposed to a salt spray environment. Flexural-fatigue tests were conducted with specimens in a normal room environment and also with specimens that had been exposed to a thermal shock environment.

Bending-beam tests: Bending-beam tests of symmetrical test specimens were conducted using the procedures specified in section 5.2.4 of reference 26. Eight 2 x 12-inch test specimens were built with 0.5-inch-thick honeycomb. Four specimens had nominal 10-cgs rayl fibermetal surfaces on both sides of the core; four had nominal 8-cgs rayl fibermetal on both sides of the core. There were no drainage slots in the honeycomb core. The results of the bending-beam tests were an average effective facing-stress of 4286 psi for the 10-cgs rayl specimens and 3835 psi for the 8-cgs rayl specimens. The effective modulus of elasticity was 1.94×10^6 and 1.45×10^6 psi for the 10- and the 8-cgs rayl specimens. As indicated in figure 72 most failures were intercellular buckling.

One of each type of test specimens was subjected to salt spray for 34 days using the procedures of paragraph 4.6 of reference 30. All specimens were installed in the test fixture shown in figure 72 with a quarter span loading as indicated.

Specimens that had been subjected to the salt spray for 34 days showed some discoloration at the edges of the fibermetal surfaces due to impurities introduced when the specimens were fabricated. No appreciable degradation in strength or any delamination in the adhesive bonds were encountered as a result of the salt spray exposure.

Flexural-fatigue tests: The flexural-fatigue test specimens were constructed similar to the bending-beam test specimens with unslotted 0.5-inch-thick honeycomb core. Nine 2 x 20-inch specimens were fabricated with symmetrical fibermetal faces that had nominal 8-cgs rayl flow resistance. Prior to flexural-fatigue testing, three specimens were thermal shocked. Flexural-fatigue tests of the nine specimens were conducted using the procedures of section 5.2.4 of reference 26. The flexural-fatigue test apparatus is shown in figure 73.

The specimens that were subjected to the thermal shock were exposed to an initial temperature gradient of 415°F by immersing one of the fibermetal faces in a flow of gaseous nitrogen at −65°F and heating the other face to 350°F with heat lamps. The thermal shock apparatus is shown in figure 74. As the thermal-shock conditioning was continued, the temperature of the cooled face gradually increased to 80°F. This 270°F temperature gradient was maintained for 10 minutes on each beam. Although midspan deflections approached 0.25 inch, no specimen took a permanent set. After the completion of the thermal-shock conditioning, flexural-fatigue tests were conducted with different quarter-span loads.

The results of the flexural-fatigue tests are shown in figure 75. The specimens that had been thermally shocked had higher peak effective stresses than those that had not been thermally shocked. This result was attributed to the post-curing of the adhesive bond that occurred during the thermal shock conditioning. The post-curing increased the fatigue life and strength of the test specimens.

Fan-duct splitter-attachment tests: The design envisioned for the static tests of the 48-inch fan-exhaust ducts had 0.25-inch-thick fiberglass laminate for the impervious backing sheet. A proposed method of attaching a flow splitter to the wall of a fan duct was simulated by bonding a piece of honeycomb core and 8-cgs rayl fibermetal to a piece of 0.25-inch-thick fiberglass laminate. A hole was drilled through the fiberglass laminate and a cylindrical insert was installed to form a hardpoint mount. The simulated splitter was then bolted to the duct wall specimen and the simulated joint was tested to determine its tensile strength. The tensile test simulated an exploding pressure in the fan-duct. The test fixture is shown in figure 76.

Typical failures occurred at the bonded interface between the fiberglass laminate and the honeycomb core as noted in figure 76. This adhesive failure allowed the compression insert to pull out of the fiberglass laminate. The average failure load was 762 lb. Failures also occurred in the L-section channels along the joint between the splitter and the duct wall. All of these channel failures were rivet shear failures and occurred at an average load of 2905 lb.

Because of these failures in the adhesive bond and in the rivets, changes were made to increase the strength of the attachment design. The rivets were changed from aluminum to monel alloy. The compression insert was installed before bonding the honeycomb core to the fiberglass laminate and did not extend through the laminate. The bolt through the joint was backed by a large washer to feed the bolt tensile load into the fiberglass laminate as a bending load, thereby eliminating the tensile load in the adhesive.

Freeze tests: Tests were conducted to determine whether water freezing in a honeycomb cell could break the bond between the fibermetal or backing surfaces and the honeycomb core. A test specimen was constructed from 0.75-inch-thick honeycomb that had 0.75-inch cells and was grooved to produce drainage slots. The fibermetal surface had a nominal 10-cgs rayl flow resistance. The backing surface was a nominal 0.063-inch-thick aluminum sheet. The specimen was bonded using two layers of film adhesive on the aluminum sheet side and one layer for the fibermetal side.

Freeze tests were conducted with three water level conditions. The first condition involved filling the specimen with water to above the level of the drain slots. The specimen was placed in a freezer until the water was frozen and then further cooled to $-70^{\circ}F$ using liquid nitrogen. The specimen was then thawed out with tap water. No visual damage was evident.

For the second condition, the specimen was filled with water to the bottom of the fibermetal surface. The specimen was frozen and thawed as in the first condition with the same result. However, it was difficult to tell if all cells of the specimen had been totally filled.

In the third condition, the specimen was completely immersed in a water bath, frozen and thawed with no visible damage. However, doubt still remained about complete filling of the cells with water and the third test was re-run carefully removing as much trapped air as possible. After this fourth test, a 1.5-inch-long crack was observed in an adhesive fillet between the honeycomb and the aluminum facing sheet. This test provided further substantiation to the decision to incorporate drainage slots in the honeycomb to ensure that no delamination would occur in the adhesive bonds should freezing conditions be encountered.

Burn-through tests: FAA regulations (ref. 22) require that firewalls withstand a $2000^{\circ}F$ flame for 15 minutes without burning through. The 15-minute period allows a pilot time to recognize the fire situation, shut down the engine and discharge the fire extinguishers. The inner wall of the fan-exhaust duct was considered a firewall because it separated the accessory and compressor sections (where a fire could occur) from the pressurized air inside the fan-exhaust duct. A burn-through test was conducted to determine the time required for a $2000^{\circ}F$ flame to burn through the fiberglass-laminate wall proposed for the static-test fan-exhaust ducts.

A burn-through test setup is shown in figure 77. The tests that were conducted gave a conservative measure of the burn-through time because no cooling fan-exhaust airflow was simulated over the side of the specimen opposite the flame. The test specimen burned through in nine minutes, a result that was considered adequate for the flight-test program.

Application of Results of Mechanical Property Tests

By using the analytical methods presented in references 27 and 29, the internal stresses in the components of the treated nacelles, caused by the applicable loads specified in the structural design criteria for the test airplane, could be compared with the mechanical properties of the duct-lining structure. The mechanical properties were derived from the structural test program. The comparisons showed that all of the acoustically treated components of the modified nacelles had high margins of safety with acceptable structural rigidity.

Repair Methods

The possibilities of foreign object damage, improper fabrication techniques, and maintenance accidents required study of a method of repairing damage to porous facings and to acoustical sandwich structures. Existing methods of repairing sandwich structures were unacceptable because they destroyed the porosity of the fibermetal surfaces. Cracks or punctures in a skin are usually repaired with a doubler, either bonded or riveted to the skin. If the crack or puncture were repaired by bonding on another piece of fibermetal, the porosity would be just as effectively lost.

If a crack or puncture were small, an impervious doubler with a surface area of not more than 20 sq in. could be bonded over the failure. The bonded doubler could be reinforced with through bolts at the edges. At least three bolts would be used for triangular doublers and at least four bolts for other shapes. A compression insert or a potting would be required under each bolt to prevent crushing the honeycomb core. The nut on the end of the bolt would be backed with a large washer to feed any bolt tensile load into the impervious backing sheet as a bending load.

In the case of a failure in a bond, the normal repair method of using a potting compound would also be unacceptable. Potting would not only fill the pores in the fibermetal, it would also clog the drainage slots in several of the interconnected honeycomb cells. The flow of potting compound through the drainage slots could affect the porosity of the porous surface over a wide area. Therefore, it was recommended that bonding failures be repaired using the same procedure described above for failures in the fibermetal surfaces.

CONCLUSIONS

The nacelle-modification design studies considered revisions to the fan-exhaust and inlet ducts for the JT3D engine on DC-8-50/61 aircraft. An acoustical design chart was developed for use in estimating the treated area required to achieve a 10-PNdB reduction in noise radiated from the fan-exhaust ducts and a 7-PNdB reduction in noise radiated from the inlet duct. The design charts were also used to estimate the noise reduction potential of the various inlet and fan-duct designs that were studied.

The fan-exhaust-duct studies included the use of acoustically treated panels to supplement the acoustical treatment installed within 24-inch-long fan-exhaust ducts. Acoustically treated 48-inch-long fan-exhaust ducts with absorptive duct linings contained entirely within the ducts were also studied. Acoustical and economic performance estimates indicated that the treated 48-inch fan ducts, with a new target thrust reverser provided a larger noise reduction with a smaller economic penalty than the treated 24-inch ducts and supplementry panels.

Acoustically treated fixed and variable-geometry inlet ducts were studied. None of the variable-geometry designs could meet the noise-reduction goal and therefore were eliminated as candidate designs. The fixed-geometry designs included acoustically treated concentric ring-vanes and radial vanes in conjunction with the existing JT3D inlet duct and centerbody. A fixed-geometry design with an enlarged, lightbulb-shaped centerbody and concentric ring-vane was also studied. Two candidate inlet designs were selected, on the basis of acoustic and economic performance estimates, for ground static testing. The selected inlet designs were a two-concentric-ring inlet with the existing

inlet duct and centerbody and a 47-percent lightbulb inlet with a lengthened inlet duct and a single concentric ring-vane.

A variable-area primary nozzle that could reduce the rotational speed of the fan stages during landing approach was also recommended for ground static testing.

Acoustical flow-resistance tests were conducted on two classes of porous metallic sheets: fibermetals with mats of sintered wire fibers, and sintered layers of woven-wire-screens. The tests showed that porous materials could be manufactured in a wide range of nominal flow resistances and that significant changes in nominal flow resistance occurred with small changes in the thickness or density of a sheet. A quality-control procedure based on flow resistance testing was developed to ensure the uniformity of the nominal flow resistance of the large sheets of porous material needed for fabricating the full-scale inlet and fan-exhaust ducts.

Acoustic absorption and impedance tests showed that the absorptivity of a duct lining was changed as the magnitude of the SPL incident on the porous surfaces increased. The nonlinear resistance of the porous material was found to be an important parameter to consider when estimating the acoustical performance of an absorptive surface installed in an inlet or fan-exhaust duct and exposed to high SPLs.

Duct transmission-loss tests determined the nominal flow resistance required for the porous surfaces, the number of layers of porous material to be included in the duct-lining design, the depth of the backing cavities, and the size of the cells in the fiberglass-honeycomb support. All tests were conducted with bonded fibermetal-honeycomb-sandwich duct-lining designs. There was no significant acoustical advantage to be gained through use of more than one layer of fibermetal in the duct lining, thus, single-layer designs were recommended for the static test articles.

It was recommended that the walls of the 48-inch fan-exhaust ducts be treated with nominal 8-cgs rayl fibermetal bonded to honeycomb with nominal 0.75-inch cells. Recommended cavity depths were 0.5-inch on the inboard walls and 0.75-inch on the outboard walls. The fan-duct airflow splitters were treated with nominal 8-cgs rayl fibermetal bonded to honeycomb with 0.75-inch cells that were 0.5 inch deep on each side of an impervious septum. The walls of the inlet duct and centerbody were treated with nominal 10-cgs rayl fibermetal bonded to honeycomb with nominal 0.75-inch cells that were 0.75 inch deep. The concentric ring vanes were treated with nominal 10-cgs rayl fibermetal bonded to honeycomb with 0.75-inch cells that were 0.5 inch deep on each side of an impervious septum. The fibermetal was screen-reinforced on two sides and made from 0.004-inch diameter stainless-steel wire fibers.

Sonic-fatigue tests evaluated the acoustic fatigue resistance of test panels simulating the design of the wall of an acoustically treated inlet duct and a fan-duct flow splitter. Panels simulating the design of the wall of the existing JT3D short fan-exhaust duct were also evaluated. The adhesive-bonding technique developed for the absorptive test panels appeared to be adequate for the acoustic environment of the ground-test articles and the flight-test treated ducts.

Structural duct-lining investigations developed an adhesive-bonding procedure that could provide adequate strength and, simultaneously, satisfy the acoustical requirement for minimal blockage of the pores in the fibermetal. Structural tests of the components of the bonded fibermetal-honeycomb sandwich and of composite sandwich structures were conducted. These tests provided structural design data used in fabricating the full-scale acoustically treated inlet and fan-exhaust ducts.

Douglas Aircraft Company
McDonnell Douglas Corporation
Long Beach, California October 1969

REFERENCES

1. Marsh, Alan H.; Elias, I.; Hoehne, J. C.; and Frasca, R. L.: A Study of Turbofan-Engine Compressor-Noise-Suppression Techniques. NASA Contractor Rept. CR-1056, June 1968. (See also Marsh, Alan H.: Study of Acoustical Treatments for Jet-Engine Nacelles. J. Acoust. Soc. Am., vol. 43, no. 5, May 1968, pp. 1137-1156.)

2. Anon.: Study and Development of Turbofan Nacelle Modifications to Minimize Fan-Compressor Noise Radiation. Volume I: Program Summary. NASA Contractor Report CR-1711, 1971.

3. Anon.: Study and Development of Turbofan Nacelle Modifications to Minimize Fan-Compressor Noise Radiation. Volume II: Acoustic Lining Development. NASA Contractor Report CR-1712, 1971.

4. Anon.: Study and Development of Turbofan Nacelle Modifications to Minimize Fan-Compressor Noise Radiation. Volume III: Concept Studies and Ground Tests. NASA Contractor Report CR-1713, 1971.

5. Anon.: Study and Development of Turbofan Nacelle Modifications to Minimize Fan-Compressor Noise Radiation. Volume IV: Flightworthy Nacelle Development. NASA Contractor Report CR-1714, 1971.

6. Anon.: Study and Development of Turbofan Nacelle Modifications to Minimize Fan-Compressor Noise Radiation. Volume V: Sonic Inlet Development. NASA Contractor Report CR-1715, 1971.

7. Anon.: Study and Development of Turbofan Nacelle Modifications to Minimize Fan-Compressor Noise Radiation. Volume VI: Economic Studies. NASA Contractor Report CR-1716, 1971.

8. Pendley, Robert E.; and Marsh, Alan H.: Investigation of DC-8 Nacelle Modifications to Reduce Fan-Compressor Noise in Airport Communities. Part I: Summary of Program Results. NASA Contractor Report CR-1705, 1970.

9. Manhart, J. Kenneth; Campbell, D. A.; Henry, C. A.; and Lowder, E. M.: Investigation of DC-8 Nacelle Modifications to Reduce Fan-Compressor Noise in Airport Communities. Part III: Static Tests of Noise Suppressor Configuration. NASA Contractor Report CR-1707, 1970.

10. Zwieback, E. L.; Lowder, E. M.; Ilkcagla, E. A.; Andresen, H.; Henry, C. A.; Marsh, Alan H.; Gordon, D. K.; and Cleveland, N. L.: Investigation of DC-8 Nacelle Modifications to Reduce Fan-Compressor Noise in Airport Communities. Part IV: Flight Acoustical and Performance Evaluations. NASA Contractor Report CR-1708, 1970.

11. Whallon, H. D.; Gabbay, Ellis J.; Ferry, G. B., Jr.; and Cleveland, N. L.: Investigation of DC-8 Nacelle Modifications to Reduce Fan-Compressor Noise in Airport Communities. Part V: Economic Implications of Retrofit. NASA Contractor Report CR-1709, 1970.

12. Langdon, Lawrence E.; Gabriel, Richard F.; and Marsh, Alan H.: Investigation of DC-8 Nacelle Modifications to Reduce Fan-Compressor Noise in Airport Communities. Part VI: Psychoacoustic Evaluation. NASA Contractor Report CR-1710, 1970.

13. Pendley, Robert E.; and Marsh, Alan H.: Turbofan-Engine Noise Suppression. J. Aircraft, vol. 5, no. 3, May-June 1968, pp. 215-220.

14. Frasca, R. L.: Sonic Fatigue Design Studies of Nacelle Acoustical Treatments. Rept. DAC-33770, Douglas Aircraft Co., May 1967. (Available from the Clearinghouse for Federal Scientific and Technical Information, Springfield, Virginia 22151 as N68-32220.)

15. Cimerol, J. J.; Erickson, A. R.; and Fisher, J. I.: Investigation of the Properties of Fiber Metal Acoustical Materials. NASA Contractor Rept. CR-66643, September 1968.

16. Patel, S. P.: Aerodynamic Losses Caused by Porous Fibermetal. Rept. DAC-33722, Douglas Aircraft Co., June 1966. (Available from the Clearinghouse for Federal Scientific and Technical Information, Springfield, Virginia 22151 as N68-32219.)

17. Cremer, Lothar: Theory of Sound Attenuation in a Rectangular Duct with an Absorbing Wall and the Resultant Maximum Attenuation Constant. Acustica, Akustische Beihefte, Heft 2, 1953, pp.249-263.

18. Morse, Phillip M.; and Ingard, K. Uno: Theoretical Acoustics. McGraw-Hill Book Co., Inc. 1968.

19. Anon: Standard Method of Test for Impedance and Absorption of Acoustical Materials by the Tube Method. Part 14 of the 1966 Book of ASTM Standards. American Society for Testing and Materials. ASTM Designation C 384-58, 1966, pp. 135-146.

20. McGowan, P. R.; and Frasca, R. L.: Structural Design for Acoustic Fatigue. Aeronautical Systems Division, USAF, Technical Report ASD-TDR-63-820, October 1963. (Available from the Defense Documentation Center, Alexandria, Virginia.)

21. Eshleman, A. L., Jr.; and Van Dyke, J. D., Jr.: A Rational Method of Analysis by Matrix Methods of Acoustically Loaded Structure for Prediction of Sonic Fatigue Strength. Paper No. 35, pp. 721-746 in Acoustical Fatigue of Aerospace Structures. Walter J. Trapp and Donald M. Forney, Jr., ed., Syracuse University Press, Syracuse, New York, 1965.

22. Anon: Federal Aviation Regulations, Air Worthiness Standards: Transport Category Airplanes, U.S. Government Printing Office, November 3, 1964.

23. Anon: Tentative Methods of Test for Tensile Properties of Plastics. ASTM Designation: D638-67T. Part 27 of 1968 Book of ASTM Standards with Related Material. American Society for Testing and Materials, 1968, pp. 189-202.

24. Anon: Plastics: Methods of Testing. Federal Test Method Standard No. 406 (Method 1042). General Services Administration, October 5, 1961.

25. Anon: Tentative Methods of Test for Repeated Flexural Stress (Fatigue) of Plastics. ASTM Designation: D671-63T. Part 27 of 1968 Book of ASTM Standards with Related Material. American

Society for Testing and Materials, 1968, pp. 217-234.

26. Anon: Sandwich Constructions and Core Materials. General Test Methods. MIL-STD-401, U.S. Department of Defense, Sept. 26, 1967.

27. Anon: Metallic Materials and Elements for Flight Vehicle Structures. MIL-HDBK-5, U.S. Department of Defense, February 8, 1966.

28. Anon: Plastic for Flight Vehicle Structures. MIL-HDBK-17, U.S. Department of Defense, November 5, 1959.

29. Anon: Composite Construction for Flight Vehicles. MIL-HDBK-23, U.S. Department of Defense, October 5, 1959.

30. Anon: General Specification for Environmental Testing. Aeronautical and Associated Equipment. MIL-E-5272C, U.S. Department of Defense, April 13, 1959.

APPENDIX A

FLOW-RESISTANCE UNIFORMITY REQUIREMENTS USED IN PURCHASING SHEETS OF POROUS MATERIALS

Sheets of porous material intended for use as acoustically absorptive linings in jet engine inlet and fan-exhaust ducts should have a nominal flow resistance reasonably uniform over the surface of the sheets. The nominal flow resistance of sheet material is defined as the desired flow resistance at an airflow velocity of 0.2 m/sec. Because of the difficulty of precisely controlling the thickness and surface density of porous materials and because the conventional method of conducting flow-resistance tests uses a 10-cm diameter test fixture, the arithmetic-mean flow resistance of a sheet will differ from the desired nominal flow resistance. The requirements described in this Appendix were developed to specify an allowable tolerance on the uniformity of flow resistance for sheet material.

Requirements

Flow-resistance uniformity requirements used in purchasing sheets of porous material were:

1. The arithmetic-mean flow resistance shall not deviate more than ±15 percent from the nominal flow resistance;

2. The standard deviation of the flow-resistance measurements from their mean value shall not exceed 15 percent of the nominal flow resistance; and

3. No two adjacent flow-resistance measurements shall differ by more than 40 percent of the nominal flow resistance.

Procedure for Determining Compliance with Requirements

Flow-resistance tests. – Flow resistance measurements shall be made under steady flow conditions with a linear airflow velocity of 0.2 m/sec through a test section area with a 10-cm diameter.

The value of the flow resistance shall be determined by the ratio of the differential pressure through the material, in dynes/cm^2, to the linear airflow velocity through the sample, in cm/sec, i.e., in cgs rayls. For each sheet, flow resistance measurements shall be made on a 6-inch grid over the entire sheet and shall be confined within a 1-inch margin around the perimeter of the sheet. The location of the first grid shall be at the upper left-hand corner. The centers of the test areas shall be permanently marked.

The minimum acceptable precision for flow resistance measurements is ±0.5 cgs rayls for nominal flow resistance greater than 5 cgs rayls.

APPENDIX A

Arithmetic-mean flow resistance. – The arithmetic mean $\overline{R}$ of the flow resistance measurements R_i at a test location i shall be determined from

$$\overline{R} = \left(\sum_{i=1}^{n} R_i\right)/n \tag{13}$$

where n is the total number of test points per sheet.

Standard deviation. – The standard deviation σ of the flow resistance measurements R_i from the arithmetic mean value $\overline{R}$ shall be determined from

$$\sigma = \sqrt{\sum_{i=1}^{n} \left[(R_i - \overline{R})^2\right] / (n-1)} \tag{14}$$

APPENDIX B

ADHESIVE-BONDING PROCEDURE USED TO FABRICATE ACOUSTICALLY TREATED TEST PANELS

The same adhesive-bonding procedure was used to fabricate all the single-layer duct transmission-loss test panels and sonic-fatigue Test Panel No. I. The procedure consisted of the following seven steps.

(1) Cut the sheets of fibermetal, aluminum, and honeycomb core to the desired size. Pre-fit the honeycomb core within the panel boundary in an assembly jig.

(2) Clean the aluminum backing sheet with solvent and wipe dry. Clean the fibermetal sheet by placing it for 20 minutes in a hot sulfuric-acid – sodium-dichromate etching solution maintained at 145° F ± 5° F. After removal from the etching solution, wash the fibermetal sheet thoroughly with water and force-air-dry in a circulating oven at 180° F for approximately one hour.

(3) Place an adhesive-coated fiberglass-scrim-cloth between the aluminum backing sheet and the honeycomb core.

(4) Assemble the panel and cover with sheets of plastic. Place the bagged assembly in a circulating oven and withdraw the air from the bag to a vacuum of 8 to 10 inches of Hg. Maintaining this partial vacuum, cure the bond between the honeycomb core and the aluminum sheet by exposure to 300° F for 30 minutes with the panel assembly in a position to allow adhesive to flow toward the aluminum sheet.

(5) Maintaining the same partial vacuum, allow the panel to cool to room temperature in the oven. When cool, remove the bagged assembly from the oven and remove the plastic sheets. Inspect the quality of the bond, using a coin-tapping process.

(6) Coat the exposed edges of the honeycomb with thixotropic epoxy-paste adhesive. Apply the adhesive to the core with a paint roller. Lay the fibermetal sheet on the adhesive-coated honeycomb core and surround the assembly again with plastic sheets.

(7) Using a partial vacuum of 8 to 10 inches of Hg, repeat the oven-curing procedure described in steps 3 to 5, except allow the assembly to cure for 60 minutes at 350° F instead of for 30 minutes at 300° F. In order to prevent filling the pores in the fibermetal with adhesive during the curing process, make sure that the assembly is cured in a position that allows the adhesive to flow away from the fibermetal and towards the backing sheet.

APPENDIX C

BURNER-CAN SOUND SOURCE

The burner-can sound source was used to solve the problem of providing a stable, reliable source of high-intensity, high-frequency acoustic power for inlet duct tests. This novel noise source could operate readily in the vacuum-pressure environment of the downstream chamber where it was impractical to use the pulse-jet sound source.

The burner was a simple device that burned aircraft-grade kerosene in a stream of high-pressure air. The heated air was exhausted through a nozzle into the downstream chamber. The acoustical power output was principally a function of the fuel-flow rate and the pressure of the air supplied to the burner.

Description of Burner

The burner was similar to the pulse jet in that it required air, fuel, and an ignition spark. Figure 78(a) shows an assembled view of the complete unit. The overall length of the assembly was 43 inches. Figure 25(b) showed the installation of the burner in the downstream chamber.

As shown in the photographs of the components of the combustor section, figure 78(b), there were only six basic parts in the section where the fuel was introduced and burned. The burner-can unit [on the right in figure 78(b)] was essentially a cylinder to house the burner-can, igniter and swirler. Exclusive of the burner-can unit, the details of the five remaining basic parts are shown in figure 78(c).

A description of the items in figure 78(c) is given below in the order of their appearance from left to right, i.e., the direction of air and fuel flow through the burner.

- The burner-tip contained twenty-eight 3/16-inch-diameter, 6-inch-long, stainless-steel tubes. Eleven of these tubes were equally spaced at a 1/2-inch radius from the center of the unit; the other 17 were equally spaced at a 13/16-inch radius. In addition, a 15-inch-long fuel pipe with an outside diameter of 5/8-inch and an inside diameter of 1/8-inch was positioned along the axial centerline of the unit, extending the length of the unit and terminating flush with the 28 stainless-steel tubes. The fuel line is not shown in figure 78.

- The burner-tip was attached to the end of the fuel line. A liquid stream of fuel was injected by the burner-tip through the swirler into the burner-can.

- The swirler was a 15/16-inch-long cylinder with a 2-inch diameter. The swirler had a hole through the center that tapered from a 9/16-inch diameter on the upstream side to a 5/16-inch diameter along a portion of the length of the swirler. The reason the tapered hole did not extend the entire length was because the cylinder was concave on one side with the thinnest depth at the center. In addition, ten equally spaced oval-shaped holes with major and minor axes of 3/16 and 1/8 inch respectively, were located at a 7/16-inch radius from the center. The oval-shaped holes were drilled through the swirler to the plane where the 28 stainless-steel tubes terminated.

The swirler mixed the air into the liquid stream of fuel in order to vaporize the fuel before it was ignited in the burner-can.

- The burner-can was a cylinder with irregularly spaced holes along its length. The holes varied in size from a minimum of 3/16-inch diameter to a maximum of 1/2-inch diameter. A tailpipe or nozzle was attached to the burner can. All of the air that flowed through the unit was forced into the burner can and was discharged through the nozzle. The dimensions of the burner can are given in the sketch below.

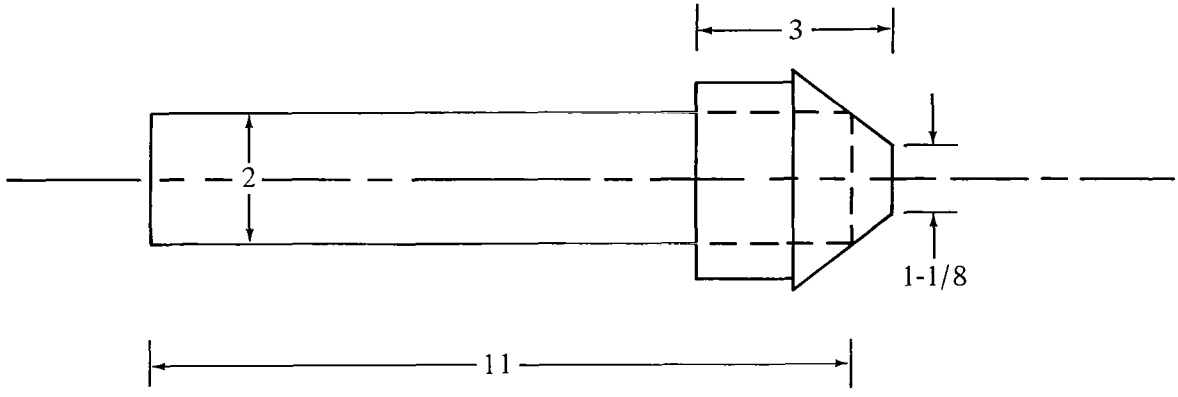

(Dimensions in inches)

- The igniter was 4-3/4 inches long with a 3/16-inch inside diameter and was located in one of the holes in the burner can.

Burner Operation

The sequence of events for operating the burner was as follows: first, shop air was allowed to flow into the assembly and through the 28 stainless-steel tubes. A portion of this air flowed through the swirler and into the burner-can. For cooling purposes, the remainder of the air flowed against the flat surface of the swirler, over the outside of, and then into, the burner-can. Next, the igniter was activated, and, finally, fuel was pumped into the fuel line, through the burner-tip, and into the burner-can where the fuel-and-air mixture was ignited.

Operational Problems

Burner-tips with fuel flow ratings of 10, 17.5, and 19.5 gal/hr (gph) were used. There were two operational problems encountered when the 19.5-gph tip was used. One problem was with the available air pressure, and the other was a possible malfunction of the microphone system due to operation in a high-temperature environment. The air pressure required to operate the burner-can with 10-gph and 17.5-gph burner tips was approximately 30 and 38 psig, respectively. The maximum available air pressure was limited to about 43 psig the majority of the time during this test program. Although the burner, with the 19.5 gph tip installed, operated satisfactorily at 43 psig, additional pressure would have been desirable because of the higher SPLs that could have been obtained.

APPENDIX C

Because more fuel was burned and consequently more heat generated with the larger burner tips, the temperature of the air in the downstream chamber increased with the size of the burner tip used. The temperature also varied with the velocity of the airflow through the test duct. Figure 79 shows the effect of duct airflow velocity on the temperature in the downstream chamber. Data are given for duct velocities ranging from 0 to 600 ft/sec and for burner tips with 10 and 19.5 gph ratings. The 19.5-gph tip was operated at an air pressure of 43 psig, the 10-gph tip at 30 psig.

If the ambient temperature were 100° F, the temperature in the downstream chamber, at zero duct velocity with the 19.5-gph burner tip installed, would reach about 300° F. Long-term exposure to 300° F would have caused a malfunction in the cable between the microphone and cathode follower. Components in the power supply and in the cathode follower would also have been affected by this temperature. Although the microphone cartridge could withstand temperatures to about 800° F continuously, the sensitivity was not stable at high temperatures and there might have been problems with the insulation under the backplate. Furthermore, the vacuum pumps were limited in the temperature of the air that could be supplied to them.

Therefore, because of the limited air pressure available and because of the potential temperature problem with the instrumentation, it was decided to wrap the microphone cable with aluminum foil and to use only the 17.5-gph tip at 38 psig.

APPENDIX D

ATTENUATION VALUES FOR DUCT TRANSMISSION-LOSS TESTS

This appendix presents a series of charts showing the effect of duct velocity on attenuation for exhaust and inlet duct transmission-loss tests. Each chart consists of a set of graphs corresponding to the duct-lining configuration tested. (For additional description of the configuration codes, see table VI.)

Chart series 1 through 25 show how attenuation varies with duct velocity for exhaust tests; chart series 26 through 49, for inlet tests. The charts were drawn by an automatic plotting machine with instructions provided by a digital computer.

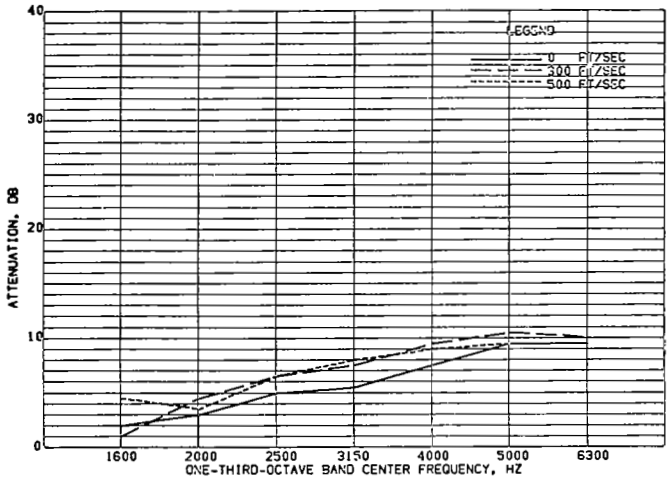

FIGURE 1.- EXHAUST MODE. EFFECT OF VELOCITY FOR CONFIGURATION R2

CONFIGURATION DESCRIPTION.- 10 RAYL FM, 0.25-IN. DEEP

* FM=FIBERMETAL. FIBERGLASS HONEYCOMB CORE WAS 0.75-IN.
TREATMENT LENGTH WAS 22.5 -IN AND BEGAN AT INLET PLANE.

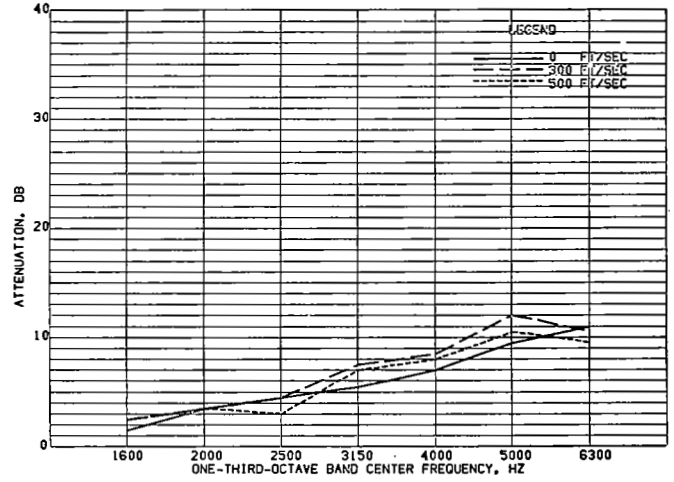

FIGURE 2.- EXHAUST MODE. EFFECT OF VELOCITY FOR CONFIGURATION R2*

CONFIGURATION DESCRIPTION.- 10 RAYL FM, 0.25-IN. DEEP
REPEAT FROM 18 JULY

* FM=FIBERMETAL. FIBERGLASS HONEYCOMB CORE WAS 0.75-IN.
TREATMENT LENGTH WAS 22.5 -IN AND BEGAN AT EXIT PLANE.

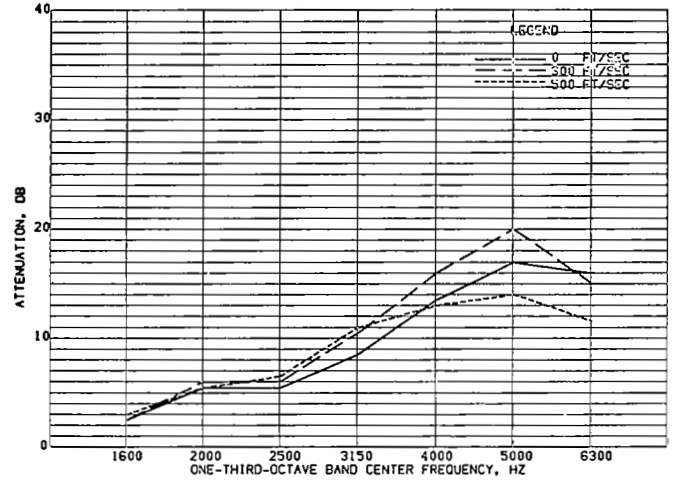

FIGURE 3.- EXHAUST MODE. EFFECT OF VELOCITY FOR CONFIGURATION R3

CONFIGURATION DESCRIPTION.- 40 RAYL FM, 0.25-IN. DEEP

* FM=FIBERMETAL. FIBERGLASS HONEYCOMB CORE WAS 0.75-IN.
TREATMENT LENGTH WAS 22.5 -IN AND BEGAN AT INLET PLANE.

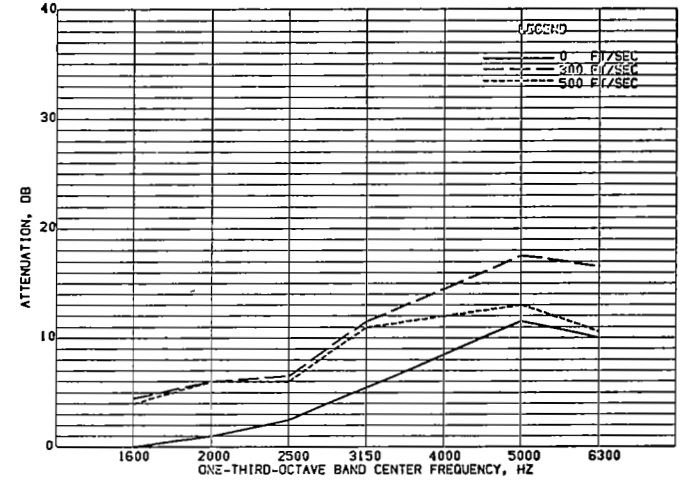

FIGURE 4.- EXHAUST MODE. EFFECT OF VELOCITY FOR CONFIGURATION R4

CONFIGURATION DESCRIPTION.- 80 RAYL FM, 0.25-IN. DEEP

* FM=FIBERMETAL. FIBERGLASS HONEYCOMB CORE WAS 0.75-IN.
TREATMENT LENGTH WAS 22.5 -IN AND BEGAN AT INLET PLANE.

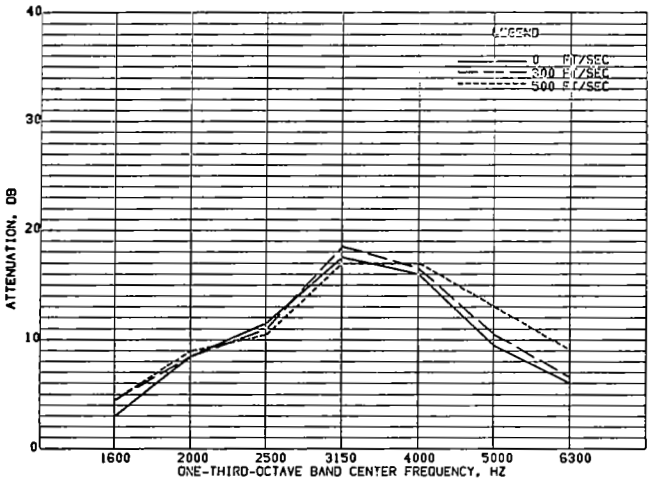

FIGURE 5.- EXHAUST MODE. EFFECT OF VELOCITY FOR CONFIGURATION R5

CONFIGURATION DESCRIPTION.- 10 RAYL FM, 0.5-IN. DEEP

*FM=FIBERMETAL. FIBERGLASS HONEYCOMB CORE WAS 0.75-IN.
TREATMENT LENGTH WAS 22.5 -IN AND BEGAN AT INLET PLANE.

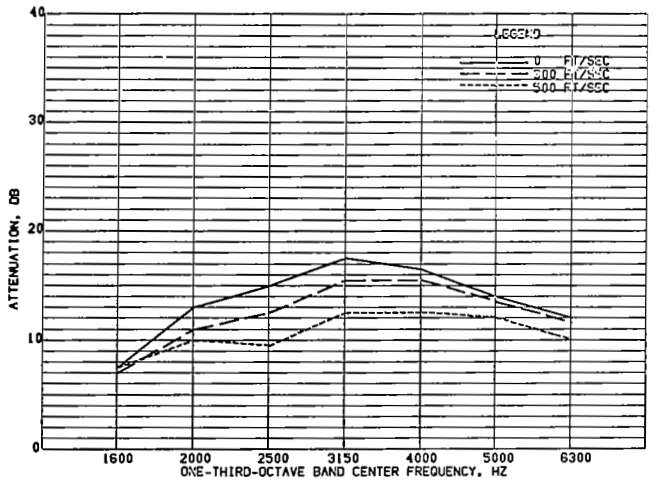

FIGURE 7.- EXHAUST MODE. EFFECT OF VELOCITY FOR CONFIGURATION R8

CONFIGURATION DESCRIPTION.- 80 RAYL FM, 0.5-IN. DEEP

*FM=FIBERMETAL. FIBERGLASS HONEYCOMB CORE WAS 0.75-IN.
TREATMENT LENGTH WAS 22.5 -IN AND BEGAN AT INLET PLANE.

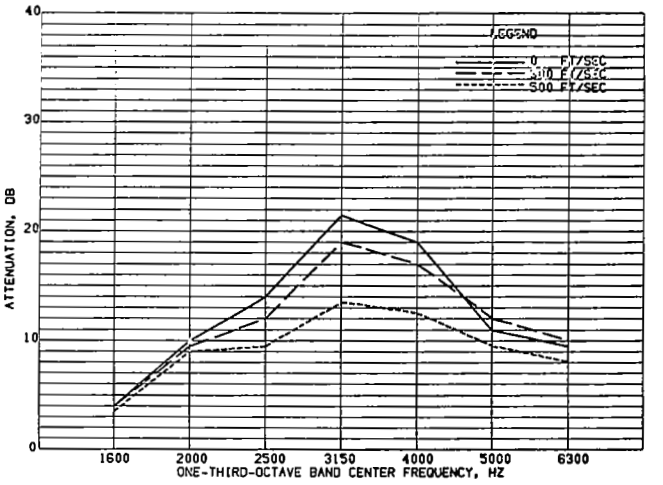

FIGURE 6.- EXHAUST MODE. EFFECT OF VELOCITY FOR CONFIGURATION R6

CONFIGURATION DESCRIPTION.- 40 RAYL FM, 0.5-IN. DEEP

*FM=FIBERMETAL. FIBERGLASS HONEYCOMB CORE WAS 0.75-IN.
TREATMENT LENGTH WAS 22.5 -IN AND BEGAN AT INLET PLANE.

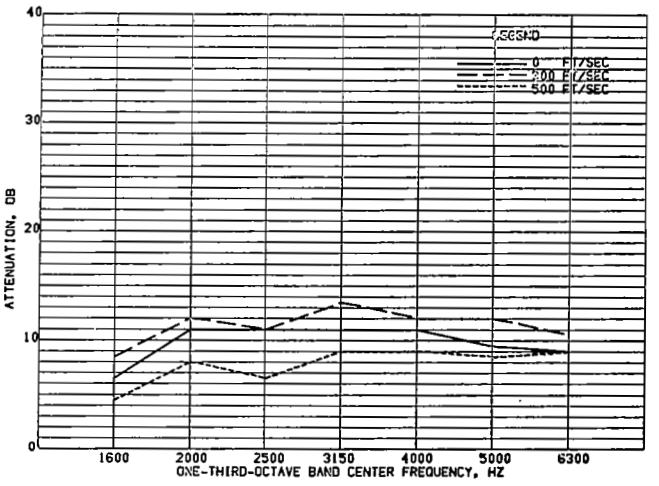

FIGURE 8.- EXHAUST MODE. EFFECT OF VELOCITY FOR CONFIGURATION R9

CONFIGURATION DESCRIPTION.- 160 RAYL FM, 0.5-IN. DEEP

*FM=FIBERMETAL. FIBERGLASS HONEYCOMB CORE WAS 0.75-IN.
TREATMENT LENGTH WAS 22.5 -IN AND BEGAN AT INLET PLANE.

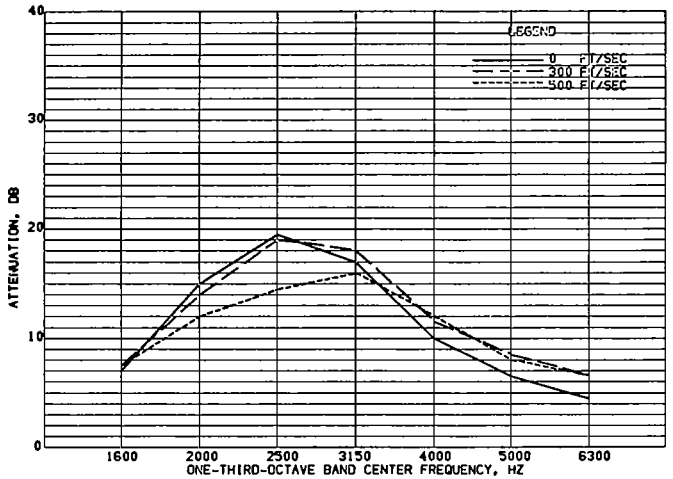

FIGURE 9.- EXHAUST MODE. EFFECT OF VELOCITY FOR CONFIGURATION R10

CONFIGURATION DESCRIPTION.- 10 RAYL FM, 0.75-IN. DEEP

• FM=FIBERMETAL. FIBERGLASS HONEYCOMB CORE WAS 0.75-IN. TREATMENT LENGTH WAS 22.5 -IN AND BEGAN AT INLET PLANE.

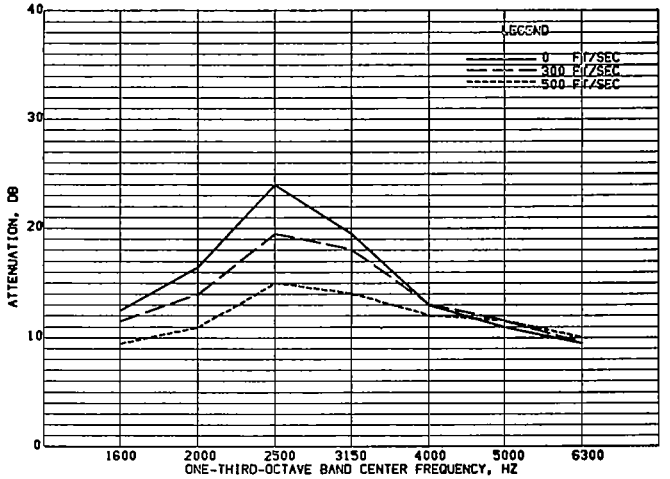

FIGURE 10.- EXHAUST MODE. EFFECT OF VELOCITY FOR CONFIGURATION R11

CONFIGURATION DESCRIPTION.- 40 RAYL FM, 0.75-IN. DEEP

• FM=FIBERMETAL. FIBERGLASS HONEYCOMB CORE WAS 0.75-IN. TREATMENT LENGTH WAS 22.5 -IN AND BEGAN AT INLET PLANE.

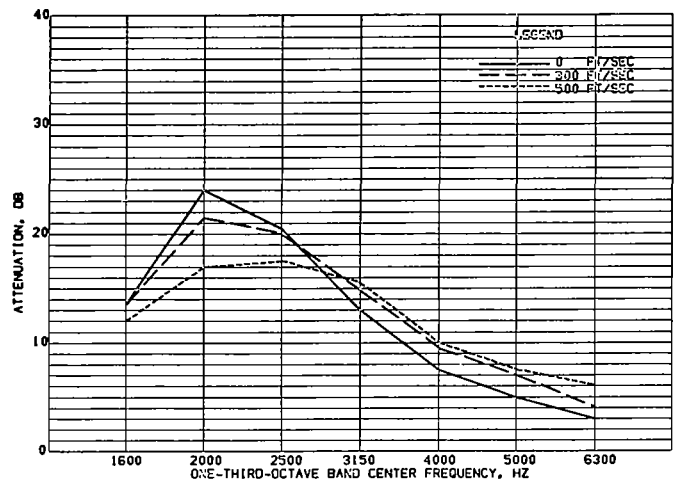

FIGURE 11.- EXHAUST MODE. EFFECT OF VELOCITY FOR CONFIGURATION R13

CONFIGURATION DESCRIPTION.- 10 RAYL FM, 1.0-IN. DEEP

• FM=FIBERMETAL. FIBERGLASS HONEYCOMB CORE WAS 0.75-IN. TREATMENT LENGTH WAS 22.5 -IN AND BEGAN AT INLET PLANE.

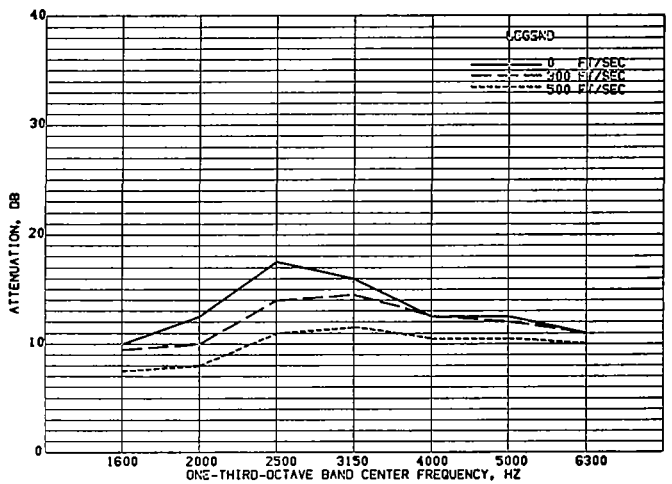

FIGURE 12.- EXHAUST MODE. EFFECT OF VELOCITY FOR CONFIGURATION R12

CONFIGURATION DESCRIPTION.- 80 RAYL FM, 0.75-IN. DEEP

• FM=FIBERMETAL. FIBERGLASS HONEYCOMB CORE WAS 0.75-IN. TREATMENT LENGTH WAS 22.5 -IN AND BEGAN AT INLET PLANE.

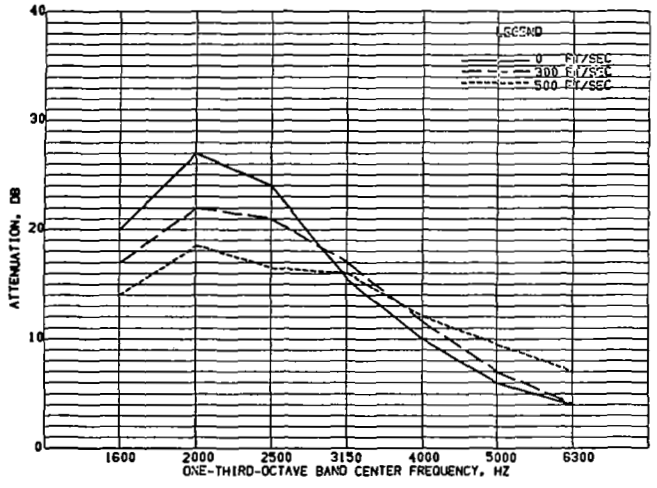

FIGURE 13.- EXHAUST MODE. EFFECT OF VELOCITY FOR CONFIGURATION R14

CONFIGURATION DESCRIPTION.- 20 RAYL FM, 1.0-IN. DEEP

* FM=FIBERMETAL. FIBERGLASS HONEYCOMB CORE WAS 0.75-IN. TREATMENT LENGTH WAS 22.5 -IN AND BEGAN AT INLET PLANE.

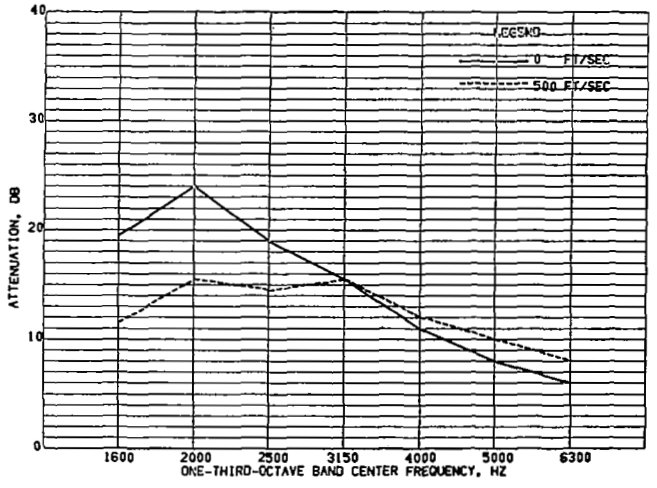

FIGURE 14.- EXHAUST MODE. EFFECT OF VELOCITY FOR CONFIGURATION R15

CONFIGURATION DESCRIPTION.- 40 RAYL FM, 1.0-IN. DEEP

* FM=FIBERMETAL. FIBERGLASS HONEYCOMB CORE WAS 0.75-IN. TREATMENT LENGTH WAS 22.5 -IN AND BEGAN AT EXIT PLANE.

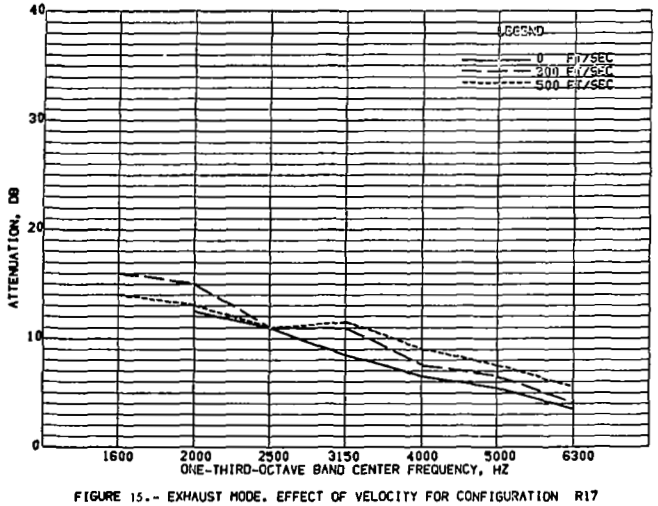

FIGURE 15.- EXHAUST MODE. EFFECT OF VELOCITY FOR CONFIGURATION R17

CONFIGURATION DESCRIPTION.- 40 RAYL FM, 1.0-IN. DEEP

* FM=FIBERMETAL. FIBERGLASS HONEYCOMB CORE WAS 0.75-IN. TREATMENT LENGTH WAS 45-IN. AND WAS INSTALLED ON ONE WALL ONLY.

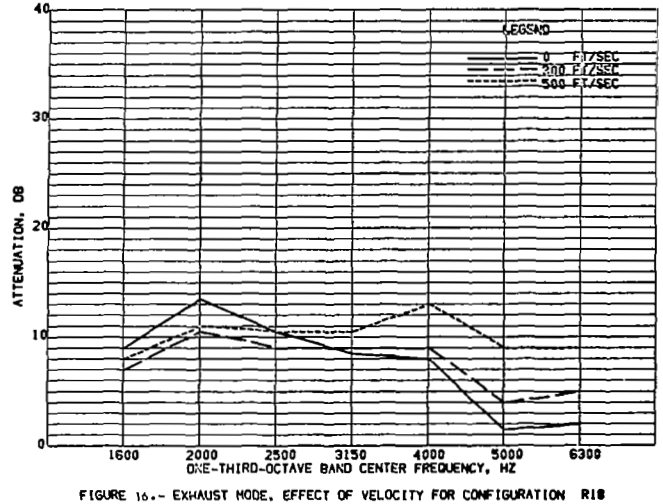

FIGURE 16.- EXHAUST MODE. EFFECT OF VELOCITY FOR CONFIGURATION R18

CONFIGURATION DESCRIPTION.- 40 RAYL FM, 1.0-IN. DEEP

* FM=FIBERMETAL. FIBERGLASS HONEYCOMB CORE WAS 0.75-IN. TREATMENT LENGTH WAS 11.25-IN AND BEGAN AT EXIT PLANE.

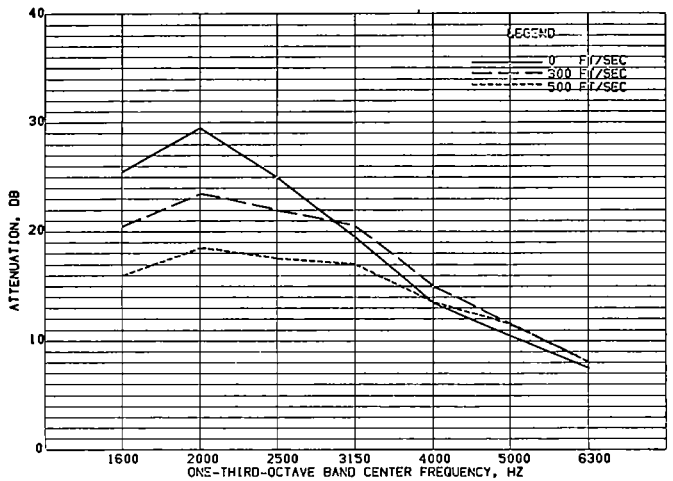

FIGURE 17.- EXHAUST MODE. EFFECT OF VELOCITY FOR CONFIGURATION R19

CONFIGURATION DESCRIPTION.- 40 RAYL FM, 1.0-IN. DEEP

* FM=FIBERMETAL. FIBERGLASS HONEYCOMB CORE WAS 0.75-IN. TREATMENT LENGTH WAS 33.75-IN AND BEGAN AT EXIT PLANE.

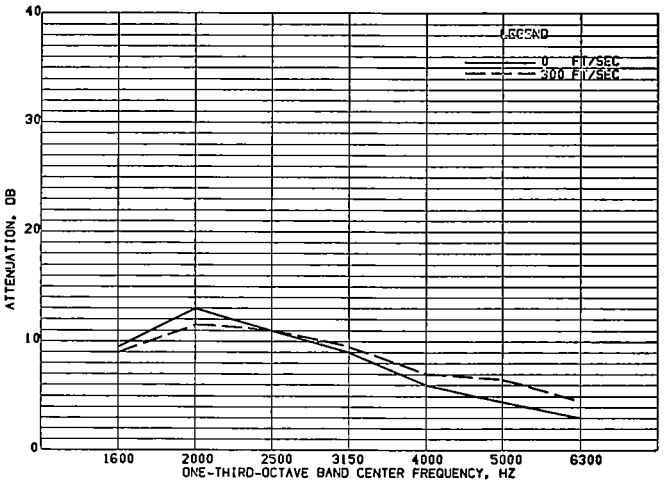

FIGURE 18.- EXHAUST MODE. EFFECT OF VELOCITY FOR CONFIGURATION R18*

CONFIGURATION DESCRIPTION.- 40 RAYL FM, 1.0-IN. DEEP

* FM=FIBERMETAL. FIBERGLASS HONEYCOMB CORE WAS 0.75-IN. TREATMENT LENGTH WAS 11.25-IN AND BEGAN AT INLET PLANE.

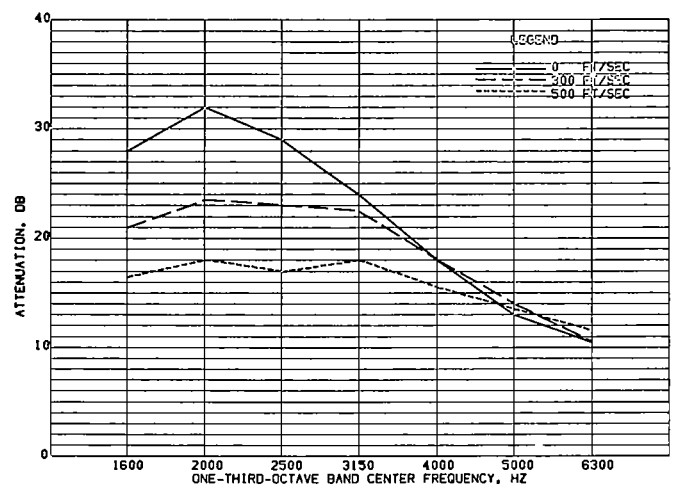

FIGURE 19.- EXHAUST MODE. EFFECT OF VELOCITY FOR CONFIGURATION R20

CONFIGURATION DESCRIPTION.- 40 RAYL FM, 1.0-IN. DEEP

* FM=FIBERMETAL. FIBERGLASS HONEYCOMB CORE WAS 0.75-IN. TREATMENT LENGTH WAS 45.0-IN.

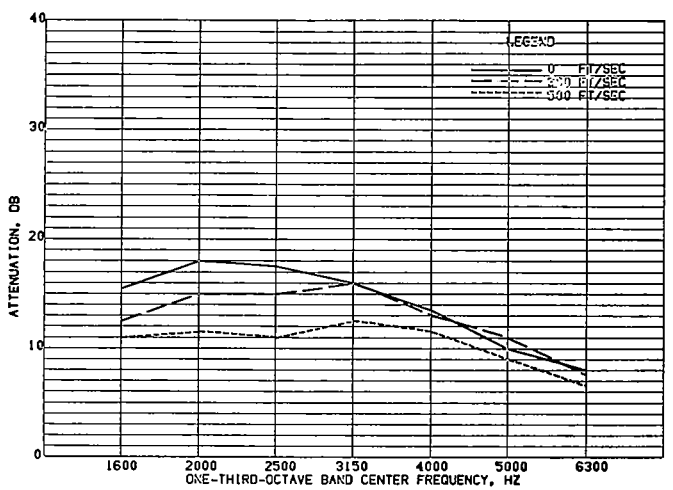

FIGURE 20.- EXHAUST MODE. EFFECT OF VELOCITY FOR CONFIGURATION R21

CONFIGURATION DESCRIPTION.- 80 RAYL FM, 1.0-IN. DEEP

* FM=FIBERMETAL. FIBERGLASS HONEYCOMB CORE WAS 0.75-IN. TREATMENT LENGTH WAS 22.5 -IN AND BEGAN AT INLET PLANE.

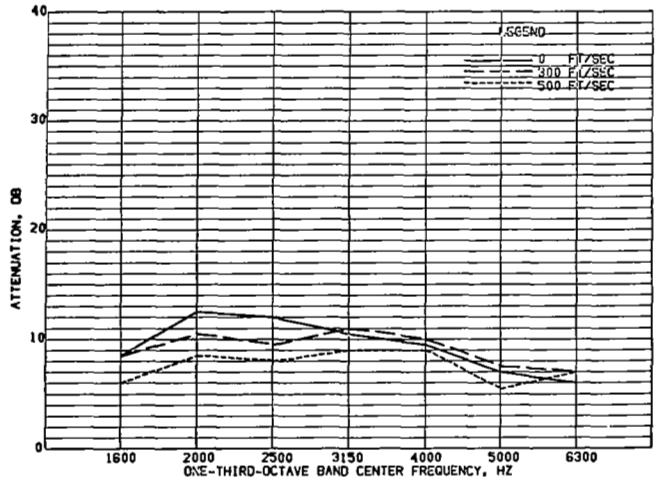

FIGURE 21.- EXHAUST MODE. EFFECT OF VELOCITY FOR CONFIGURATION R22

CONFIGURATION DESCRIPTION.- 160 RAYL FM, 1.0-IN. DEEP

* FM=FIBERMETAL. FIBERGLASS HONEYCOMB CORE WAS 0.75-IN.
TREATMENT LENGTH WAS 22.5 -IN AND BEGAN AT INLET PLANE.

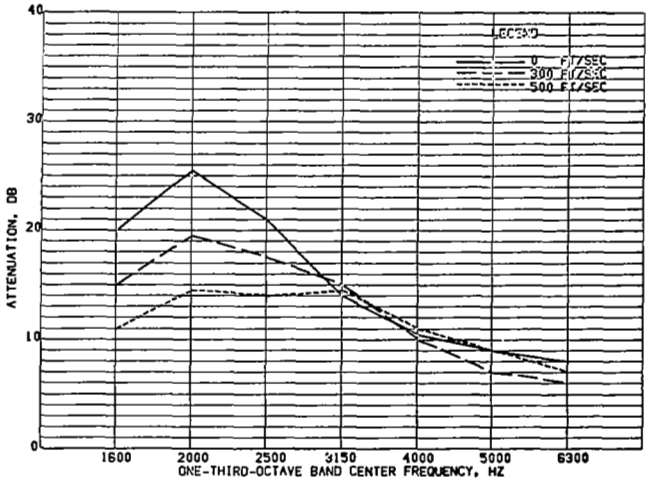

FIGURE 22.- EXHAUST MODE. EFFECT OF VELOCITY FOR CONFIGURATION R23

CONFIGURATION DESCRIPTION.- 40 RAYL FM, 1.0-IN. DEEP

*FM=FIBERMETAL. FIBERGLASS HONEYCOMB CORE WAS 0.375-IN.
TREATMENT LENGTH WAS 22.5-IN AND BEGAN AT INLET PLANE.

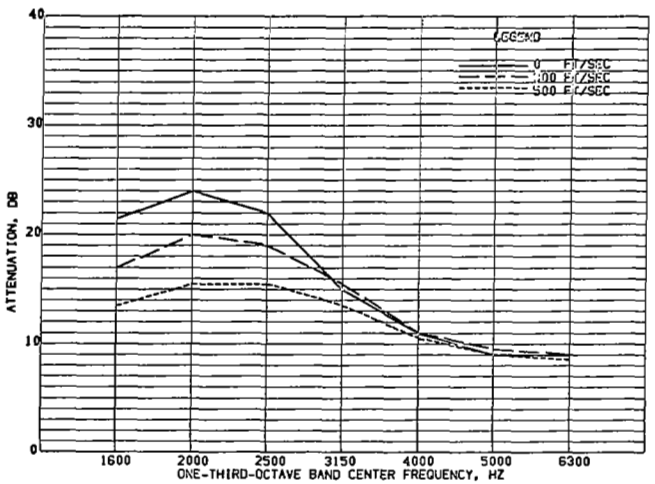

FIGURE 23.- EXHAUST MODE. EFFECT OF VELOCITY FOR CONFIGURATION R24

CONFIGURATION DESCRIPTION.- 40 RAYL FM, 1.0-IN. DEEP

*FM=FIBERMETAL. FIBERGLASS HONEYCOMB CORE WAS 1.125-IN.
TREATMENT LENGTH WAS 22.5-IN. AND BEGAN AT INLET PLANE.

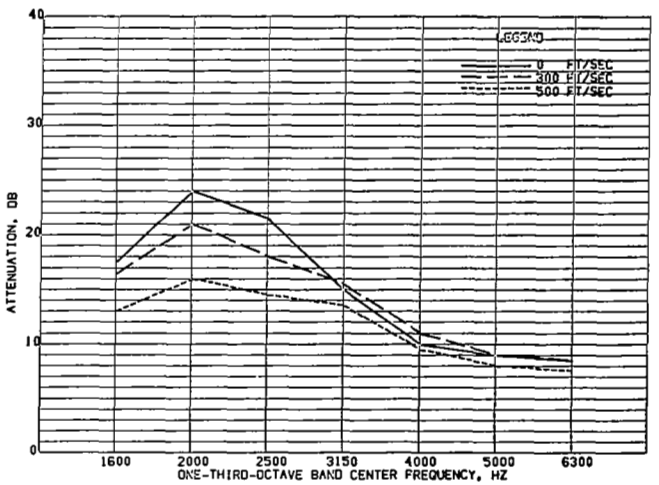

FIGURE 24.- EXHAUST MODE. EFFECT OF VELOCITY FOR CONFIGURATION R24

CONFIGURATION DESCRIPTION.- 40 RAYL FM, 1.0-IN. DEEP

*FM=FIBERMETAL. FIBERGLASS HONEYCOMB CORE WAS 1.125-IN.
TREATMENT LENGTH WAS 22.5-IN AND BEGAN AT EXIT PLANE.

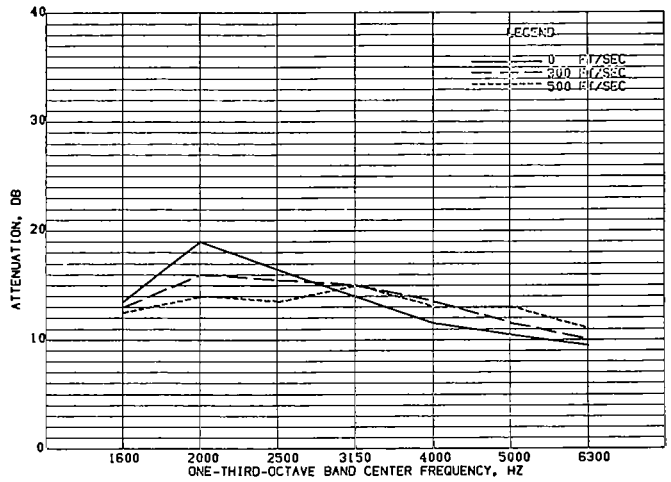

FIGURE 33.- EXHAUST MODE. EFFECT OF VELOCITY FOR CONFIGURATION R34

CONFIGURATION DESCRIPTION.- SPLITTER = 40 RAYL FM ON TWO SIDES OF FLAT SHEET ALUMINUM SEPTUM. 1.0-IN. DUCT WALLS WERE AS R18

• FM=FIBERMETAL. FIBERGLASS HONEYCOMB CORE WAS 0.75-IN.

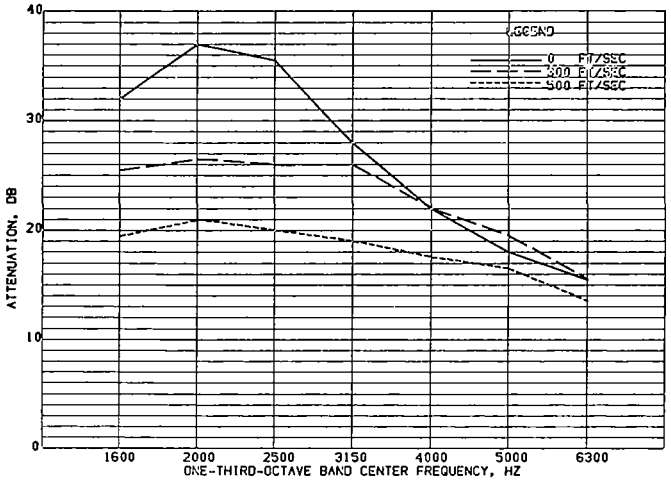

FIGURE 35.- EXHAUST MODE. EFFECT OF VELOCITY FOR CONFIGURATION R36

CONFIGURATION DESCRIPTION.- SPLITTER = 40 RAYL FM ON TWO SIDES OF FLAT SHEET ALUMINUM SEPTUM. 1.0-IN. DUCT WALLS WERE AS R20

• FM=FIBERMETAL. FIBERGLASS HONEYCOMB CORE WAS 0.75-IN.

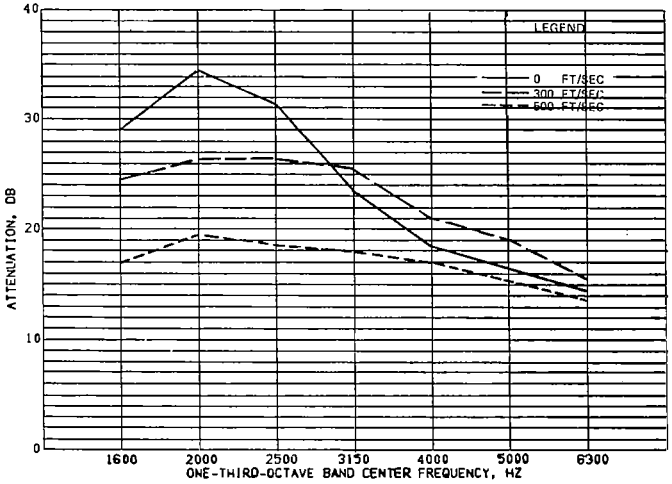

FIGURE 34.- EXHAUST MODE. EFFECT OF VELOCITY FOR CONFIGURATION R35

CONFIGURATION DESCRIPTION.- SPLITTER = 40 RAYL FM ON TWO SIDES OF FLAT SHEET ALUMINUM SEPTUM. 1.0-IN. DUCT WALLS WERE AS R19

• FM=FIBERMETAL. FIBERGLASS HONEYCOMB CORE WAS 0.75-IN.

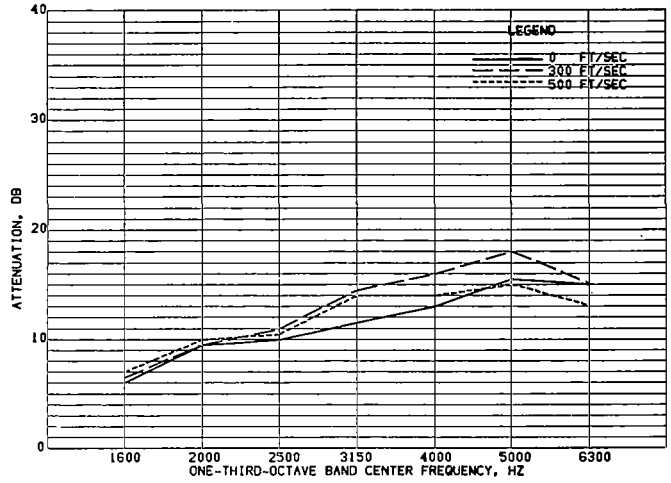

FIGURE 36.- EXHAUST MODE. EFFECT OF VELOCITY FOR CONFIGURATION R101

CONFIGURATION DESCRIPTION.- SURFACE NO 1=10 RAYL FM CAVITY NO 1=0.25-IN DEEP SURFACE NO 2=40 RAYL FM CAVITY NO 2=0.25-IN DEEP

• FM=FIBERMETAL. FIBERGLASS HONEYCOMB CORE WAS 0.75-IN. TREATMENT LENGTH WAS 22.5-IN. AND BEGAN AT INLET PLANE. SURFACE AND CAVITY NO 1 IS NEXT TO AIRFLOW. SURFACE AND CAVITY NO 2 IS NEXT TO OUTER DUCT WALL.

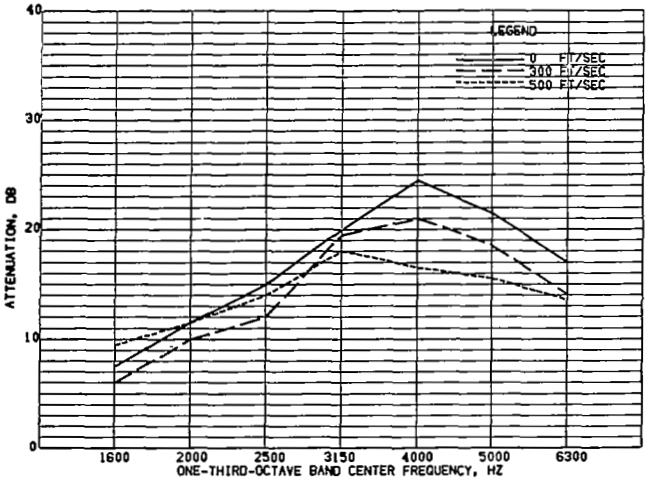

FIGURE 37.- EXHAUST MODE. EFFECT OF VELOCITY FOR CONFIGURATION R102

CONFIGURATION DESCRIPTION.- SURFACE NO 1=10 RAYL FM
CAVITY NO 1=0.25-IN DEEP
SURFACE NO 2=80 RAYL FM
CAVITY NO 2=0.25-IN DEEP

* FM=FIBERMETAL. FIBERGLASS HONEYCOMB CORE WAS 0.75-IN. TREATMENT LENGTH WAS 22.5-IN. AND BEGAN AT INLET PLANE. SURFACE AND CAVITY NO 1 IS NEXT TO AIRFLOW. SURFACE AND CAVITY NO 2 IS NEXT TO OUTER DUCT WALL.

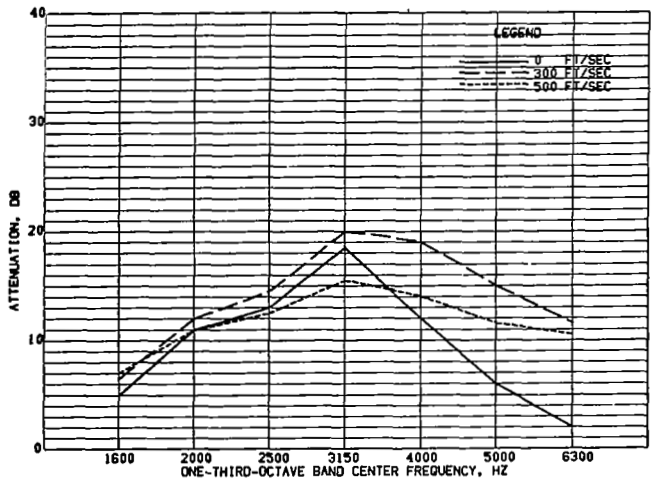

FIGURE 39.- EXHAUST MODE. EFFECT OF VELOCITY FOR CONFIGURATION R104

CONFIGURATION DESCRIPTION.- SURFACE NO 1=40 RAYL FM
CAVITY NO 1=0.25-IN DEEP
SURFACE NO 2=10 RAYL FM
CAVITY NO 2=0.25-IN DEEP

* FM=FIBERMETAL. FIBERGLASS HONEYCOMB CORE WAS 0.75-IN. TREATMENT LENGTH WAS 22.5-IN. AND BEGAN AT INLET PLANE. SURFACE AND CAVITY NO 1 IS NEXT TO AIRFLOW. SURFACE AND CAVITY NO 2 IS NEXT TO OUTER DUCT WALL.

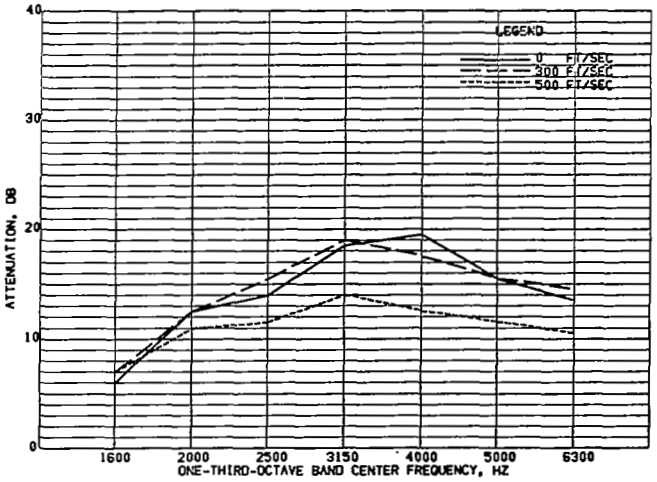

FIGURE 38.- EXHAUST MODE. EFFECT OF VELOCITY FOR CONFIGURATION R103

CONFIGURATION DESCRIPTION.- SURFACE NO 1=40 RAYL FM
CAVITY NO 1=0.25-IN DEEP
SURFACE NO 2=80 RAYL FM
CAVITY NO 2=0.25-IN DEEP

* FM=FIBERMETAL. FIBERGLASS HONEYCOMB CORE WAS 0.75-IN. TREATMENT LENGTH WAS 22.5-IN. AND BEGAN AT INLET PLANE. SURFACE AND CAVITY NO 1 IS NEXT TO AIRFLOW. SURFACE AND CAVITY NO 2 IS NEXT TO OUTER DUCT WALL.

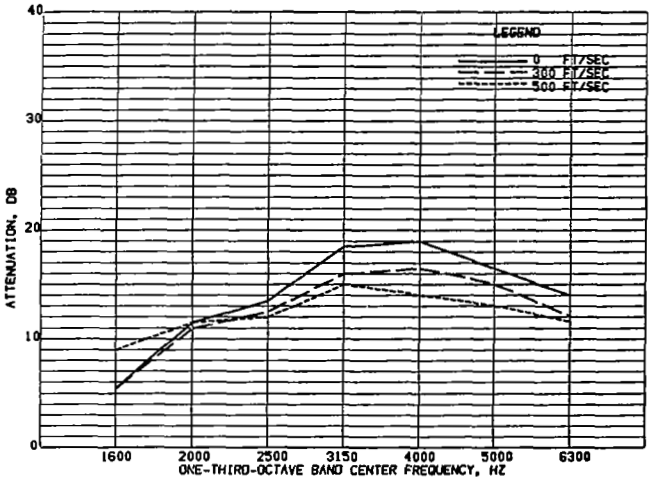

FIGURE 40.- EXHAUST MODE. EFFECT OF VELOCITY FOR CONFIGURATION R105

CONFIGURATION DESCRIPTION.- SURFACE NO 1=80 RAYL FM
CAVITY NO 1=0.25-IN DEEP
SURFACE NO 2=10 RAYL FM
CAVITY NO 2=0.25-IN DEEP

* FM=FIBERMETAL. FIBERGLASS HONEYCOMB CORE WAS 0.75-IN. TREATMENT LENGTH WAS 22.5-IN. AND BEGAN AT INLET PLANE. SURFACE AND CAVITY NO 1 IS NEXT TO AIRFLOW. SURFACE AND CAVITY NO 2 IS NEXT TO OUTER DUCT WALL.

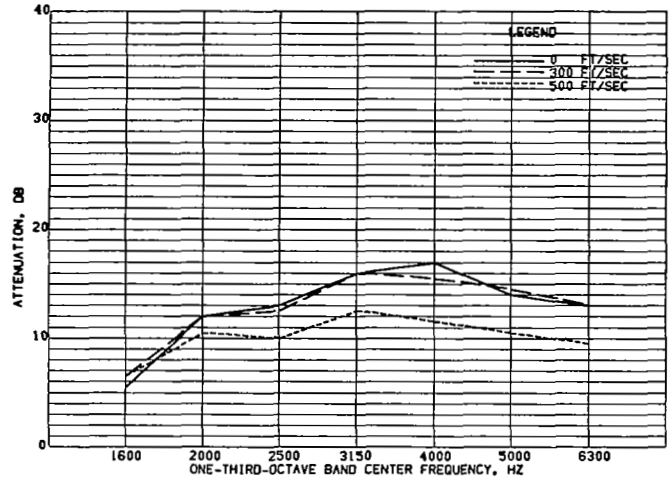

FIGURE 41.- EXHAUST MODE. EFFECT OF VELOCITY FOR CONFIGURATION R106

CONFIGURATION DESCRIPTION.- SURFACE NO 1=80 RAYL FM
CAVITY NO 1=0.25-IN DEEP
SURFACE NO 2=40 RAYL FM
CAVITY NO 2=0.25-IN DEEP

* FM=FIBERMETAL. FIBERGLASS HONEYCOMB CORE WAS 0.75-IN. TREATMENT LENGTH WAS 22.5-IN. AND BEGAN AT INLET PLANE. SURFACE AND CAVITY NO 1 IS NEXT TO AIRFLOW. SURFACE AND CAVITY NO 2 IS NEXT TO OUTER DUCT WALL.

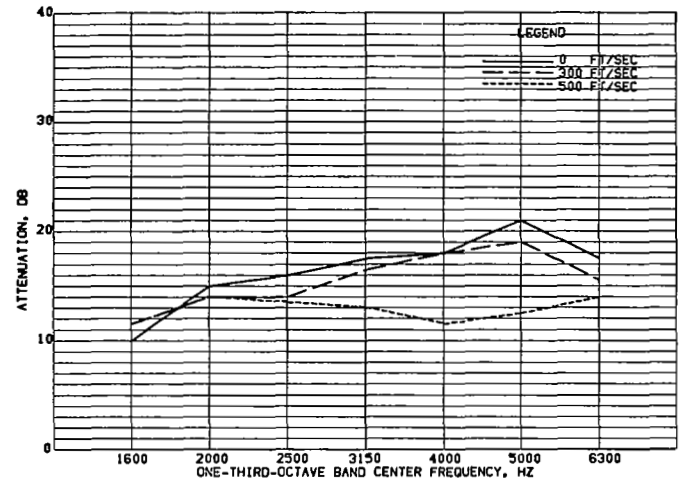

FIGURE 43.- EXHAUST MODE. EFFECT OF VELOCITY FOR CONFIGURATION R110

CONFIGURATION DESCRIPTION.- SURFACE NO 1=10 RAYL FM
CAVITY NO 1=0.25-IN DEEP
SURFACE NO 2=160 RAYL FM
CAVITY NO 2=0.5-IN DEEP

* FM=FIBERMETAL. FIBERGLASS HONEYCOMB CORE WAS 0.75-IN. TREATMENT LENGTH WAS 22.5-IN. AND BEGAN AT INLET PLANE. SURFACE AND CAVITY NO 1 IS NEXT TO AIRFLOW. SURFACE AND CAVITY NO 2 IS NEXT TO OUTER DUCT WALL.

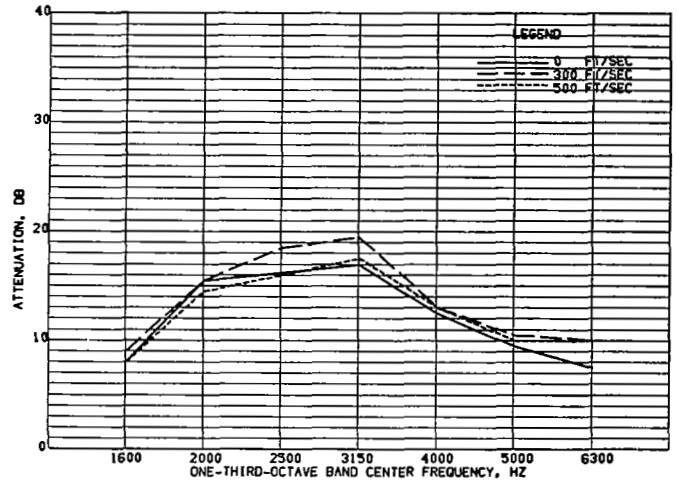

FIGURE 42.- EXHAUST MODE. EFFECT OF VELOCITY FOR CONFIGURATION R107

CONFIGURATION DESCRIPTION.- SURFACE NO 1=10 RAYL FM
CAVITY NO 1=0.25-IN DEEP
SURFACE NO 2=10 RAYL FM
CAVITY NO 2=0.5-IN DEEP

* FM=FIBERMETAL. FIBERGLASS HONEYCOMB CORE WAS 0.75-IN. TREATMENT LENGTH WAS 22.5-IN. AND BEGAN AT INLET PLANE. SURFACE AND CAVITY NO 1 IS NEXT TO AIRFLOW. SURFACE AND CAVITY NO 2 IS NEXT TO OUTER DUCT WALL.

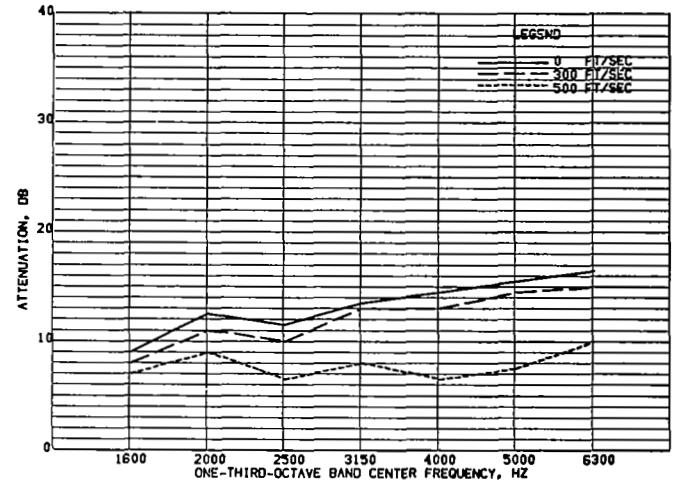

FIGURE 44.- EXHAUST MODE. EFFECT OF VELOCITY FOR CONFIGURATION R115

CONFIGURATION DESCRIPTION.- SURFACE NO 1=80 RAYL FM
CAVITY NO 1=0.25-IN DEEP
SURFACE NO 2=160 RAYL FM
CAVITY NO 2=0.5-IN DEEP

* FM=FIBERMETAL. FIBERGLASS HONEYCOMB CORE WAS 0.75-IN. TREATMENT LENGTH WAS 22.5-IN. AND BEGAN AT INLET PLANE. SURFACE AND CAVITY NO 1 IS NEXT TO AIRFLOW. SURFACE AND CAVITY NO 2 IS NEXT TO OUTER DUCT WALL.

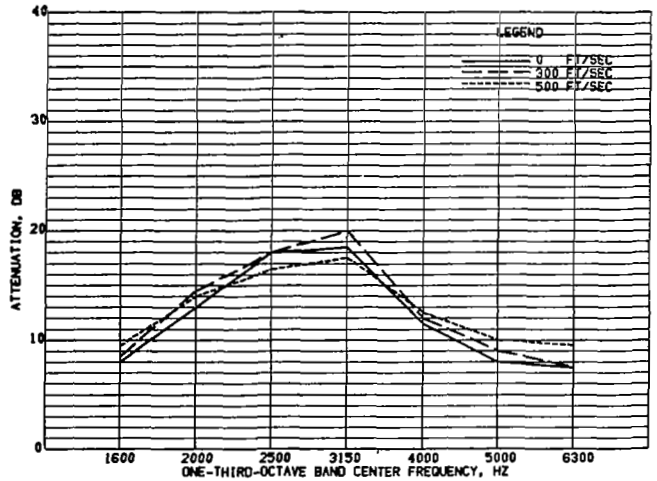

FIGURE 45.- EXHAUST MODE. EFFECT OF VELOCITY FOR CONFIGURATION R116

CONFIGURATION DESCRIPTION.- SURFACE NO 1=10 RAYL FM
CAVITY NO 1=0.5-IN DEEP
SURFACE NO 2=10 RAYL FM
CAVITY NO 2=0.25-IN DEEP

* FM=FIBERMETAL. FIBERGLASS HONEYCOMB CORE WAS 0.75-IN. TREATMENT LENGTH WAS 22.5-IN. AND BEGAN AT INLET PLANE. SURFACE AND CAVITY NO 1 IS NEXT TO AIRFLOW. SURFACE AND CAVITY NO 2 IS NEXT TO OUTER DUCT WALL.

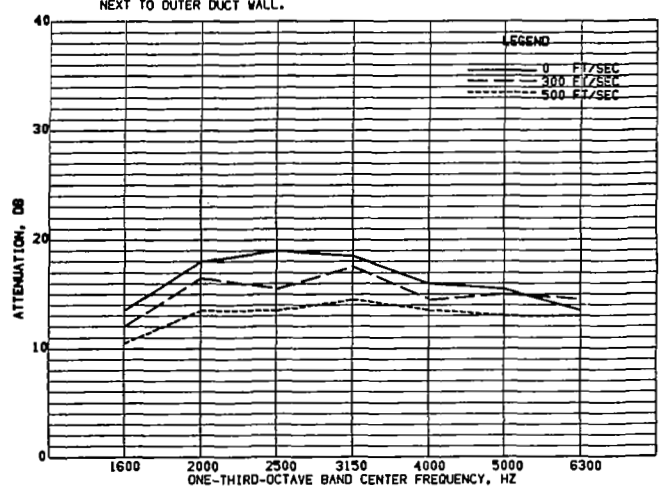

FIGURE 47.- EXHAUST MODE. EFFECT OF VELOCITY FOR CONFIGURATION R121

CONFIGURATION DESCRIPTION.- SURFACE NO 1=80 RAYL FM
CAVITY NO 1=0.5-IN DEEP
SURFACE NO 2=80 RAYL FM
CAVITY NO 2=0.25-IN DEEP

* FM=FIBERMETAL. FIBERGLASS HONEYCOMB CORE WAS 0.75-IN. TREATMENT LENGTH WAS 22.5-IN. AND BEGAN AT INLET PLANE. SURFACE AND CAVITY NO 1 IS NEXT TO AIRFLOW. SURFACE AND CAVITY NO 2 IS NEXT TO OUTER DUCT WALL.

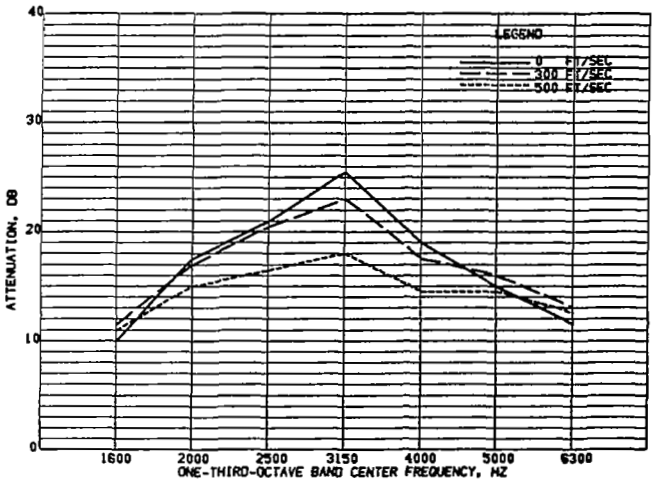

FIGURE 46.- EXHAUST MODE. EFFECT OF VELOCITY FOR CONFIGURATION R117

CONFIGURATION DESCRIPTION.- SURFACE NO 1=40 RAYL FM
CAVITY NO 1=0.5-IN DEEP
SURFACE NO 2=10 RAYL FM
CAVITY NO 2=0.25-IN DEEP

* FM=FIBERMETAL. FIBERGLASS HONEYCOMB CORE WAS 0.75-IN. TREATMENT LENGTH WAS 22.5-IN. AND BEGAN AT INLET PLANE. SURFACE AND CAVITY NO 1 IS NEXT TO AIRFLOW. SURFACE AND CAVITY NO 2 IS NEXT TO OUTER DUCT WALL.

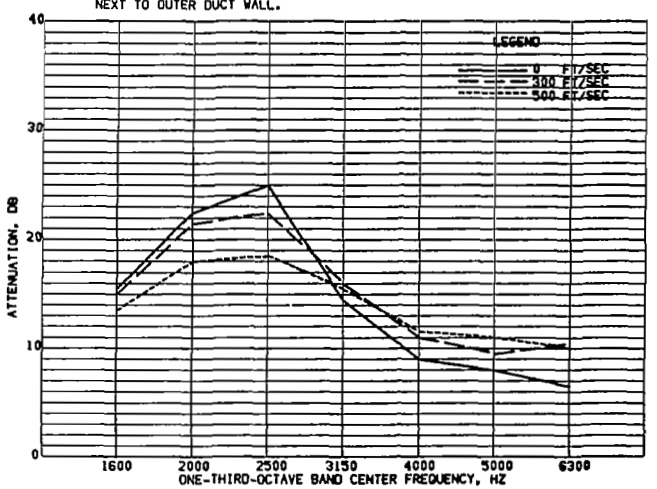

FIGURE 48.- EXHAUST MODE. EFFECT OF VELOCITY FOR CONFIGURATION R122

CONFIGURATION DESCRIPTION.- SURFACE NO 1=10 RAYL FM
CAVITY NO 1=0.25-IN DEEP
SURFACE NO 2=10 RAYL FM
CAVITY NO 2=0.75-IN DEEP

* FM=FIBERMETAL. FIBERGLASS HONEYCOMB CORE WAS 0.75-IN. TREATMENT LENGTH WAS 22.5-IN. AND BEGAN AT INLET PLANE. SURFACE AND CAVITY NO 1 IS NEXT TO AIRFLOW. SURFACE AND CAVITY NO 2 IS NEXT TO OUTER DUCT WALL.

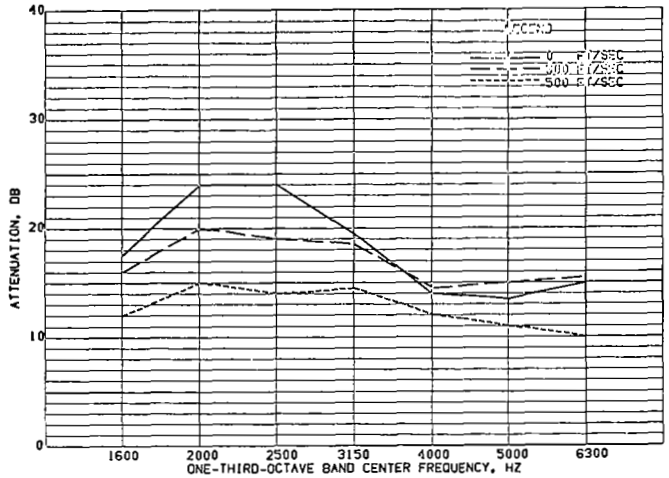

FIGURE 49.- EXHAUST MODE. EFFECT OF VELOCITY FOR CONFIGURATION R123

CONFIGURATION DESCRIPTION.- SURFACE NO 1=10 RAYL FM
CAVITY NO 1=0.25-IN DEEP
SURFACE NO 2=40 RAYL FM
CAVITY NO 2=0.75-IN DEEP

* FM=FIBERMETAL. FIBERGLASS HONEYCOMB CORE WAS 0.75-IN. TREATMENT LENGTH WAS 22.5-IN. AND BEGAN AT INLET PLANE. SURFACE AND CAVITY NO 1 IS NEXT TO AIRFLOW. SURFACE AND CAVITY NO 2 IS NEXT TO OUTER DUCT WALL.

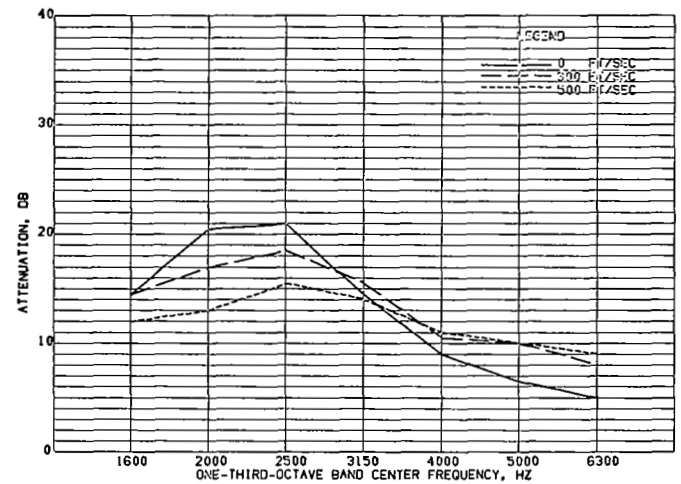

FIGURE 51.- EXHAUST MODE. EFFECT OF VELOCITY FOR CONFIGURATION R125

CONFIGURATION DESCRIPTION.- SURFACE NO 1=40 RAYL FM
CAVITY NO 1=0.25-IN DEEP
SURFACE NO 2=10 RAYL FM
CAVITY NO 2=0.75-IN DEEP

* FM=FIBERMETAL. FIBERGLASS HONEYCOMB CORE WAS 0.75-IN. TREATMENT LENGTH WAS 22.5-IN. AND BEGAN AT INLET PLANE. SURFACE AND CAVITY NO 1 IS NEXT TO AIRFLOW. SURFACE AND CAVITY NO 2 IS NEXT TO OUTER DUCT WALL.

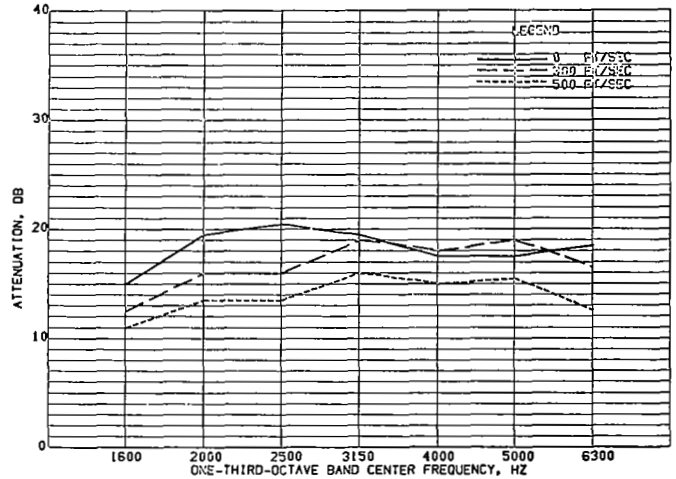

FIGURE 50.- EXHAUST MODE. EFFECT OF VELOCITY FOR CONFIGURATION R124

CONFIGURATION DESCRIPTION.- SURFACE NO 1=10 RAYL FM
CAVITY NO 1=0.25-IN DEEP
SURFACE NO 2=80 RAYL FM
CAVITY NO 2=0.75-IN DEEP

* FM=FIBERMETAL. FIBERGLASS HONEYCOMB CORE WAS 0.75-IN. TREATMENT LENGTH WAS 22.5-IN. AND BEGAN AT INLET PLANE. SURFACE AND CAVITY NO 1 IS NEXT TO AIRFLOW. SURFACE AND CAVITY NO 2 IS NEXT TO OUTER DUCT WALL.

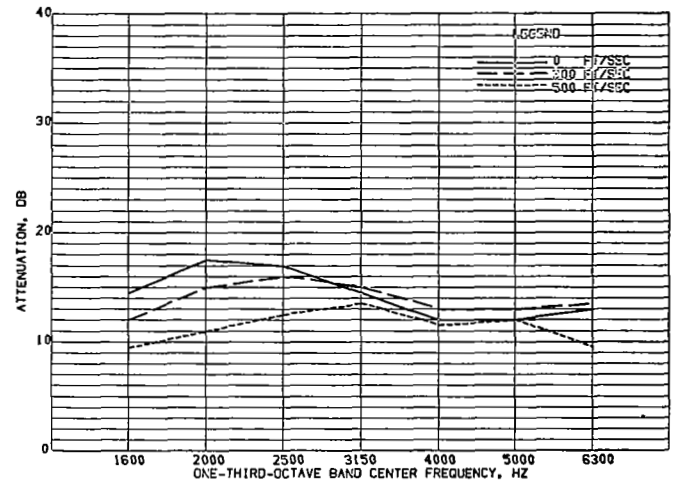

FIGURE 52.- EXHAUST MODE. EFFECT OF VELOCITY FOR CONFIGURATION R126

CONFIGURATION DESCRIPTION.- SURFACE NO 1=40 RAYL FM
CAVITY NO 1=0.25-IN DEEP
SURFACE NO 2=40 RAYL FM
CAVITY NO 2=0.75-IN DEEP

* FM=FIBERMETAL. FIBERGLASS HONEYCOMB CORE WAS 0.75-IN. TREATMENT LENGTH WAS 22.5-IN. AND BEGAN AT INLET PLANE. SURFACE AND CAVITY NO 1 IS NEXT TO AIRFLOW. SURFACE AND CAVITY NO 2 IS NEXT TO OUTER DUCT WALL.

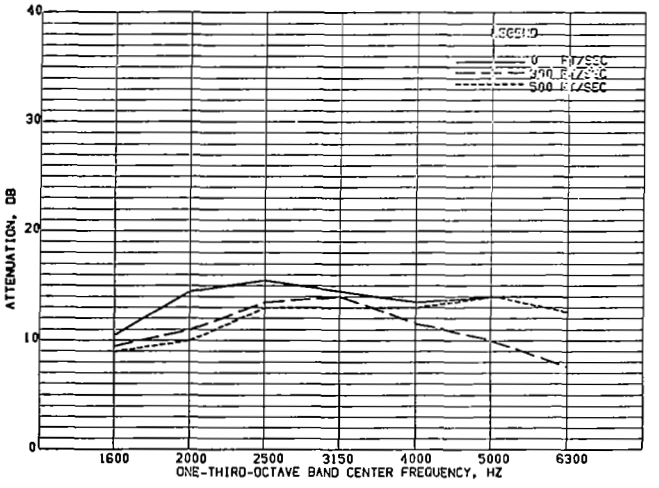

FIGURE 53.- EXHAUST MODE. EFFECT OF VELOCITY FOR CONFIGURATION R127

CONFIGURATION DESCRIPTION.- SURFACE NO 1=40 RAYL FM
CAVITY NO 1=0.25-IN DEEP
SURFACE NO 2=80 RAYL FM
CAVITY NO 2=0.75-IN DEEP

* FM=FIBERMETAL. FIBERGLASS HONEYCOMB CORE WAS 0.75-IN. TREATMENT LENGTH WAS 22.5-IN. AND BEGAN AT INLET PLANE. SURFACE AND CAVITY NO 1 IS NEXT TO AIRFLOW. SURFACE AND CAVITY NO 2 IS NEXT TO OUTER DUCT WALL.

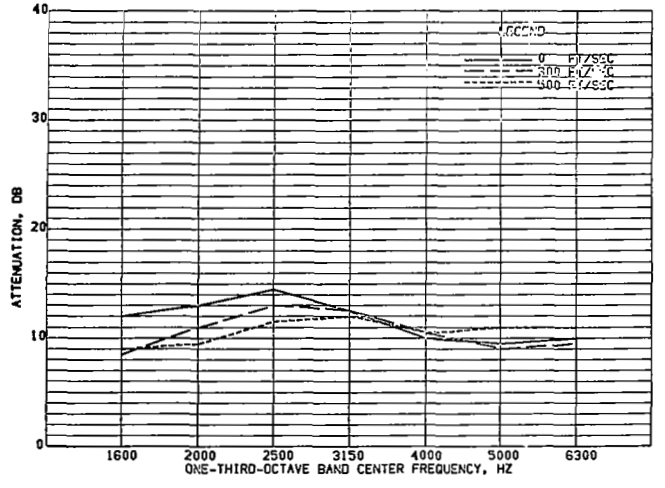

FIGURE 55.- EXHAUST MODE. EFFECT OF VELOCITY FOR CONFIGURATION R129

CONFIGURATION DESCRIPTION.- SURFACE NO 1=80 RAYL FM
CAVITY NO 1=0.25-IN DEEP
SURFACE NO 2=40 RAYL FM
CAVITY NO 2=0.75-IN DEEP

* FM=FIBERMETAL. FIBERGLASS HONEYCOMB CORE WAS 0.75-IN. TREATMENT LENGTH WAS 22.5-IN. AND BEGAN AT INLET PLANE. SURFACE AND CAVITY NO 1 IS NEXT TO AIRFLOW. SURFACE AND CAVITY NO 2 IS NEXT TO OUTER DUCT WALL.

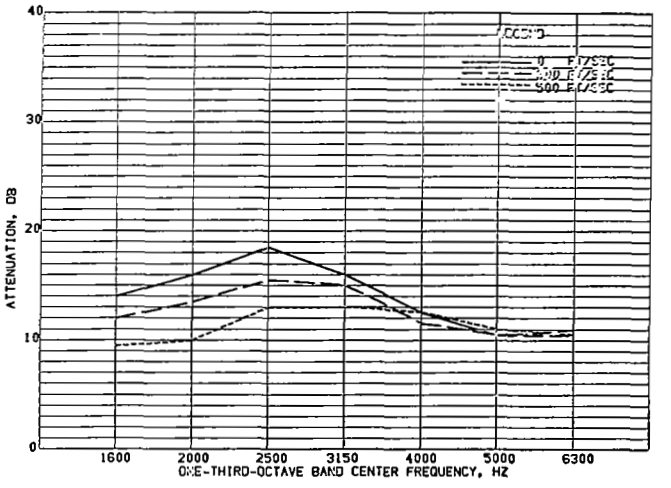

FIGURE 54.- EXHAUST MODE. EFFECT OF VELOCITY FOR CONFIGURATION R128

CONFIGURATION DESCRIPTION.- SURFACE NO 1=80 RAYL FM
CAVITY NO 1=0.25-IN DEEP
SURFACE NO 2=10 RAYL FM
CAVITY NO 2=0.75-IN DEEP

* FM=FIBERMETAL. FIBERGLASS HONEYCOMB CORE WAS 0.75-IN. TREATMENT LENGTH WAS 22.5-IN. AND BEGAN AT INLET PLANE. SURFACE AND CAVITY NO 1 IS NEXT TO AIRFLOW. SURFACE AND CAVITY NO 2 IS NEXT TO OUTER DUCT WALL.

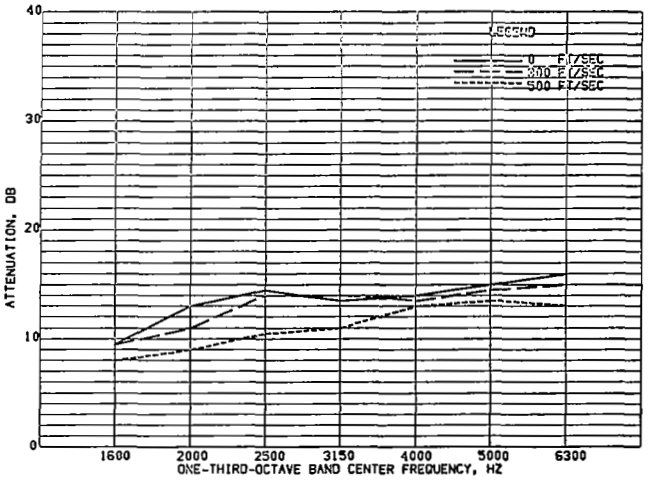

FIGURE 56.- EXHAUST MODE. EFFECT OF VELOCITY FOR CONFIGURATION R130

CONFIGURATION DESCRIPTION.- SURFACE NO 1=80 RAYL FM
CAVITY NO 1=0.25-IN DEEP
SURFACE NO 2=80 RAYL FM
CAVITY NO 2=0.75-IN DEEP

* FM=FIBERMETAL. FIBERGLASS HONEYCOMB CORE WAS 0.75-IN. TREATMENT LENGTH WAS 22.5-IN. AND BEGAN AT INLET PLANE. SURFACE AND CAVITY NO 1 IS NEXT TO AIRFLOW. SURFACE AND CAVITY NO 2 IS NEXT TO OUTER DUCT WALL.

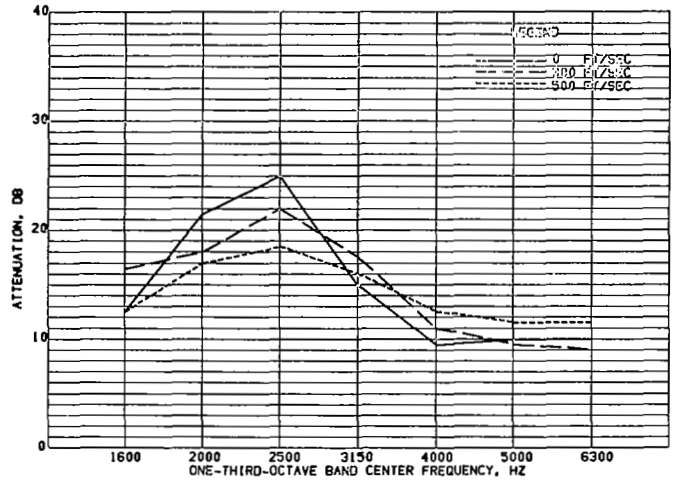

FIGURE 57.- EXHAUST MODE. EFFECT OF VELOCITY FOR CONFIGURATION R131

CONFIGURATION DESCRIPTION.- SURFACE NO 1=10 RAYL FM
CAVITY NO 1=0.5-IN DEEP
SURFACE NO 2=10 RAYL FM
CAVITY NO 2=0.5-IN DEEP

* FM=FIBERMETAL. FIBERGLASS HONEYCOMB CORE WAS 0.75-IN. TREATMENT LENGTH WAS 22.5-IN. AND BEGAN AT INLET PLANE. SURFACE AND CAVITY NO 1 IS NEXT TO AIRFLOW. SURFACE AND CAVITY NO 2 IS NEXT TO OUTER DUCT WALL.

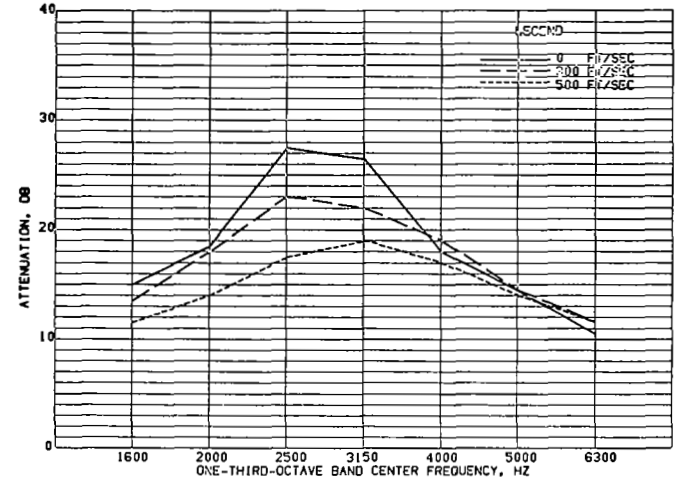

FIGURE 59.- EXHAUST MODE. EFFECT OF VELOCITY FOR CONFIGURATION R133

CONFIGURATION DESCRIPTION.- SURFACE NO 1=10 RAYL FM
CAVITY NO 1=0.5-IN DEEP
SURFACE NO 2=80 RAYL FM
CAVITY NO 2=0.5-IN DEEP

* FM=FIBERMETAL. FIBERGLASS HONEYCOMB CORE WAS 0.75-IN. TREATMENT LENGTH WAS 22.5-IN. AND BEGAN AT INLET PLANE. SURFACE AND CAVITY NO 1 IS NEXT TO AIRFLOW. SURFACE AND CAVITY NO 2 IS NEXT TO OUTER DUCT WALL.

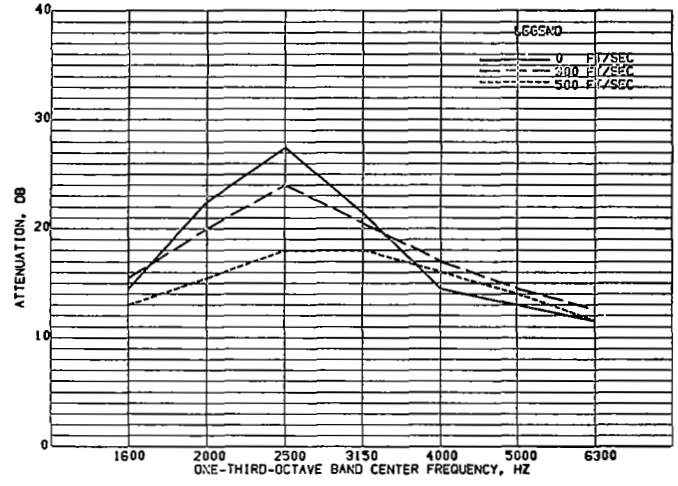

FIGURE 58.- EXHAUST MODE. EFFECT OF VELOCITY FOR CONFIGURATION R132

CONFIGURATION DESCRIPTION.- SURFACE NO 1=10 RAYL FM
CAVITY NO 1=0.5-IN DEEP
SURFACE NO 2=40 RAYL FM
CAVITY NO 2=0.5-IN DEEP

* FM=FIBERMETAL. FIBERGLASS HONEYCOMB CORE WAS 0.75-IN. TREATMENT LENGTH WAS 22.5-IN. AND BEGAN AT INLET PLANE. SURFACE AND CAVITY NO 1 IS NEXT TO AIRFLOW. SURFACE AND CAVITY NO 2 IS NEXT TO OUTER DUCT WALL.

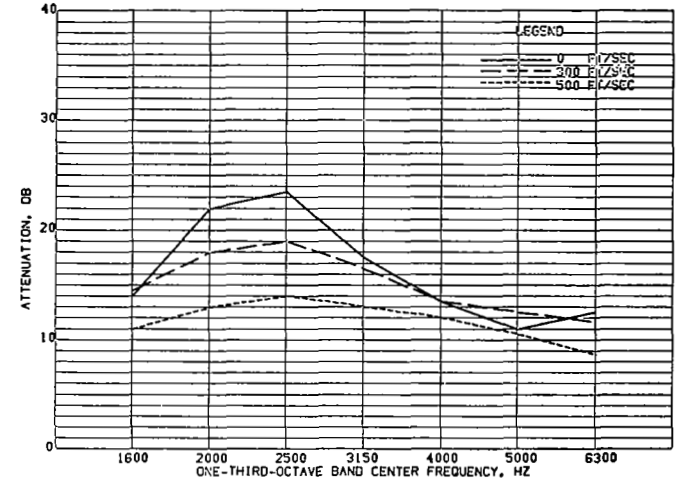

FIGURE 60.- EXHAUST MODE. EFFECT OF VELOCITY FOR CONFIGURATION R134

CONFIGURATION DESCRIPTION.- SURFACE NO 1=40 RAYL FM
CAVITY NO 1=0.5-IN DEEP
SURFACE NO 2=10 RAYL FM
CAVITY NO 2=0.5-IN DEEP

* FM=FIBERMETAL. FIBERGLASS HONEYCOMB CORE WAS 0.75-IN. TREATMENT LENGTH WAS 22.5-IN. AND BEGAN AT INLET PLANE. SURFACE AND CAVITY NO 1 IS NEXT TO AIRFLOW. SURFACE AND CAVITY NO 2 IS NEXT TO OUTER DUCT WALL.

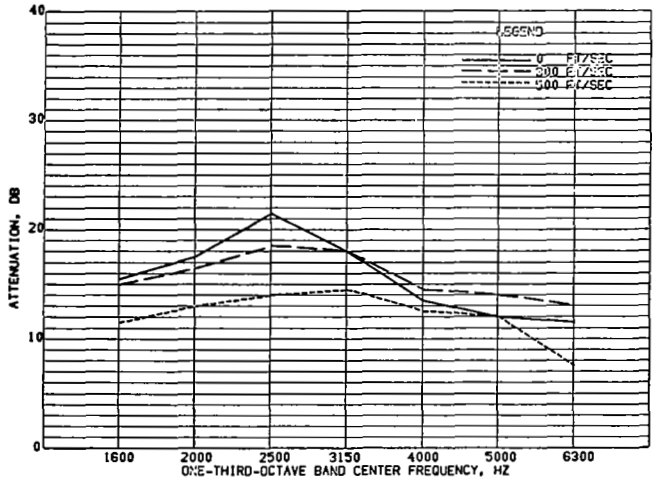

FIGURE 61.- EXHAUST MODE. EFFECT OF VELOCITY FOR CONFIGURATION R135

CONFIGURATION DESCRIPTION.- SURFACE NO 1=40 RAYL FM
CAVITY NO 1=0.5-IN DEEP
SURFACE NO 2=40 RAYL FM
CAVITY NO 2=0.5-IN DEEP

* FM=FIBERMETAL. FIBERGLASS HONEYCOMB CORE WAS 0.75-IN. TREATMENT LENGTH WAS 22.5-IN. AND BEGAN AT INLET PLANE. SURFACE AND CAVITY NO 1 IS NEXT TO AIRFLOW. SURFACE AND CAVITY NO 2 IS NEXT TO OUTER DUCT WALL.

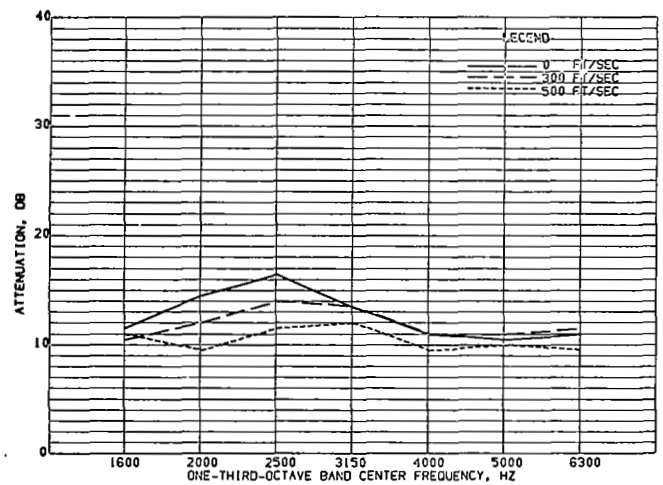

FIGURE 63.- EXHAUST MODE. EFFECT OF VELOCITY FOR CONFIGURATION R137

CONFIGURATION DESCRIPTION.- SURFACE NO 1=80 RAYL FM
CAVITY NO 1=0.5-IN DEEP
SURFACE NO 2=10 RAYL FM
CAVITY NO 2=0.5-IN DEEP

* FM=FIBERMETAL. FIBERGLASS HONEYCOMB CORE WAS 0.75-IN. TREATMENT LENGTH WAS 22.5-IN. AND BEGAN AT INLET PLANE. SURFACE AND CAVITY NO 1 IS NEXT TO AIRFLOW. SURFACE AND CAVITY NO 2 IS NEXT TO OUTER DUCT WALL.

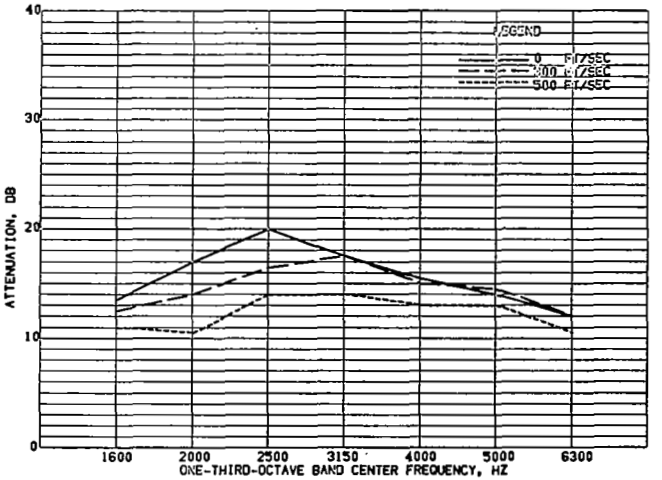

FIGURE 62.- EXHAUST MODE. EFFECT OF VELOCITY FOR CONFIGURATION R136

CONFIGURATION DESCRIPTION.- SURFACE NO 1=40 RAYL FM
CAVITY NO 1=0.5-IN DEEP
SURFACE NO 2=80 RAYL FM
CAVITY NO 2=0.5-IN DEEP

* FM=FIBERMETAL. FIBERGLASS HONEYCOMB CORE WAS 0.75-IN. TREATMENT LENGTH WAS 22.5-IN. AND BEGAN AT INLET PLANE. SURFACE AND CAVITY NO 1 IS NEXT TO AIRFLOW. SURFACE AND CAVITY NO 2 IS NEXT TO OUTER DUCT WALL.

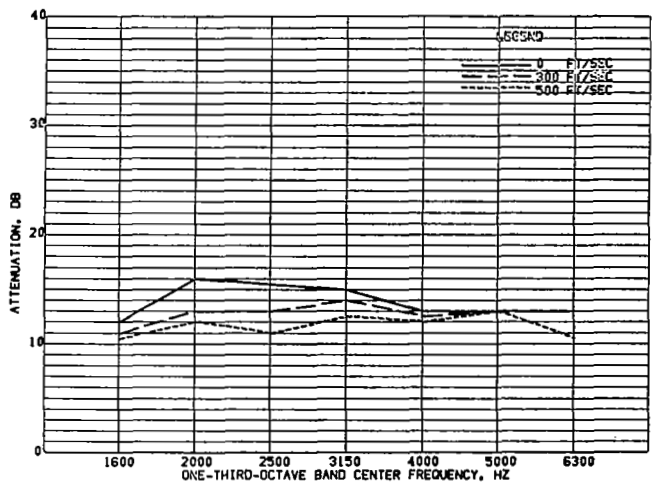

FIGURE 64.- EXHAUST MODE. EFFECT OF VELOCITY FOR CONFIGURATION R138

CONFIGURATION DESCRIPTION.- SURFACE NO 1=80 RAYL FM
CAVITY NO 1=0.5-IN DEEP
SURFACE NO 2=40 RAYL FM
CAVITY NO 2=0.5-IN DEEP

* FM=FIBERMETAL. FIBERGLASS HONEYCOMB CORE WAS 0.75-IN. TREATMENT LENGTH WAS 22.5-IN. AND BEGAN AT INLET PLANE. SURFACE AND CAVITY NO 1 IS NEXT TO AIRFLOW. SURFACE AND CAVITY NO 2 IS NEXT TO OUTER DUCT WALL.

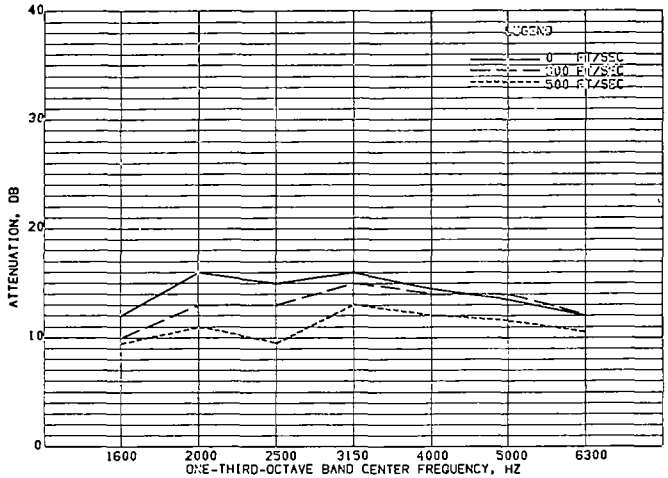

FIGURE 65.- EXHAUST MODE. EFFECT OF VELOCITY FOR CONFIGURATION R139

CONFIGURATION DESCRIPTION.- *SURFACE NO 1=80 RAYL FM*
CAVITY NO 1=0.5-IN DEEP
SURFACE NO 2=80 RAYL FM
CAVITY NO 2=0.5-IN DEEP

• FM=FIBERMETAL. FIBERGLASS HONEYCOMB CORE WAS 0.75-IN. TREATMENT LENGTH WAS 22.5-IN. AND BEGAN AT INLET PLANE. SURFACE AND CAVITY NO 1 IS NEXT TO AIRFLOW. SURFACE AND CAVITY NO 2 IS NEXT TO OUTER DUCT WALL.

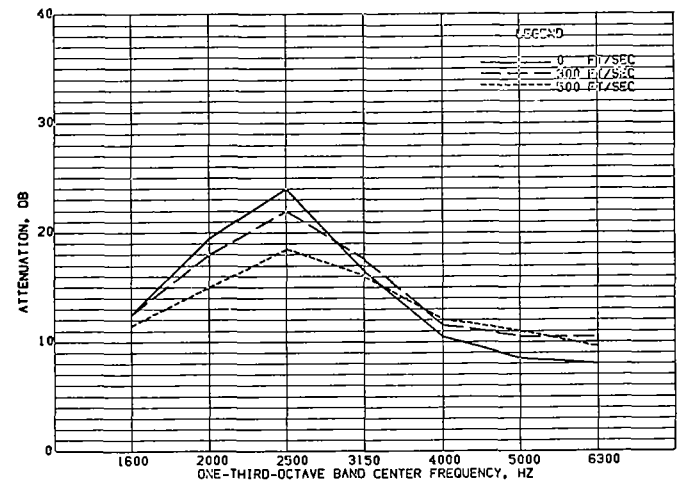

FIGURE 67.- EXHAUST MODE. EFFECT OF VELOCITY FOR CONFIGURATION R141

CONFIGURATION DESCRIPTION.- SURFACE NO 1=10 RAYL FM
CAVITY NO 1=0.75-IN DEEP
SURFACE NO 2=40 RAYL FM
CAVITY NO 2=0.25-IN DEEP

• FM=FIBERMETAL. FIBERGLASS HONEYCOMB CORE WAS 0.75-IN. TREATMENT LENGTH WAS 22.5-IN. AND BEGAN AT INLET PLANE. SURFACE AND CAVITY NO 1 IS NEXT TO AIRFLOW. SURFACE AND CAVITY NO 2 IS NEXT TO OUTER DUCT WALL.

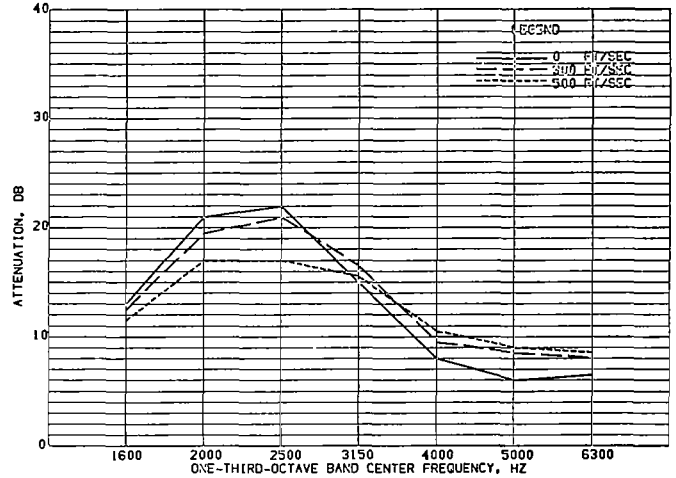

FIGURE 66.- EXHAUST MODE. EFFECT OF VELOCITY FOR CONFIGURATION R140

CONFIGURATION DESCRIPTION.- SURFACE NO 1=10 RAYL FM
CAVITY NO 1=0.75-IN DEEP
SURFACE NO 2=10 RAYL FM
CAVITY NO 2=0.25-IN DEEP

• FM=FIBERMETAL. FIBERGLASS HONEYCOMB CORE WAS 0.75-IN. TREATMENT LENGTH WAS 22.5-IN. AND BEGAN AT INLET PLANE. SURFACE AND CAVITY NO 1 IS NEXT TO AIRFLOW. SURFACE AND CAVITY NO 2 IS NEXT TO OUTER DUCT WALL.

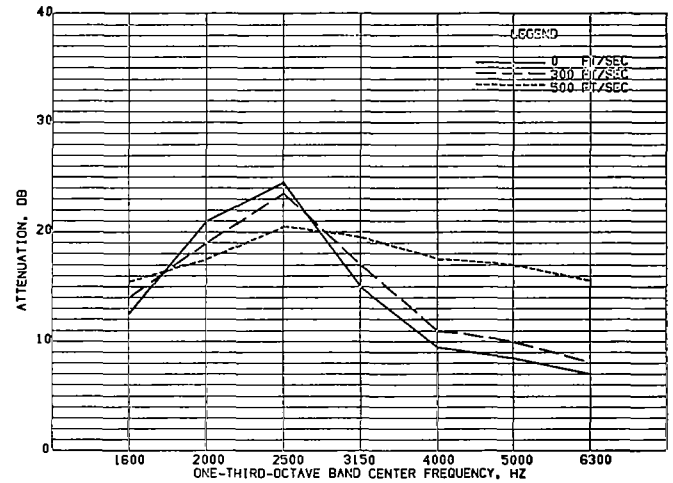

FIGURE 68.- EXHAUST MODE. EFFECT OF VELOCITY FOR CONFIGURATION R142

CONFIGURATION DESCRIPTION.- SURFACE NO 1=10 RAYL FM
CAVITY NO 1=0.75-IN DEEP
SURFACE NO 2=80 RAYL FM
CAVITY NO 2=0.25-IN DEEP

• FM=FIBERMETAL. FIBERGLASS HONEYCOMB CORE WAS 0.75-IN. TREATMENT LENGTH WAS 22.5-IN. AND BEGAN AT INLET PLANE. SURFACE AND CAVITY NO 1 IS NEXT TO AIRFLOW. SURFACE AND CAVITY NO 2 IS NEXT TO OUTER DUCT WALL.

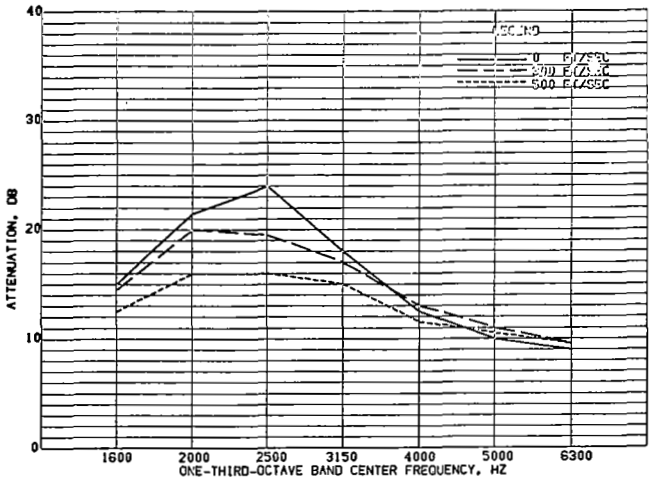

FIGURE 69.- EXHAUST MODE. EFFECT OF VELOCITY FOR CONFIGURATION R143

CONFIGURATION DESCRIPTION.- SURFACE NO 1=40 RAYL FM
CAVITY NO 1=0.75-IN DEEP
SURFACE NO 2=10 RAYL FM
CAVITY NO 2=0.25-IN DEEP

* FM=FIBERMETAL. FIBERGLASS HONEYCOMB CORE WAS 0.75-IN. TREATMENT LENGTH WAS 22.5-IN. AND BEGAN AT INLET PLANE. SURFACE AND CAVITY NO 1 IS NEXT TO AIRFLOW. SURFACE AND CAVITY NO 2 IS NEXT TO OUTER DUCT WALL.

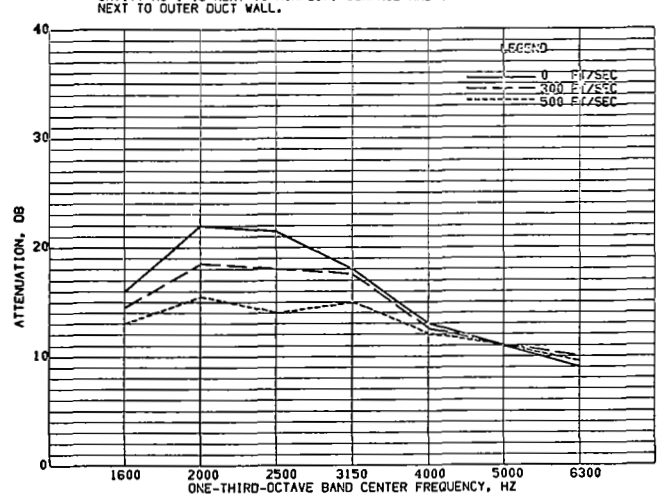

FIGURE 71.- EXHAUST MODE. EFFECT OF VELOCITY FOR CONFIGURATION R145

CONFIGURATION DESCRIPTION.- SURFACE NO 1=40 RAYL FM
CAVITY NO 1=0.75-IN DEEP
SURFACE NO 2=80 RAYL FM
CAVITY NO 2=0.25-IN DEEP

* FM=FIBERMETAL. FIBERGLASS HONEYCOMB CORE WAS 0.75-IN. TREATMENT LENGTH WAS 22.5-IN. AND BEGAN AT INLET PLANE. SURFACE AND CAVITY NO 1 IS NEXT TO AIRFLOW. SURFACE AND CAVITY NO 2 IS NEXT TO OUTER DUCT WALL.

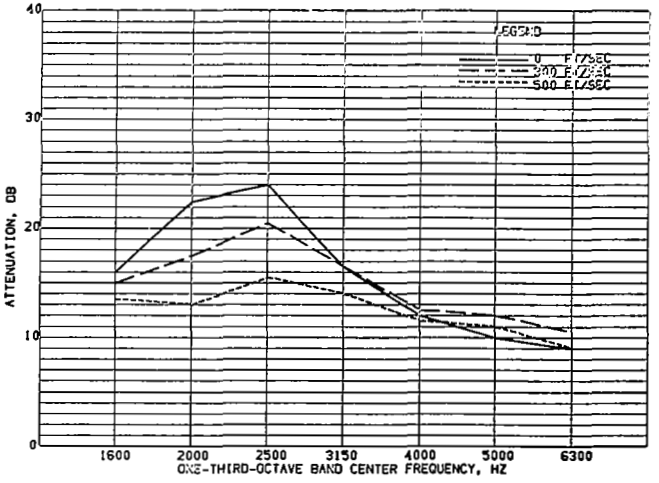

FIGURE 70.- EXHAUST MODE. EFFECT OF VELOCITY FOR CONFIGURATION R144

CONFIGURATION DESCRIPTION.- SURFACE NO 1=40 RAYL FM
CAVITY NO 1=0.75-IN DEEP
SURFACE NO 2=40 RAYL FM
CAVITY NO 2=0.25-IN DEEP

* FM=FIBERMETAL. FIBERGLASS HONEYCOMB CORE WAS 0.75-IN. TREATMENT LENGTH WAS 22.5-IN. AND BEGAN AT INLET PLANE. SURFACE AND CAVITY NO 1 IS NEXT TO AIRFLOW. SURFACE AND CAVITY NO 2 IS NEXT TO OUTER DUCT WALL.

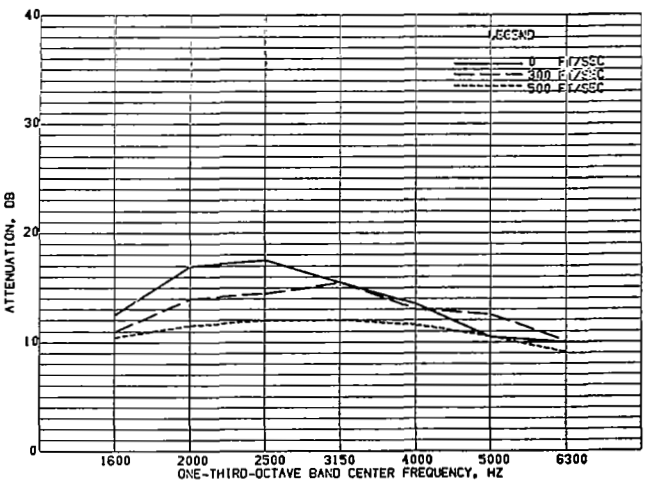

FIGURE 72.- EXHAUST MODE. EFFECT OF VELOCITY FOR CONFIGURATION R146

CONFIGURATION DESCRIPTION.- SURFACE NO 1=80 RAYL FM
CAVITY NO 1=0.75-IN DEEP
SURFACE NO 2=10 RAYL FM
CAVITY NO 2=0.25-IN DEEP

* FM=FIBERMETAL. FIBERGLASS HONEYCOMB CORE WAS 0.75-IN. TREATMENT LENGTH WAS 22.5-IN. AND BEGAN AT INLET PLANE. SURFACE AND CAVITY NO 1 IS NEXT TO AIRFLOW. SURFACE AND CAVITY NO 2 IS NEXT TO OUTER DUCT WALL.

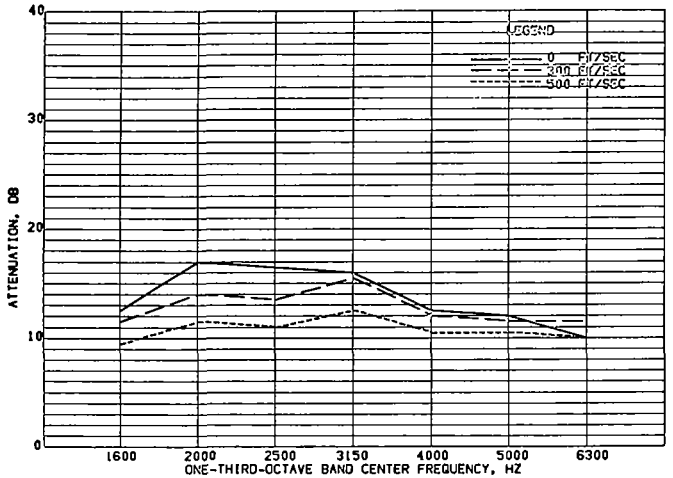

FIGURE 73.- EXHAUST MODE. EFFECT OF VELOCITY FOR CONFIGURATION R147

CONFIGURATION DESCRIPTION.- SURFACE NO 1=80 RAYL FM
CAVITY NO 1=0.75-IN DEEP
SURFACE NO 2=40 RAYL FM
CAVITY NO 2=0.25-IN DEEP

* FM=FIBERMETAL. FIBERGLASS HONEYCOMB CORE WAS 0.75-IN. TREATMENT LENGTH WAS 22.5-IN. AND BEGAN AT INLET PLANE. SURFACE AND CAVITY NO 1 IS NEXT TO AIRFLOW. SURFACE AND CAVITY NO 2 IS NEXT TO OUTER DUCT WALL.

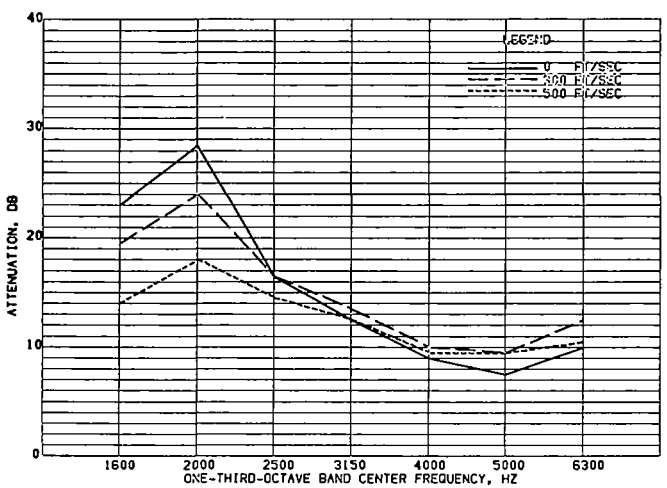

FIGURE 75.- EXHAUST MODE. EFFECT OF VELOCITY FOR CONFIGURATION R155

CONFIGURATION DESCRIPTION.- SURFACE NO 1=10 RAYL FM
CAVITY NO 1=0.25-IN DEEP
SURFACE NO 2=10 RAYL FM
CAVITY NO 2=1.0-IN DEEP

* FM=FIBERMETAL. FIBERGLASS HONEYCOMB CORE WAS 0.75-IN. TREATMENT LENGTH WAS 22.5-IN. AND BEGAN AT INLET PLANE. SURFACE AND CAVITY NO 1 IS NEXT TO AIRFLOW. SURFACE AND CAVITY NO 2 IS NEXT TO OUTER DUCT WALL.

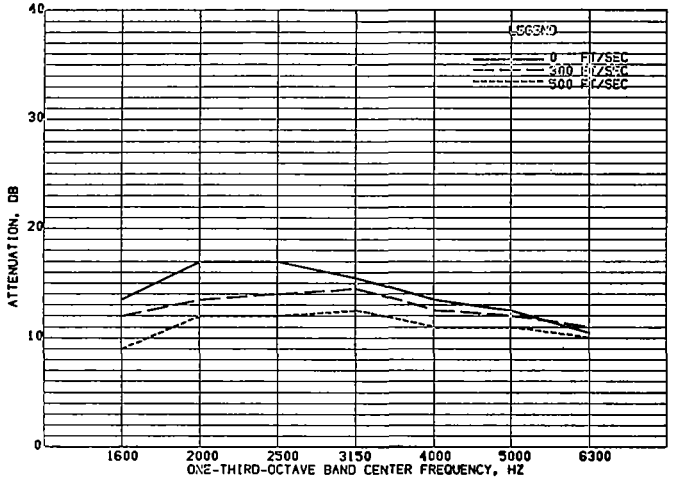

FIGURE 74.- EXHAUST MODE. EFFECT OF VELOCITY FOR CONFIGURATION R148

CONFIGURATION DESCRIPTION.- SURFACE NO 1=80 RAYL FM
CAVITY NO 1=0.75-IN DEEP
SURFACE NO 2=80 RAYL FM
CAVITY NO 2=0.25-IN DEEP

* FM=FIBERMETAL. FIBERGLASS HONEYCOMB CORE WAS 0.75-IN. TREATMENT LENGTH WAS 22.5-IN. AND BEGAN AT INLET PLANE. SURFACE AND CAVITY NO 1 IS NEXT TO AIRFLOW. SURFACE AND CAVITY NO 2 IS NEXT TO OUTER DUCT WALL.

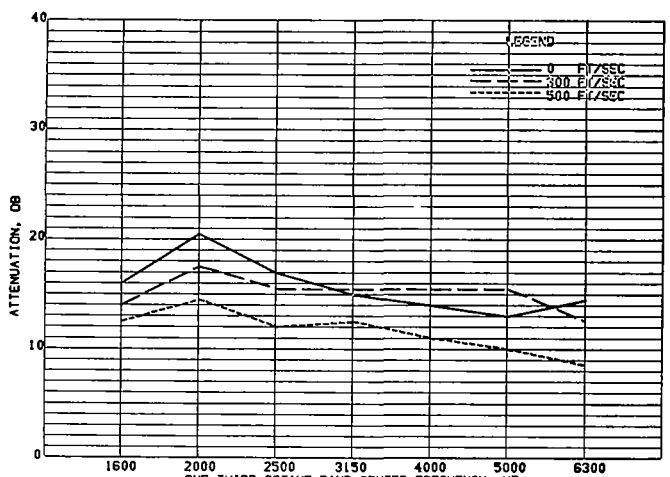

FIGURE 76.- EXHAUST MODE. EFFECT OF VELOCITY FOR CONFIGURATION R158

CONFIGURATION DESCRIPTION.- SURFACE NO 1=10 RAYL FM
CAVITY NO 1=0.25-IN DEEP
SURFACE NO 2=80 RAYL FM
CAVITY NO 2=1.0-IN DEEP

* FM=FIBERMETAL. FIBERGLASS HONEYCOMB CORE WAS 0.75-IN. TREATMENT LENGTH WAS 22.5-IN. AND BEGAN AT INLET PLANE. SURFACE AND CAVITY NO 1 IS NEXT TO AIRFLOW. SURFACE AND CAVITY NO 2 IS NEXT TO OUTER DUCT WALL.

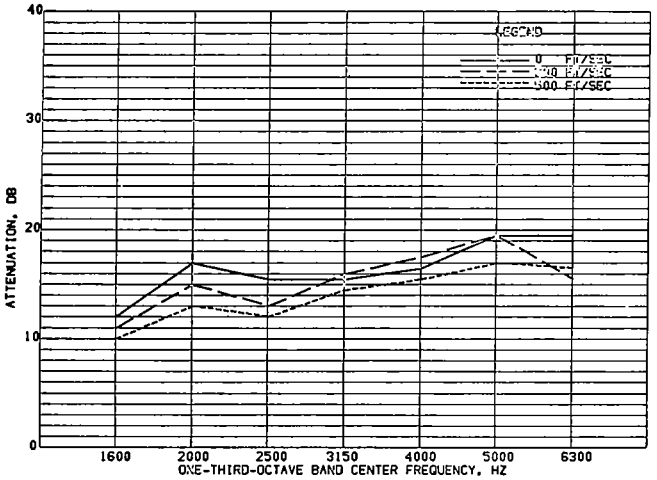

FIGURE 77.- EXHAUST MODE. EFFECT OF VELOCITY FOR CONFIGURATION R159

CONFIGURATION DESCRIPTION.- SURFACE NO 1=10 RAYL FM
CAVITY NO 1=0.25-IN DEEP
SURFACE NO 2=160 RAYL FM
CAVITY NO 2=1.0-IN DEEP

• FM=FIBERMETAL. FIBERGLASS HONEYCOMB CORE WAS 0.75-IN. TREATMENT LENGTH WAS 22.5-IN. AND BEGAN AT INLET PLANE. SURFACE AND CAVITY NO 1 IS NEXT TO AIRFLOW. SURFACE AND CAVITY NO 2 IS NEXT TO OUTER DUCT WALL.

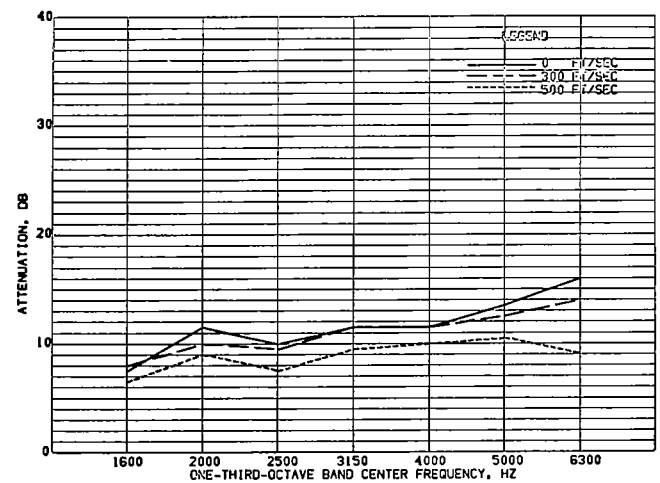

FIGURE 79.- EXHAUST MODE. EFFECT OF VELOCITY FOR CONFIGURATION R169

CONFIGURATION DESCRIPTION.- SURFACE NO 1=80 RAYL FM
CAVITY NO 1=0.25-IN DEEP
SURFACE NO 2=160 RAYL FM
CAVITY NO 2=1.0-IN DEEP

• FM=FIBERMETAL. FIBERGLASS HONEYCOMB CORE WAS 0.75-IN. TREATMENT LENGTH WAS 22.5-IN. AND BEGAN AT INLET PLANE. SURFACE AND CAVITY NO 1 IS NEXT TO AIRFLOW. SURFACE AND CAVITY NO 2 IS NEXT TO OUTER DUCT WALL.

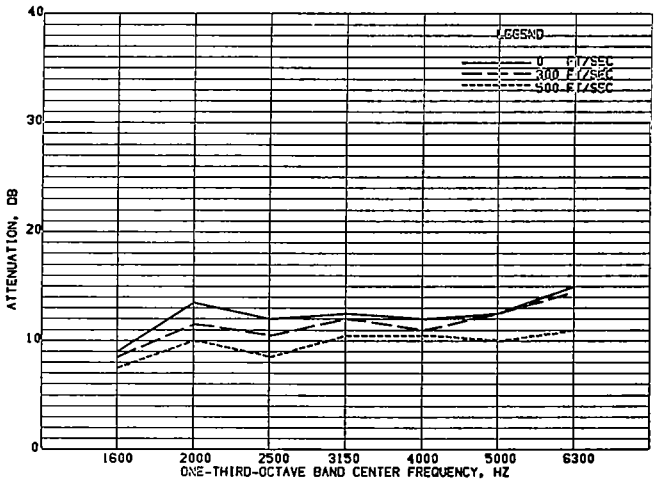

FIGURE 78.- EXHAUST MODE. EFFECT OF VELOCITY FOR CONFIGURATION R168

CONFIGURATION DESCRIPTION.- SURFACE NO 1=80 RAYL FM
CAVITY NO 1=0.25-IN DEEP
SURFACE NO 2=80 RAYL FM
CAVITY NO 2=1.0-IN DEEP

• FM=FIBERMETAL. FIBERGLASS HONEYCOMB CORE WAS 0.75-IN. TREATMENT LENGTH WAS 22.5-IN. AND BEGAN AT INLET PLANE. SURFACE AND CAVITY NO 1 IS NEXT TO AIRFLOW. SURFACE AND CAVITY NO 2 IS NEXT TO OUTER DUCT WALL.

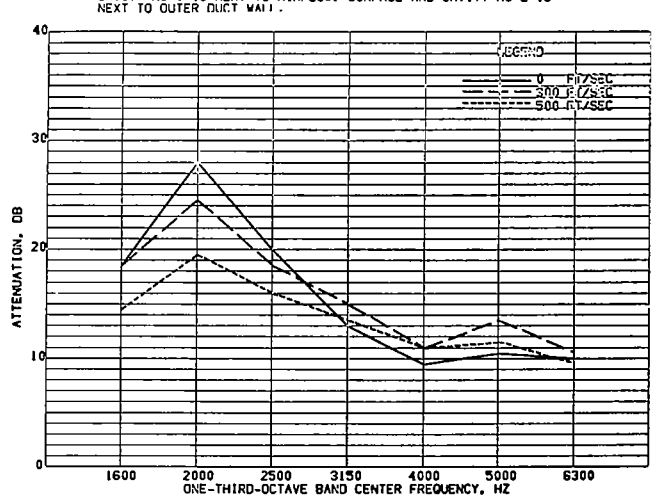

FIGURE 80.- EXHAUST MODE. EFFECT OF VELOCITY FOR CONFIGURATION R179

CONFIGURATION DESCRIPTION.- SURFACE NO 1=10 RAYL FM
CAVITY NO 1=0.75-IN DEEP
SURFACE NO 2=10 RAYL FM
CAVITY NO 2=0.5-IN DEEP

• FM=FIBERMETAL. FIBERGLASS HONEYCOMB CORE WAS 0.75-IN. TREATMENT LENGTH WAS 22.5-IN. AND BEGAN AT INLET PLANE. SURFACE AND CAVITY NO 1 IS NEXT TO AIRFLOW. SURFACE AND CAVITY NO 2 IS NEXT TO OUTER DUCT WALL.

FIGURE 81.- EXHAUST MODE. EFFECT OF VELOCITY FOR CONFIGURATION R185

CONFIGURATION DESCRIPTION.- SURFACE NO 1=10 RAYL FM
CAVITY NO 1=0.75-IN DEEP
SURFACE NO 2=80 RAYL FM
CAVITY NO 2=0.5-IN DEEP

* FM=FIBERMETAL. FIBERGLASS HONEYCOMB CORE WAS 0.75-IN. TREATMENT LENGTH WAS 22.5-IN. AND BEGAN AT INLET PLANE. SURFACE AND CAVITY NO 1 IS NEXT TO AIRFLOW. SURFACE AND CAVITY NO 2 IS NEXT TO OUTER DUCT WALL.

FIGURE 83.- EXHAUST MODE. EFFECT OF VELOCITY FOR CONFIGURATION R188

CONFIGURATION DESCRIPTION.- SURFACE NO 1=10 RAYL FM
CAVITY NO 1=0.5-IN DEEP
SURFACE NO 2=10 RAYL FM
CAVITY NO 2=1.0-IN DEEP

* FM=FIBERMETAL. FIBERGLASS HONEYCOMB CORE WAS 0.75-IN. TREATMENT

FIGURE 82.- EXHAUST MODE. EFFECT OF VELOCITY FOR CONFIGURATION R185

CONFIGURATION DESCRIPTION.- SURFACE NO 1=80 RAYL FM
CAVITY NO 1=0.75-IN DEEP
SURFACE NO 2=80 RAYL FM
CAVITY NO 2=0.5-IN DEEP

* FM=FIBERMETAL. FIBERGLASS HONEYCOMB CORE WAS 0.75-IN. TREATMENT LENGTH WAS 22.5-IN. AND BEGAN AT INLET PLANE. SURFACE AND CAVITY NO 1 IS NEXT TO AIRFLOW. SURFACE AND CAVITY NO 2 IS NEXT TO OUTER DUCT WALL.

FIGURE 84.- EXHAUST MODE. EFFECT OF VELOCITY FOR CONFIGURATION R192

CONFIGURATION DESCRIPTION.- SURFACE NO 1=10 RAYL FM
CAVITY NO 1=0.5-IN DEEP
SURFACE NO 2=160 RAYL FM
CAVITY NO 2=1.0-IN DEEP

* FM=FIBERMETAL. FIBERGLASS HONEYCOMB CORE WAS 0.75-IN. TREATMENT LENGTH WAS 22.5-IN. AND BEGAN AT INLET PLANE. SURFACE AND CAVITY NO 1 IS NEXT TO AIRFLOW. SURFACE AND CAVITY NO 2 IS NEXT TO OUTER DUCT WALL.

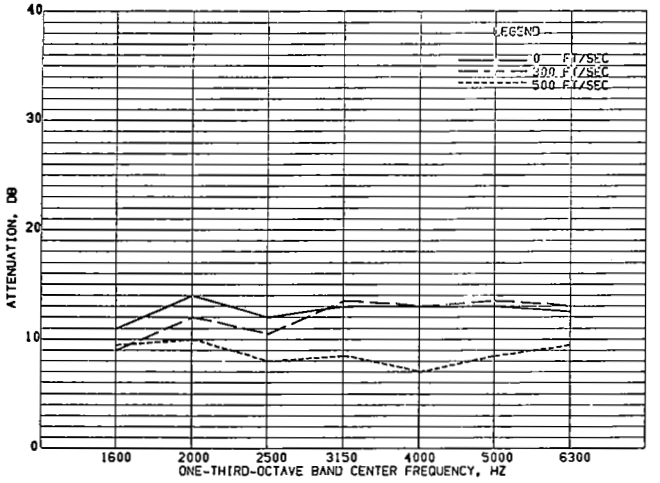

FIGURE 85.- EXHAUST MODE. EFFECT OF VELOCITY FOR CONFIGURATION R201

CONFIGURATION DESCRIPTION.- SURFACE NO 1=80 RAYL FM
CAVITY NO 1=0.5-IN DEEP
SURFACE NO 2=80 RAYL FM
CAVITY NO 2=1.0-IN DEEP

% FM=FIBERMETAL. FIBERGLASS HONEYCOMB CORE WAS 0.75-IN. TREATMENT LENGTH WAS 22.5-IN. AND BEGAN AT INLET PLANE. SURFACE AND CAVITY NO 1 IS NEXT TO AIRFLOW. SURFACE AND CAVITY NO 2 IS NEXT TO OUTER DUCT WALL.

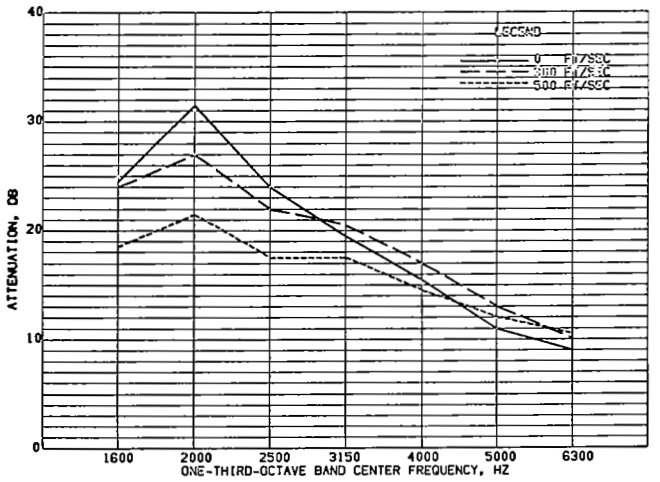

FIGURE 87.- EXHAUST MODE. EFFECT OF VELOCITY FOR CONFIGURATION R203

CONFIGURATION DESCRIPTION.- SURFACE NO 1=10 RAYL FM
CAVITY NO 1=0.75-IN DEEP
SURFACE NO 2=40 RAYL FM
CAVITY NO 2=0.75-IN DEEP

% FM=FIBERMETAL. FIBERGLASS HONEYCOMB CORE WAS 0.75-IN. TREATMENT LENGTH WAS 22.5-IN. AND BEGAN AT INLET PLANE. SURFACE AND CAVITY NO 1 IS NEXT TO AIRFLOW. SURFACE AND CAVITY NO 2 IS NEXT TO OUTER DUCT WALL.

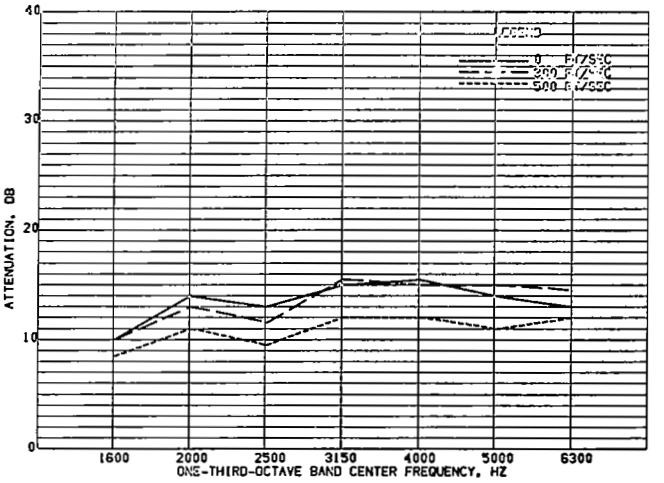

FIGURE 86.- EXHAUST MODE. EFFECT OF VELOCITY FOR CONFIGURATION R202

CONFIGURATION DESCRIPTION.- SURFACE NO 1=80 RAYL FM
CAVITY NO 1=0.5-IN DEEP
SURFACE NO 2=160 RAYL FM
CAVITY NO 2=1.0-IN DEEP

% FM=FIBERMETAL. FIBERGLASS HONEYCOMB CORE WAS 0.75-IN. TREATMENT LENGTH WAS 22.5-IN. AND BEGAN AT INLET PLANE. SURFACE AND CAVITY NO 1 IS NEXT TO AIRFLOW. SURFACE AND CAVITY NO 2 IS NEXT TO OUTER DUCT WALL.

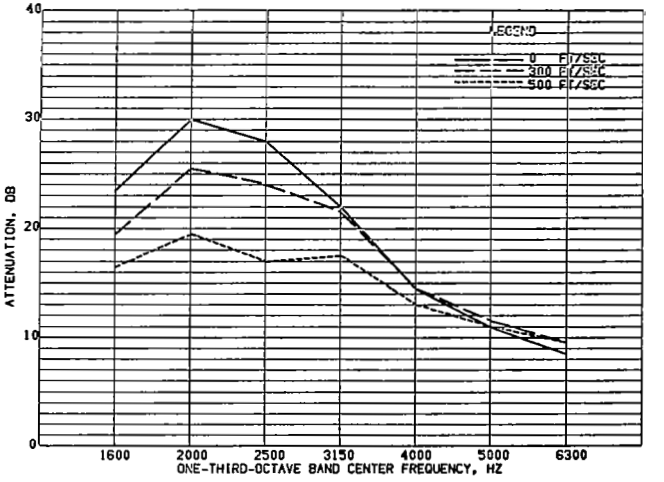

FIGURE 88.- EXHAUST MODE. EFFECT OF VELOCITY FOR CONFIGURATION R204

CONFIGURATION DESCRIPTION.- SURFACE NO 1=10 RAYL FM
CAVITY NO 1=0.75-IN DEEP
SURFACE NO 2=80 RAYL FM
CAVITY NO 2=0.75-IN DEEP

% FM=FIBERMETAL. FIBERGLASS HONEYCOMB CORE WAS 0.75-IN. TREATMENT LENGTH WAS 22.5-IN. AND BEGAN AT INLET PLANE. SURFACE AND CAVITY NO 1 IS NEXT TO AIRFLOW. SURFACE AND CAVITY NO 2 IS NEXT TO OUTER DUCT WALL.

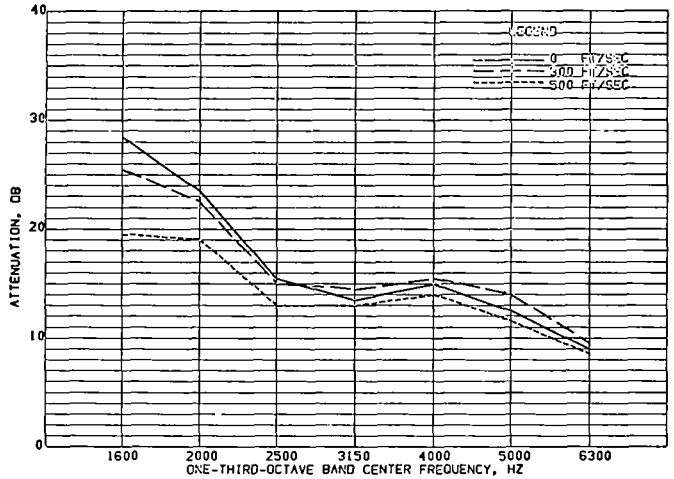

FIGURE 89.- EXHAUST MODE. EFFECT OF VELOCITY FOR CONFIGURATION R209

CONFIGURATION DESCRIPTION.- SURFACE NO 1=10 RAYL FM
CAVITY NO 1=0.75-IN DEEP
SURFACE NO 2=10 RAYL FM
CAVITY NO 2=1.0-IN DEEP

• FM=FIBERMETAL. FIBERGLASS HONEYCOMB CORE WAS 0.75-IN. TREATMENT LENGTH WAS 22.5-IN. AND BEGAN AT INLET PLANE. SURFACE AND CAVITY NO 1 IS NEXT TO AIRFLOW. SURFACE AND CAVITY NO 2 IS NEXT TO OUTER DUCT WALL.

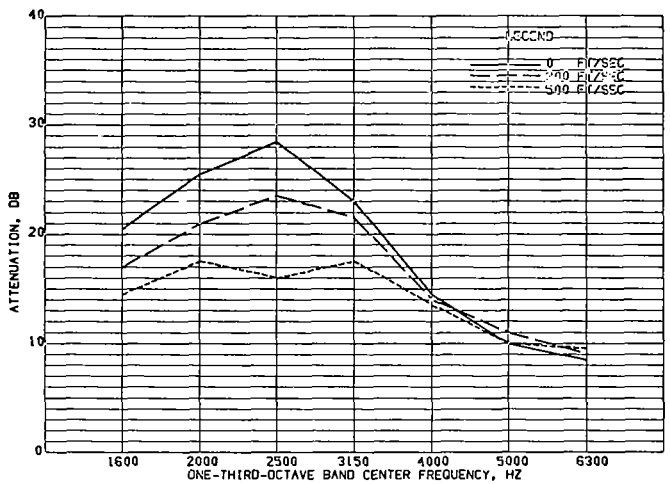

FIGURE 91.- EXHAUST MODE. EFFECT OF VELOCITY FOR CONFIGURATION R213

CONFIGURATION DESCRIPTION.- SURFACE NO 1=10 RAYL FM
CAVITY NO 1=0.75-IN DEEP
SURFACE NO 2=160 RAYL FM
CAVITY NO 2=1.0-IN DEEP

• FM=FIBERMETAL. FIBERGLASS HONEYCOMB CORE WAS 0.75-IN. TREATMENT LENGTH WAS 22.5-IN. AND BEGAN AT INLET PLANE. SURFACE AND CAVITY NO 1 IS NEXT TO AIRFLOW. SURFACE AND CAVITY NO 2 IS NEXT TO OUTER DUCT WALL.

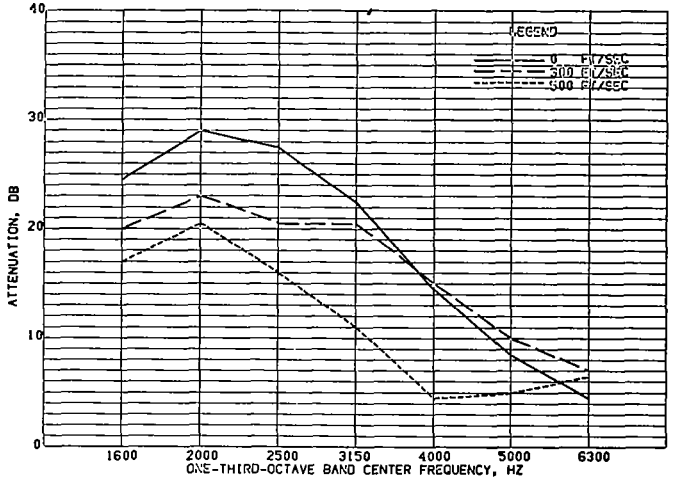

FIGURE 90.- EXHAUST MODE. EFFECT OF VELOCITY FOR CONFIGURATION R212

CONFIGURATION DESCRIPTION.- SURFACE NO 1=10 RAYL FM
CAVITY NO 1=0.75-IN DEEP
SURFACE NO 2=80 RAYL FM
CAVITY NO 2=1.0-IN DEEP

• FM=FIBERMETAL. FIBERGLASS HONEYCOMB CORE WAS 0.75-IN. TREATMENT LENGTH WAS 22.5-IN. AND BEGAN AT INLET PLANE. SURFACE AND CAVITY NO 1 IS NEXT TO AIRFLOW. SURFACE AND CAVITY NO 2 IS NEXT TO OUTER DUCT WALL.

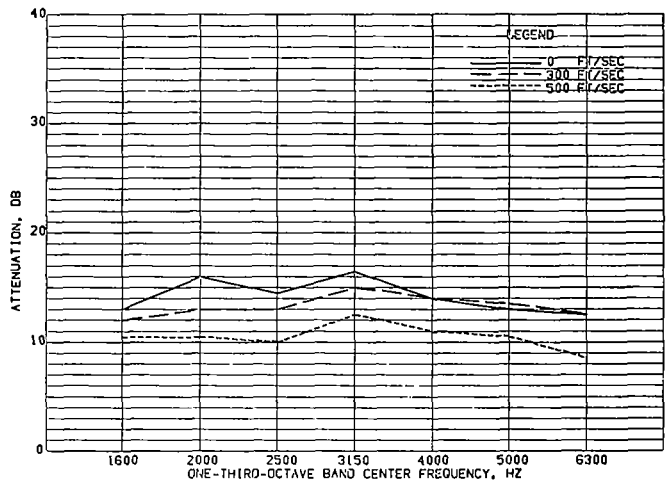

FIGURE 92.- EXHAUST MODE. EFFECT OF VELOCITY FOR CONFIGURATION R222

CONFIGURATION DESCRIPTION.- SURFACE NO 1=80 RAYL FM
CAVITY NO 1=0.75-IN DEEP
SURFACE NO 2=80 RAYL FM
CAVITY NO 2=1.0-IN DEEP

• FM=FIBERMETAL. FIBERGLASS HONEYCOMB CORE WAS 0.75-IN. TREATMENT LENGTH WAS 22.5-IN. AND BEGAN AT INLET PLANE. SURFACE AND CAVITY NO 1 IS NEXT TO AIRFLOW. SURFACE AND CAVITY NO 2 IS NEXT TO OUTER DUCT WALL.

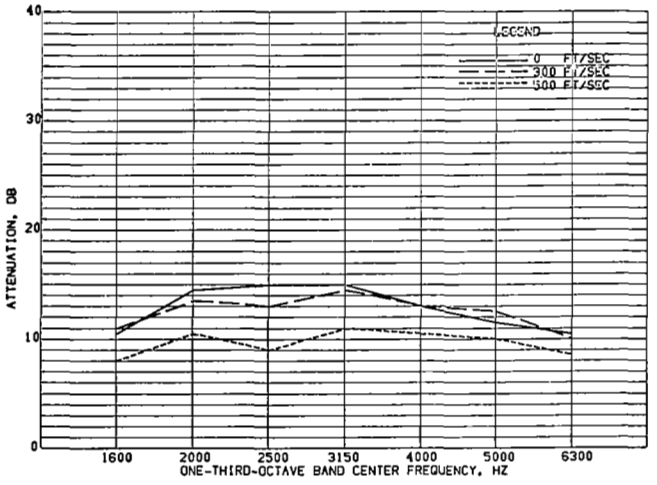

FIGURE 93.- EXHAUST MODE. EFFECT OF VELOCITY FOR CONFIGURATION R223

CONFIGURATION DESCRIPTION.- SURFACE NO 1=80 RAYL FM
CAVITY NO 1=0.75-IN DEEP
SURFACE NO 2=160 RAYL FM
CAVITY NO 2=1.0-IN DEEP

* FM=FIBERMETAL. FIBERGLASS HONEYCOMB CORE WAS 0.75-IN. TREATMENT LENGTH WAS 22.5-IN. AND BEGAN AT INLET PLANE. SURFACE AND CAVITY NO 1 IS NEXT TO AIRFLOW. SURFACE AND CAVITY NO 2 IS NEXT TO OUTER DUCT WALL.

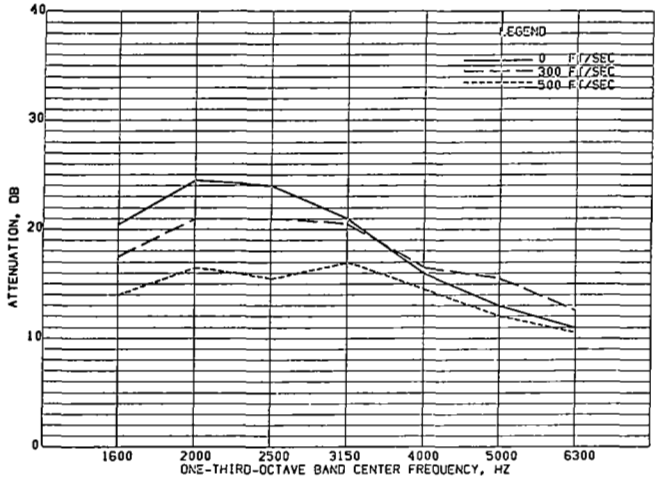

FIGURE 95.- EXHAUST MODE. EFFECT OF VELOCITY FOR CONFIGURATION R1002

CONFIGURATION DESCRIPTION.- SURFACES AND CAVITIES 1, 2 AND 3 = 10, 40 AND 80 RAYL FM-AND 0.5, 0.5 AND 0.5-IN RESPECTIVELY.

* FM=FIBERMETAL. FIBERGLASS HONEYCOMB CORE WAS 0.75-IN. TREATMENT LENGTH WAS 22.5-IN. AND BEGAN AT INLET PLANE. SURFACE AND CAVITY NO 1 IS NEXT TO AIRFLOW. SURFACE AND CAVITY NO 3 IS NEXT TO OUTER DUCT WALL.

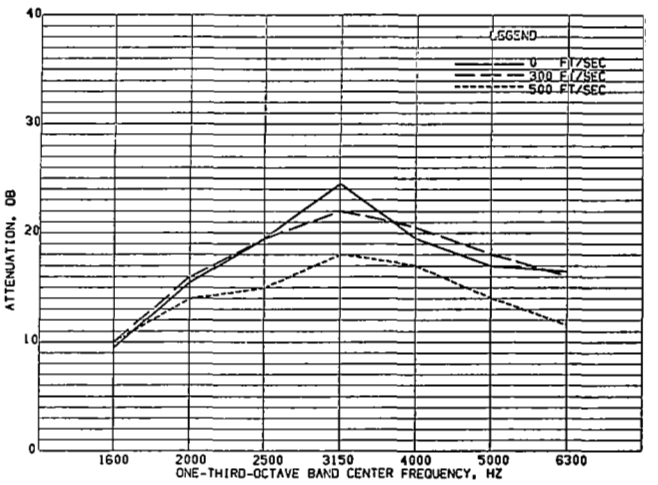

FIGURE 94.- EXHAUST MODE. EFFECT OF VELOCITY FOR CONFIGURATION R1001

CONFIGURATION DESCRIPTION.- SURFACES AND CAVITIES 1, 2 AND 3 = 10, 40 AND 80 RAYL FM-AND 0.25, 0.25, AND 0.25-IN RESPECTIVELY

* FM=FIBERMETAL. FIBERGLASS HONEYCOMB CORE WAS 0.75-IN. TREATMENT LENGTH WAS 22.5-IN. AND BEGAN AT INLET PLANE. SURFACE AND CAVITY NO 1 IS NEXT TO AIRFLOW. SURFACE AND CAVITY NO 3 IS NEXT TO OUTER DUCT WALL.

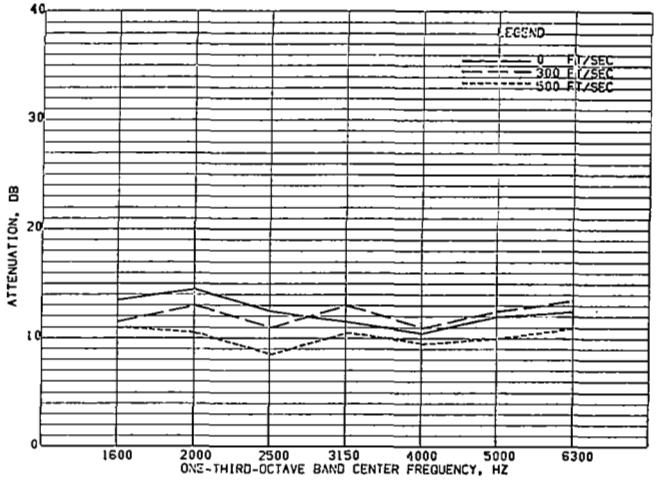

FIGURE 96.- EXHAUST MODE. EFFECT OF VELOCITY FOR CONFIGURATION R1003

CONFIGURATION DESCRIPTION.- SURFACES AND CAVITIES 1, 2 AND 3 = 80, 10 AND 40 RAYL FM-AND 0.5, 0.5 AND 0.5-IN RESPECTIVELY.

* FM=FIBERMETAL. FIBERGLASS HONEYCOMB CORE WAS 0.75-IN. TREATMENT LENGTH WAS 22.5-IN. AND BEGAN AT INLET PLANE. SURFACE AND CAVITY NO 1 IS NEXT TO AIRFLOW. SURFACE AND CAVITY NO 3 IS NEXT TO OUTER DUCT WALL.

FIGURE 97.- EXHAUST MODE. EFFECT OF VELOCITY FOR CONFIGURATION R1005

CONFIGURATION DESCRIPTION.- SURFACES AND CAVITIES 1, 2, 3, AND 4 = 10, 80, 10 AND 40 RAYL FM-AND 0.5, 0.25, 0.5 AND 0.75-IN

• FM=FIBERMETAL. FIBERGLASS HONEYCOMB CORE WAS 0.75-IN. TREATMENT LENGTH WAS 22.5-IN. AND BEGAN AT INLET PLANE. SURFACE AND CAVITY NO 1 IS NEXT TO AIRFLOW. SURFACE AND CAVITY NO 4 IS NEXT TO OUTER DUCT WALL.

FIGURE 98.- EXHAUST MODE. EFFECT OF VELOCITY FOR CONFIGURATION R1004

CONFIGURATION DESCRIPTION.- SURFACES AND CAVITIES 1, 2 AND 3 = 10, 80 AND 10 RAYL FM-AND 0.5, 0.5 AND 1-IN RESPECTIVELY.

• FM=FIBERMETAL. FIBERGLASS HONEYCOMB CORE WAS 0.75-IN. TREATMENT LENGTH WAS 22.5-IN. AND BEGAN AT INLET PLANE. SURFACE AND CAVITY NO 1 IS NEXT TO AIRFLOW. SURFACE AND CAVITY NO 3 IS NEXT TO OUTER DUCT WALL.

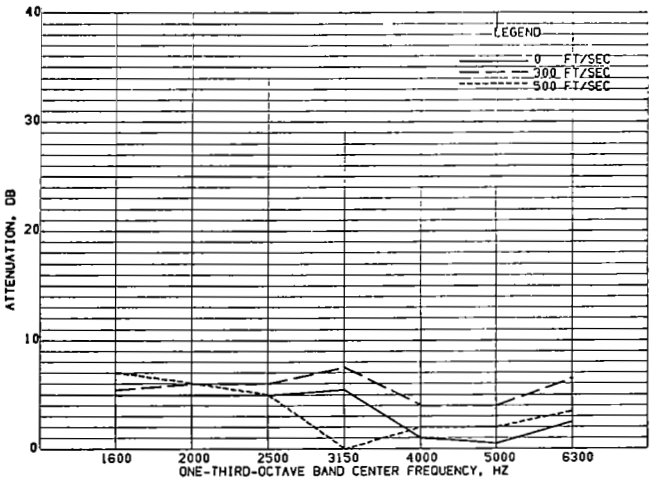

FIGURE 1.- INLET MODE. EFFECT OF VELOCITY FOR CONFIGURATION R2

CONFIGURATION DESCRIPTION.- 10 RAYL FM, 0.25-IN. DEEP

% FM=FIBERMETAL. FIBERGLASS HONEYCOMB CORE WAS 0.75-IN. TREATMENT LENGTH WAS 22.5 -IN AND BEGAN AT INLET PLANE.

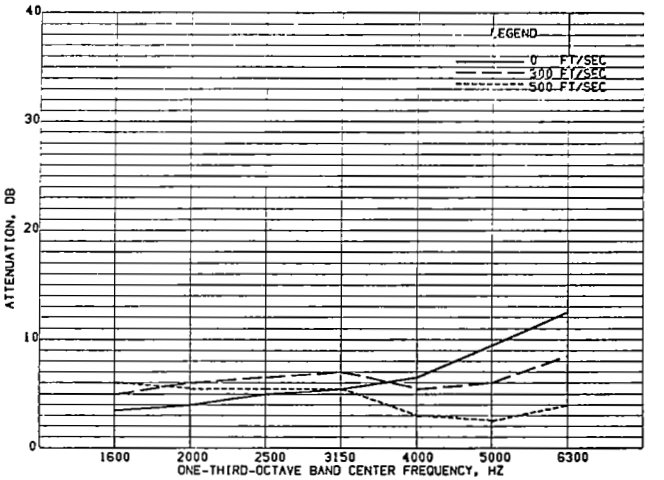

FIGURE 2.- INLET MODE. EFFECT OF VELOCITY FOR CONFIGURATION R3

CONFIGURATION DESCRIPTION.- 40 RAYL FM, 0.25-IN. DEEP

% FM=FIBERMETAL. FIBERGLASS HONEYCOMB CORE WAS 0.75-IN. TREATMENT LENGTH WAS 22.5 -IN AND BEGAN AT INLET PLANE.

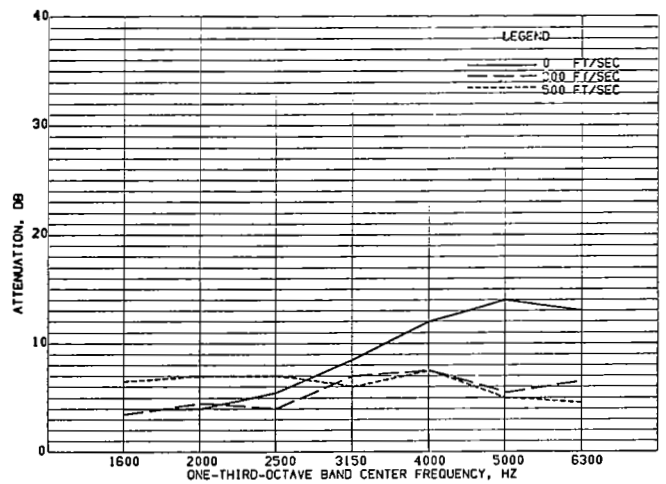

FIGURE 3.- INLET MODE. EFFECT OF VELOCITY FOR CONFIGURATION R4

CONFIGURATION DESCRIPTION.- 80 RAYL FM, 0.25-IN. DEEP

% FM=FIBERMETAL. FIBERGLASS HONEYCOMB CORE WAS 0.75-IN. TREATMENT LENGTH WAS 22.5 -IN AND BEGAN AT INLET PLANE.

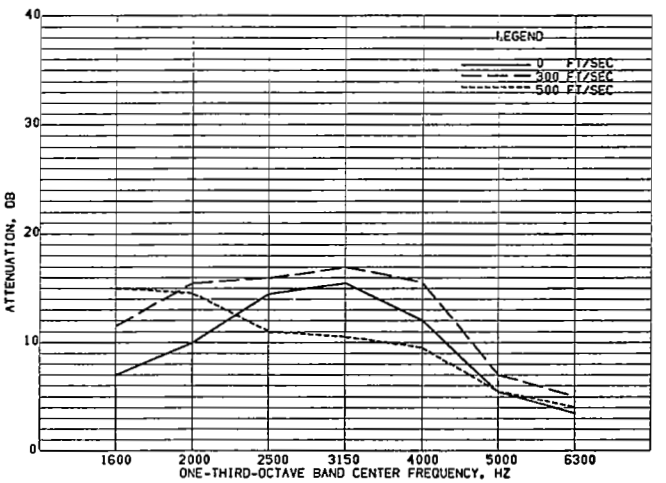

FIGURE 4.- INLET MODE. EFFECT OF VELOCITY FOR CONFIGURATION R5

CONFIGURATION DESCRIPTION.- 10 RAYL FM, 0.5-IN. DEEP

% FM=FIBERMETAL. FIBERGLASS HONEYCOMB CORE WAS 0.75-IN. TREATMENT LENGTH WAS 22.5 -IN AND BEGAN AT INLET PLANE.

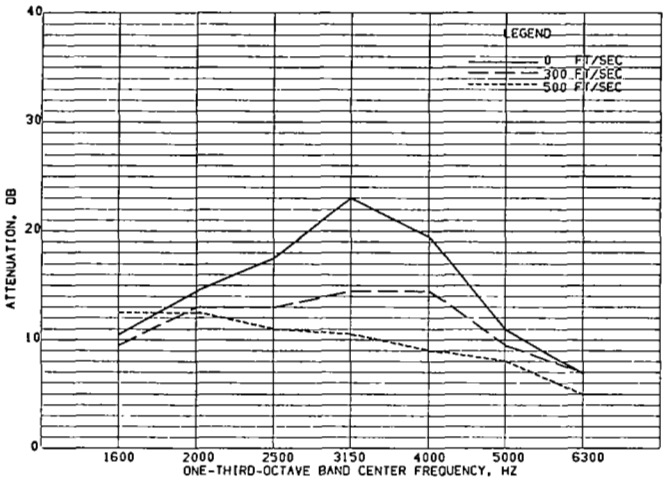

FIGURE 5.- INLET MODE. EFFECT OF VELOCITY FOR CONFIGURATION R6

CONFIGURATION DESCRIPTION.- 40 RAYL FM, 0.5-IN. DEEP

* FM=FIBERMETAL. FIBERGLASS HONEYCOMB CORE WAS 0.75-IN. TREATMENT LENGTH WAS 22.5 -IN AND BEGAN AT INLET PLANE.

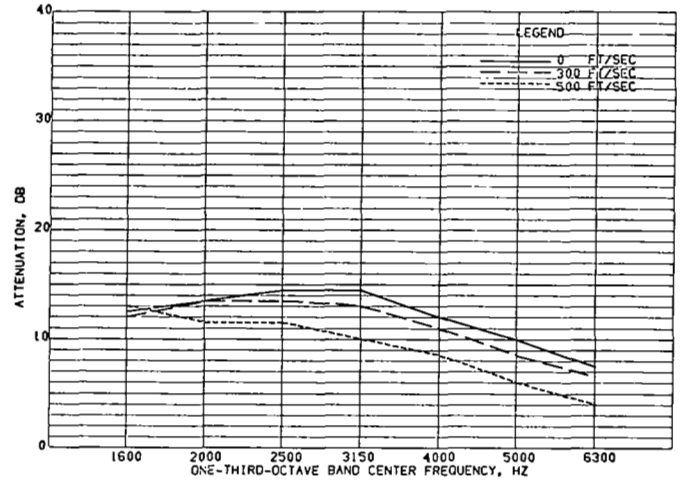

FIGURE 7.- INLET MODE. EFFECT OF VELOCITY FOR CONFIGURATION R9

CONFIGURATION DESCRIPTION.- 160 RAYL FM, 0.5-IN. DEEP

* FM=FIBERMETAL. FIBERGLASS HONEYCOMB CORE WAS 0.75-IN. TREATMENT LENGTH WAS 22.5 -IN AND BEGAN AT INLET PLANE.

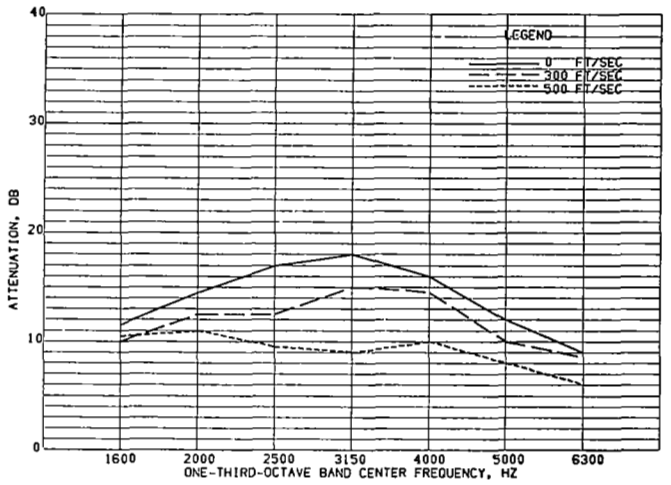

FIGURE 6.- INLET MODE. EFFECT OF VELOCITY FOR CONFIGURATION R8

CONFIGURATION DESCRIPTION.- 80 RAYL FM, 0.5-IN. DEEP

* FM=FIBERMETAL. FIBERGLASS HONEYCOMB CORE WAS 0.75-IN. TREATMENT LENGTH WAS 22.5 -IN AND BEGAN AT INLET PLANE.

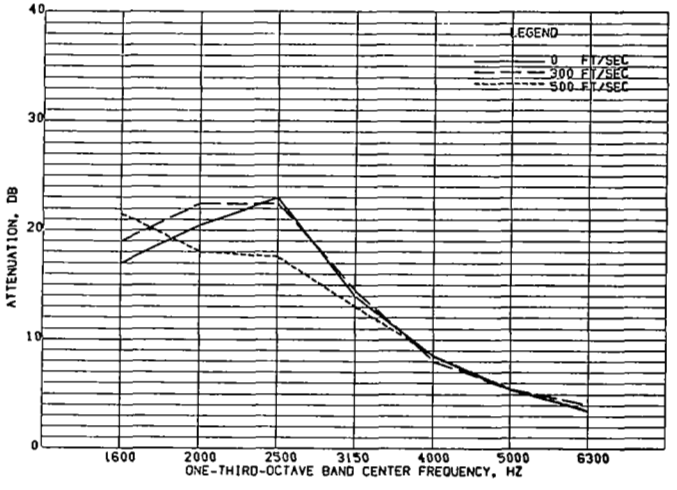

FIGURE 8.- INLET MODE. EFFECT OF VELOCITY FOR CONFIGURATION R10

CONFIGURATION DESCRIPTION.- 10 RAYL FM, 0.75-IN. DEEP

* FM=FIBERMETAL. FIBERGLASS HONEYCOMB CORE WAS 0.75-IN. TREATMENT LENGTH WAS 22.5 -IN AND BEGAN AT INLET PLANE.

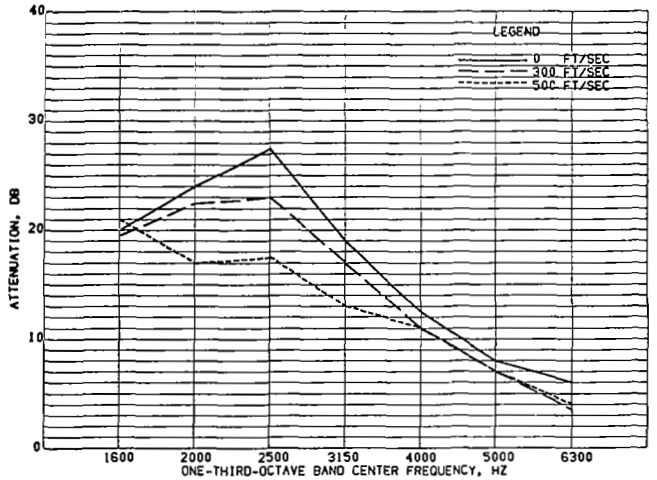

FIGURE 9.- INLET MODE. EFFECT OF VELOCITY FOR CONFIGURATION R11

CONFIGURATION DESCRIPTION.- 40 RAYL FM, 0.75-IN. DEEP

* FM=FIBERMETAL, FIBERGLASS HONEYCOMB CORE WAS 0.75-IN. TREATMENT LENGTH WAS 22.5 -IN AND BEGAN AT INLET PLANE.

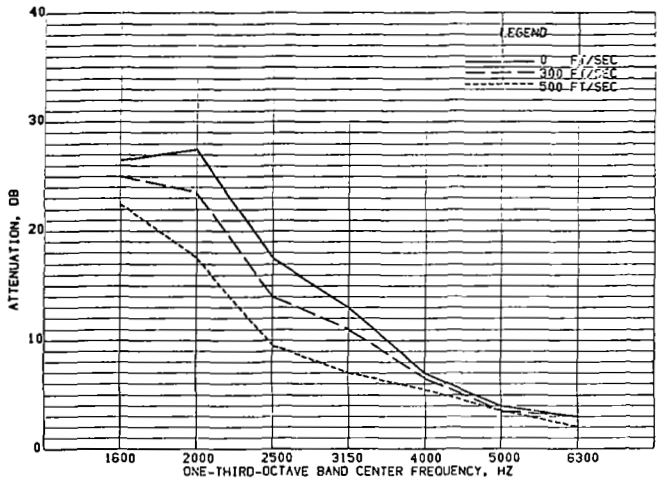

FIGURE 11.- INLET MODE. EFFECT OF VELOCITY FOR CONFIGURATION R13

CONFIGURATION DESCRIPTION.- 10 RAYL FM, 1.0-IN. DEEP

* FM=FIBERMETAL, FIBERGLASS HONEYCOMB CORE WAS 0.75-IN. TREATMENT LENGTH WAS 22.5 -IN AND BEGAN AT INLET PLANE.

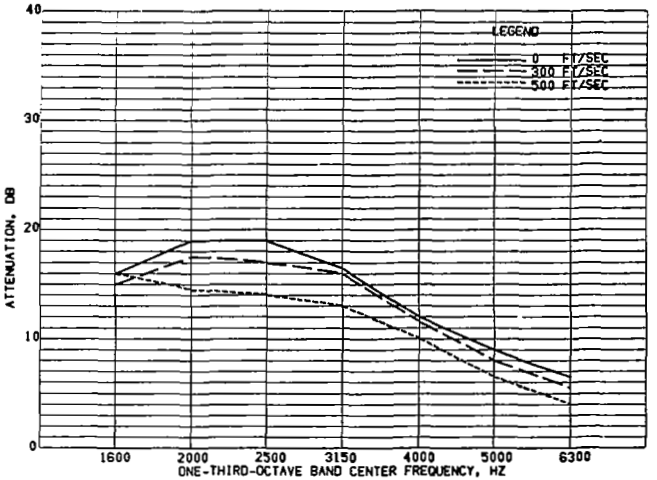

FIGURE 10.- INLET MODE. EFFECT OF VELOCITY FOR CONFIGURATION R12

CONFIGURATION DESCRIPTION.- 80 RAYL FM, 0.75-IN. DEEP

* FM=FIBERMETAL, FIBERGLASS HONEYCOMB CORE WAS 0.75-IN. TREATMENT LENGTH WAS 22.5 -IN AND BEGAN AT INLET PLANE.

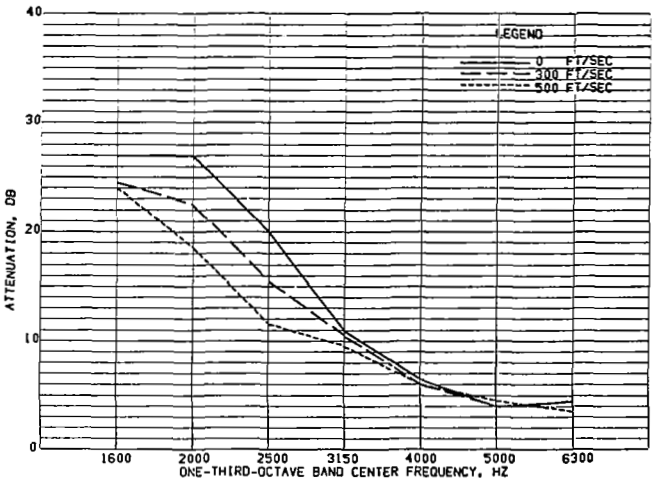

FIGURE 12.- INLET MODE. EFFECT OF VELOCITY FOR CONFIGURATION R14

CONFIGURATION DESCRIPTION.- 20 RAYL FM, 1.0-IN. DEEP

* FM=FIBERMETAL, FIBERGLASS HONEYCOMB CORE WAS 0.75-IN. TREATMENT LENGTH WAS 22.5 -IN AND BEGAN AT INLET PLANE.

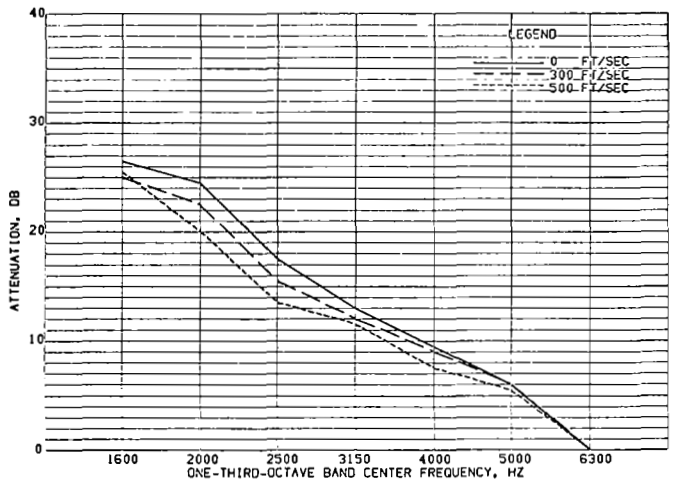

FIGURE 13.- INLET MODE. EFFECT OF VELOCITY FOR CONFIGURATION R15

CONFIGURATION DESCRIPTION.- 40 RAYL FM, 1.0-IN. DEEP
REPEAT FROM 18 AUGUST

% FM=FIBERMETAL. FIBERGLASS HONEYCOMB CORE WAS 0.75-IN.
TREATMENT LENGTH WAS 22.5 -IN AND BEGAN AT EXIT PLANE.

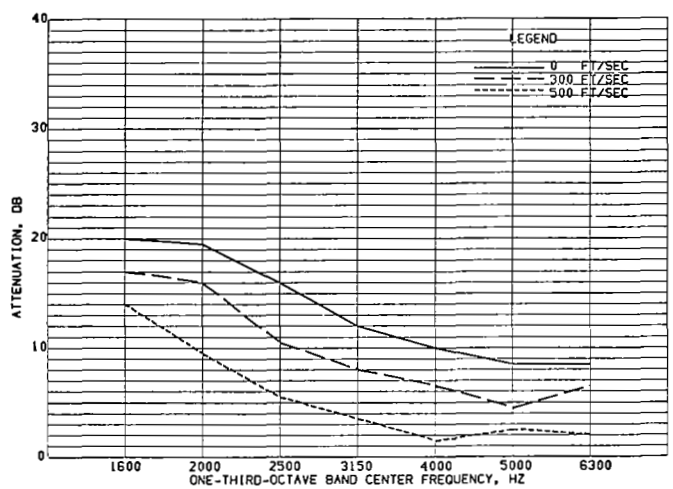

FIGURE 15.- INLET MODE. EFFECT OF VELOCITY FOR CONFIGURATION R18

CONFIGURATION DESCRIPTION.- 40 RAYL FM, 1.0-IN. DEEP

% FM=FIBERMETAL. FIBERGLASS HONEYCOMB CORE WAS 0.75-IN.
TREATMENT LENGTH WAS 11.25-IN AND BEGAN AT EXIT PLANE.

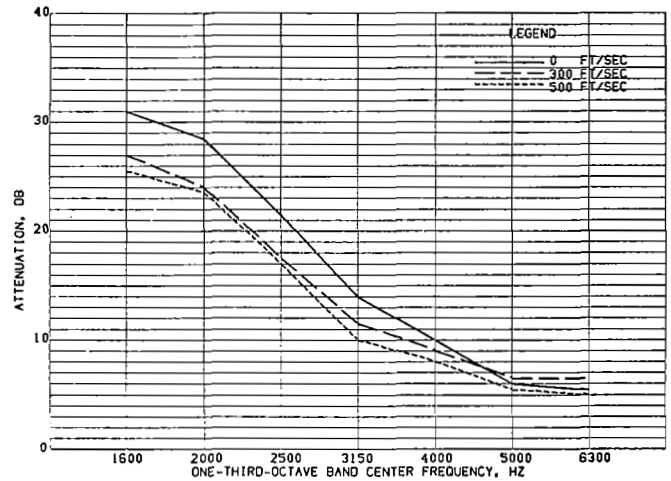

FIGURE 14.- INLET MODE. EFFECT OF VELOCITY FOR CONFIGURATION R17

CONFIGURATION DESCRIPTION.- 40 RAYL FM, 1.0-IN. DEEP

% FM=FIBERMETAL. FIBERGLASS HONEYCOMB CORE WAS 0.75-IN.
TREATMENT LENGTH WAS 45-IN. AND WAS INSTALLED ON ONE WALL ONLY.

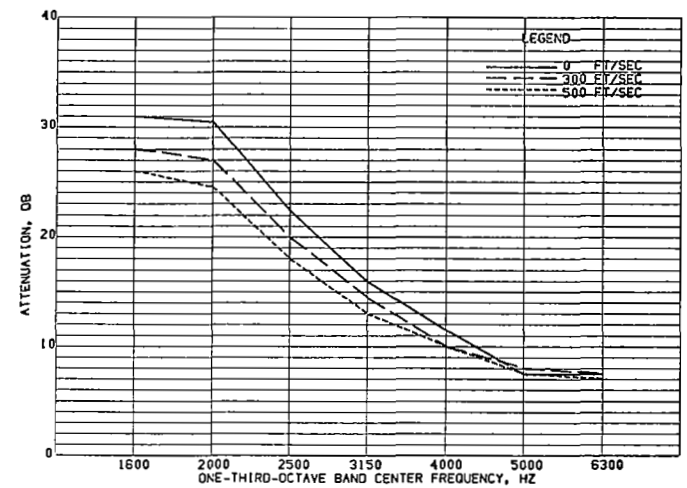

FIGURE 16.- INLET MODE. EFFECT OF VELOCITY FOR CONFIGURATION R19

CONFIGURATION DESCRIPTION.- 40 RAYL FM, 1.0-IN. DEEP

% FM=FIBERMETAL. FIBERGLASS HONEYCOMB CORE WAS 0.75-IN.
TREATMENT LENGTH WAS 33.75-IN AND BEGAN AT EXIT PLANE.

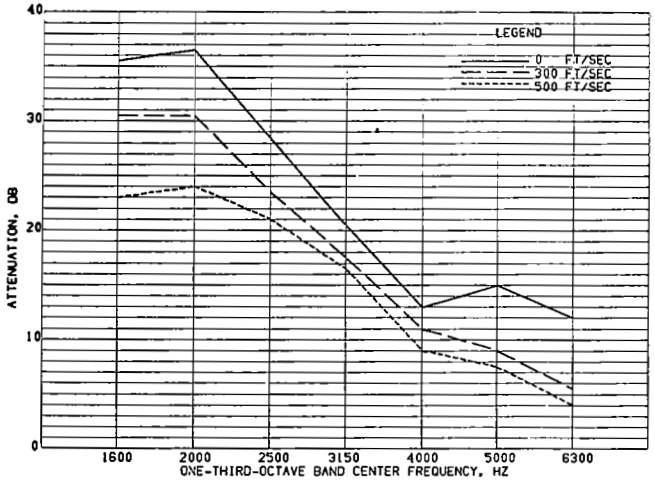

FIGURE 17.- INLET MODE. EFFECT OF VELOCITY FOR CONFIGURATION R20

CONFIGURATION DESCRIPTION.- 40 RAYL FM, 1.0-IN. DEEP

*FM=FIBERMETAL. FIBERGLASS HONEYCOMB CORE WAS 0.75-IN. TREATMENT LENGTH WAS 45.0-IN.

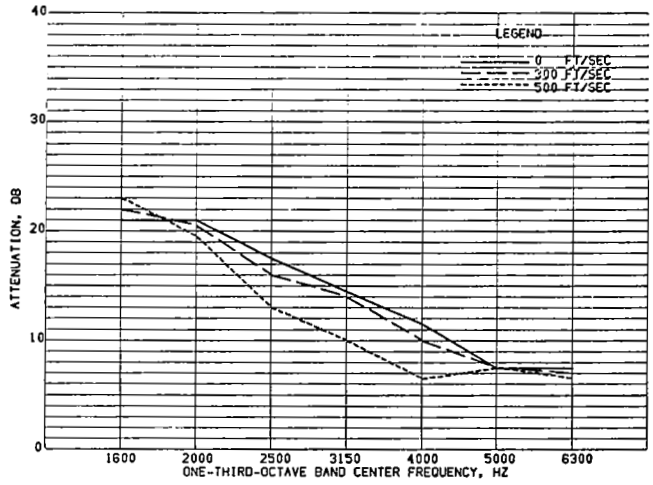

FIGURE 18.- INLET MODE. EFFECT OF VELOCITY FOR CONFIGURATION R21

CONFIGURATION DESCRIPTION.- 80 RAYL FM, 1.0-IN. DEEP

*FM=FIBERMETAL. FIBERGLASS HONEYCOMB CORE WAS 0.75-IN. TREATMENT LENGTH WAS 22.5 -IN AND BEGAN AT INLET PLANE.

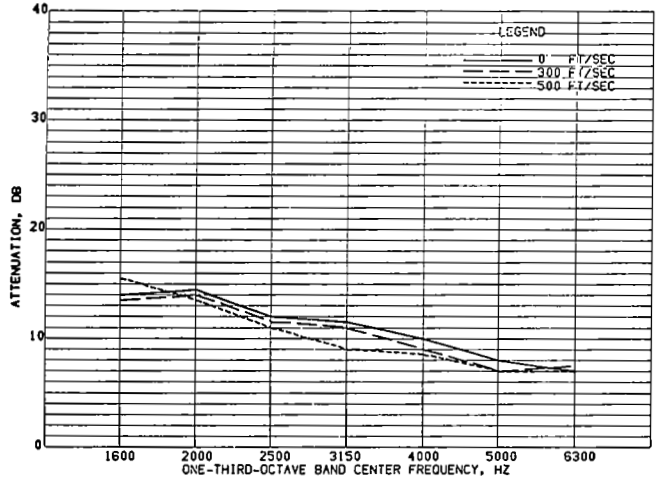

FIGURE 19.- INLET MODE. EFFECT OF VELOCITY FOR CONFIGURATION R22

CONFIGURATION DESCRIPTION.- 160 RAYL FM, 1.0-IN. DEEP

*FM=FIBERMETAL. FIBERGLASS HONEYCOMB CORE WAS 0.75-IN. TREATMENT LENGTH WAS 22.5 -IN AND BEGAN AT INLET PLANE.

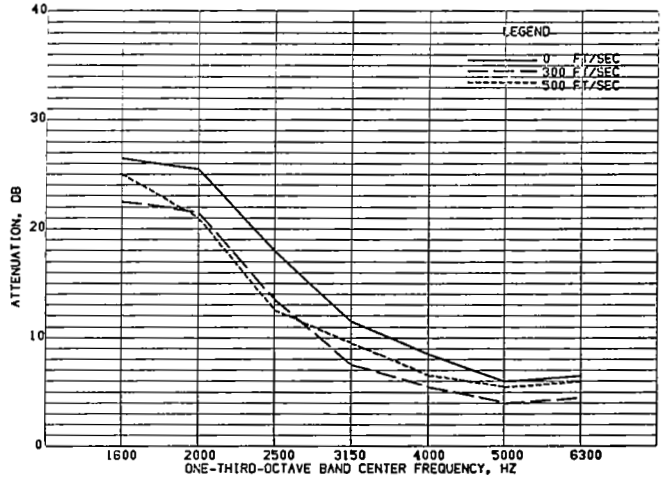

FIGURE 20.- INLET MODE. EFFECT OF VELOCITY FOR CONFIGURATION R23

CONFIGURATION DESCRIPTION.- 40 RAYL FM, 1.0-IN. DEEP

*FM=FIBERMETAL. FIBERGLASS HONEYCOMB CORE WAS 0.375-IN. TREATMENT LENGTH WAS 22.5-IN AND BEGAN AT INLET PLANE.

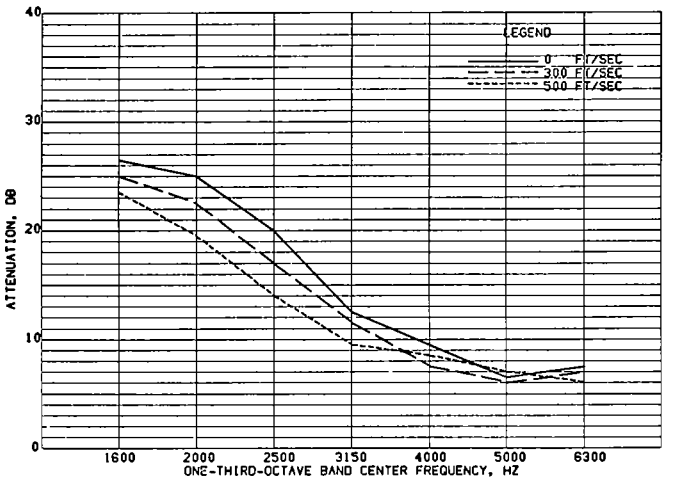

FIGURE 21.- INLET MODE. EFFECT OF VELOCITY FOR CONFIGURATION R24*

CONFIGURATION DESCRIPTION.- 40 RAYL FM, 1.0-IN. DEEP

* FM=FIBERMETAL. FIBERGLASS HONEYCOMB CORE WAS 1.125-IN. TREATMENT LENGTH WAS 22.5-IN AND BEGAN AT EXIT PLANE.

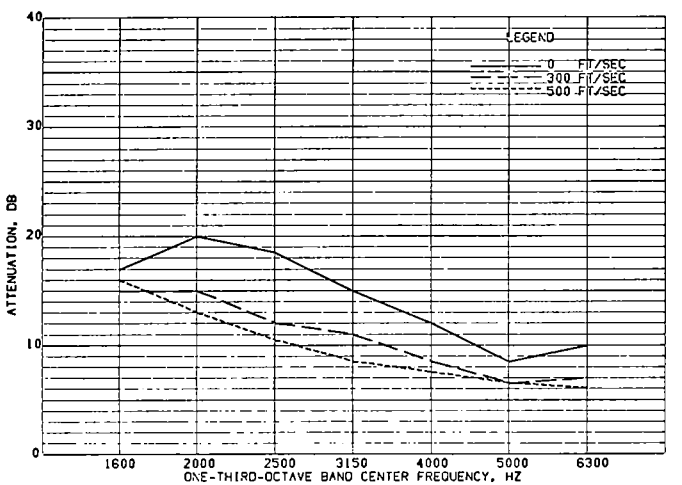

FIGURE 23.- INLET MODE. EFFECT OF VELOCITY FOR CONFIGURATION R26

CONFIGURATION DESCRIPTION.- 40 RAYL FM, 1.0-IN. DEEP
3.0-IN. HC CELLS

* FM=FIBERMETAL. FIBERGLASS HONEYCOMB CORE WAS 3.0-IN. TREATMENT LENGTH WAS 22.5-IN AND BEGAN AT INLET PLANE.

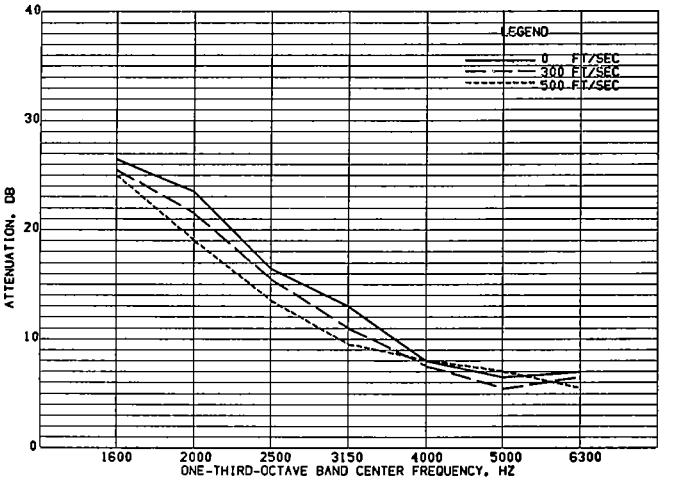

FIGURE 22.- INLET MODE. EFFECT OF VELOCITY FOR CONFIGURATION R24**

CONFIGURATION DESCRIPTION.- 40 RAYL FM, 1.0-IN. DEEP

* FM=FIBERMETAL. FIBERGLASS HONEYCOMB CORE WAS 1.125-IN. TREATMENT LENGTH WAS 22.5-IN AND BEGAN AT INLET PLANE.

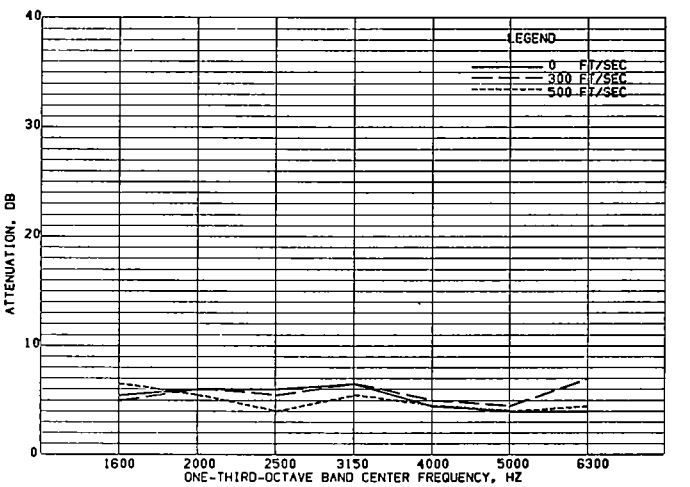

FIGURE 24.- INLET MODE. EFFECT OF VELOCITY FOR CONFIGURATION R29

CONFIGURATION DESCRIPTION.- SPLITTER = 40 RAYL FM ON TWO SIDES OF CORRUGATED ALUMINUM SEPTUM
DUCT WALLS WERE HARD

* FM-FIBERMETAL.

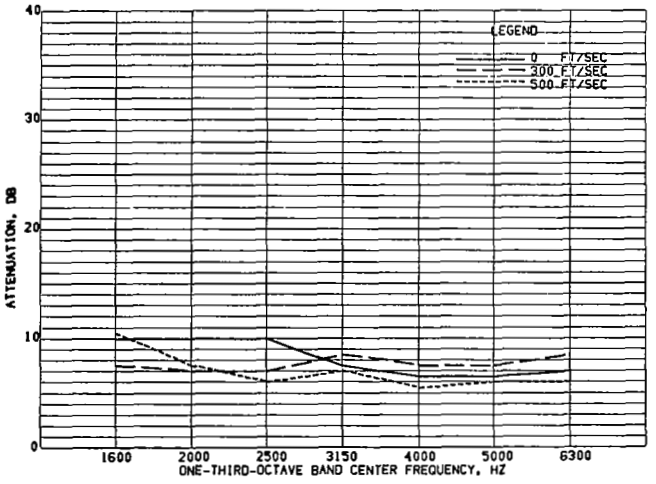

FIGURE 25.- INLET MODE. EFFECT OF VELOCITY FOR CONFIGURATION R30

CONFIGURATION DESCRIPTION.- SPLITTER = 40 RAYL FM ON
TWO SIDES OF FLAT SHEET
ALUMINUM SEPTUM
DUCT WALLS WERE HARD

% FM=FIBERMETAL. FIBERGLASS HONEYCOMB CORE WAS 0.75-IN.

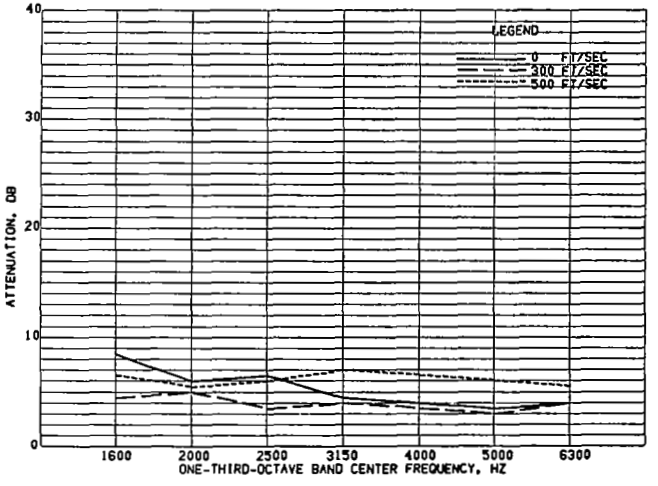

FIGURE 26.- INLET MODE. EFFECT OF VELOCITY FOR CONFIGURATION R31

CONFIGURATION DESCRIPTION.- SPLITTER = 40 RAYL FM ON
ONE SIDE ONLY.1.0-IN.
DUCT WALLS WERE HARD

% FM=FIBERMETAL. FIBERGLASS HONEYCOMB CORE WAS 0.75-IN.

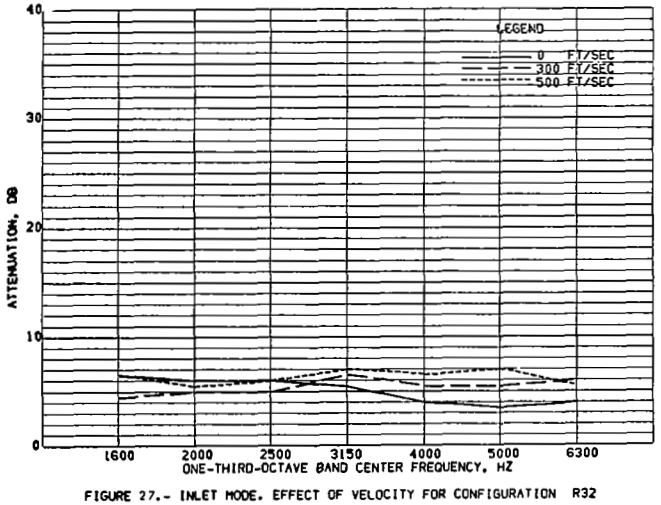

FIGURE 27.- INLET MODE. EFFECT OF VELOCITY FOR CONFIGURATION R32

CONFIGURATION DESCRIPTION.- SPLITTER = 10 RAYL FM ON
SURFACE NO 1 AND 40 RAYL
FM ON SURFACE NO 2.0.5IN
DUCT WALLS WERE HARD

% FM=FIBERMETAL. FIBERGLASS HONEYCOMB CORE WAS 0.75-IN.

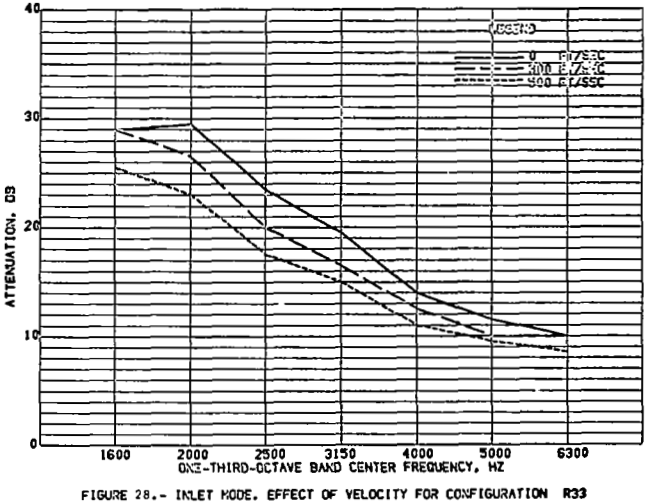

FIGURE 28.- INLET MODE. EFFECT OF VELOCITY FOR CONFIGURATION R33

CONFIGURATION DESCRIPTION.- SPLITTER = 40 RAYL FM ON
TWO SIDES OF FLAT SHEET
ALUMINUM SEPTUM.1.0-IN.
DUCT WALLS WERE AS R15

% FM=FIBERMETAL. FIBERGLASS HONEYCOMB CORE WAS 0.75-IN.

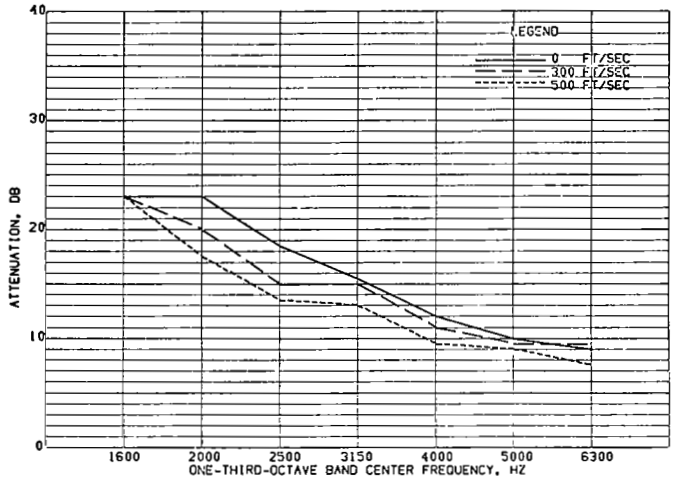

FIGURE 29.- INLET MODE. EFFECT OF VELOCITY FOR CONFIGURATION R34

CONFIGURATION DESCRIPTION.- SPLITTER = 40 RAYL FM ON TWO SIDES OF FLAT SHEET ALUMINUM SEPTUM. 1.0-IN. DUCT WALLS WERE AS R18

* FM=FIBERMETAL. FIBERGLASS HONEYCOMB CORE WAS 0.75-IN.

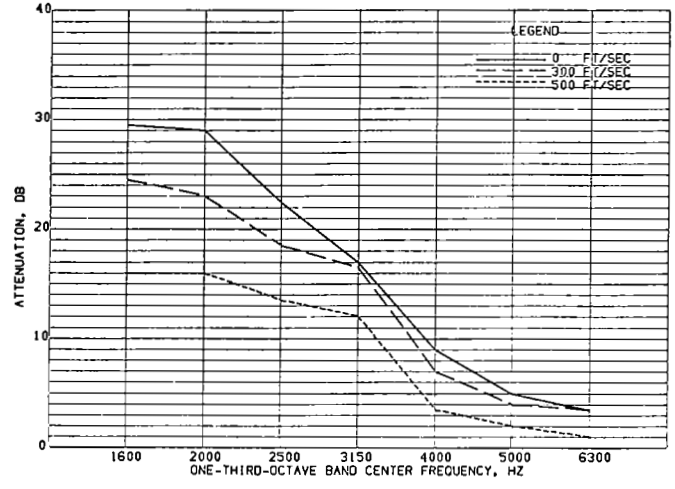

FIGURE 31.- INLET MODE. EFFECT OF VELOCITY FOR CONFIGURATION R36

CONFIGURATION DESCRIPTION.- SPLITTER = 40 RAYL FM ON TWO SIDES OF FLAT SHEET ALUMINUM SEPTUM. 1.0-IN. DUCT WALLS WERE AS R20

* FM=FIBERMETAL. FIBERGLASS HONEYCOMB CORE WAS 0.75-IN.

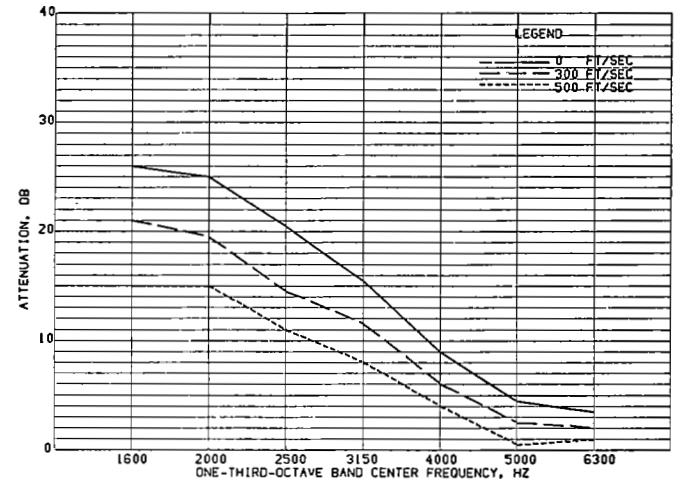

FIGURE 30.- INLET MODE. EFFECT OF VELOCITY FOR CONFIGURATION R35

CONFIGURATION DESCRIPTION.- SPLITTER = 40 RAYL FM ON TWO SIDES OF FLAT SHEET ALUMINUM SEPTUM. 1.0-IN. DUCT WALLS WERE AS R19

* FM=FIBERMETAL. FIBERGLASS HONEYCOMB CORE WAS 0.75-IN.

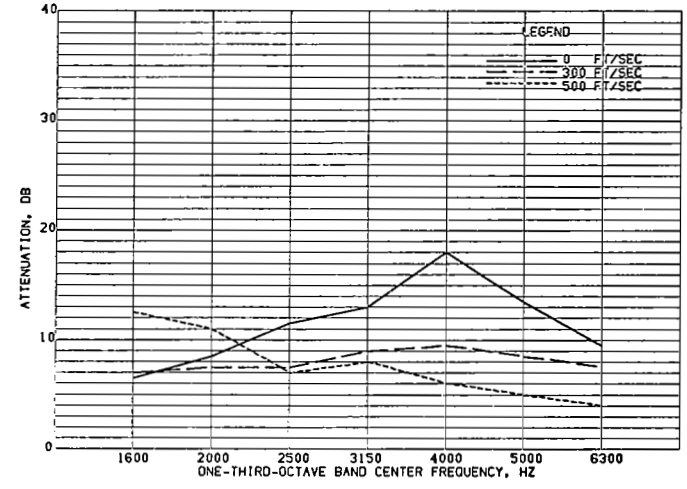

FIGURE 32.- INLET MODE. EFFECT OF VELOCITY FOR CONFIGURATION R101

CONFIGURATION DESCRIPTION.- SURFACE NO 1=10 RAYL FM
CAVITY NO 1=0.25-IN DEEP
SURFACE NO 2=40 RAYL FM
CAVITY NO 2=0.25-IN DEEP

** FM=FIBERMETAL. FIBERGLASS HONEYCOMB CORE WAS 0.75-IN. TREATMENT LENGTH WAS 22.5-IN. AND BEGAN AT INLET PLANE. SURFACE AND CAVITY NO 1 IS NEXT TO AIRFLOW. SURFACE AND CAVITY NO 2 IS NEXT TO OUTER DUCT WALL.

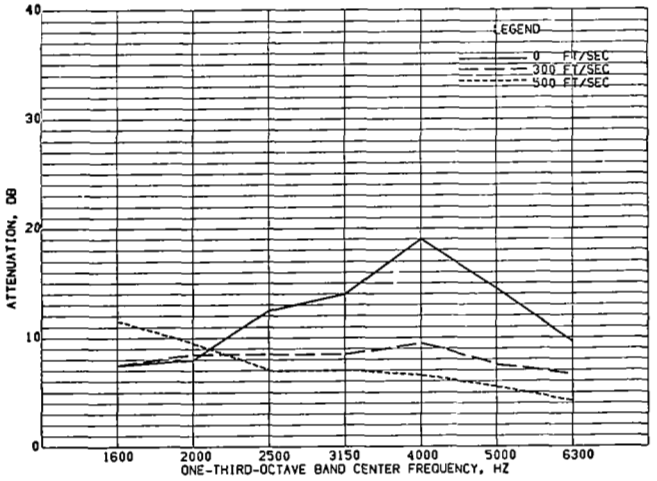

FIGURE 33.- INLET MODE. EFFECT OF VELOCITY FOR CONFIGURATION R102

CONFIGURATION DESCRIPTION.- SURFACE NO 1=10 RAYL FM
CAVITY NO 1=0.25-IN DEEP
SURFACE NO 2=80 RAYL FM
CAVITY NO 2=0.25-IN DEEP

* FM=FIBERMETAL. FIBERGLASS HONEYCOMB CORE WAS 0.75-IN. TREATMENT LENGTH WAS 22.5-IN. AND BEGAN AT INLET PLANE. SURFACE AND CAVITY NO 1 IS NEXT TO AIRFLOW. SURFACE AND CAVITY NO 2 IS NEXT TO OUTER DUCT WALL.

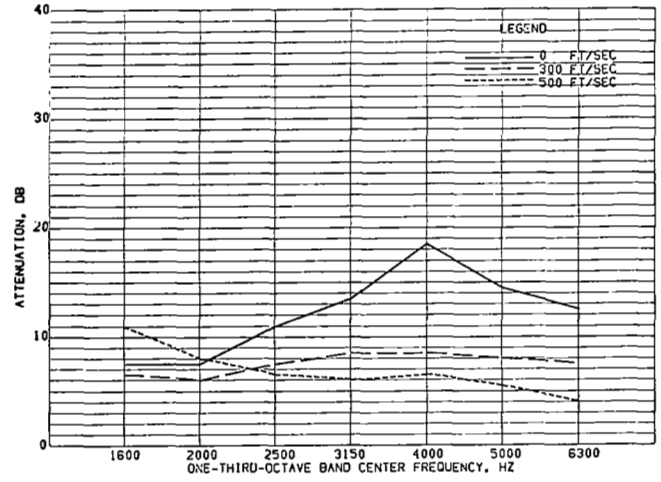

FIGURE 35.- INLET MODE. EFFECT OF VELOCITY FOR CONFIGURATION R104

CONFIGURATION DESCRIPTION.- SURFACE NO 1=40 RAYL FM
CAVITY NO 1=0.25-IN DEEP
SURFACE NO 2=10 RAYL FM
CAVITY NO 2=0.25-IN DEEP

* FM=FIBERMETAL. FIBERGLASS HONEYCOMB CORE WAS 0.75-IN. TREATMENT LENGTH WAS 22.5-IN. AND BEGAN AT INLET PLANE. SURFACE AND CAVITY NO 1 IS NEXT TO AIRFLOW. SURFACE AND CAVITY NO 2 IS NEXT TO OUTER DUCT WALL.

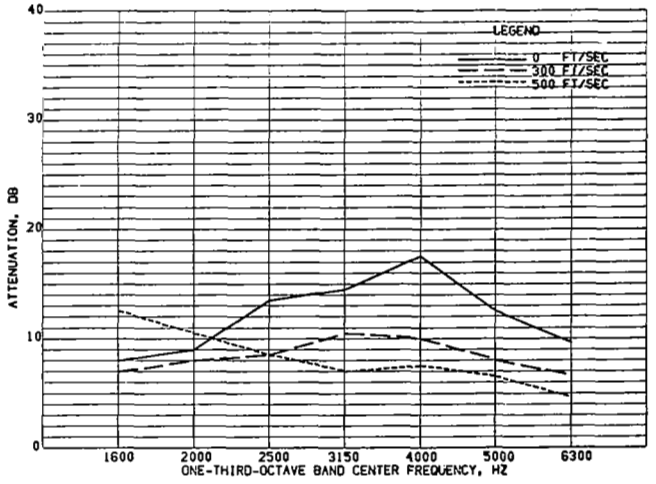

FIGURE 34.- INLET MODE. EFFECT OF VELOCITY FOR CONFIGURATION R103

CONFIGURATION DESCRIPTION.- SURFACE NO 1=40 RAYL FM
CAVITY NO 1=0.25-IN DEEP
SURFACE NO 2=80 RAYL FM
CAVITY NO 2=0.25-IN DEEP

* FM=FIBERMETAL. FIBERGLASS HONEYCOMB CORE WAS 0.75-IN. TREATMENT LENGTH WAS 22.5-IN. AND BEGAN AT INLET PLANE. SURFACE AND CAVITY NO 1 IS NEXT TO AIRFLOW. SURFACE AND CAVITY NO 2 IS NEXT TO OUTER DUCT WALL.

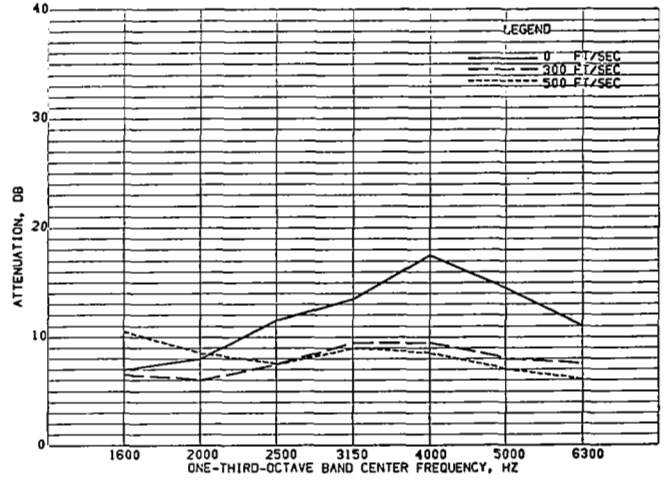

FIGURE 36.- INLET MODE. EFFECT OF VELOCITY FOR CONFIGURATION R105

CONFIGURATION DESCRIPTION.- SURFACE NO 1=80 RAYL FM
CAVITY NO 1=0.25-IN DEEP
SURFACE NO 2=10 RAYL FM
CAVITY NO 2=0.25-IN DEEP

* FM=FIBERMETAL. FIBERGLASS HONEYCOMB CORE WAS 0.75-IN. TREATMENT LENGTH WAS 22.5-IN. AND BEGAN AT INLET PLANE. SURFACE AND CAVITY NO 1 IS NEXT TO AIRFLOW. SURFACE AND CAVITY NO 2 IS NEXT TO OUTER DUCT WALL.

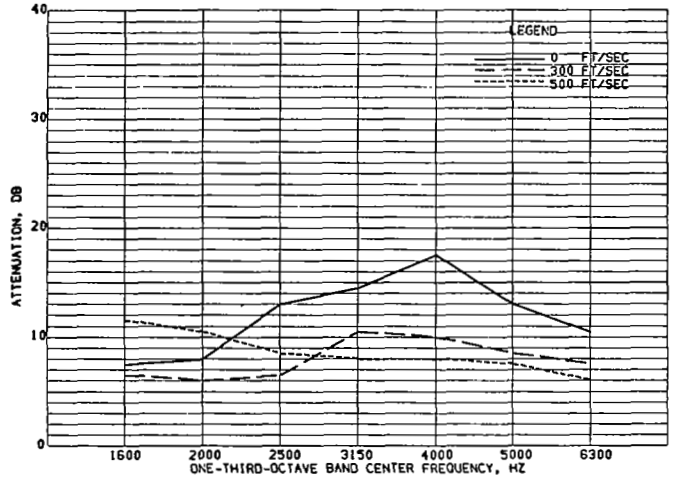

FIGURE 37.- INLET MODE. EFFECT OF VELOCITY FOR CONFIGURATION R106

CONFIGURATION DESCRIPTION.- SURFACE NO 1=80 RAYL FM
CAVITY NO 1=0.25-IN DEEP
SURFACE NO 2=40 RAYL FM
CAVITY NO 2=0.25-IN DEEP

* FM=FIBERMETAL. FIBERGLASS HONEYCOMB CORE WAS 0.75-IN. TREATMENT LENGTH WAS 22.5-IN. AND BEGAN AT INLET PLANE. SURFACE AND CAVITY NO 1 IS NEXT TO AIRFLOW. SURFACE AND CAVITY NO 2 IS NEXT TO OUTER DUCT WALL.

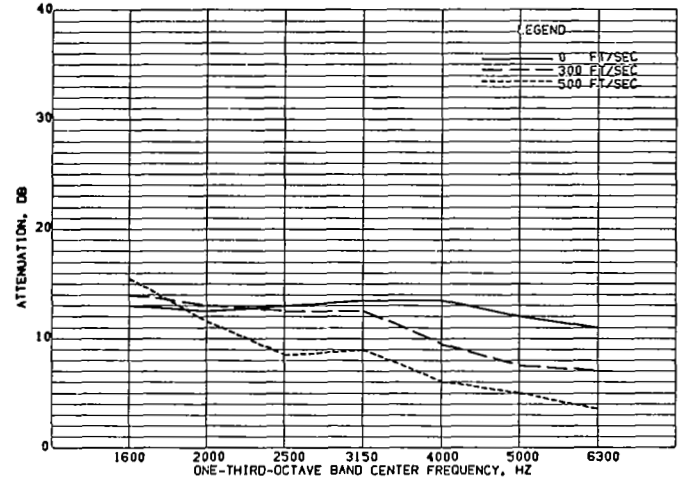

FIGURE 39.- INLET MODE. EFFECT OF VELOCITY FOR CONFIGURATION R110

CONFIGURATION DESCRIPTION.- SURFACE NO 1=10 RAYL FM
CAVITY NO 1=0.25-IN DEEP
SURFACE NO 2=10 RAYL FM
CAVITY NO 2=0.5-IN DEEP

* FM=FIBERMETAL. FIBERGLASS HONEYCOMB CORE WAS 0.75-IN. TREATMENT LENGTH WAS 22.5-IN. AND BEGAN AT INLET PLANE. SURFACE AND CAVITY NO 1 IS NEXT TO AIRFLOW. SURFACE AND CAVITY NO 2 IS NEXT TO OUTER DUCT WALL.

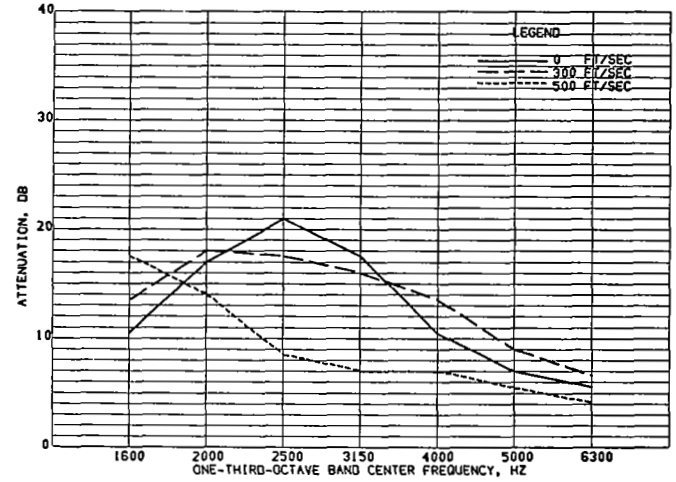

FIGURE 38.- INLET MODE. EFFECT OF VELOCITY FOR CONFIGURATION R107

CONFIGURATION DESCRIPTION.- SURFACE NO 1=10 RAYL FM
CAVITY NO 1=0.25-IN DEEP
SURFACE NO 2=10 RAYL FM
CAVITY NO 2=0.5-IN. DEEP

* FM=FIBERMETAL. FIBERGLASS HONEYCOMB CORE WAS 0.75-IN. TREATMENT LENGTH WAS 22.5-IN. AND BEGAN AT INLET PLANE. SURFACE AND CAVITY NO 1 IS NEXT TO AIRFLOW. SURFACE AND CAVITY NO 2 IS NEXT TO OUTER DUCT WALL.

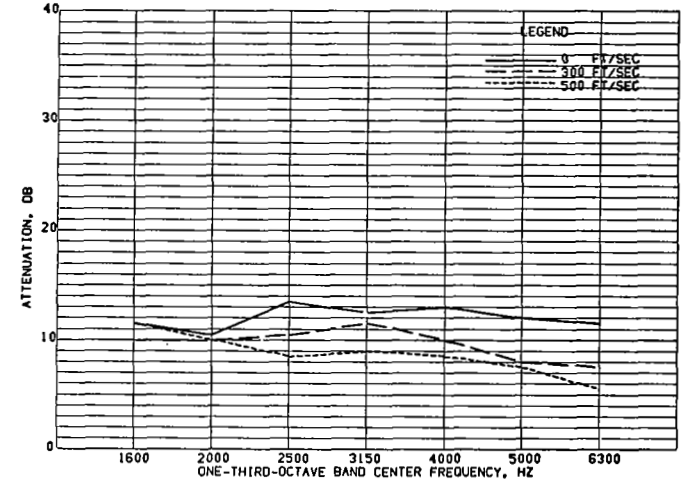

FIGURE 40.- INLET MODE. EFFECT OF VELOCITY FOR CONFIGURATION R115

CONFIGURATION DESCRIPTION.- SURFACE NO 1=80 RAYL FM
CAVITY NO 1=0.25-IN DEEP
SURFACE NO 2=160 RAYL FM
CAVITY NO 2=0.5-IN DEEP

* FM=FIBERMETAL. FIBERGLASS HONEYCOMB CORE WAS 0.75-IN. TREATMENT LENGTH WAS 22.5-IN. AND BEGAN AT INLET PLANE. SURFACE AND CAVITY NO 1 IS NEXT TO AIRFLOW. SURFACE AND CAVITY NO 2 IS NEXT TO OUTER DUCT WALL.

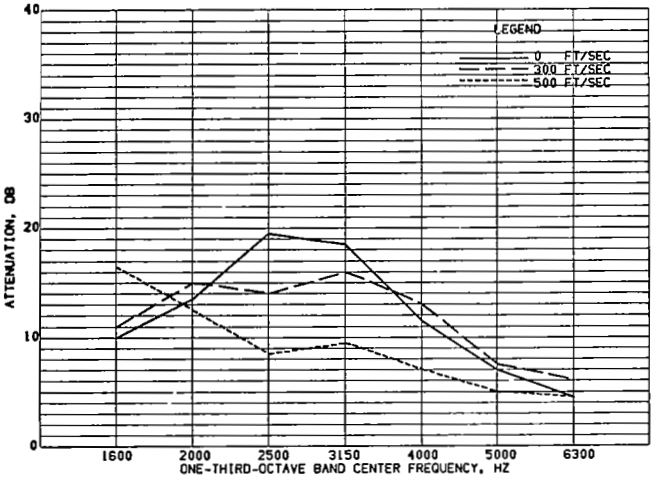

FIGURE 41.- INLET MODE. EFFECT OF VELOCITY FOR CONFIGURATION R116

CONFIGURATION DESCRIPTION.- SURFACE NO 1=10 RAYL FM
CAVITY NO 1=0.5-IN DEEP
SURFACE NO 2=10 RAYL FM
CAVITY NO 2=0.25-IN DEEP

* FM=FIBERMETAL. FIBERGLASS HONEYCOMB CORE WAS 0.75-IN. TREATMENT LENGTH WAS 22.5-IN. AND BEGAN AT INLET PLANE. SURFACE AND CAVITY NO 1 IS NEXT TO AIRFLOW. SURFACE AND CAVITY NO 2 IS NEXT TO OUTER DUCT WALL.

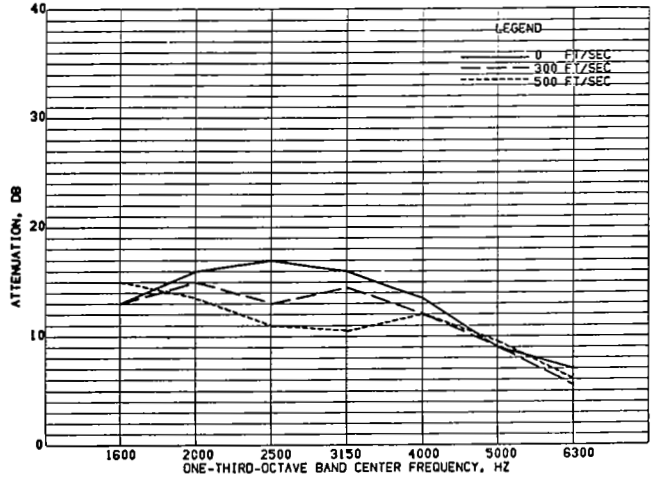

FIGURE 43.- INLET MODE. EFFECT OF VELOCITY FOR CONFIGURATION R121

CONFIGURATION DESCRIPTION.- SURFACE NO 1=80 RAYL FM
CAVITY NO 1=0.5-IN DEEP
SURFACE NO 2=80 RAYF FM
CAVITY NO 2=0.25-IN DEEP

* FM=FIBERMETAL. FIBERGLASS HONEYCOMB CORE WAS 0.75-IN. TREATMENT LENGTH WAS 22.5-IN. AND BEGAN AT INLET PLANE. SURFACE AND CAVITY NO 1 IS NEXT TO AIRFLOW. SURFACE AND CAVITY NO 2 IS NEXT TO OUTER DUCT WALL.

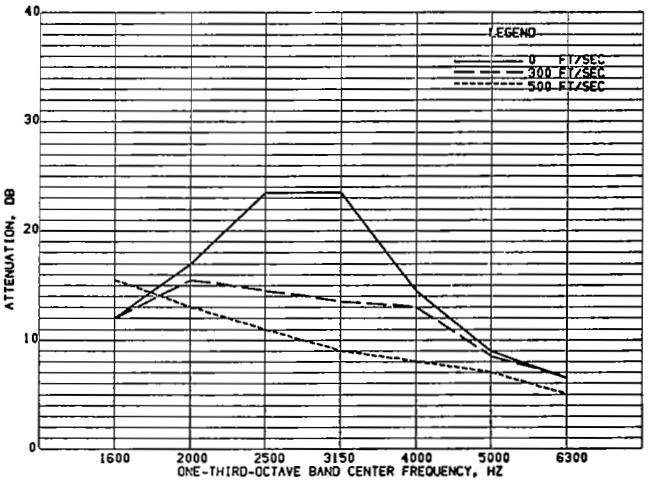

FIGURE 42.- INLET MODE. EFFECT OF VELOCITY FOR CONFIGURATION R117

CONFIGURATION DESCRIPTION.- SURFACE NO 1=40 RAYL FM
CAVITY NO 1=0.5-IN DEEP
SURFACE NO 2=10 RAYL FM
CAVITY NO 2=0.25-IN DEEP

* FM=FIBERMETAL. FIBERGLASS HONEYCOMB CORE WAS 0.75-IN. TREATMENT LENGTH WAS 22.5-IN. AND BEGAN AT INLET PLANE. SURFACE AND CAVITY NO 1 IS NEXT TO AIRFLOW. SURFACE AND CAVITY NO 2 IS NEXT TO OUTER DUCT WALL.

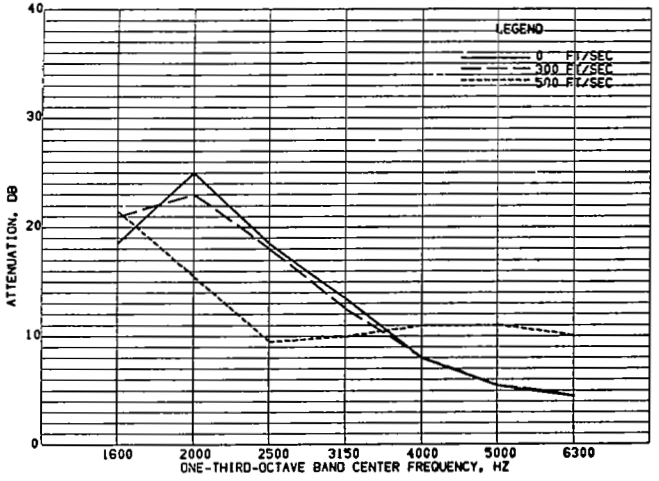

FIGURE 44.- INLET MODE. EFFECT OF VELOCITY FOR CONFIGURATION R122

CONFIGURATION DESCRIPTION.- SURFACE NO 1=10 RAYL FM
CAVITY NO 1=0.25-IN DEEP
SURFACE NO 2=10 RAYL FM
CAVITY NO 2=0.75-IN DEEP

* FM=FIBERMETAL. FIBERGLASS HONEYCOMB CORE WAS 0.75-IN. TREATMENT LENGTH WAS 22.5-IN. AND BEGAN AT INLET PLANE. SURFACE AND CAVITY NO 1 IS NEXT TO AIRFLOW. SURFACE AND CAVITY NO 2 IS NEXT TO OUTER DUCT WALL.

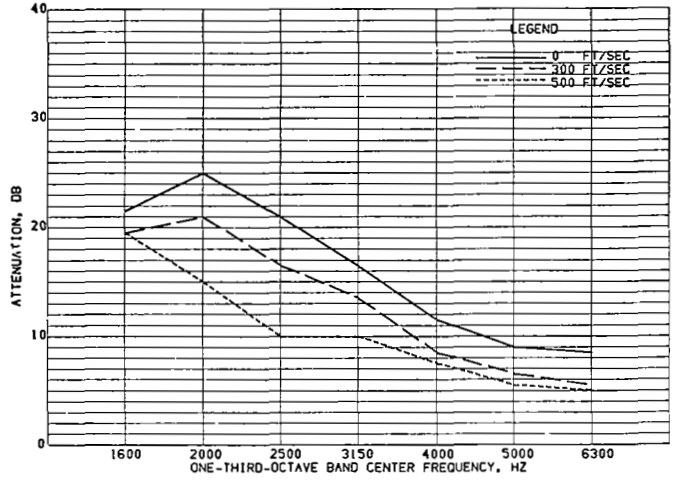

FIGURE 45.- INLET MODE. EFFECT OF VELOCITY FOR CONFIGURATION R123

CONFIGURATION DESCRIPTION.- SURFACE NO 1=10 RAYL FM
CAVITY NO 1=0.25-IN DEEP
SURFACE NO 2=40 RAYL FM
CAVITY NO 2=0.75-IN DEEP

* FM=FIBERMETAL. FIBERGLASS HONEYCOMB CORE WAS 0.75-IN. TREATMENT LENGTH WAS 22.5-IN. AND BEGAN AT INLET PLANE. SURFACE AND CAVITY NO 1 IS NEXT TO AIRFLOW. SURFACE AND CAVITY NO 2 IS NEXT TO OUTER DUCT WALL.

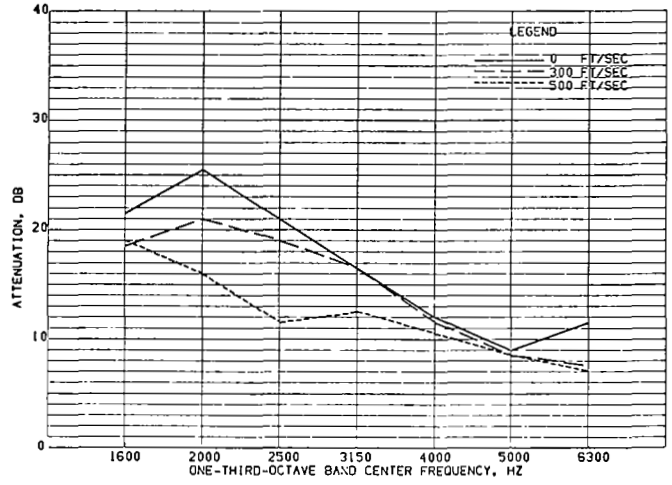

FIGURE 47.- INLET MODE. EFFECT OF VELOCITY FOR CONFIGURATION R125

CONFIGURATION DESCRIPTION.- SURFACE NO 1=40 RAYL FM
CAVITY NO 1=0.25-IN DEEP
SURFACE NO 2=10 RAYL FM
CAVITY NO 2=0.75-IN DEEP

* FM=FIBERMETAL. FIBERGLASS HONEYCOMB CORE WAS 0.75-IN. TREATMENT LENGTH WAS 22.5-IN. AND BEGAN AT INLET PLANE. SURFACE AND CAVITY NO 1 IS NEXT TO AIRFLOW. SURFACE AND CAVITY NO 2 IS NEXT TO OUTER DUCT WALL.

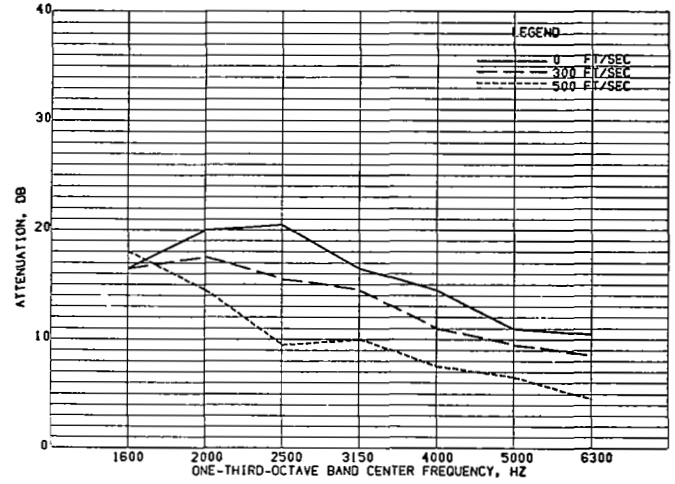

FIGURE 46.- INLET MODE. EFFECT OF VELOCITY FOR CONFIGURATION R124

CONFIGURATION DESCRIPTION.- SURFACE NO 1=10 RAYL FM
CAVITY NO 1=0.25-IN DEEP
SURFACE NO 2=80 RAYL FM
CAVITY NO 2=0.75-IN DEEP

* FM=FIBERMETAL. FIBERGLASS HONEYCOMB CORE WAS 0.75-IN. TREATMENT LENGTH WAS 22.5-IN. AND BEGAN AT INLET PLANE. SURFACE AND CAVITY NO 1 IS NEXT TO AIRFLOW. SURFACE AND CAVITY NO 2 IS NEXT TO OUTER DUCT WALL.

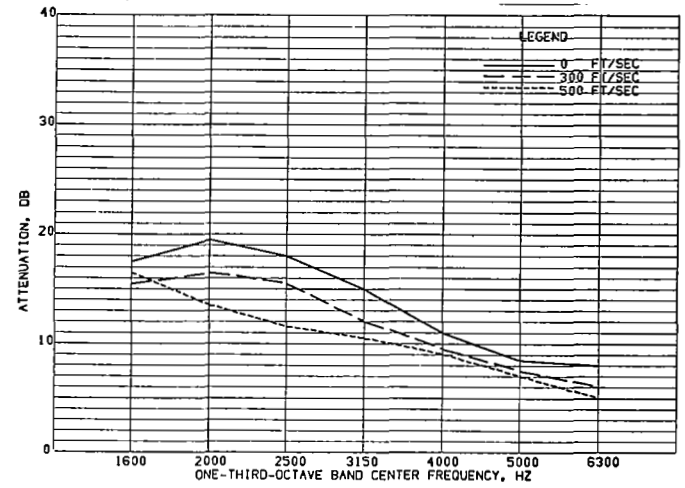

FIGURE 48.- INLET MODE. EFFECT OF VELOCITY FOR CONFIGURATION R126

CONFIGURATION DESCRIPTION.- SURFACE NO 1=40 RAYL FM
CAVITY NO 1=0.25-IN DEEP
SURFACE NO 2=40 RAYL FM
CAVITY NO 2=0.75-IN DEEP

* FM=FIBERMETAL. FIBERGLASS HONEYCOMB CORE WAS 0.75-IN. TREATMENT LENGTH WAS 22.5-IN. AND BEGAN AT INLET PLANE. SURFACE AND CAVITY NO 1 IS NEXT TO AIRFLOW. SURFACE AND CAVITY NO 2 IS NEXT TO OUTER DUCT WALL.

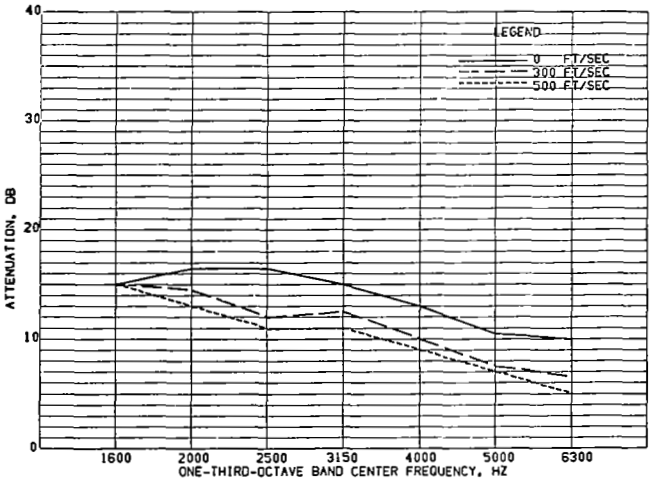

FIGURE 49.- INLET MODE. EFFECT OF VELOCITY FOR CONFIGURATION R127

CONFIGURATION DESCRIPTION.- SURFACE NO 1=40 RAYL FM
CAVITY NO 1=0.25-IN DEEP
SURFACE NO 2=80 RAYL FM
CAVITY NO 2=0.75-IN DEEP

* FM=FIBERMETAL. FIBERGLASS HONEYCOMB CORE WAS 0.75-IN. TREATMENT LENGTH WAS 22.5-IN. AND BEGAN AT INLET PLANE. SURFACE AND CAVITY NO 1 IS NEXT TO AIRFLOW. SURFACE AND CAVITY NO 2 IS NEXT TO OUTER DUCT WALL.

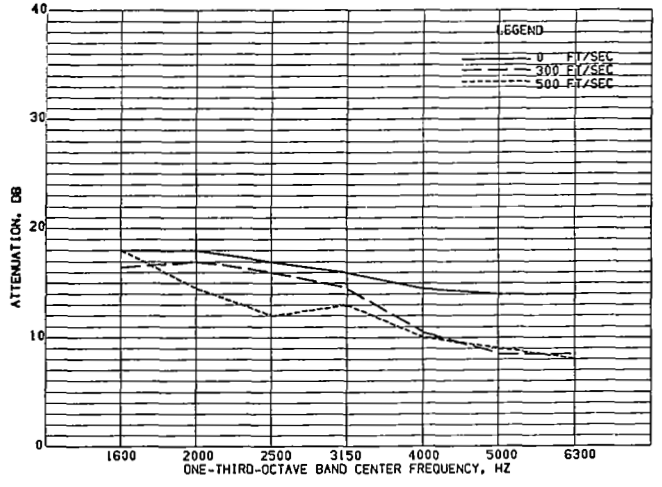

FIGURE 51.- INLET MODE. EFFECT OF VELOCITY FOR CONFIGURATION R129

CONFIGURATION DESCRIPTION.- SURFACE NO 1=80 RAYL FM
CAVITY NO 1=0.25-IN DEEP
SURFACE NO 2=40 RAYL FM
CAVITY NO 2=0.75-IN DEEP

* FM=FIBERMETAL. FIBERGLASS HONEYCOMB CORE WAS 0.75-IN. TREATMENT LENGTH WAS 22.5-IN. AND BEGAN AT INLET PLANE. SURFACE AND CAVITY NO 1 IS NEXT TO AIRFLOW. SURFACE AND CAVITY NO 2 IS NEXT TO OUTER DUCT WALL.

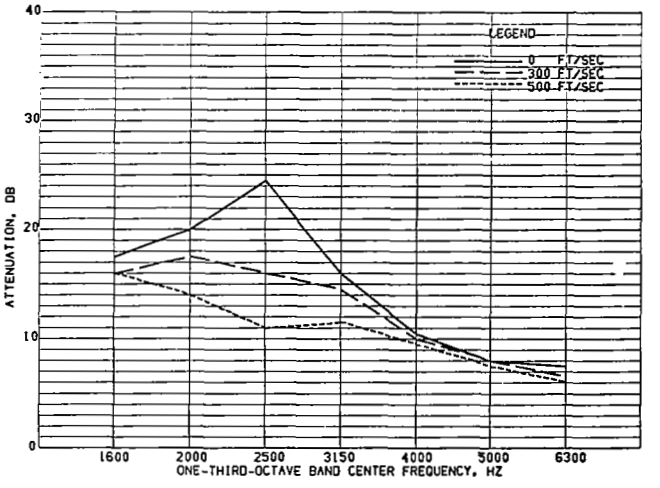

FIGURE 50.- INLET MODE. EFFECT OF VELOCITY FOR CONFIGURATION R128

CONFIGURATION DESCRIPTION.- SURFACE NO 1=80 RAYL FM
CAVITY NO 1=0.25-IN DEEP
SURFACE NO 2=10 RAYL FM
CAVITY NO 2=0.75-IN DEEP

* FM=FIBERMETAL. FIBERGLASS HONEYCOMB CORE WAS 0.75-IN. TREATMENT LENGTH WAS 22.5-IN. AND BEGAN AT INLET PLANE. SURFACE AND CAVITY NO 1 IS NEXT TO AIRFLOW. SURFACE AND CAVITY NO 2 IS NEXT TO OUTER DUCT WALL.

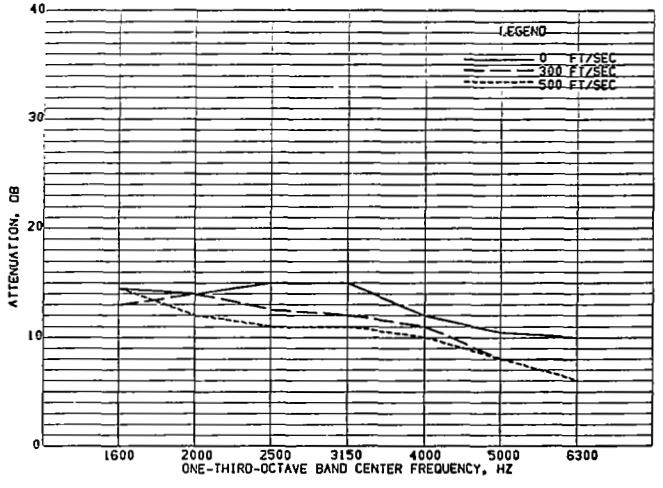

FIGURE 52.- INLET MODE. EFFECT OF VELOCITY FOR CONFIGURATION R130

CONFIGURATION DESCRIPTION.- SURFACE NO 1=80 RAYL FM
CAVITY NO 1=0.25-IN DEEP
SURFACE NO 2=80 RAYL FM
CAVITY NO 2=0.75-IN DEEP

* FM=FIBERMETAL. FIBERGLASS HONEYCOMB CORE WAS 0.75-IN. TREATMENT LENGTH WAS 22.5-IN. AND BEGAN AT INLET PLANE. SURFACE AND CAVITY NO 1 IS NEXT TO AIRFLOW. SURFACE AND CAVITY NO 2 IS NEXT TO OUTER DUCT WALL.

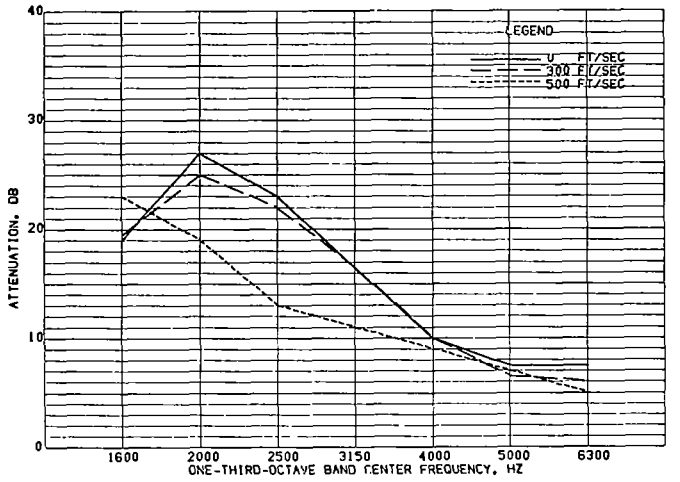

FIGURE 53.- INLET MODE. EFFECT OF VELOCITY FOR CONFIGURATION R131

CONFIGURATION DESCRIPTION.- SURFACE NO 1=10 RAYL FM
CAVITY NO 1=0.5-IN DEEP
SURFACE NO 2=10 RAYL FM
CAVITY NO 2=0.5-IN DEEP

* FM=FIBERMETAL. FIBERGLASS HONEYCOMB CORE WAS 0.75-IN. TREATMENT LENGTH WAS 22.5-IN. AND BEGAN AT INLET PLANE. SURFACE AND CAVITY NO 1 IS NEXT TO AIRFLOW. SURFACE AND CAVITY NO 2 IS NEXT TO OUTER DUCT WALL.

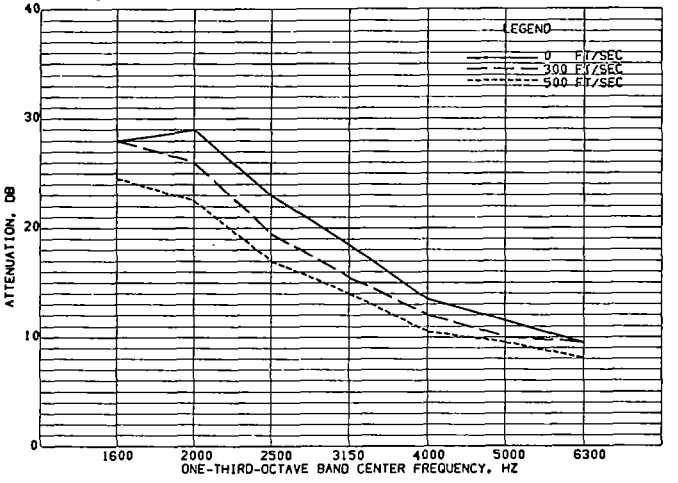

FIGURE 55.- INLET MODE. EFFECT OF VELOCITY FOR CONFIGURATION R133

CONFIGURATION DESCRIPTION.- SURFACE NO 1=10 RAYL FM
CAVITY NO 1=0.5-IN DEEP
SURFACE NO 2=80 RAYL FM
CAVITY NO 2=0.5-IN DEEP

* FM=FIBERMETAL. FIBERGLASS HONEYCOMB CORE WAS 0.75-IN. TREATMENT LENGTH WAS 22.5-IN. AND BEGAN AT INLET PLANE. SURFACE AND CAVITY NO 1 IS NEXT TO AIRFLOW. SURFACE AND CAVITY NO 2 IS NEXT TO OUTER DUCT WALL.

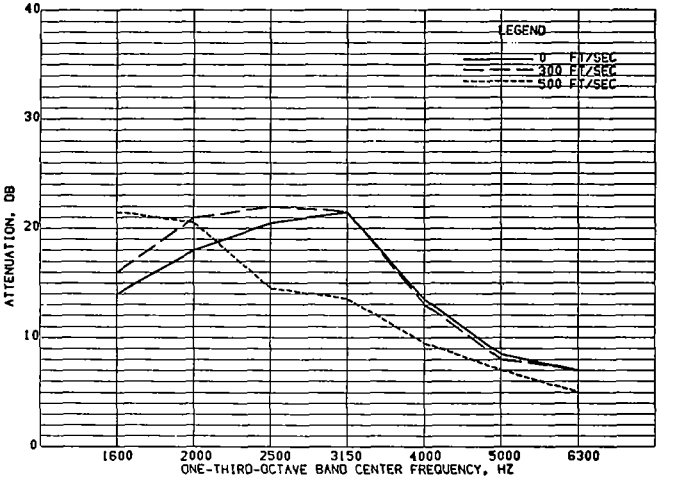

FIGURE 54.- INLET MODE. EFFECT OF VELOCITY FOR CONFIGURATION R132

CONFIGURATION DESCRIPTION.- SURFACE NO 1=10 RAYL FM
CAVITY NO 1=0.5-IN DEEP
SURFACE NO 2=40 RAYL FM
CAVITY NO 2=0.5-IN DEEP

* FM=FIBERMETAL. FIBERGLASS HONEYCOMB CORE WAS 0.75-IN. TREATMENT LENGTH WAS 22.5-IN. AND BEGAN AT INLET PLANE. SURFACE AND CAVITY NO 1 IS NEXT TO AIRFLOW. SURFACE AND CAVITY NO 2 IS NEXT TO OUTER DUCT WALL.

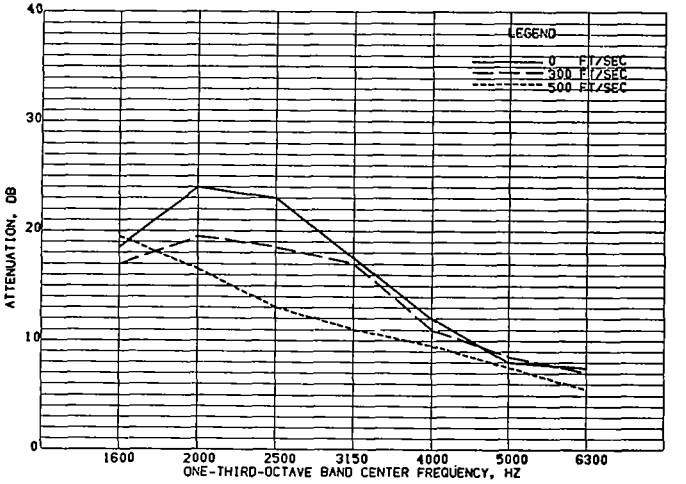

FIGURE 56.- INLET MODE. EFFECT OF VELOCITY FOR CONFIGURATION R134

CONFIGURATION DESCRIPTION.- SURFACE NO 1=40 RAYL FM
CAVITY NO 1=0.5-IN DEEP
SURFACE NO 2=10 RAYL FM
CAVITY NO 2=0.5-IN DEEP

* FM=FIBERMETAL. FIBERGLASS HONEYCOMB CORE WAS 0.75-IN. TREATMENT LENGTH WAS 22.5-IN. AND BEGAN AT INLET PLANE. SURFACE AND CAVITY NO 1 IS NEXT TO AIRFLOW. SURFACE AND CAVITY NO 2 IS NEXT TO OUTER DUCT WALL.

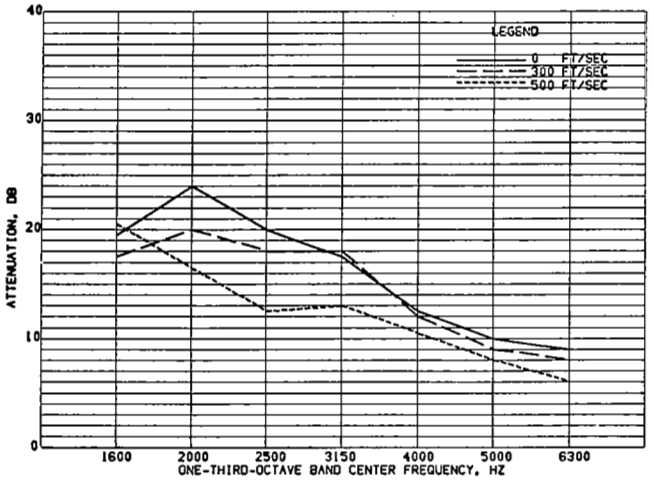

FIGURE 57.- INLET MODE. EFFECT OF VELOCITY FOR CONFIGURATION R135

CONFIGURATION DESCRIPTION.- SURFACE NO 1=40 RAYL FM
CAVITY NO 1=0.5-IN DEEP
SURFACE NO 2=40 RAYL FM
CAVITY NO 2=0.5-IN DEEP

• FM=FIBERMETAL. FIBERGLASS HONEYCOMB CORE WAS 0.75-IN. TREATMENT LENGTH WAS 22.5-IN. AND BEGAN AT INLET PLANE. SURFACE AND CAVITY NO 1 IS NEXT TO AIRFLOW. SURFACE AND CAVITY NO 2 IS NEXT TO OUTER DUCT WALL.

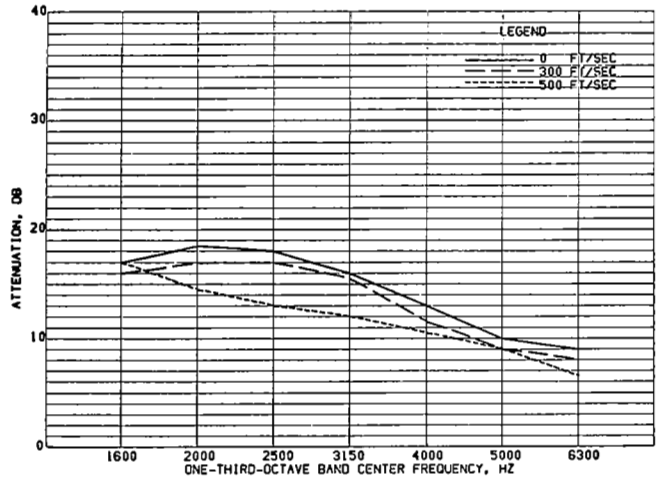

FIGURE 59.- INLET MODE. EFFECT OF VELOCITY FOR CONFIGURATION R137

CONFIGURATION DESCRIPTION.- SURFACE NO 1=80 RAYL FM
CAVITY NO 1=0.5-IN DEEP
SURFACE NO 2=10 RAYL FM
CAVITY NO 2=0.5-IN DEEP

• FM=FIBERMETAL. FIBERGLASS HONEYCOMB CORE WAS 0.75-IN. TREATMENT LENGTH WAS 22.5-IN. AND BEGAN AT INLET PLANE. SURFACE AND CAVITY NO 1 IS NEXT TO AIRFLOW. SURFACE AND CAVITY NO 2 IS NEXT TO OUTER DUCT WALL.

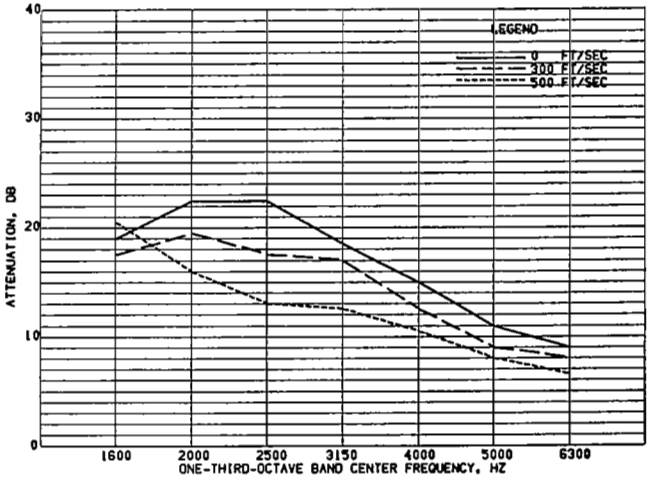

FIGURE 58.- INLET MODE. EFFECT OF VELOCITY FOR CONFIGURATION R136

CONFIGURATION DESCRIPTION.- SURFACE NO 1=40 RAYL FM
CAVITY NO 1=0.5-IN DEEP
SURFACE NO 2=80 RAYL FM
CAVITY NO 2=0.5-IN DEEP

• FM=FIBERMETAL. FIBERGLASS HONEYCOMB CORE WAS 0.75-IN. TREATMENT LENGTH WAS 22.5-IN. AND BEGAN AT INLET PLANE. SURFACE AND CAVITY NO 1 IS NEXT TO AIRFLOW. SURFACE AND CAVITY NO 2 IS NEXT TO OUTER DUCT WALL.

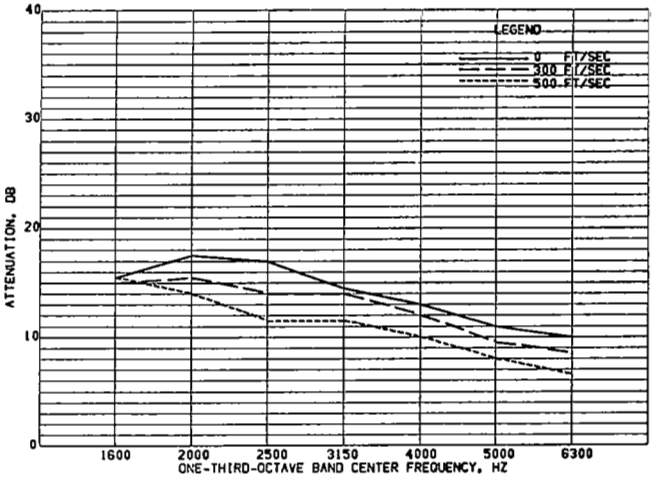

FIGURE 60.- INLET MODE. EFFECT OF VELOCITY FOR CONFIGURATION R138

CONFIGURATION DESCRIPTION.- SURFACE NO 1=80 RAYL FM
CAVITY NO 1=0.5-IN DEEP
SURFACE NO 2=40 RAYL FM
CAVITY NO 2=0.5-IN DEEP

• FM=FIBERMETAL. FIBERGLASS HONEYCOMB CORE WAS 0.75-IN. TREATMENT LENGTH WAS 22.5-IN. AND BEGAN AT INLET PLANE. SURFACE AND CAVITY NO 1 IS NEXT TO AIRFLOW. SURFACE AND CAVITY NO 2 IS NEXT TO OUTER DUCT WALL.

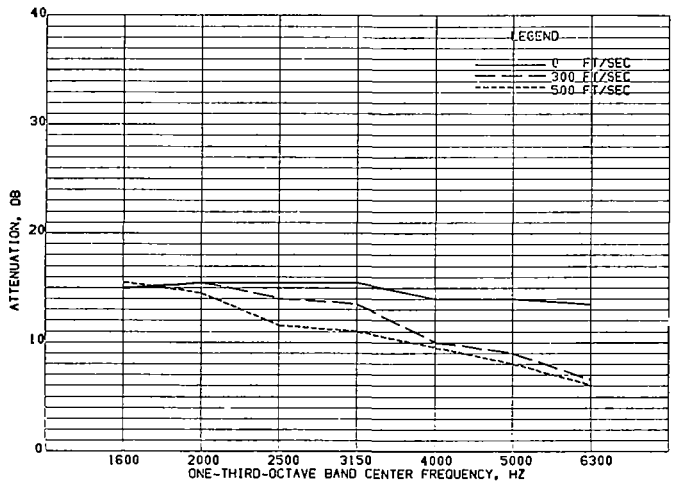

FIGURE 61.- INLET MODE. EFFECT OF VELOCITY FOR CONFIGURATION R139

CONFIGURATION DESCRIPTION.- SURFACE NO 1=80 RAYL FM
CAVITY NO 1=0.5-IN DEEP
SURFACE NO 2=80 RAYL FM
CAVITY NO 2=0.5-IN DEEP

• FM=FIBERMETAL. FIBERGLASS HONEYCOMB CORE WAS 0.75-IN. TREATMENT LENGTH WAS 22.5-IN. AND BEGAN AT INLET PLANE. SURFACE AND CAVITY NO 1 IS NEXT TO AIRFLOW. SURFACE AND CAVITY NO 2 IS NEXT TO OUTER DUCT WALL.

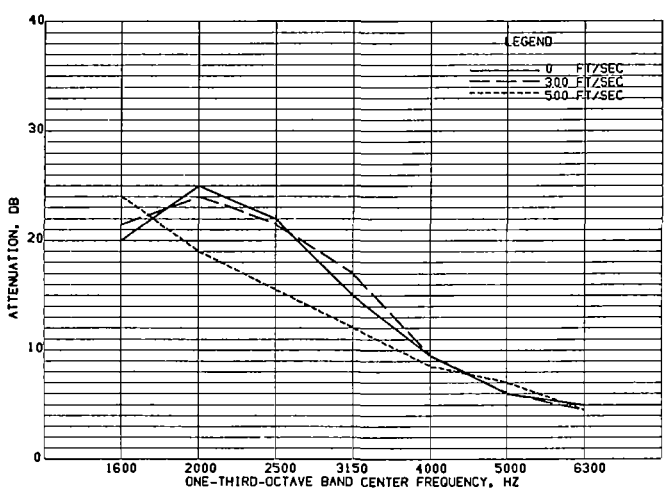

FIGURE 63.- INLET MODE. EFFECT OF VELOCITY FOR CONFIGURATION R141

CONFIGURATION DESCRIPTION.- SURFACE NO 1=10 RAYL FM
CAVITY NO 1=0.75-IN DEEP
SURFACE NO 2=40 RAYL FM
CAVITY NO 2=0.25-IN DEEP

• FM=FIBERMETAL. FIBERGLASS HONEYCOMB CORE WAS 0.75-IN. TREATMENT LENGTH WAS 22.5-IN. AND BEGAN AT INLET PLANE. SURFACE AND CAVITY NO 1 IS NEXT TO AIRFLOW. SURFACE AND CAVITY NO 2 IS NEXT TO OUTER DUCT WALL.

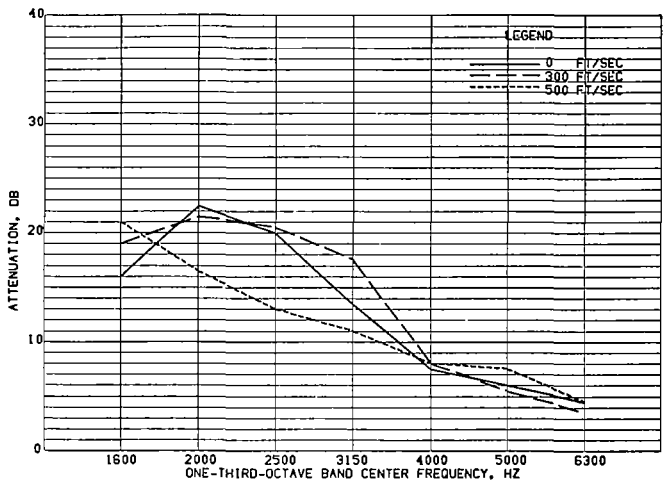

FIGURE 62.- INLET MODE. EFFECT OF VELOCITY FOR CONFIGURATION R140

CONFIGURATION DESCRIPTION.- SURFACE NO 1=10 RAYL FM
CAVITY NO 1=0.75-IN DEEP
SURFACE NO 2=10 RAYL FM
CAVITY NO 2=0.25-IN DEEP

• FM=FIBERMETAL. FIBERGLASS HONEYCOMB CORE WAS 0.75-IN. TREATMENT LENGTH WAS 22.5-IN. AND BEGAN AT INLET PLANE. SURFACE AND CAVITY NO 1 IS NEXT TO AIRFLOW. SURFACE AND CAVITY NO 2 IS NEXT TO OUTER DUCT WALL.

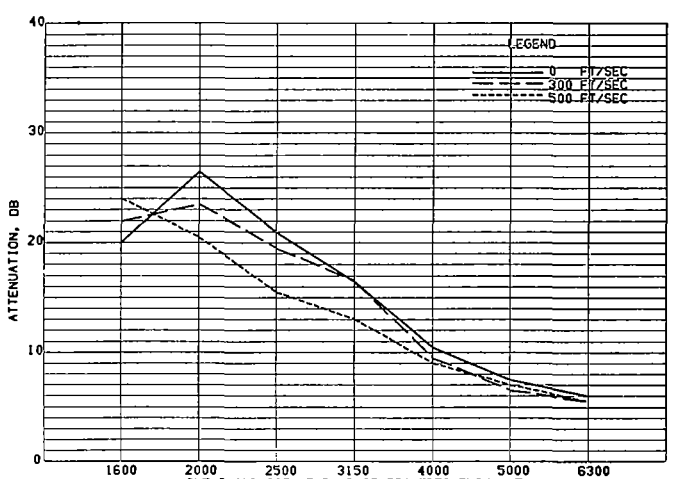

FIGURE 64.- INLET MODE. EFFECT OF VELOCITY FOR CONFIGURATION R142

CONFIGURATION DESCRIPTION.- SURFACE NO 1=10 RAYL FM
CAVITY NO 1=0.75-IN DEEP
SURFACE NO 2=80 RAYL FM
CAVITY NO 2=0.25-IN DEEP

• FM=FIBERMETAL. FIBERGLASS HONEYCOMB CORE WAS 0.75-IN. TREATMENT LENGTH WAS 22.5-IN. AND BEGAN AT INLET PLANE. SURFACE AND CAVITY NO 1 IS NEXT TO AIRFLOW. SURFACE AND CAVITY NO 2 IS NEXT TO OUTER DUCT WALL.

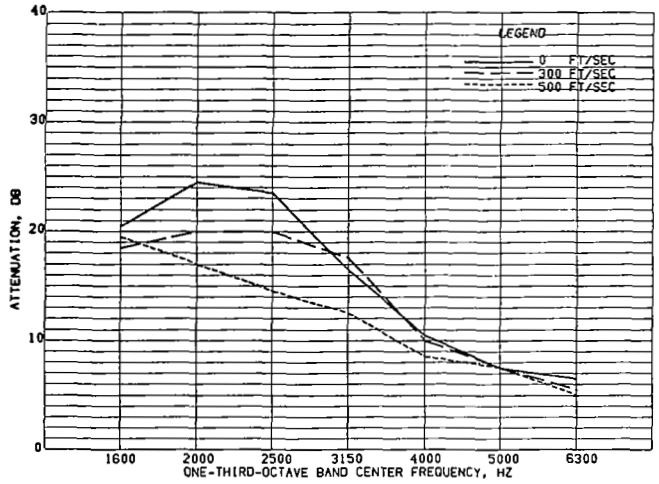

FIGURE 65.- INLET MODE. EFFECT OF VELOCITY FOR CONFIGURATION R143

CONFIGURATION DESCRIPTION.- SURFACE NO 1=40 RAYL FM
CAVITY NO 1=0.75-IN DEEP
SURFACE NO 2=10 RAYL FM
CAVITY NO 2=0.25-IN DEEP

* FM=FIBERMETAL. FIBERGLASS HONEYCOMB CORE WAS 0.75-IN. TREATMENT LENGTH WAS 22.5-IN. AND BEGAN AT INLET PLANE. SURFACE AND CAVITY NO 1 IS NEXT TO AIRFLOW. SURFACE AND CAVITY NO 2 IS NEXT TO OUTER DUCT WALL.

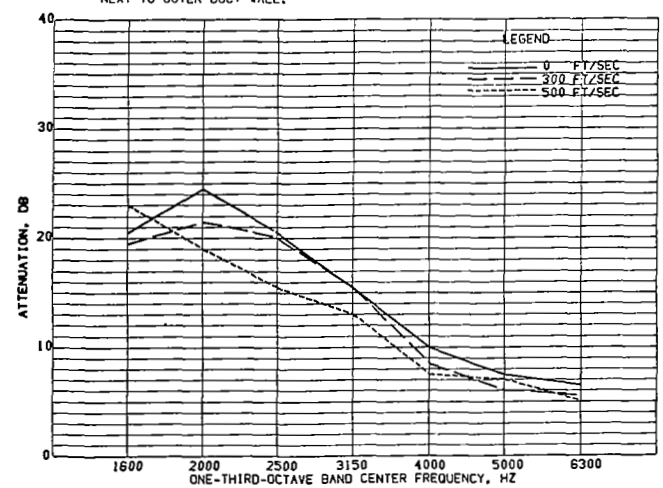

FIGURE 67.- INLET MODE. EFFECT OF VELOCITY FOR CONFIGURATION R145

CONFIGURATION DESCRIPTION.- SURFACE NO 1=40 RAYL FM
CAVITY NO 1=0.75-IN DEEP
SURFACE NO 2=80 RAYL FM
CAVITY NO 2=0.25-IN DEEP

* FM=FIBERMETAL. FIBERGLASS HONEYCOMB CORE WAS 0.75-IN. TREATMENT LENGTH WAS 22.5-IN. AND BEGAN AT INLET PLANE. SURFACE AND CAVITY NO 1 IS NEXT TO AIRFLOW. SURFACE AND CAVITY NO 2 IS NEXT TO OUTER DUCT WALL.

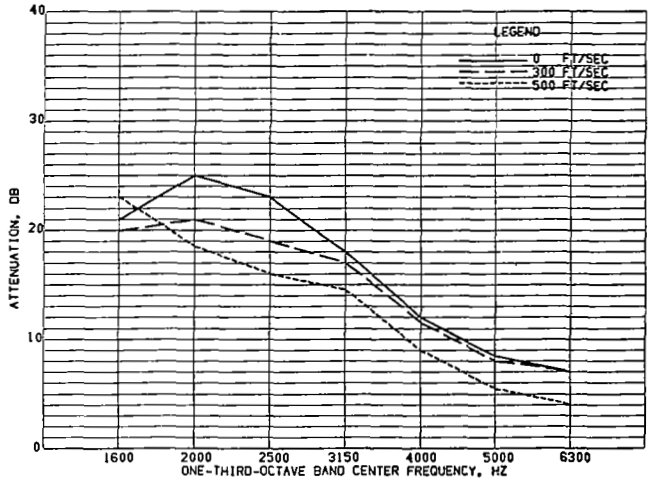

FIGURE 66.- INLET MODE. EFFECT OF VELOCITY FOR CONFIGURATION R144

CONFIGURATION DESCRIPTION.- SURFACE NO 1=40 RAYL FM
CAVITY NO 1=0.75-IN DEEP
SURFACE NO 2=40 RAYL FM
CAVITY NO 2=0.25-IN DEEP

* FM=FIBERMETAL. FIBERGLASS HONEYCOMB CORE WAS 0.75-IN. TREATMENT LENGTH WAS 22.5-IN. AND BEGAN AT INLET PLANE. SURFACE AND CAVITY NO 1 IS NEXT TO AIRFLOW. SURFACE AND CAVITY NO 2 IS NEXT TO OUTER DUCT WALL.

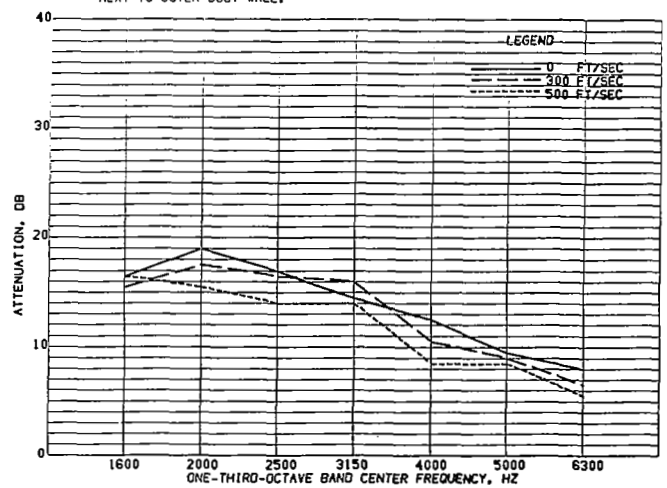

FIGURE 68.- INLET MODE. EFFECT OF VELOCITY FOR CONFIGURATION R146

CONFIGURATION DESCRIPTION.- SURFACE NO 1=80 RAYL FM
CAVITY NO 1=0.75-IN DEEP
SURFACE NO 2=10 RAYL FM
CAVITY NO 2=0.25-IN DEEP

* FM=FIBERMETAL. FIBERGLASS HONEYCOMB CORE WAS 0.75-IN. TREATMENT LENGTH WAS 22.5-IN. AND BEGAN AT INLET PLANE. SURFACE AND CAVITY NO 1 IS NEXT TO AIRFLOW. SURFACE AND CAVITY NO 2 IS NEXT TO OUTER DUCT WALL.

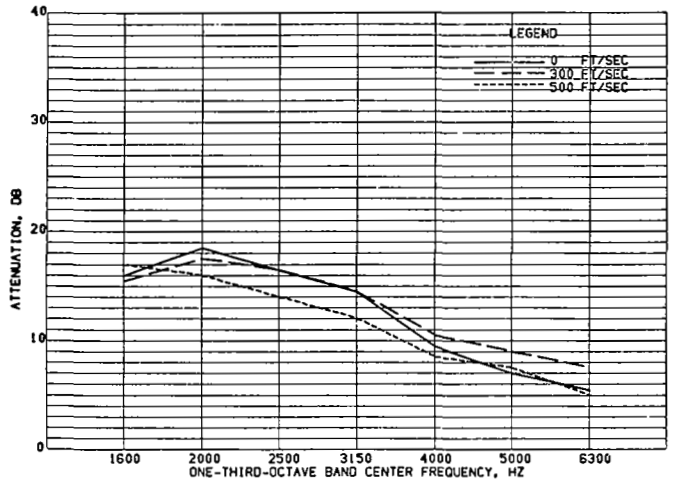

FIGURE 69.- INLET MODE. EFFECT OF VELOCITY FOR CONFIGURATION R147

CONFIGURATION DESCRIPTION.- SURFACE NO 1=80 RAYL FM
CAVITY NO 1=0.75-IN DEEP
SURFACE NO 2=40 RAYL FM
CAVITY NO 2=0.25-IN DEEP

♦ FM=FIBERMETAL. FIBERGLASS HONEYCOMB CORE WAS 0.75-IN. TREATMENT LENGTH WAS 22.5-IN. AND BEGAN AT INLET PLANE. SURFACE AND CAVITY NO 1 IS NEXT TO AIRFLOW. SURFACE AND CAVITY NO 2 IS NEXT TO OUTER DUCT WALL.

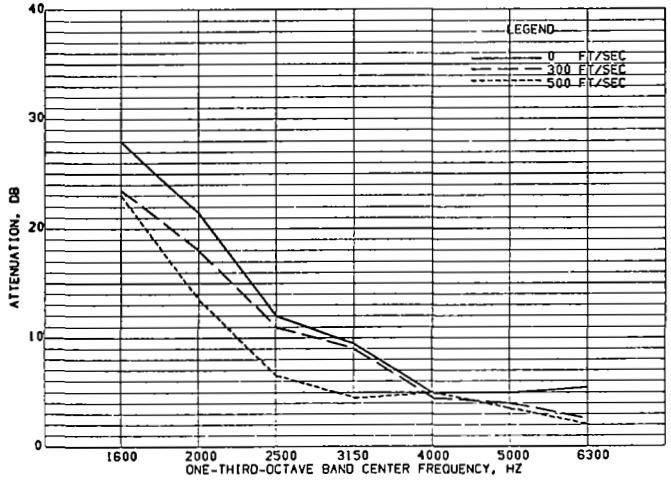

FIGURE 71.- INLET MODE. EFFECT OF VELOCITY FOR CONFIGURATION R155

CONFIGURATION DESCRIPTION.- SURFACE NO 1=10 RAYL FM
CAVITY NO 1=0.25-IN DEEP
SURFACE NO 2=10 RAYL FM
CAVITY NO 2=1.0-IN DEEP

♦ FM=FIBERMETAL. FIBERGLASS HONEYCOMB CORE WAS 0.75-IN. TREATMENT LENGTH WAS 22.5-IN. AND BEGAN AT INLET PLANE. SURFACE AND CAVITY NO 1 IS NEXT TO AIRFLOW. SURFACE AND CAVITY NO 2 IS NEXT TO OUTER DUCT WALL.

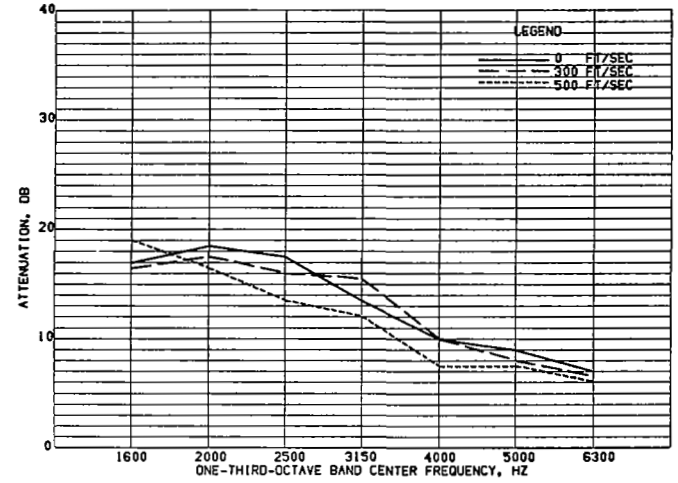

FIGURE 70.- INLET MODE. EFFECT OF VELOCITY FOR CONFIGURATION R148

CONFIGURATION DESCRIPTION.- SURFACE NO 1=80 RAYL FM
CAVITY NO 1=0.75-IN DEEP
SURFACE NO 2=80 RAYL FM
CAVITY NO 2=0.25-IN DEEP

♦ FM=FIBERMETAL. FIBERGLASS HONEYCOMB CORE WAS 0.75-IN. TREATMENT LENGTH WAS 22.5-IN. AND BEGAN AT INLET PLANE. SURFACE AND CAVITY NO 1 IS NEXT TO AIRFLOW. SURFACE AND CAVITY NO 2 IS NEXT TO OUTER DUCT WALL.

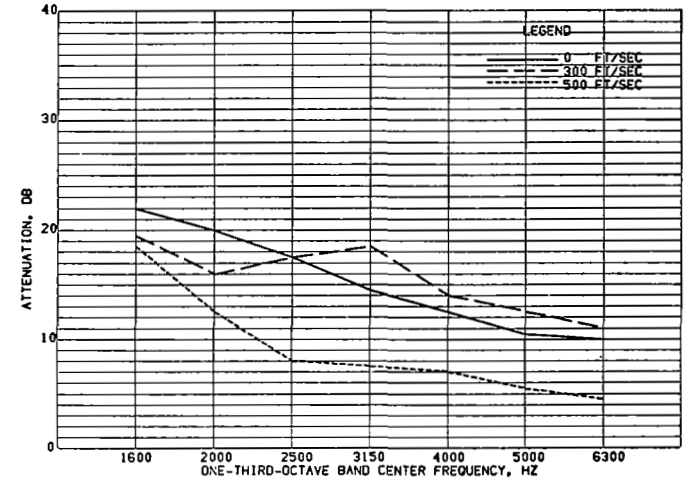

FIGURE 72.- INLET MODE. EFFECT OF VELOCITY FOR CONFIGURATION R158

CONFIGURATION DESCRIPTION.- SURFACE NO 1=10 RAYL FM
CAVITY NO 1=0.25-IN DEEP
SURFACE NO 2=80 RAYL FM
CAVITY NO 2=1.0-IN DEEP

♦ FM=FIBERMETAL. FIBERGLASS HONEYCOMB CORE WAS 0.75-IN. TREATMENT LENGTH WAS 22.5-IN. AND BEGAN AT INLET PLANE. SURFACE AND CAVITY NO 1 IS NEXT TO AIRFLOW. SURFACE AND CAVITY NO 2 IS NEXT TO OUTER DUCT WALL.

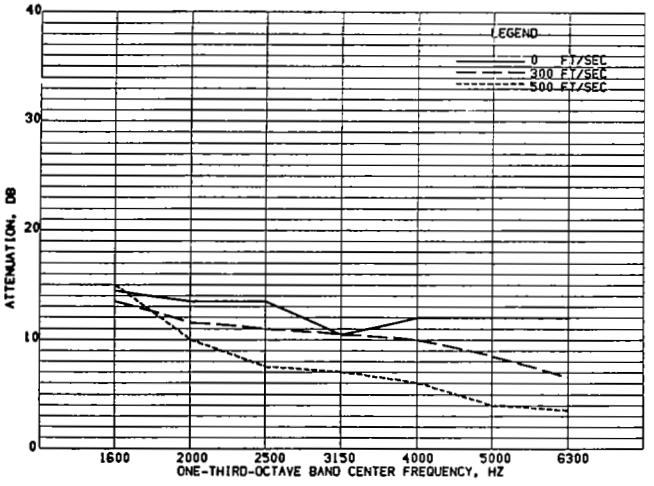

FIGURE 73.- INLET MODE. EFFECT OF VELOCITY FOR CONFIGURATION R159

CONFIGURATION DESCRIPTION.- SURFACE NO 1=10 RAYL FM
CAVITY NO 1=0.25-IN DEEP
SURFACE NO 2=160 RAYL FM
CAVITY NO 2=1.0-IN DEEP

* FM=FIBERMETAL. FIBERGLASS HONEYCOMB CORE WAS 0.75-IN. TREATMENT LENGTH WAS 22.5-IN. AND BEGAN AT INLET PLANE. SURFACE AND CAVITY NO 1 IS NEXT TO AIRFLOW. SURFACE AND CAVITY NO 2 IS NEXT TO OUTER DUCT WALL.

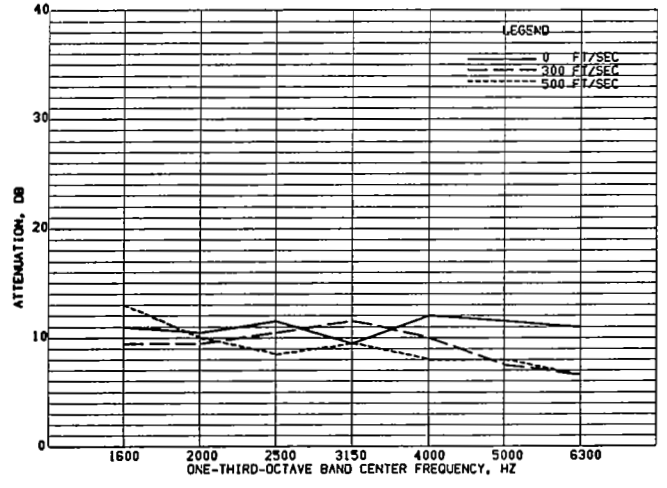

FIGURE 75.- INLET MODE. EFFECT OF VELOCITY FOR CONFIGURATION R169

CONFIGURATION DESCRIPTION.- SURFACE NO 1=80 RAYL FM
CAVITY NO 1=0.25-IN DEEP
SURFACE NO 2=160 RAYL FM
CAVITY NO 2=1.0-IN DEEP

* FM=FIBERMETAL. FIBERGLASS HONEYCOMB CORE WAS 0.75-IN. TREATMENT LENGTH WAS 22.5-IN. AND BEGAN AT INLET PLANE. SURFACE AND CAVITY NO 1 IS NEXT TO AIRFLOW. SURFACE AND CAVITY NO 2 IS NEXT TO OUTER DUCT WALL.

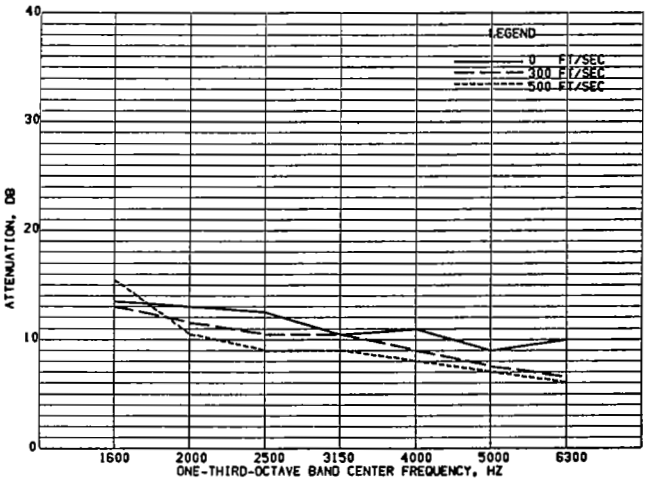

FIGURE 74.- INLET MODE. EFFECT OF VELOCITY FOR CONFIGURATION R168

CONFIGURATION DESCRIPTION.- SURFACE NO 1=80 RAYL FM
CAVITY NO 1=0.25-IN DEEP
SURFACE NO 2=80 RAYL FM
CAVITY NO 2=1.0-IN DEEP

* FM=FIBERMETAL. FIBERGLASS HONEYCOMB CORE WAS 0.75-IN. TREATMENT LENGTH WAS 22.5-IN. AND BEGAN AT INLET PLANE. SURFACE AND CAVITY NO 1 IS NEXT TO AIRFLOW. SURFACE AND CAVITY NO 2 IS NEXT TO OUTER DUCT WALL.

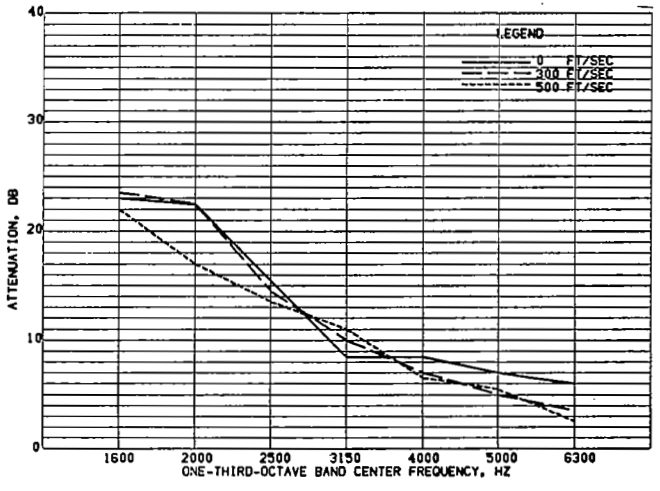

FIGURE 76.- INLET MODE. EFFECT OF VELOCITY FOR CONFIGURATION R179

CONFIGURATION DESCRIPTION.- SURFACE NO 1=10 RAYL FM
CAVITY NO 1=0.75-IN DEEP
SURFACE NO 2=10 RAYL FM
CAVITY NO 2=0.5-IN DEEP

* FM=FIBERMETAL. FIBERGLASS HONEYCOMB CORE WAS 0.75-IN. TREATMENT LENGTH WAS 22.5-IN. AND BEGAN AT INLET PLANE. SURFACE AND CAVITY NO 1 IS NEXT TO AIRFLOW. SURFACE AND CAVITY NO 2 IS NEXT TO OUTER DUCT WALL.

FIGURE 77.- INLET MODE. EFFECT OF VELOCITY FOR CONFIGURATION R185

CONFIGURATION DESCRIPTION.- SURFACE NO 1=10 RAYL FM
CAVITY NO 1=0.75-IN DEEP
SURFACE NO 2=80 RAYL FM
CAVITY NO 2=0.5-IN DEEP

• FM=FIBERMETAL. FIBERGLASS HONEYCOMB CORE WAS 0.75-IN. TREATMENT LENGTH WAS 22.5-IN. AND BEGAN AT INLET PLANE. SURFACE AND CAVITY NO 1 IS NEXT TO AIRFLOW. SURFACE AND CAVITY NO 2 IS NEXT TO OUTER DUCT WALL.

FIGURE 79.- INLET MODE. EFFECT OF VELOCITY FOR CONFIGURATION R188

CONFIGURATION DESCRIPTION.- SURFACE NO 1=10 RAYL FM
CAVITY NO 1=0.5-IN DEEP
SURFACE NO 2=10 RAYL FM
CAVITY NO 2=1.0-IN DEEP

• FM=FIBERMETAL. FIBERGLASS HONEYCOMB CORE WAS 0.75-IN. TREATMENT LENGTH WAS 22.5-IN. AND BEGAN AT INLET PLANE. SURFACE AND CAVITY NO 1 IS NEXT TO AIRFLOW. SURFACE AND CAVITY NO 2 IS NEXT TO OUTER DUCT WALL.

FIGURE 78.- INLET MODE. EFFECT OF VELOCITY FOR CONFIGURATION R187

CONFIGURATION DESCRIPTION.- SURFACE NO 1=80 RAYL FM
CAVITY NO 1=0.75-IN DEEP
SURFACE NO 2=80 RAYL FM
CAVITY NO 2=0.5-IN DEEP

• FM=FIBERMETAL. FIBERGLASS HONEYCOMB CORE WAS 0.75-IN. TREATMENT LENGTH WAS 22.5-IN. AND BEGAN AT INLET PLANE. SURFACE AND CAVITY NO 1 IS NEXT TO AIRFLOW. SURFACE AND CAVITY NO 2 IS NEXT TO OUTER DUCT WALL.

FIGURE 80.- INLET MODE. EFFECT OF VELOCITY FOR CONFIGURATION R192

CONFIGURATION DESCRIPTION.- SURFACE NO 1=10 RAYL FM
CAVITY NO 1=0.5-IN DEEP
SURFACE NO 2=160 RAYL FM
CAVITY NO 2=1.0-IN DEEP

• FM=FIBERMETAL. FIBERGLASS HONEYCOMB CORE WAS 0.75-IN. TREATMENT LENGTH WAS 22.5-IN. AND BEGAN AT INLET PLANE. SURFACE AND CAVITY NO 1 IS NEXT TO AIRFLOW. SURFACE AND CAVITY NO 2 IS NEXT TO OUTER DUCT WALL.

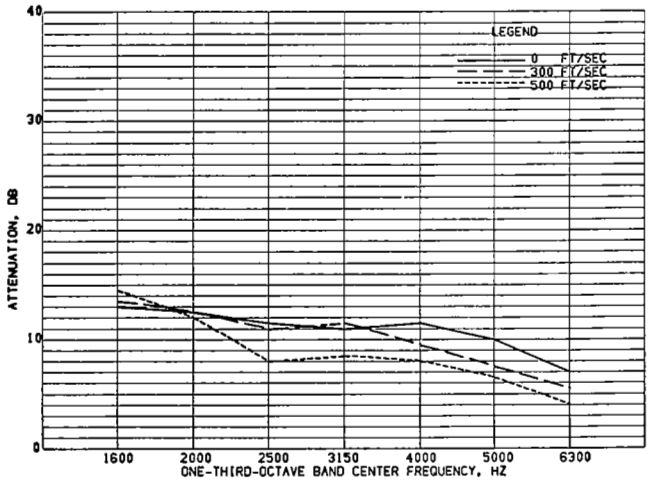

FIGURE 81.- INLET MODE. EFFECT OF VELOCITY FOR CONFIGURATION R201

CONFIGURATION DESCRIPTION.- SURFACE NO 1=80 RAYL FM
CAVITY NO 1=0.5-IN DEEP
SURFACE NO 2=80 RAYL FM
CAVITY NO 2=1.0-IN DEEP

• FM=FIBERMETAL. FIBERGLASS HONEYCOMB CORE WAS 0.75-IN. TREATMENT LENGTH WAS 22.5-IN. AND BEGAN AT INLET PLANE. SURFACE AND CAVITY NO 1 IS NEXT TO AIRFLOW. SURFACE AND CAVITY NO 2 IS NEXT TO OUTER DUCT WALL.

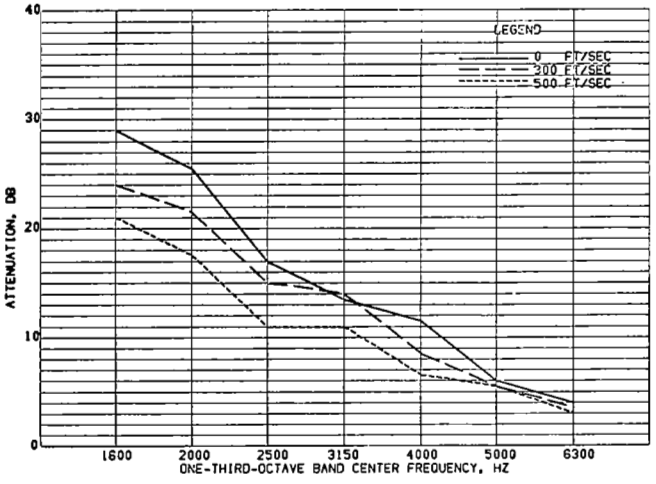

FIGURE 83.- INLET MODE. EFFECT OF VELOCITY FOR CONFIGURATION R203

CONFIGURATION DESCRIPTION.- SURFACE NO 1=10 RAYL FM
CAVITY NO 1=0.75-IN DEEP
SURFACE NO 2=40 RAYL FM
CAVITY NO 2=0.75-IN DEEP

• FM=FIBERMETAL. FIBERGLASS HONEYCOMB CORE WAS 0.75-IN. TREATMENT LENGTH WAS 22.5-IN. AND BEGAN AT INLET PLANE. SURFACE AND CAVITY NO 1 IS NEXT TO AIRFLOW. SURFACE AND CAVITY NO 2 IS NEXT TO OUTER DUCT WALL.

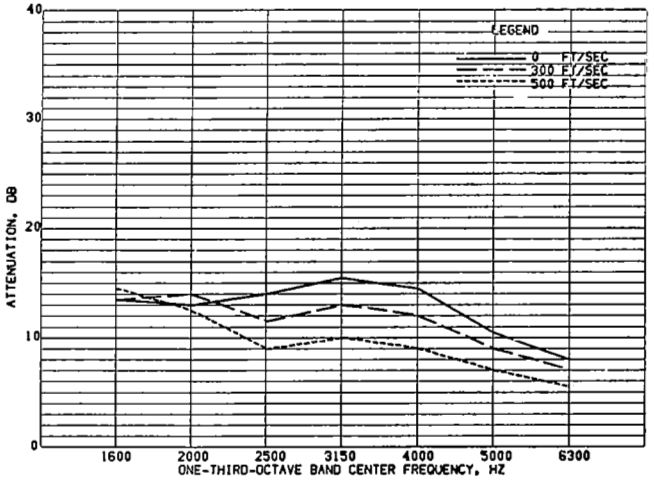

FIGURE 82.- INLET MODE. EFFECT OF VELOCITY FOR CONFIGURATION R202

CONFIGURATION DESCRIPTION.- SURFACE NO 1=80 RAYL FM
CAVITY NO 1=0.5-IN DEEP
SURFACE NO 2=160 RAYL FM
CAVITY NO 2=1.0-IN DEEP

• FM=FIBERMETAL. FIBERGLASS HONEYCOMB CORE WAS 0.75-IN. TREATMENT LENGTH WAS 22.5-IN. AND BEGAN AT INLET PLANE. SURFACE AND CAVITY NO 1 IS NEXT TO AIRFLOW. SURFACE AND CAVITY NO 2 IS NEXT TO OUTER DUCT WALL.

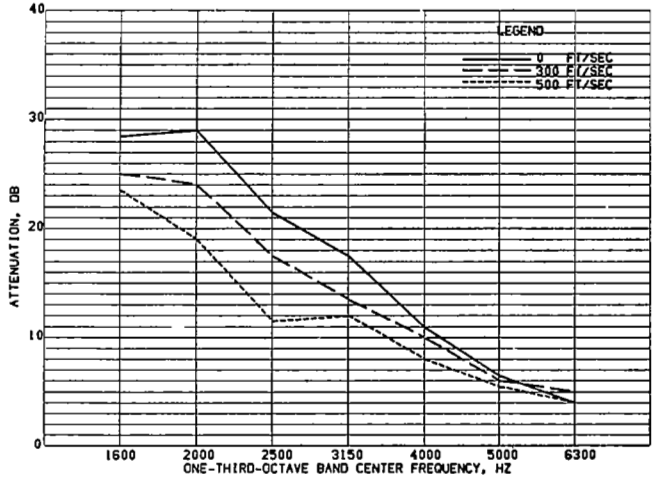

FIGURE 84.- INLET MODE. EFFECT OF VELOCITY FOR CONFIGURATION R204

CONFIGURATION DESCRIPTION.- SURFACE NO 1=10 RAYL FM
CAVITY NO 1=0.75-IN DEEP
SURFACE NO 2=80 RAYL FM
CAVITY NO 2=0.75-IN DEEP

• FM=FIBERMETAL. FIBERGLASS HONEYCOMB CORE WAS 0.75-IN. TREATMENT LENGTH WAS 22.5-IN. AND BEGAN AT INLET PLANE. SURFACE AND CAVITY NO 1 IS NEXT TO AIRFLOW. SURFACE AND CAVITY NO 2 IS NEXT TO OUTER DUCT WALL.

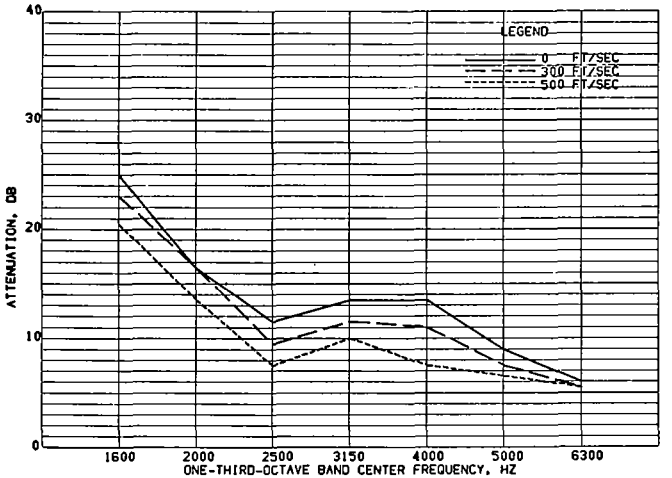

FIGURE 85.- INLET MODE. EFFECT OF VELOCITY FOR CONFIGURATION R209

CONFIGURATION DESCRIPTION.- SURFACE NO 1=10 RAYL FM
CAVITY NO 1=0.75-IN DEEP
SURFACE NO 2=10 RAYL FM
CAVITY NO 2=1.0-IN DEEP

• FM=FIBERMETAL. FIBERGLASS HONEYCOMB CORE WAS 0.75-IN. TREATMENT LENGTH WAS 22.5-IN. AND BEGAN AT INLET PLANE. SURFACE AND CAVITY NO 1 IS NEXT TO AIRFLOW. SURFACE AND CAVITY NO 2 IS NEXT TO OUTER DUCT WALL.

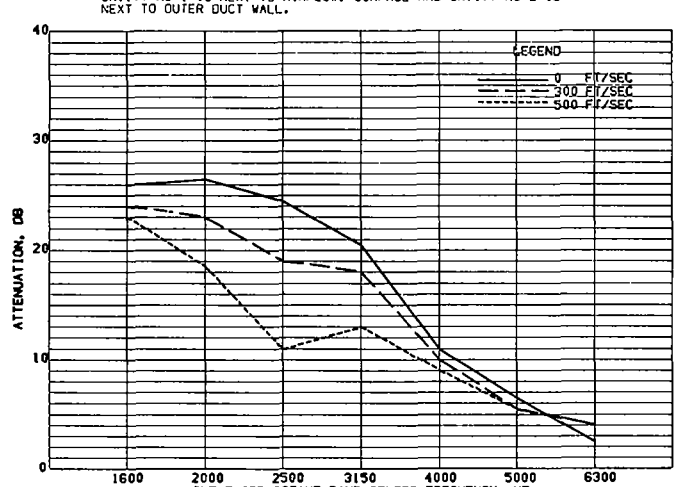

FIGURE 87.- INLET MODE. EFFECT OF VELOCITY FOR CONFIGURATION R213

CONFIGURATION DESCRIPTION.- SURFACE NO 1=10 RAYL FM
CAVITY NO 1=0.75-IN DEEP
SURFACE NO 2=160 RAYL FM
CAVITY NO 2=1.0-IN DEEP

• FM=FIBERMETAL. FIBERGLASS HONEYCOMB CORE WAS 0.75-IN. TREATMENT LENGTH WAS 22.5-IN. AND BEGAN AT INLET PLANE. SURFACE AND CAVITY NO 1 IS NEXT TO AIRFLOW. SURFACE AND CAVITY NO 2 IS NEXT TO OUTER DUCT WALL.

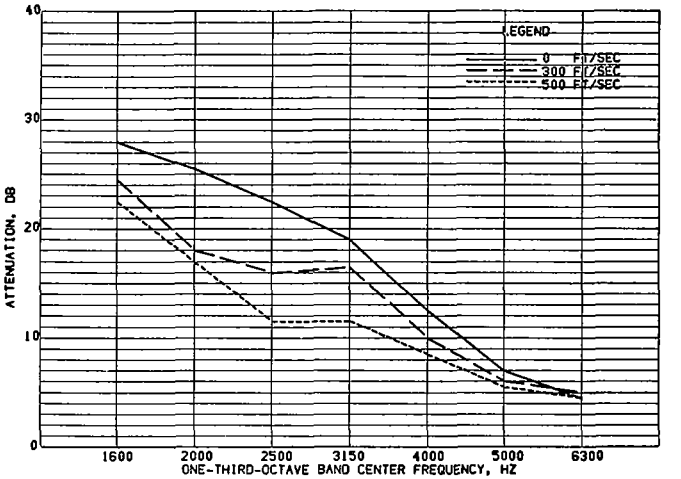

FIGURE 86.- INLET MODE. EFFECT OF VELOCITY FOR CONFIGURATION R212

CONFIGURATION DESCRIPTION.- SURFACE NO 1=10 RAYL FM
CAVITY NO 1=0.75-IN DEEP
SURFACE NO 2=80 RAYL FM
CAVITY NO 2=1.0-IN DEEP

• FM=FIBERMETAL. FIBERGLASS HONEYCOMB CORE WAS 0.75-IN. TREATMENT LENGTH WAS 22.5-IN. AND BEGAN AT INLET PLANE. SURFACE AND CAVITY NO 1 IS NEXT TO AIRFLOW. SURFACE AND CAVITY NO 2 IS NEXT TO OUTER DUCT WALL.

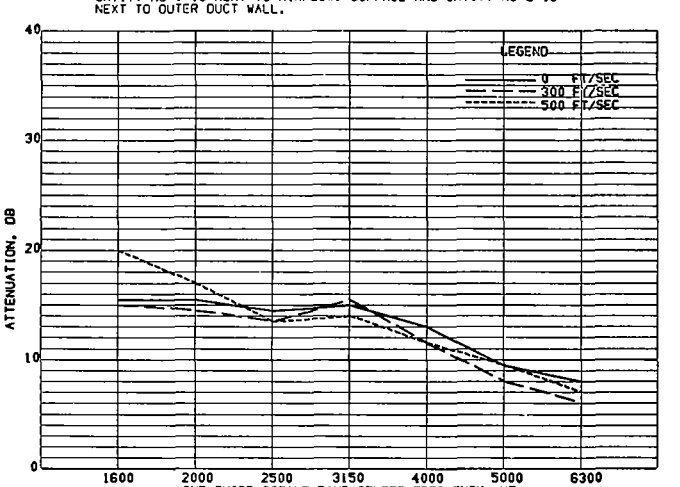

FIGURE 88.- INLET MODE. EFFECT OF VELOCITY FOR CONFIGURATION R222

CONFIGURATION DESCRIPTION.- SURFACE NO 1=80 RAYL FM
CAVITY NO 1=0.75-IN DEEP
SURFACE NO 2=80 RAYL FM
CAVITY NO 2=1.0-IN DEEP

• FM=FIBERMETAL. FIBERGLASS HONEYCOMB CORE WAS 0.75-IN. TREATMENT LENGTH WAS 22.5-IN. AND BEGAN AT INLET PLANE. SURFACE AND CAVITY NO 1 IS NEXT TO AIRFLOW. SURFACE AND CAVITY NO 2 IS NEXT TO OUTER DUCT WALL.

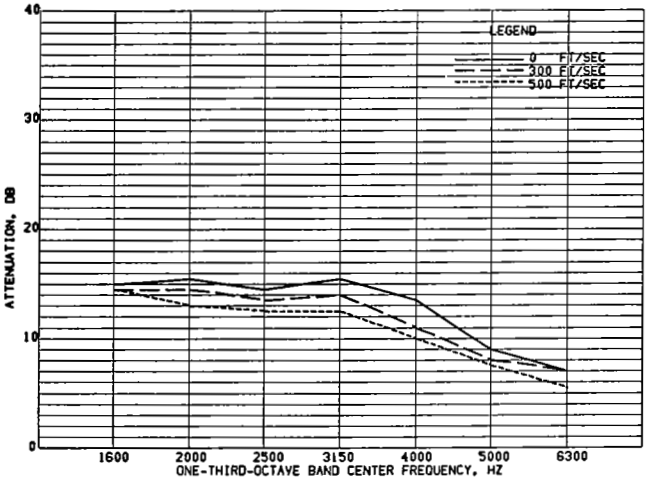

FIGURE 89.- INLET MODE. EFFECT OF VELOCITY FOR CONFIGURATION R223

CONFIGURATION DESCRIPTION.- SURFACE NO 1=80 RAYL FM
CAVITY NO 1=0.75-IN DEEP
SURFACE NO 2=160 RAYL FM
CAVITY NO 2=1.0-IN DEEP

* FM=FIBERMETAL. FIBERGLASS HONEYCOMB CORE WAS 0.75-IN. TREATMENT LENGTH WAS 22.5-IN. AND BEGAN AT INLET PLANE. SURFACE AND CAVITY NO 1 IS NEXT TO AIRFLOW. SURFACE AND CAVITY NO 2 IS NEXT TO OUTER DUCT WALL.

FIGURE 91.- INLET MODE. EFFECT OF VELOCITY FOR CONFIGURATION R1002

CONFIGURATION DESCRIPTION.- SURFACES AND CAVITIES 1, 2 AND 3 = 10, 40 AND 80 RAYL FM-AND 0.5, 0.5 AND 0.5-IN RESPECTIVELY.

* FM=FIBERMETAL. FIBERGLASS HONEYCOMB CORE WAS 0.75-IN. TREATMENT LENGTH WAS 22.5-IN. AND BEGAN AT INLET PLANE. SURFACE AND CAVITY NO 1 IS NEXT TO AIRFLOW. SURFACE AND CAVITY NO 3 IS NEXT TO OUTER DUCT WALL.

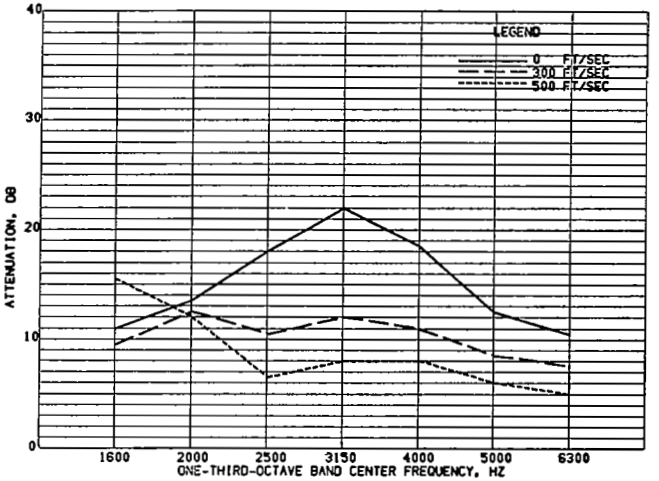

FIGURE 90.- INLET MODE. EFFECT OF VELOCITY FOR CONFIGURATION R1001

CONFIGURATION DESCRIPTION.- SURFACES AND CAVITIES 1, 2 AND 3 = 10, 40 AND 80 RAYL FM-AND 0.25, 0.25, AND 0.25-IN RESPECTIVELY

* FM=FIBERMETAL. FIBERGLASS HONEYCOMB CORE WAS 0.75-IN. TREATMENT LENGTH WAS 22.5-IN. AND BEGAN AT INLET PLANE. SURFACE AND CAVITY NO 1 IS NEXT TO AIRFLOW. SURFACE AND CAVITY NO 3 IS NEXT TO OUTER DUCT WALL.

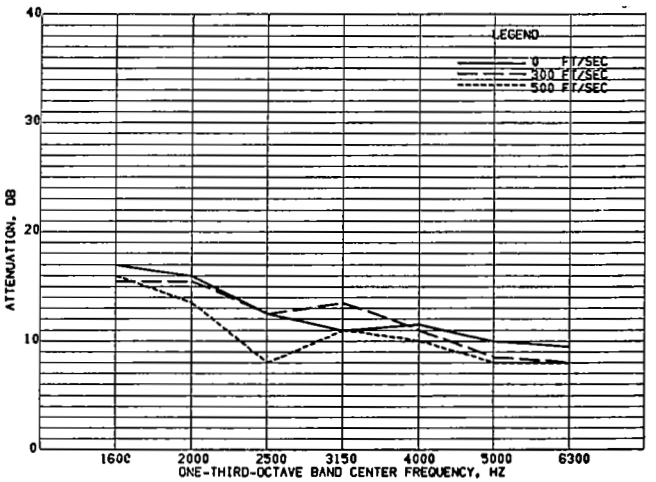

FIGURE 92.- INLET MODE. EFFECT OF VELOCITY FOR CONFIGURATION R1003

CONFIGURATION DESCRIPTION.- SURFACES AND CAVITIES 1, 2 AND 3 = 80, 10 AND 40 RAYL FM-AND 0.5, 0.5 AND 0.5-IN RESPECTIVELY.

* FM=FIBERMETAL. FIBERGLASS HONEYCOMB CORE WAS 0.75-IN. TREATMENT LENGTH WAS 22.5-IN. AND BEGAN AT INLET PLANE. SURFACE AND CAVITY NO 1 IS NEXT TO AIRFLOW. SURFACE AND CAVITY NO 3 IS NEXT TO OUTER DUCT WALL.

APPENDIX D

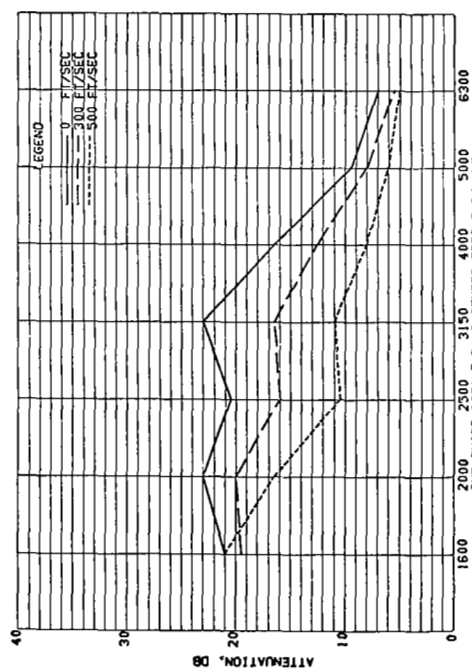

FIGURE 93.- INLET MODE. EFFECT OF VELOCITY FOR CONFIGURATION R1005

CONFIGURATION DESCRIPTION.- SURFACES AND CAVITIES 1, 2, 3, AND 4 = 10, 80, 10 AND 40 RAYL FM-AND 0.5, 0.25, 0.5 AND 0.75-IN

• FM=FIBERMETAL. FIBERGLASS HONEYCOMB CORE WAS 0.75-IN. TREATMENT LENGTH WAS 22.5-IN AND BEGAN AT INLET PLANE. SURFACE AND CAVITY NO 1 IS NEXT TO AIRFLOW. SURFACE AND CAVITY NO 4 IS NEXT TO OUTER DUCT WALL.

Chart series 49

TABLE I. – SUMMARY OF ACOUSTICAL AND ECONOMIC PERFORMANCE OF FAN-DUCT DESIGNS

Configuration	Estimated noise reduction, ΔPNLM, PNdB	Estimated increment in DOC, percent
24-inch treated ducts with supplementary treated panels	7 to 9	1.5
48-inch treated ducts	9 to 11	1.3

TABLE II. – COMPARISON OF ACOUSTICALLY TREATED INLET DESIGNS TO EXISTING INLET DESIGN

Item	Description of inlet design	Gross treated surface area, sq ft	Increase in inlet length, in. (a)	Increase in inlet maximum diameter, in. (b)	Increase in inlet weight, lb (c)
1	One concentric ring vane, existing inlet duct and centerbody	55	0	0	105
2	Two concentric ring vanes, existing inlet duct and centerbody	73	0	0	150
3	Sixteen radial vanes, existing inlet duct and centerbody	83	9	0	295
4	Lightbulb centerbody, lengthened inlet duct, and one ring vane	83	21	3.6	255
5	Same as item 4, but maximum treated area	100	21	3.6	300
6	Retractable inlet flaps	53	30	0	440
7	Retractable radial vanes	46	14	0	330
8	Retractable curved vanes	82	6	1.5	435

[a]Length of existing JT3D inlet is 45 in.

[b]Maximum diameter of existing JT3D inlet at engine attach flange is 72 in. in profile view and 67.2 in. in plan view.

[c]Weight of existing JT3D inlet, less 190 lb of nacelle subsystems, is 236 lb.

TABLE III. – SUMMARY OF ACOUSTICAL AND ECONOMIC PERFORMANCE OF INLET DESIGNS

Item	Description of inlet design	Estimated noise reduction, ΔPNLM, PNdB	Estimated increment in DOC, percent
1	One concentric ring vane, existing inlet duct and centerbody	4 to 6	1.0
2	Two concentric ring vanes, existing inlet duct and centerbody	8 to 10	1.2
3	Sixteen radial vanes, existing inlet duct and centerbody	6 to 8	1.7
4	Lightbulb centerbody, lengthened inlet duct, and one ring vane	6 to 9	1.7
5	Same as item 4, but maximum treated area	7 to 10	1.9
6	Retractable inlet flaps	2 to 5	2.2
7	Retractable radial vanes	1 to 4	1.7
8	Retractable curved vanes	5 to 9	1.9

TABLE IV. – SUMMARY OF CHARACTERISTICS OF POROUS MATERIALS FOR FLOW-RESISTANCE TESTS

(a) Fibermetal samples supplied by the Brunswick Corporation[a]

0.0004-in. diameter wire fibers

Item	Nominal flow resistance, cgs rayls	Nonlinearity factor	Thickness, in.	Surface density, lb/ft^2
1	28.3	1.8	0.032	0.3
2	38.3	1.8	0.009	0.2

0.0005-in. diameter wire fibers

3	9.5	1.6	0.028	0.2
4	11.4	1.4	0.020	0.3
5	36.0	1.5	0.018	0.3
6	39.1	1.4	0.037	0.3
7	40.1	1.3	0.039	0.3
8	41.4	1.7	0.011	0.2
9	42.3	1.6	0.013	0.3
10	42.5	1.4	0.037	0.3
11	54.0	1.7	0.010	0.2
12	60.0	–	0.020	0.2
13	64.0	1.3	0.032	0.3
14	116.0	1.3	0.020	0.3
15	171.0	1.3	0.039	0.4

0.001-in. diameter wire fibers

16	9.2	1.8	0.030	0.3
17	9.4	1.6	0.024	0.2
18	12.4	1.7	0.011	0.2
19	15.0	1.6	0.026	0.2
20	16.6	–	0.020	0.2
21	20.0	1.7	0.041	0.4
22	20.2	1.8	0.042	0.4
23	36.9	1.7	0.028	0.4
24	38.2	1.8	0.029	0.4
25	43.9	1.8	0.015	0.2
26	44.1	1.7	0.040	0.5
27	52.5	1.8	0.021	0.4
28	85.0	1.6	0.030	0.5
29	94.0	–	0.011	0.2
30	100.8	1.8	0.010	0.2
31	123.1	2.5	0.011	0.2
32	132.0	1.9	0.021	0.5
33	132.8	2.5	0.011	0.2
34	200.0	1.7	0.013	0.3

[a]Brunswick Corporation, Needham, Massachusetts. All samples were made from type 304 stainless steel wire fibers. Items 1 through 15 and item 20 were reinforced on both sides with 18 x 18 mesh, 0.009-in. dia, type 304 stainless-steel wire screen. Items 16 through 19 and 21 through 34 had no reinforcing screens.

TABLE IV. – SUMMARY OF CHARACTERISTICS OF POROUS MATERIALS FOR FLOW-RESISTANCE TESTS – Continued

(b) Fibermetal samples supplied by the Huyck Metals Company[a]

0.003-in. diameter wire fibers

Item	Nominal flow resistance, cgs rayls	Nonlinearity factor	Thickness, in.	Surface density, lb/ft^2
1	10.1	2.5	0.048	0.8
2	12.1	2.5	0.048	0.8
3	12.4	2.5	0.049	0.8
4	12.7	2.4	0.048	0.8
5	12.8	2.5	0.049	0.8
6	13.5	2.5	0.049	0.8
7	31.5	2.5	0.047	1.0
8	38.8	2.5	0.048	1.2
9	46.0	2.5	0.049	1.1
10	48.2	2.5	0.048	1.1
11	57.6	2.6	0.049	1.1
12	65.0	2.7	0.045	1.1
13	66.0	2.4	0.045	1.0
14	66.0	2.5	0.045	1.1
15	66.0	2.6	0.049	1.1
16	70.0	2.5	0.045	1.1
17	77.0	2.7	0.049	1.2
18	82.0	2.9	0.049	1.2

0.004-in. diameter wire fibers

19	7.4	2.9	0.040	0.8
20	7.8	2.9	0.040	0.8
21	10.2	2.9	0.040	0.8
22	10.4	3.0	0.040	0.8

[a]Huyck Metals Company, Milford, Connecticut. All samples were made from type 347 stainless-steel wire fibers and were reinforced on both sides with 18 x 18 mesh, 0.009-inch dia, type 347 stainless-steel wire screen.

TABLE IV. – SUMMARY OF CHARACTERISTICS OF POROUS MATERIALS FOR FLOW-RESISTANCE TESTS – Concluded

(c) Woven wire-screen samples supplied by the Aircraft Porous Media Company[a]

Item	Nominal flow resistance, cgs rayls	Nonlinearity factor	Thickness, in.	Surface density, lb/ft^2	Number of wire screen layers
1	8.1	1.7	0.025	0.3	3
2	8.7	1.7	0.026	0.4	3
3	9.3	3.9	0.018	0.4	–
4	10.2	2.1	0.022	0.5	2
5	10.4	2.2	0.030	0.5	3
6	10.5	2.2	0.032	0.5	2
7	10.6	2.4	0.032	0.5	3
8	11.0	2.3	0.036	0.6	3
9	12.0	3.2	0.044	0.9	2
10	12.0	5.8	0.052	1.3	2
11	12.5	1.8	0.033	0.6	2
12	12.8	–	0.031	0.6	2
13	13.5	5.8	0.027	0.7	1
14	15.9	4.4	0.041	1.0	2
15	18.2	2.6	0.027	0.6	2
16	18.6	3.0	0.043	0.9	2
17	20.8	3.1	0.063	1.4	4
18	22.8	6.1	0.048	1.3	2
19	23.3	4.9	0.038	1.0	2
20	25.2	6.2	0.025	0.6	1
21	28.8	2.0	0.020	0.4	–
22	29.6	1.5	0.038	0.7	2
23	30.8	1.5	0.037	0.7	3
24	31.8	2.2	0.020	0.4	–
25	32.2	3.1	0.034	0.8	–
26	33.9	2.9	0.063	0.9	2
27	37.7	1.5	0.042	0.8	4
28	41.7	1.5	0.043	0.8	4
29	42.2	3.5	0.021	0.6	2
30	43.7	2.9	0.044	1.1	–
31	53.0	1.2	0.048	0.9	5
32	58.0	4.7	0.034	1.0	2
33	63.0	2.1	0.020	0.6	2
34	65.0	–	0.018	0.5	2
35	70.1	5.9	0.027	0.6	1
36	74.0	6.0	0.041	1.3	2
37	100.4	3.5	0.041	1.0	2

[a]Aircraft Porous Media Co., Glen Cove, Long Island, New York. All samples, except items 3, 21, 24, 25, and 30 were made from type 304 stainless steel. Items 3, 21, 24, 25, and 30 were made from continuous filaments of type 347 stainless steel wire that were laid down in a repetitive loop pattern rather than woven in one of the conventional weaving patterns.

TABLE V. – SUMMARY OF PARAMETERS INVESTIGATED IN DUCT-MODEL TRANSMISSION-LOSS TESTS CONDUCTED PRIOR TO THE PROGRAM REPORTED IN THIS DOCUMENT

(a) Test series[a] No. 1 conducted 16 November 1965 to 5 March 1966 with results reported in reference 1.

Test configuration	Range of cavity depths, in.	Cavity filling materials[b]	Nominal flow resistances[c], cgs rayls	Range of treated areas, sq in.	Range of duct velocities, ft/sec	No. of config. tested	Total no. of tests
Original center fan-exhaust duct							
A. No splitter	0.25 to 1.0	Air, CPF 3-900, CPF 4-900	25	202 to 1217	100 to 400	8	16
B. Radial splitter	0.25 to 1.0	Air, CPF 3-900, CPF 4-900	25 and 60	842 to 1217	100 to 300	26	31
C. Radial and circumferential splitters	0.5 to 1.0	Air, CPF 3-900, CPF 4-900, CF-600	25	1217 to 1626	100 to 300	7	9
End fan-exhaust duct	0.25 to 1.0	Air, CPF 3-900, CPF 4-900	25	1003 to 1444	300	10	10
55 % inlet duct	0.5 to 1.0	Air, CPF 3-900, CPF 4-900, FG	25 and 60	107 to 804	75 to 465	32	80
75 % inlet duct	0.5 to 1.0	Air, CPF 3-900, CPF 4-900	25 and 60	764 to 1012	75 to 465	6	20
Standard inlet duct	0.5 to 1.0	Air, CPF 3-900, CPF 4-900	25 and 60	48 to 391	61 to 358	12	32

(b) Test series[a] No. 2 conducted 25 April to 25 May 1966.

Original center fan-exhaust duct	0.5 to 1.0	Air, CPF 3-900	25	1217	100 to 600	3	12
Revised center fan-exhaust duct	–[d]	Air, FG	10 and 40	247 to 579	0 to 600	21	91
End fan-exhaust duct	0.5 to 1.0	Air, CPF 3-900	25 and 60	1003 to 1444	100 to 600	7	31

[a,b,c]See end of table for these footnotes.

[d]The cavity depth on the revised center fan-exhaust duct varied along the length of the duct. The cavity depths tested ranged from the full cavity depth to a depth that was 0.75 inch less than the full depth.

TABLE V. – SUMMARY OF PARAMETERS INVESTIGATED IN DUCT-MODEL TRANSMISSION-LOSS TESTS CONDUCTED PRIOR TO THE PROGRAM REPORTED IN THIS DOCUMENT - Concluded

(c) Test series[a] No. 3 conducted 29 September to 29 November 1966.

Test configuration	Range of cavity depths, in.	Cavity filling materials[b]	Nominal flow resistances[c], cgs rayls	Range of treated areas, sq in.	Range of duct velocities, ft/sec	No. of config. tested	Total no. of tests
Revised center fan-exhaust duct	–[d]	Air, FG	10 and 40	247 to 579	100 to 700	9	57
Original center fan-exhaust duct							
A. No splitter	0.5 to 1.0	Air, CPF 3-900	25	1218	100 to 600	5	23
B. Radial splitter	0.5 to 1.0	Air, CPF 3-900	25	1119 to 1420	0 to 600	6	32
C. Radial and circumferential splitters	0.5 to 1.0	Air, CPF 3-900	25	515 to 2006	0 to 700	13	54

[a]Except for six configurations, all porous duct lining surfaces were sheets of fibermetal made from type 347 stainless-steel fibers with a nominal fiber diameter of 0.004 in. and were reinforced on both sides with a boxweave, type 347 stainless steel wire screen. The six configurations that were not made from stainless steel fibers included five made from aluminum fibers and one made from a steel sheet with thin slits. The nominal thickness of the stainless-steel fibermetal sheets and the slitted steel sheet was 0.040 in., that of the aluminum fibermetal sheets was 0.038 in. All porous surfaces were bolted to rib frames. For exhaust-duct tests. the sound source was a pulse jet. For inlet-duct tests in test series no. 1, the sound source was two electropneumatic transducers.

[b]CPF was open-cell compressed-polyurethane-foam having a pore count of 90 pores/in. before compression. The density of type 3-900 was 5.4 lb/cu ft, that of type 4-900 was 7.2 lb/cu ft. CF-600 was 6.0 lb/cu ft ceramic-fiber felt. FG was type AA fiberglass with nominal fiber diameter of 0.00004 in. and a density of 1.2 lb/cu ft.

[c]The stainless-steel fibermetal had a nominal flow resistance of 25 rayls and a density of 1.1 lb/cu ft. The density of the nominal 60 rayl material was 1.3 lb/cu ft. The aluminum fibermetal had a nominal flow resistance of 25 rayls. The slitted metal had 0.002 x 0.25-in. slits, a nominal flow resistance of 25 rayls, and a density of 1.4 lb/cu ft.

[d]The cavity depth on the revised center fan-exhaust duct varied along the length of the duct. The cavity depths tested ranged from the full cavity depth to a depth that was 0.75-in. less than the full depth.

TABLE VI. – EXPLANATION OF CONFIGURATION CODES FOR DUCT TRANSMISSION-LOSS TESTS

(a) Test configurations[a] with duct-lining designs having one layer of porous material and with no splitter installed.

Conf. code[b]	Description of lining on walls			
	Honeycomb[c] cell size, in.	Cavity depth, in.	Nominal flow resistance of fibermetal,[d] cgs rayls	Length of treatment, in.
R1	–	–	hardwall	–
R2	0.75	0.25	10	22.5
R2′	0.75	0.25	10	22.5
R3	0.75	0.25	40	22.5
R4	0.75	0.25	80	22.5
R5	0.75	0.5	10	22.5
R6	0.75	0.5	40	22.5
R7*[e]	0.75	0.5	40	22.5
R8	0.75	0.5	80	22.5
R9	0.75	0.5	160	22.5
R10	0.75	0.75	10	22.5
R11	0.75	0.75	40	22.5
R12	0.75	0.75	80	22.5
R13	0.75	1.0	10	22.5
R14	0.75	1.0	20	22.5
(R15)	0.75	1.0	40	22.5
R16*	0.75	1.0	40	22.5
R17[f]	0.75	1.0	40	45.0
(R18)	0.75	1.0	40	11.25
(R18′)	0.75	1.0	40	11.25
(R19)	0.75	1.0	40	33.75
R20	0.75	1.0	40	45.0
R21	0.75	1.0	80	22.5
R22	0.75	1.0	160	22.5
R23	0.375	1.0	40	22.5
R24	1.125	1.0	40	22.5
R24′	1.125	1.0	40	22.5
R24″[g]	1.125	1.0	40	22.5
R25	1.5	1.0	40	22.5
R26	3.0	1.0	40	22.5
R27[h]	–	–	–	–

a, b, c, d, *See end of the table for footnotes a, b, c, d, and *.

[e]Same as configuration R6 except fibermetal surface not bonded to honeycomb core.

[f]Same as configuration R15 except that a 45-in. length of treatment was installed on one wall only, the opposite wall was untreated.

[g]Same as configuration R24 except fibermetal surface not bonded to honeycomb core.

[h]Configuration was eliminated.

TABLE VI. – EXPLANATION OF CONFIGURATION CODES
FOR DUCT TRANSMISSION-LOSS TESTS – Continued

(b) Test configurations[a] with duct-lining designs having one layer of porous material and with a 1-inch-thick splitter installed.

Description of lining on walls					Description of lining on splitter			
Conf code[b]	Honeycomb[c] cell size, in.	Cavity depth, in.	Nominal flow resistance of fibermetal[d], cgs rayls	Length of treatment, in.	Honeycomb[c] cell size, in.	Cavity depth, in.	Nominal flow resistance of fibermetal[d], cgs rayls	Length of treatment, in.
R28	–	–	hardwall	–	–	–	hardwall	–
R29	–	–	hardwall	–	–[i]	–[i]	40	45
R30	–	–	hardwall	–	0.75	0.5[j]	40	45
R31	–	–	hardwall	–	0.75	1.0[k]	40	45
R32	–	–	hardwall	–	0.75	0.5/0.5[l]	10/40[l]	45
R33	0.75	1.0	40	22.5	0.75	0.5[j]	40	45
(R34)	0.75	1.0	40	11.25	0.75	0.5[j]	40	45
(R35)	0.75	1.0	40	33.75	0.75	0.5[j]	40	45
R36*	0.75	1.0	40	45.0	0.75	0.5[j]	40	45

[i] Corrugated aluminum-truss core, 1-inch-deep truss, corrugations 5-inch on centers. Fibermetal surfaces on both sides of splitter.

[j] Cavities were 0.5-inch-deep on either side of a steel septum, giving the splitter two porous surfaces.

[k] Cavities were 1.0-inch-deep on one side of the splitter, giving the splitter one porous and one hard surface.

[l] This was a two layer design, giving the splitter one hard surface and one absorptive surface. For the absorptive surface, the 10-rayl sheet faced the air stream and was backed by a 0.5-inch-deep cavity. The second porous surface was a 40-rayl sheet backed by another 0.5-inch-deep cavity.

TABLE VI. – EXPLANATION OF CONFIGURATION CODES FOR DUCT TRANSMISSION-LOSS TESTS–Continued

(c) Test configurations[a] with duct-lining designs having two layers of porous material[m] and with no splitter installed.

Conf. code[b]	Description of lining with porous surface next to air flow		Description of lining with porous surface between airflow and impervious backing sheet		
	Cavity depth, in.	Nominal flow resistance of fibermetal,[d] cgs rayls	Cavity depth, in.	Nominal flow resistance of fibermetal,[d] cgs rayls	Total depth of lining, in.
R101	0.25	10	0.25	40	0.5
R102	0.25	10	0.25	80	0.5
R103	0.25	40	0.25	80	0.5
R104	0.25	40	0.25	10	0.5
R105	0.25	80	0.25	10	0.5
R106	0.25	80	0.25	40	0.5
R107	0.25	10	0.5	10	0.75
R108*	0.25	10	0.5	40	0.75
R109*	0.25	10	0.5	80	0.75
R110	0.25	10	0.5	160	0.75
R111*	0.25	40	0.5	40	0.75
R112*	0.25	40	0.5	80	0.75
R113*	0.25	40	0.5	160	0.75
R114*	0.25	80	0.5	80	0.75
R115	0.25	80	0.5	160	0.75
R116	0.5	10	0.25	10	0.75
R117	0.5	40	0.25	10	0.75
R118*	0.5	80	0.25	10	0.75
R119*	0.5	40	0.25	40	0.75
R120*	0.5	80	0.25	40	0.75
R121	0.5	80	0.25	80	0.75
R122	0.25	10	0.75	10	1.0
R123	0.25	10	0.75	40	1.0
R124	0.25	10	0.75	80	1.0
R125	0.25	40	0.75	10	1.0
R126	0.25	40	0.75	40	1.0
R127	0.25	40	0.75	80	1.0
R128	0.25	80	0.75	10	1.0
R129	0.25	80	0.75	40	1.0

[m]The honeycomb core used to support the fibermetal surfaces was the same type of fiberglass honeycomb as used for the one-layer lining designs. For all configurations, the honeycomb cell size was 0.75 in. and the length of treatment was 22.5 in. For all configurations except R149, the treatment was installed beginning at the upstream end of the duct.

TABLE VI. – EXPLANATION OF CONFIGURATION CODES FOR DUCT TRANSMISSION-LOSS TESTS – Continued

(c) Test configurations[a] with duct-lining designs having two layers of porous material[m] and with no splitter installed-Continued

Conf. code[b]	Description of lining with porous surface next to airflow		Description of lining with porous surface between airflow and impervious backing sheet		Total depth of lining, in.
	Cavity depth, in.	Nominal flow resistance of fibermetal,[d] cgs rayls	Cavity depth, in.	Nominal flow resistance of fibermetal,[d] cgs rayls	
R130	0.25	80	0.75	80	1.0
R131	0.5	10	0.5	10	1.0
R132	0.5	10	0.5	40	1.0
R133	0.5	10	0.5	80	1.0
R134	0.5	40	0.5	10	1.0
R135	0.5	40	0.5	40	1.0
R136	0.5	40	0.5	80	1.0
R137	0.5	80	0.5	10	1.0
R138	0.5	80	0.5	40	1.0
R139	0.5	80	0.5	80	1.0
R140	0.75	10	0.25	10	1.0
R141	0.75	10	0.25	40	1.0
R142	0.75	10	0.25	80	1.0
R143	0.75	40	0.25	10	1.0
R144	0.75	40	0.25	40	1.0
R145	0.75	40	0.25	80	1.0
R146	0.75	80	0.25	10	1.0
R147	0.75	80	0.25	40	1.0
R148	0.75	80	0.25	80	1.0
R149*	– n	–n	– n	–n	1.0
R155	0.25	10	1.0	10	1.25
R156	0.25	10	1.0	20	1.25
R157	0.25	10	1.0	40	1.25
R158	0.25	10	1.0	80	1.25
R159	0.25	10	1.0	160	1.25
R160	0.25	40	1.0	10	1.25
R161*	0.25	40	1.0	20	1.25
R162*	0.25	40	1.0	40	1.25
R163*	0.25	40	1.0	80	1.25
R164*	0.25	40	1.0	160	1.25

[n]Choice of linings was to have been made after examination of results of tests of configurations R122 through R148. The selected lining was also to have been installed with the treatment beginning at the downstream end of the sheet rather than the upstream end.

TABLE VI. – EXPLANATION OF CONFIGURATION CODES FOR DUCT TRANSMISSION-LOSS TESTS – Continued

(c) Test configurations[a] with duct-lining designs having two layers of porous material[m] and with no splitter installed–Continued

Conf. code[b]	Description of lining with porous surface next to airflow		Description of lining with porous surface between airflow and impervious backing sheet		Total depth of lining, in.
	Cavity depth, in.	Nominal flow resistance of fibermetal,[d] cgs rayls	Cavity depth, in.	Nominal flow resistance of fibermetal,[d] cgs rayls	
R165*	0.25	80	1.0	10	1.25
R166*	0.25	80	1.0	20	1.25
R167*	0.25	80	1.0	40	1.25
R168	0.25	80	1.0	80	1.25
R169	0.25	80	1.0	160	1.25
R170*	0.5	10	0.75	10	1.25
R171*	0.5	10	0.75	40	1.25
R172*	0.5	10	0.75	80	1.25
R173*	0.5	40	0.75	10	1.25
R174*	0.5	40	0.75	40	1.25
R175*	0.5	40	0.75	80	1.25
R176*	0.5	80	0.75	10	1.25
R177*	0.5	80	0.75	40	1.25
R178*	0.5	80	0.75	80	1.25
R179	0.75	10	0.5	10	1.25
R180*	0.75	40	0.5	10	1.25
R181*	0.75	80	0.5	10	1.25
R182*	0.75	10	0.5	40	1.25
R183*	0.75	40	0.5	40	1.25
R184*	0.75	80	0.5	40	1.25
R185	0.75	10	0.5	80	1.25
R186*	0.75	40	0.5	80	1.25
R187	0.75	80	0.5	80	1.25
R188	0.5	10	1.0	10	1.5
R189*	0.5	10	1.0	20	1.5
R190*	0.5	10	1.0	40	1.5
R191*	0.5	10	1.0	80	1.5
R192	0.5	10	1.0	160	1.5
R193*	0.5	40	1.0	10	1.5
R194*	0.5	40	1.0	20	1.5
R195*	0.5	40	1.0	40	1.5

TABLE VI. – EXPLANATION OF CONFIGURATION CODES FOR DUCT TRANSMISSION-LOSS TESTS – Continued

(c) Test configurations[a] with duct-lining designs having two layers of porous material[m] and with no splitter installed-Concluded

Conf. code[b]	Description of lining with porous surface next to airflow		Description of lining with porous surface between airflow and impervious backing sheet		Total depth of lining, in.
	Cavity depth, in.	Nominal flow resistance of fibermetal,[d] cgs rayls	Cavity depth, in.	Nominal flow resistance of fibermetal,[d] cgs rayls	
R196*	0.5	40	1.0	80	1.5
R197*	0.5	40	1.0	160	1.5
R198*	0.5	80	1.0	10	1.5
R199*	0.5	80	1.0	20	1.5
R200*	0.5	80	1.0	40	1.5
R201	0.5	80	1.0	80	1.5
R202	0.5	80	1.0	160	1.5
R203	0.75	10	0.75	40	1.5
R204	0.75	10	0.75	80	1.5
R205*	0.75	40	0.75	80	1.5
R206*	0.75	40	0.75	10	1.5
R207*	0.75	80	0.75	10	1.5
R208*	0.75	80	0.75	40	1.5
R209	0.75	10	1.0	10	1.75
R210*	0.75	10	1.0	20	1.75
R211*	0.75	10	1.0	40	1.75
R212	0.75	10	1.0	80	1.75
R213	0.75	40	1.0	10	1.75
R214*	0.75	40	1.0	10	1.75
R215*	0.75	40	1.0	20	1.75
R216*	0.75	40	1.0	40	1.75
R217*	0.75	40	1.0	80	1.75
R218*	0.75	40	1.0	160	1.75
R219*	0.75	80	1.0	10	1.75
R220*	0.75	80	1.0	20	1.75
R221*	0.75	80	1.0	40	1.75
R222	0.75	80	1.0	80	1.75
R223	0.75	80	1.0	160	1.75

TABLE VI. – EXPLANATION OF CONFIGURATION CODES FOR DUCT TRANSMISSION-LOSS TESTS - Continued

(d) Test configurations[a] with 1.0-inch thick duct-lining designs having two layers of porous material[m] and with a 1-inch-thick splitter installed.

Conf. code[b]	Description of lining with porous surface next to airflow		Description of lining with porous surface between airflow and impervious backing sheet		Description of lining on splitter			
	Cavity depth, in.	Nominal flow resistance of fibermetal,[d] cgs rayls	Cavity depth, in.	Nominal flow resistance of fibermetal,[d] cgs rayls	Honeycomb cell size, in.	Cavity depth, in.	Nominal flow resistance of fibermetal,[d] cgs rayls	Length of treatment, in.
R150*	–[o]	–[o]	–[o]	–[o]	–	–	hardwall	–
R151*	–[o]	–[o]	–[o]	–[o]	–[i]	–[i]	40	45
R152*	–[o]	–[o]	–[o]	–[o]	0.75	0.5[j]	40	45
R153*	–[o]	–[o]	–[o]	–[o]	0.75	1.0[k]	40	45
R154*	–[o]	–[o]	–[o]	–[o]	0.75	0.5/0.5[l]	10/40[l]	45

[o]Choice of lining was to have been made after examination of results of tests of configurations R122 through R148.

[Footnotes i, j, k, and l explained in table VI (b); footnote m explained in table VI (c)]

TABLE VI. – EXPLANATION OF CONFIGURATION CODES FOR DUCT TRANSMISSION-LOSS TESTS – Continued

(e) Test configurations[a] with duct-lining designs having three layers of porous material[m] and with no splitter installed.

Conf. code[b]	Description of lining with porous surface next to air flow		Description of intermediate lining		Description of lining with porous surface nearest the impervious backing sheets		Total depth of lining in.
	Cavity depth, in.	Nominal flow resistance of fibermetal,[d] cgs rayls	Cavity depth, in.	Nominal flow resistance of fibermetal,[d] cgs rayls	Cavity depth, in.	Nominal flow resistance of fibermetal,[d] cgs rayls	
R1001	0.25	10	0.25	40	0.25	80	0.75
R1002	0.5	10	0.5	40	0.5	80	1.5
R1003	0.5	80	0.5	10	0.5	40	1.5
R1004	0.5	10	0.5	80	1.0	10	2.0

(f) Test configuration[a] with duct-lining design having four layers of porous material[m] and with no splitter installed.

Conf. code[b]	Description of lining with porous surface next to airflow		Description of first intermediate lining		Description of second intermediate lining		Description of lining with porous surface nearest the impervious backing sheets		Total depth of lining in.
	Cavity depth, in.	Nominal flow resistance of fibermetal,[d] cgs rayls	Cavity depth, in.	Nominal flow resistance of fibermetal,[d] cgs rayls	Cavity depth, in.	Nominal flow resistance of fibermetal,[d] cgs rayls	Cavity depth, in.	Nominal flow resistance of fibermetal,[d] cgs rayls	
R1005	0.5	10	0.25	80	0.5	10	0.75	40	2.0

TABLE VI. – EXPLANATION OF CONFIGURATION CODES
FOR DUCT TRANSMISSION-LOSS TESTS - Concluded

The following footnotes apply to all configurations in this table:

[a] The backing cavities behind the fibermetal facing sheets were air filled. Absorptive linings were installed only on portions of one or both the two 20 x 45-in. walls. The two 5 x 45-in. walls were always hard, 0.093-in.-thick sheet-aluminum. All porous sheets, except in configurations R7 and R24", were adhesively bonded to a honeycomb core.

[b] The R in the configuration core denotes the rectangular test duct. Configuration codes with primes indicate that the acoustical treatment was installed beginning at the downstream end of duct rather than beginning at the upstream end of the duct as it was for all configuration codes without primes. Except for configuration R17 the treatment was always installed on the two 20 x 45-in. walls. For configuration codes within parentheses, the length of treatment was determined by laying sheet aluminum over the fibermetal surface as required.

[c] The honeycomb core was made from heat-resistant phenolic-coated fiberglass cloth. The walls of the cells were approximately 0.004-in. thick.

[d] The fibermetal surfaces all had a nominal thickness of 0.040-in. Sheets with nominal flow resistances of 10, 20 and 40 cgs rayls were made from nominal 0.004-in. diameter, type 347 stainless-steel wire fibers. Sheets with nominal flow resistances of 80 and 160 cgs rayls were made from nominal 0.003-in. diameter, type 347 stainless-steel wire fibers.

* The asterisk in the configuration code indicates a configuration that was available but was not tested.

TABLE VII. – SUMMARY OF RESULTS OF SONIC-FATIGUE TESTS CONDUCTED PRIOR TO STUDIES REPORTED IN THIS DOCUMENT

Test panel no.	Description of panel construction	Description of facing material (a)	Maximum overall SPL, dB	Duration at maximum overall SPL, min	Description of failure after duration at max overall SPL
I.	Skin and rib – 1.0 x 24.0 x 26.75 in. with six Z-frames	FM = 0.020 in., 25 rayl 0.004-in. fibers	159	60	FM separated from rib at rivets
II.	Same as no. I	FM = 0.056 in., 35 rayl 0.004-in. fibers	162	60	FM surface was severely damaged
III.	Same as no. I except 1.0 x 24 x 26.75-in.	SM = 0.040 in., 25 rayl (0.002 x 0.25 in. slits)	166	180	No failure
IV.	Same as no. I	FM = 0.040 in., 25 rayl 0.004-in. fibers	162	60	4 in. crack in middle of center bay
V.	Same as no. I	FM = 0.040 in., 10 rayl 0.004-in. fibers	159	30	2 in. crack in middle of bay no. 2
VI.	Honeycomb – 1.125 x 20 x 26.75 in. 1.125-in. cells	FM = 0.040 in., 10 rayl 0.004-in. fibers	159	30	2 sq in. hole near vertical downstream edge
VII.	Same as no. VI	FM = 0.020 in., 25 rayl 0.003-in. fibers	165	90	3 x 5 in. area at top center of panel detached
VIII.	Same as no. VI	FM = 0.020 in., 25 rayl 0.003-in. fibers	165	30	1 in. crack + lower vertical downstream buckling
IX.	Same as no. VI except 1-in. core + 0.020-in. Ti backing	FM = 0.040 in., 10 rayl 0.004-in. fibers	162	30	2 sq in. hole near vertical upstream edge
X.	Same as no. VI except three pieces of 1.0-in. cores + added doubler	FM = 0.040 in., 10 rayl 0.004-in. fibers	159	45	5 in. vertical crack at panel center

[a]The notation FM indicates fibermetal and SM indicates slitted metal.

TABLE VIII. – DESCRIPTION OF 20.0 x 26.75-INCH SONIC-FATIGUE TEST PANELS

(a) Acoustically treated panels I, II and IV

Items common to the three panels were:

1. The duct-lining designs all had a single layer of porous material in front of an impervious backing sheet.

2. The porous surfaces were fibermetal sheets with a nominal thickness of 0.040-inch.

3. The fibermetal was made from type 347 stainless-steel wire fibers with a nominal diameter of 0.004-inch and was screen-reinforced on both sides with stainless-steel wire screen.

4. The solid backing surfaces were aluminum sheets with a nominal thickness of 0.050-inch.

5. The fibermetal and aluminum surfaces were adhesively bonded to heat-resistant phenolic-coated fiberglass-cloth honeycomb core with a sine-wave ribbon pattern.

6. The honeycomb core had 0.002-inch-thick walls and a density of approximately 1.6 lb/cu ft feet.

7. The ribbon direction of the honeycomb was oriented parallel to the 26.75-inch sides of the panel.

8. A 0.040 x 2.0-in. stainless-steel doubler was bonded and reveted to the porous fibermetal surface around the perimeter of the side of the panel facing into the progressive-wave tube.

9. A 0.063 x 4.0-in. aluminum doubler was bonded and riveted around the surface of the panel outside the progressive-wave tube.

Items different among the three panels were:

1. Panels I and II used fibermetal with a nominal flow resistance of 10 cgs rayls, a nominal relative density of 53.5 percent, and a density of 0.78 lb/cu feet.

2. Panel IV used fibermetal with a nominal flow resistance of 8 cgs rayls, a nominal relative density of 44.7 percent, and a density of 0.745 lb/cu feet.

3. Panel I used honeycomb with a nominal cell size of 1.125-inch. Panels II and IV used honeycomb with a nominal cell size of 0.75-inch.

4. Panels I and II were built to simulate the lining on the wall of a duct with a cavity depth of 1.0-inch. Panel IV simulated the design of a fan-duct flow splitter or inlet ring vane with 0.5-inch-deep cavities on both sides of a 0.020-inch-thick stainless-steel septum.

TABLE VIII. – DESCRIPTION OF 20.0 x 26.75-INCH SONIC-FATIGUE TEST PANELS – Concluded

(b) Baseline reference panel III

1. The panel design was a single sheet of nominal 0.050-inch-thick aluminum alloy stiffened by five Z-section frames that were 0.063-inch-thick.

2. The width of the flange on the frames was 0.75-inch.

3. The aluminum skin was riveted to the frames with 0.156-inch diameter rivets.

4. The frames were installed parallel to the 20-inch sides of the panel.

5. The four center bays were spaced 4.5-inch apart. The two end bays were spaced 3.6-inch apart.

6. The panels were bonded along the 26.75-inch sides by 0.125-inch thick, L-section structural-steel angles, along the 20-inch sides by 0.063-inch U-Section aluminum channels.

7. The Z-section frames were tied to the L-section steel angles by aluminum shear clips.

8. The rivets attaching the skin to the Z-section frames were spaced 0.9-inch on center.

9. The depth of the Z-section frames was 1.44-inch.

10. The aluminum shear clips were 0.071-inch-thick.

11. The shear clips were fastened to the Z-section frames with three rivets per clip.

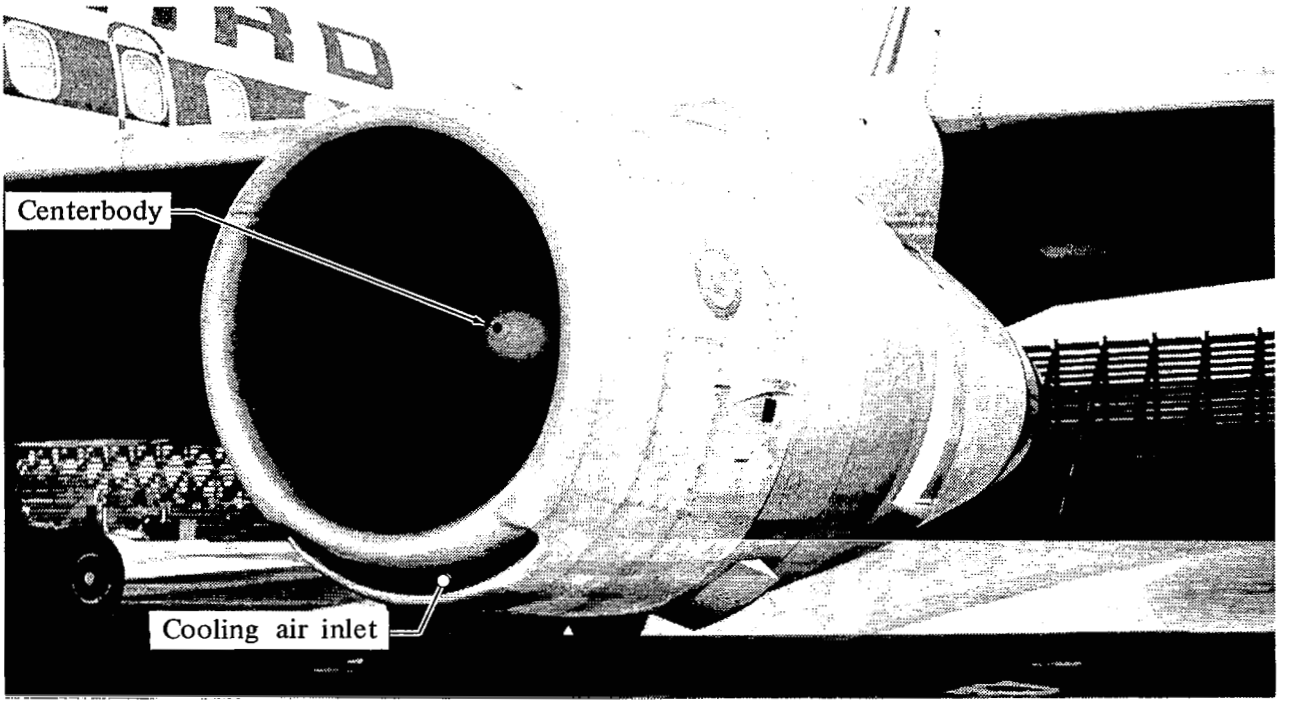

(a) Three-quarter front view.

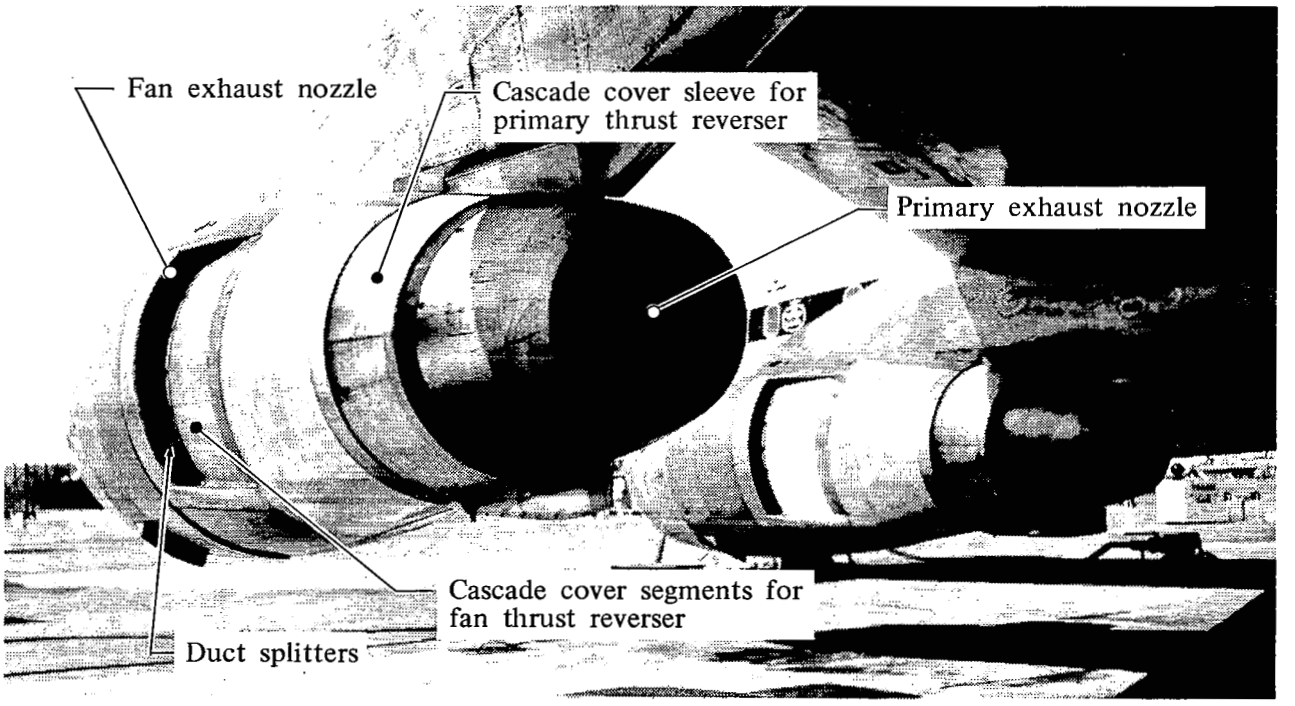

(b) Three-quarter rear view.

Figure 1. Major components of nacelle installation on existing DC-8-50/61 aircraft.

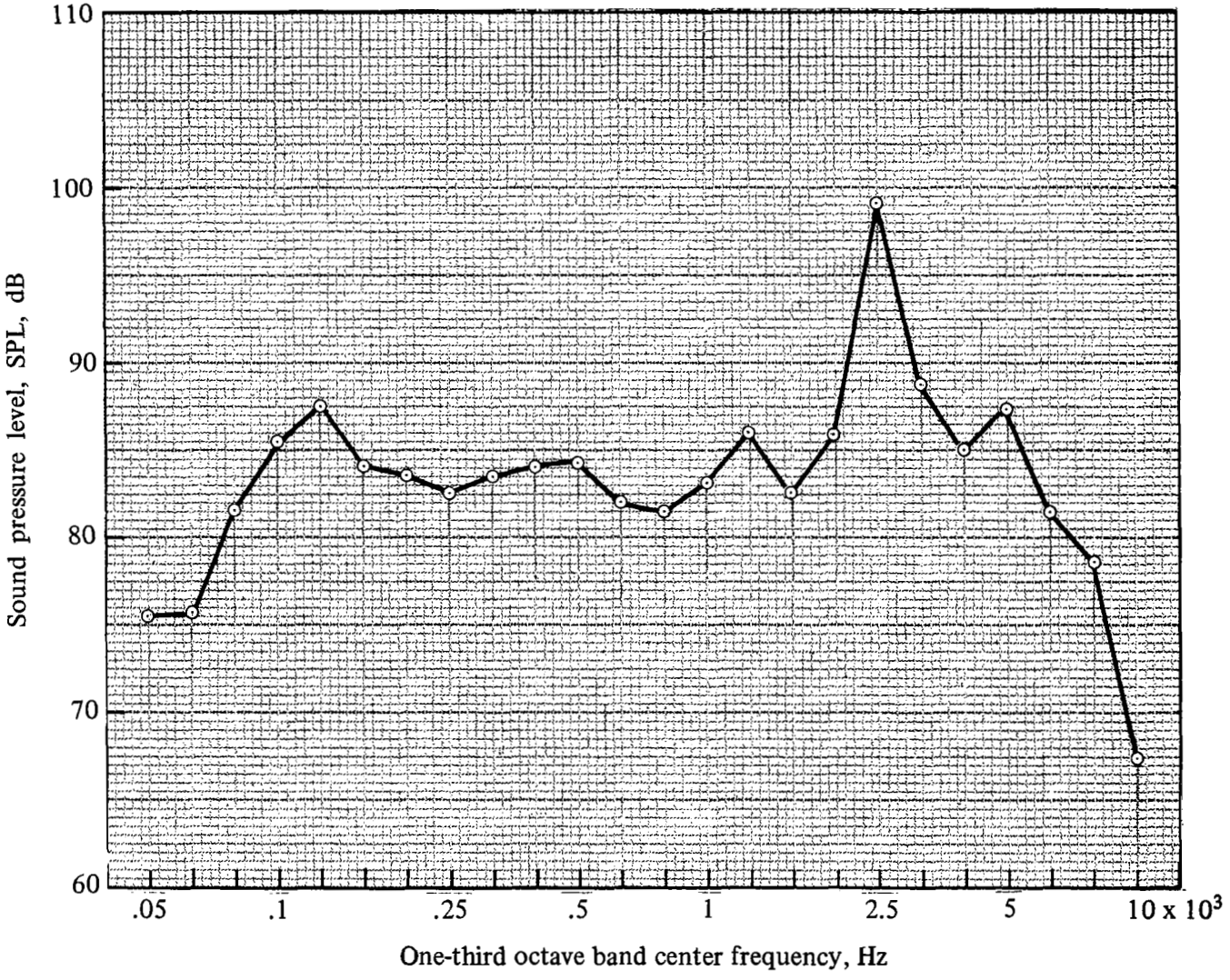

Figure 2. – Sound spectrum of a JT3D-powered DC-8 during landing approach at an altitude of approximately 500 feet.

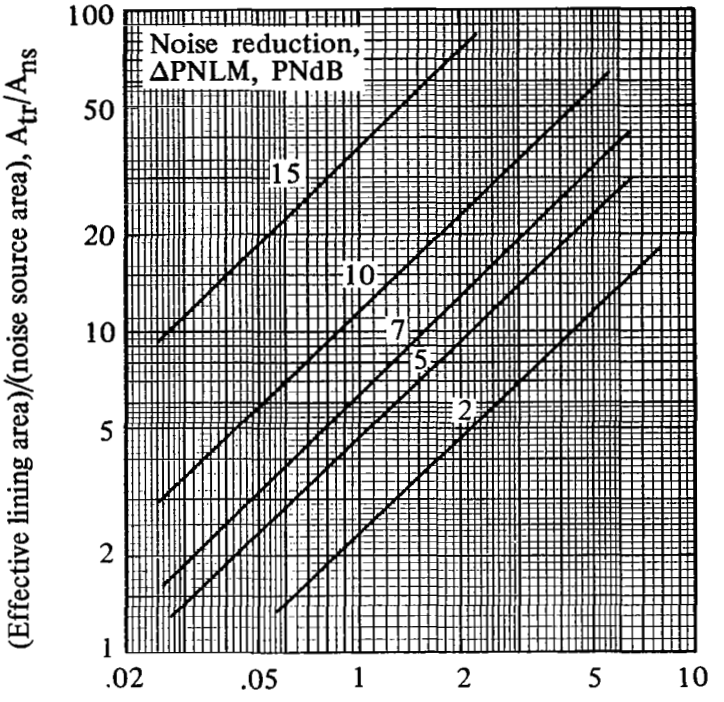

(a) Chart for estimating required area of duct lining, given specific values for h/λ, ΔPNLM, and A_{ns}.

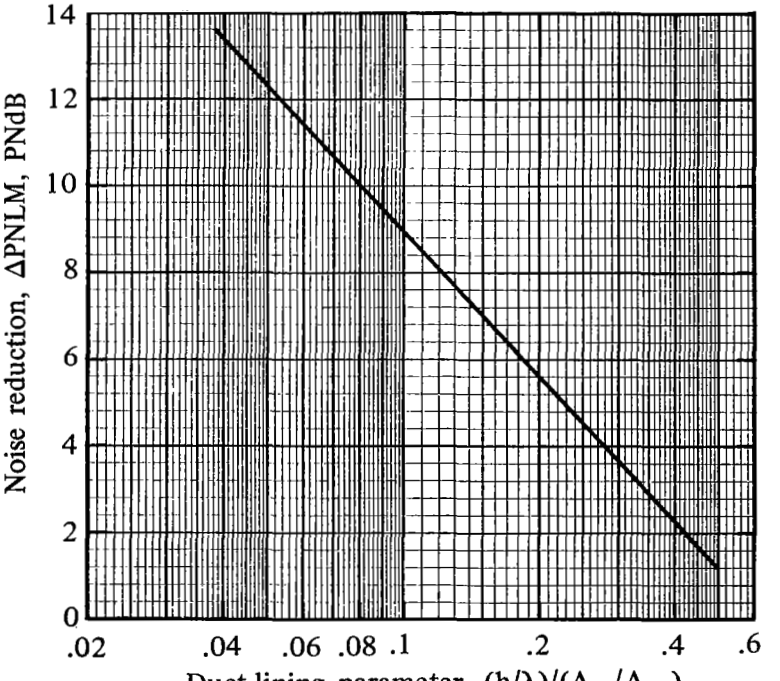

(b) Chart for evaluating specific nacelle designs.

Figure 3. – Acoustical design charts.

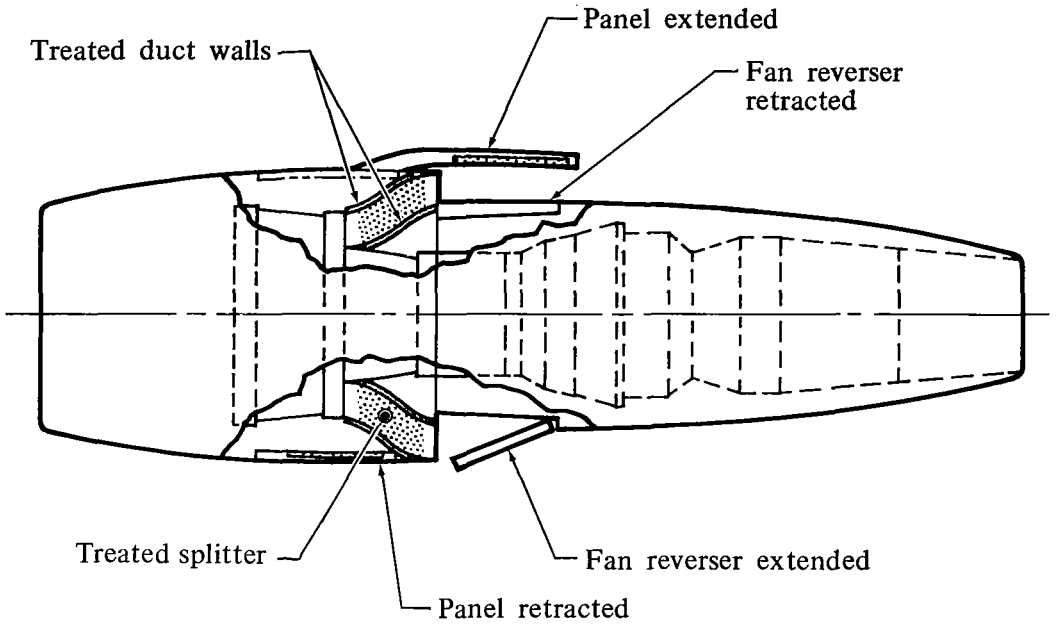

Figure 4. – 24-inch fan-exhaust ducts with supplementary treated panels.

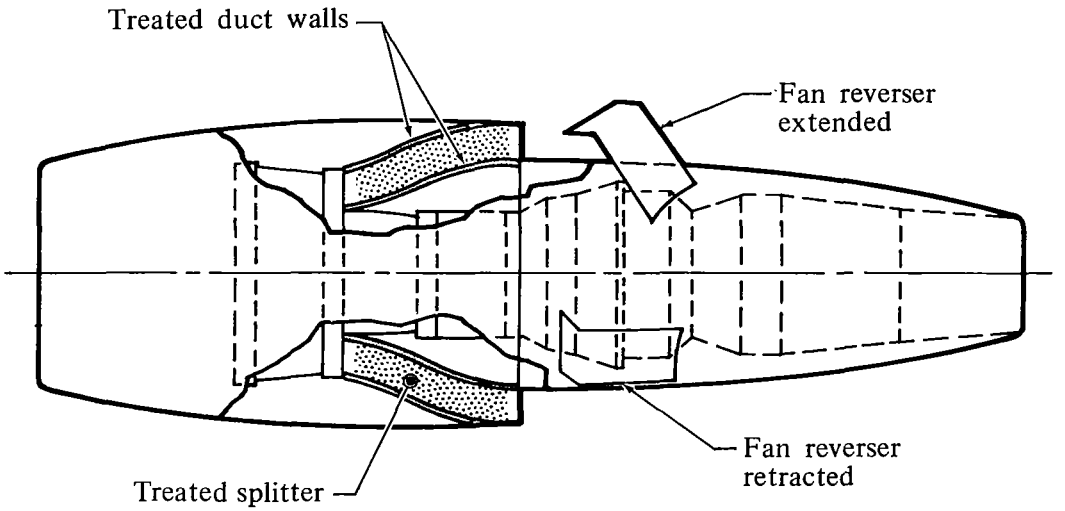

Figure 5. – 48-inch fan-exhaust ducts.

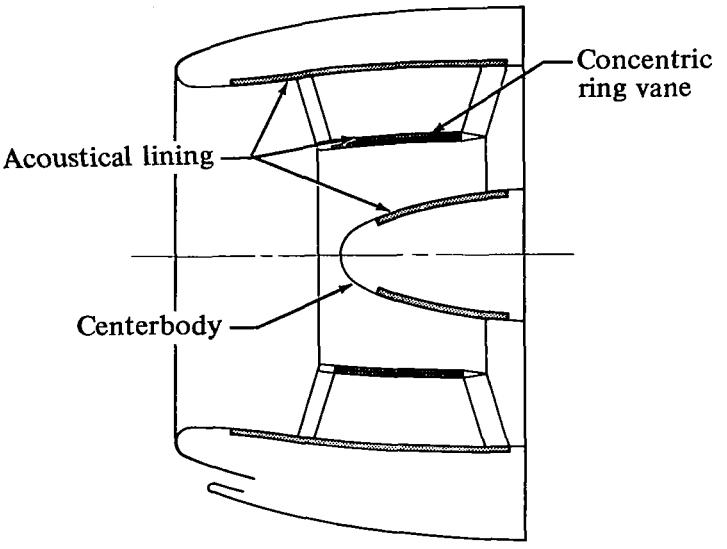

(a) One ring vane.

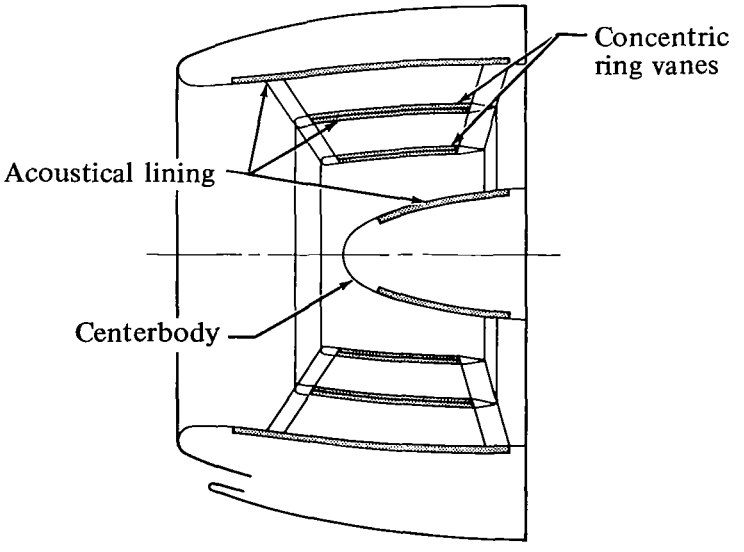

(b) Two ring vanes.

Figure 6. – Ring-vaned inlets.

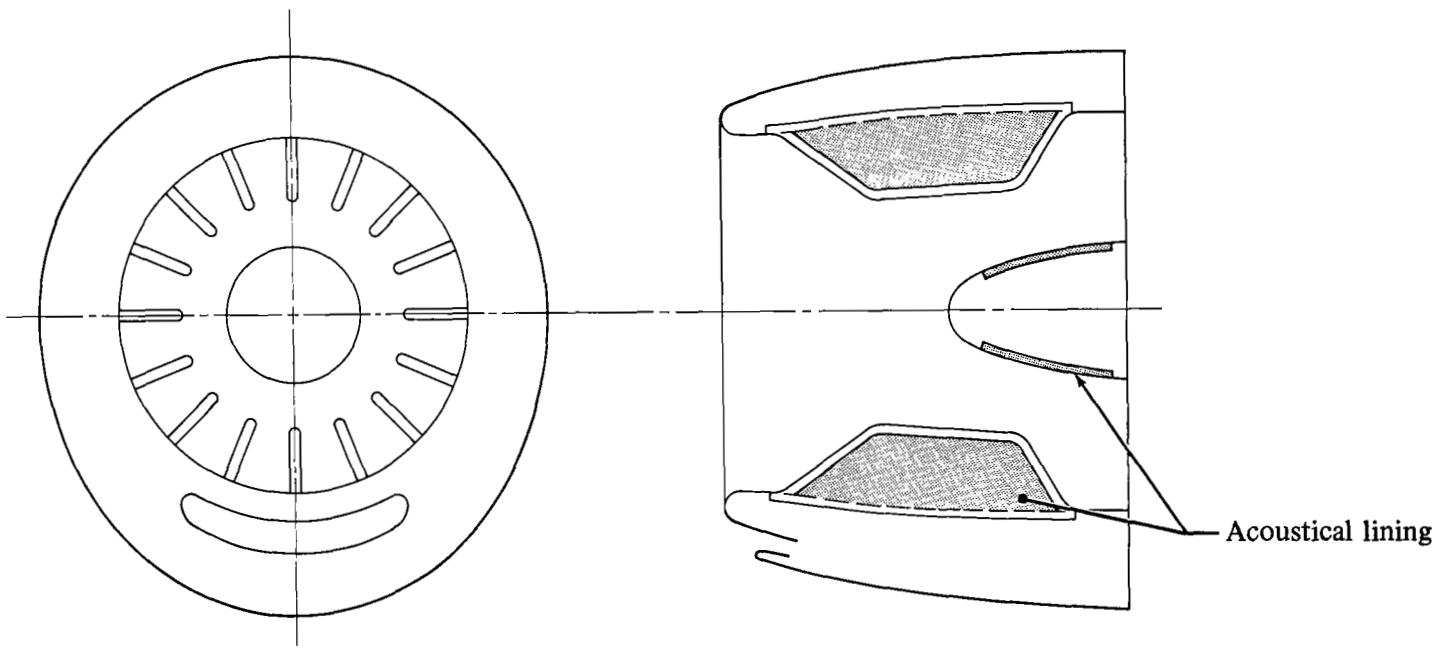

Figure 7. – Radial-vane inlet with 16 equally spaced vanes.

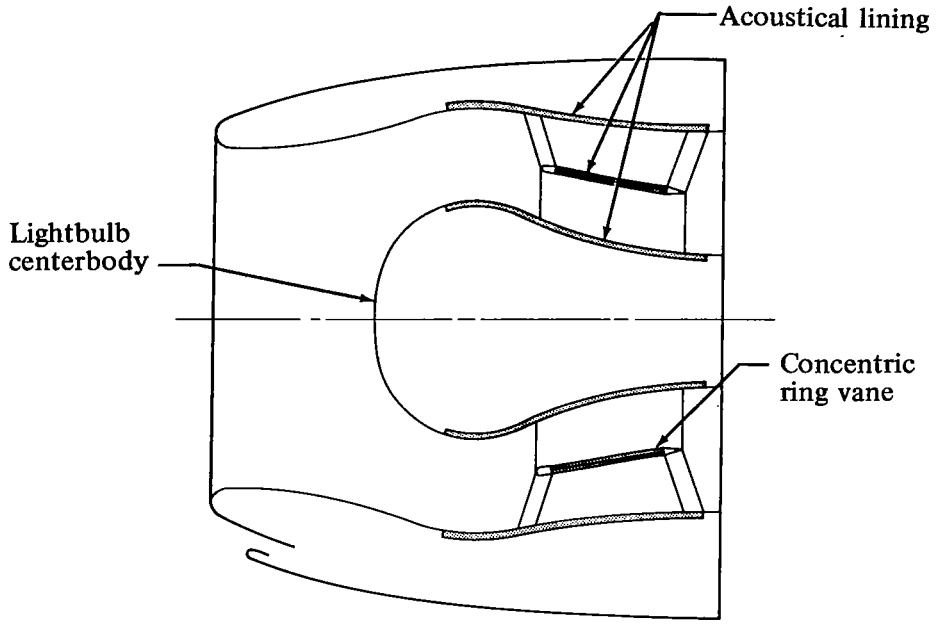

(a) Moderate amount of treated area.

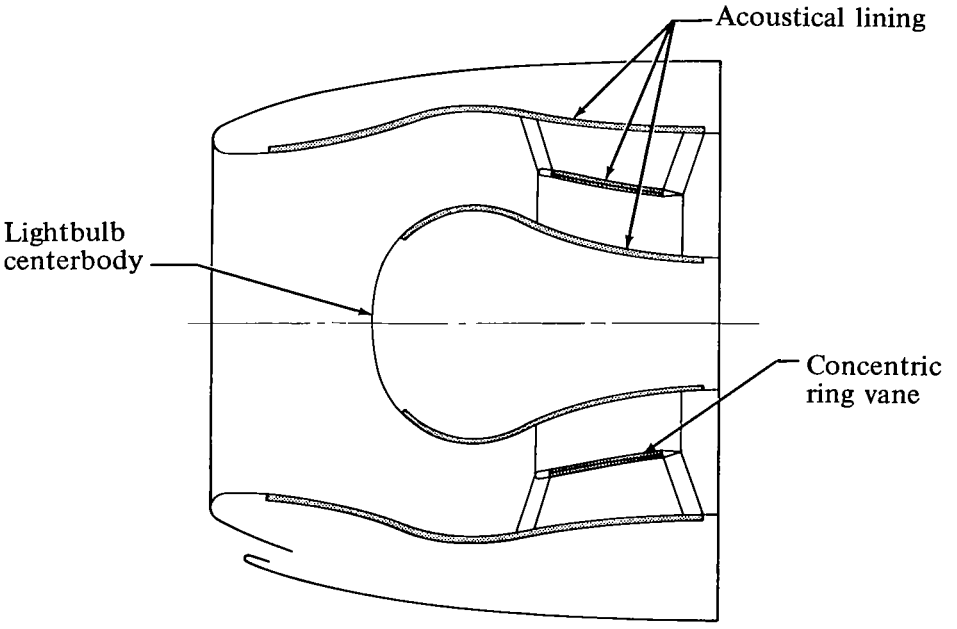

(b) Maximum amount of treated area.

Figure 8. – 47-percent lightbulb inlets.

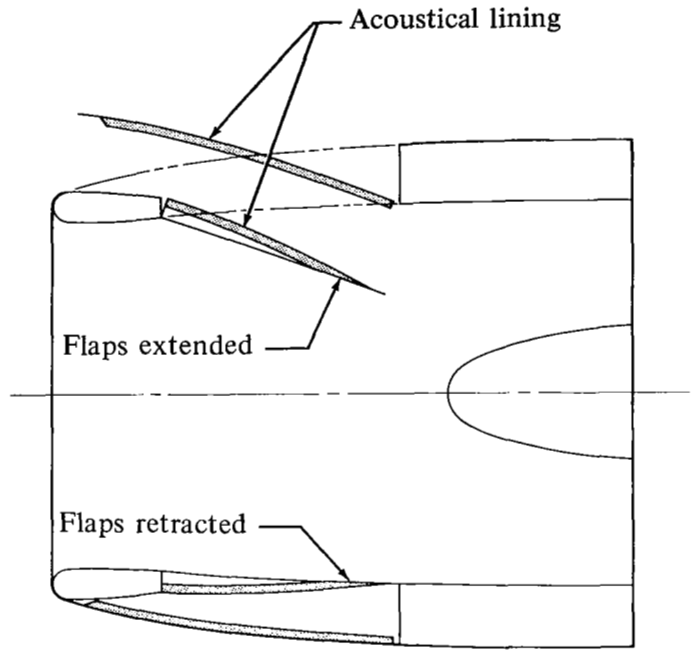

(a) Retractable inlet flaps.

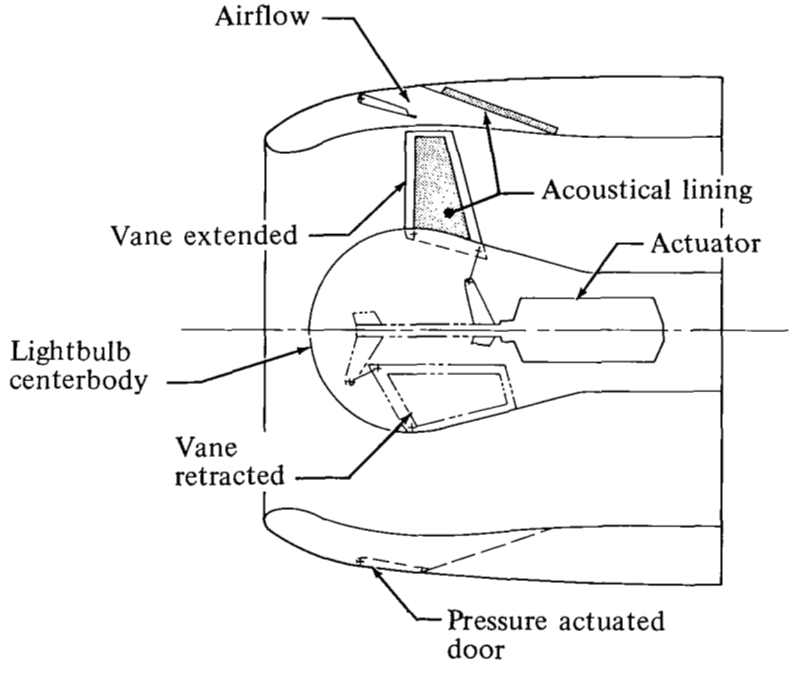

(b) Retractable radial vanes.

Figure 9. – Variable-geometry inlets.

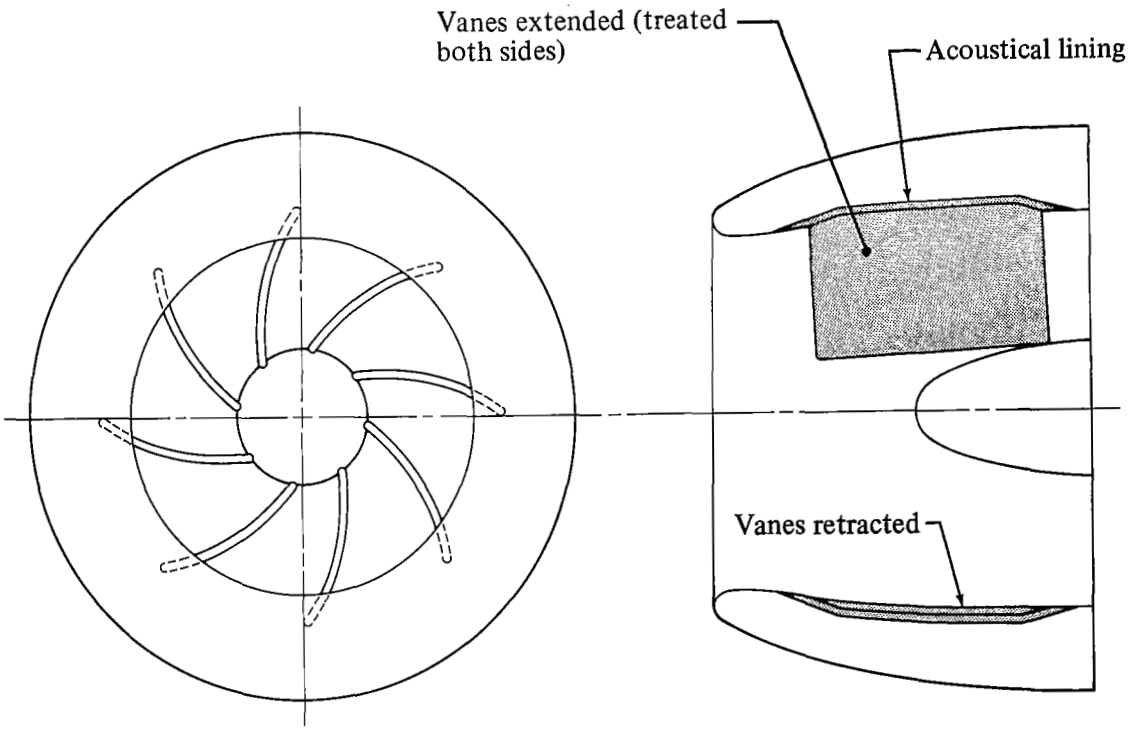

Figure 10. – Retractable-curved-vane inlet.

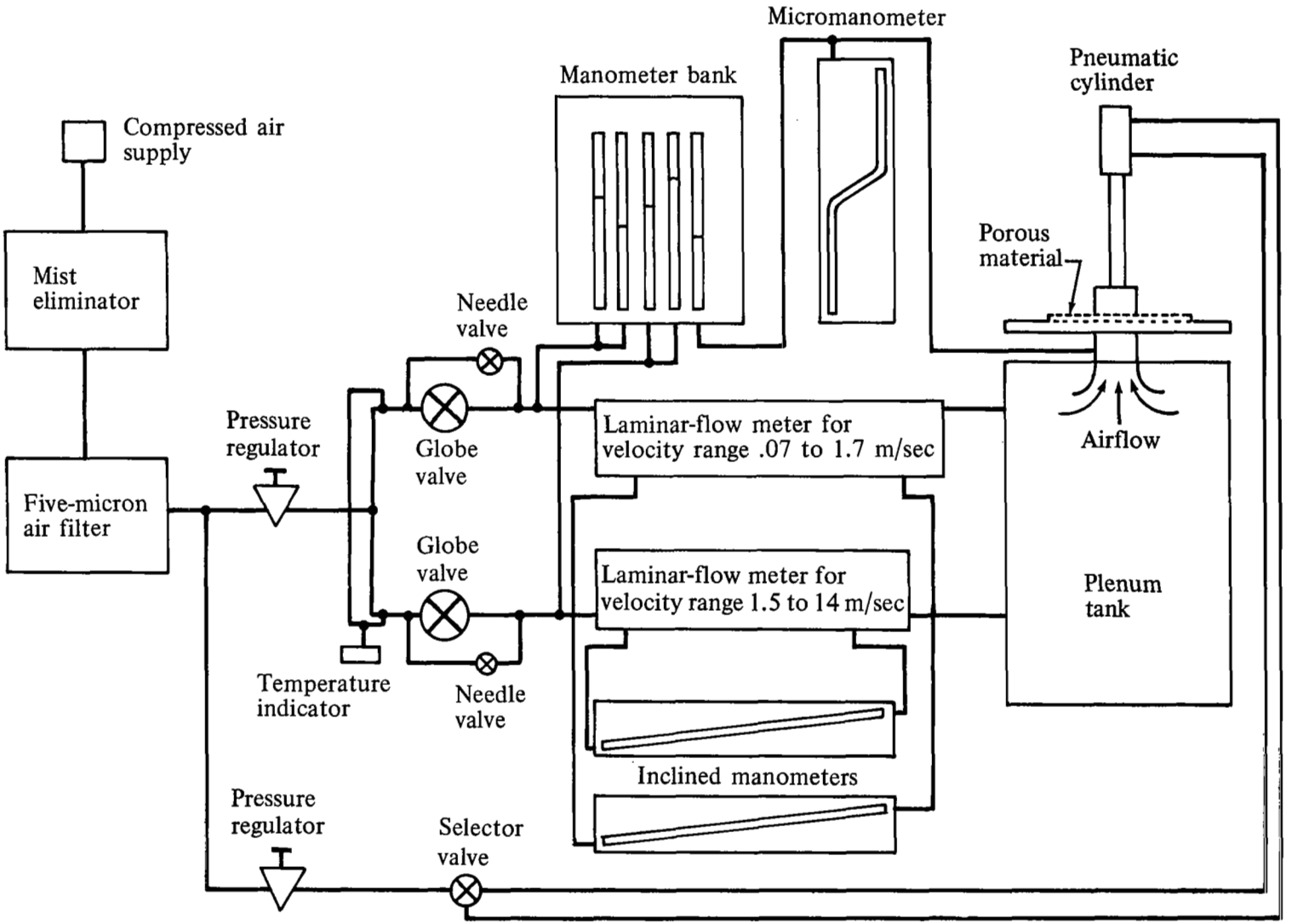

Figure 11. – Apparatus for flow-resistance tests of porous materials.

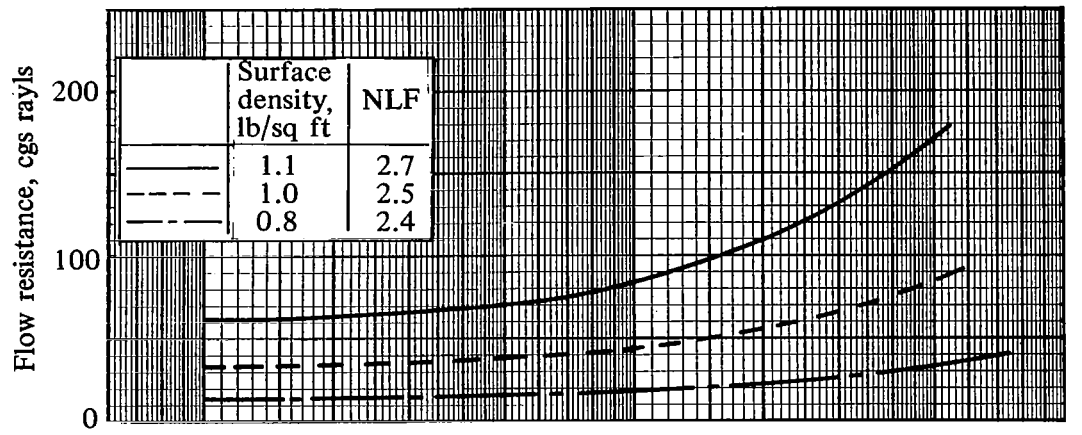

Figure 12. – Variation of flow resistance of fibermetal with changes in surface density. Test samples had .003-in. diameter wire fibers and a nominal thickness of .048 inches.

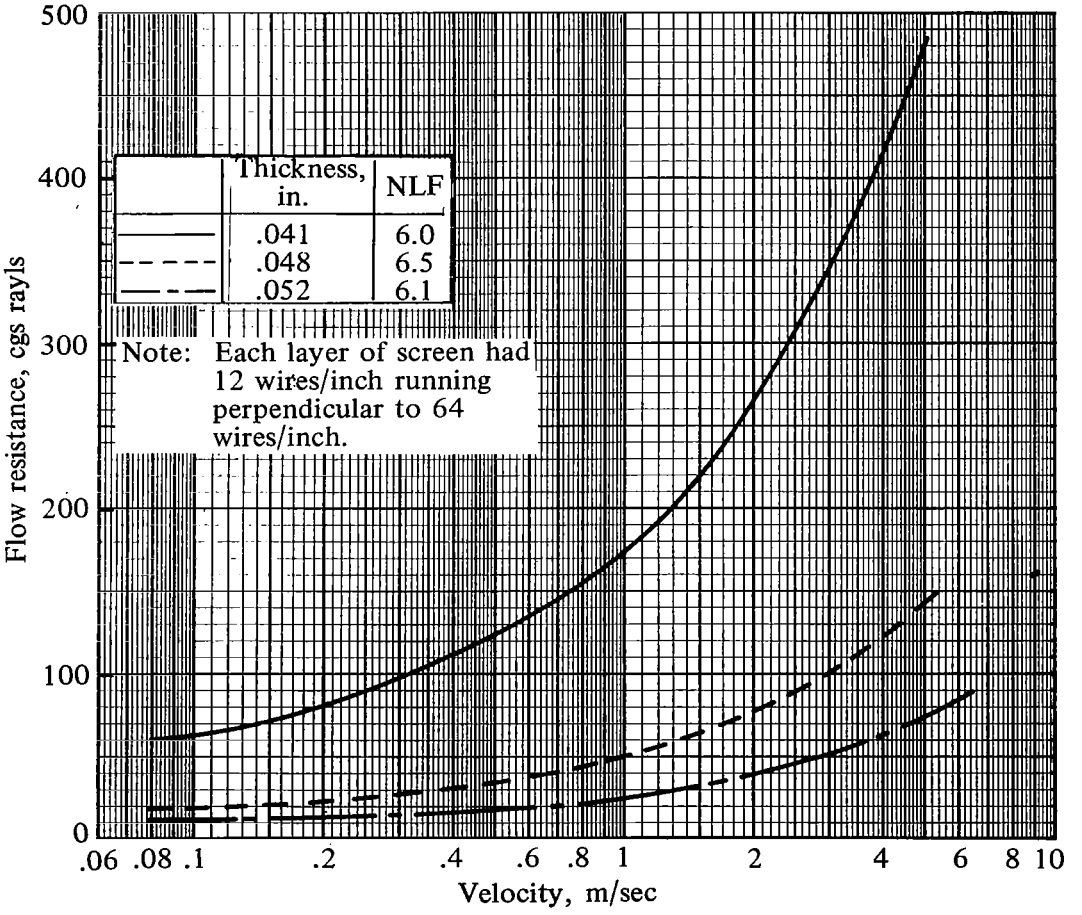

Figure 13. – Variation of flow resistance of two-layer woven wire-screen with changes in thickness. Test samples had a surface density of 1.3 lb/sq ft.

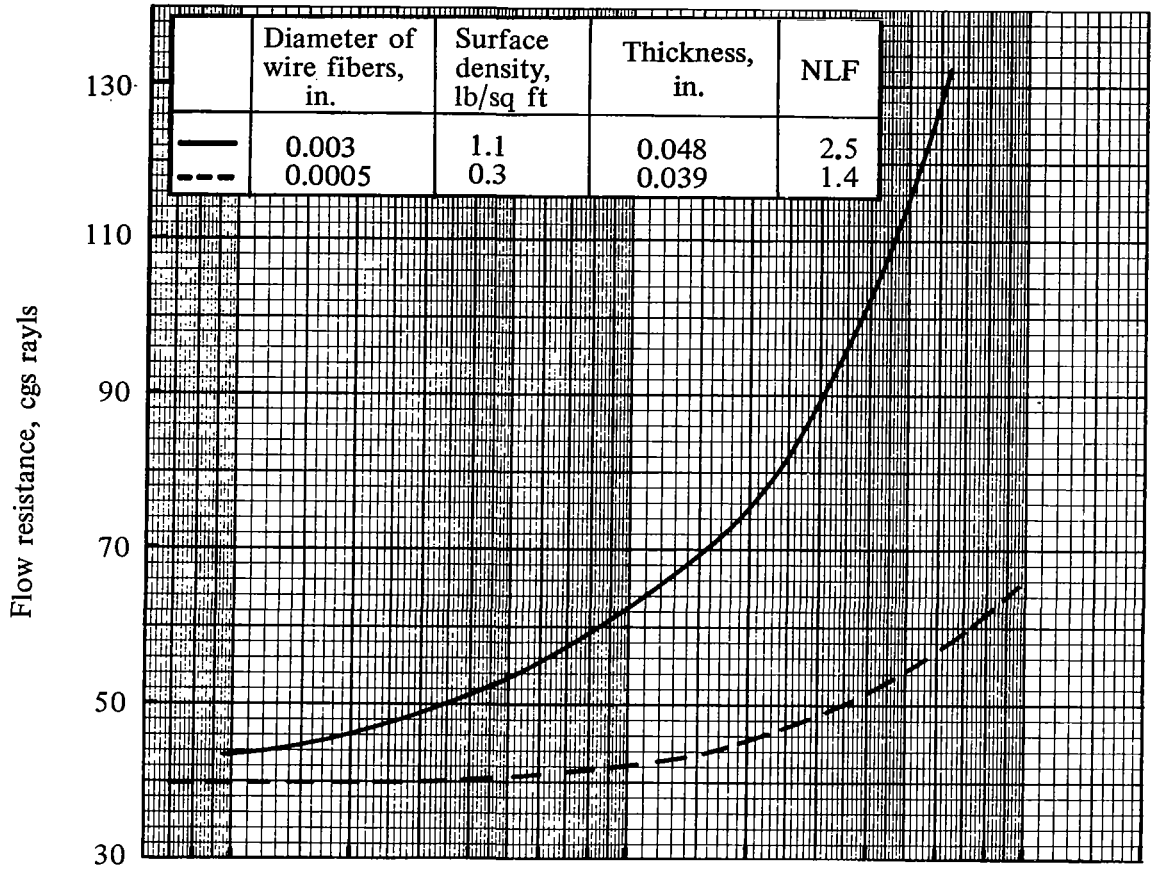

(a) Nominal 40 cgs rayl material.

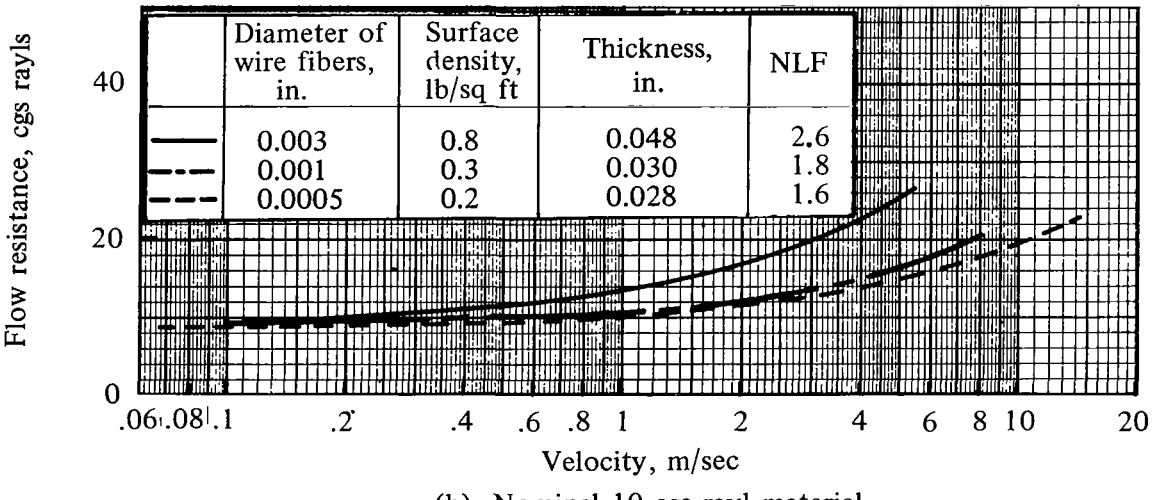

(b) Nominal 10 cgs rayl material.

Figure 14. – Variation of flow resistance of fibermetals with changes in wire fiber diameter, surface density, and thickness.

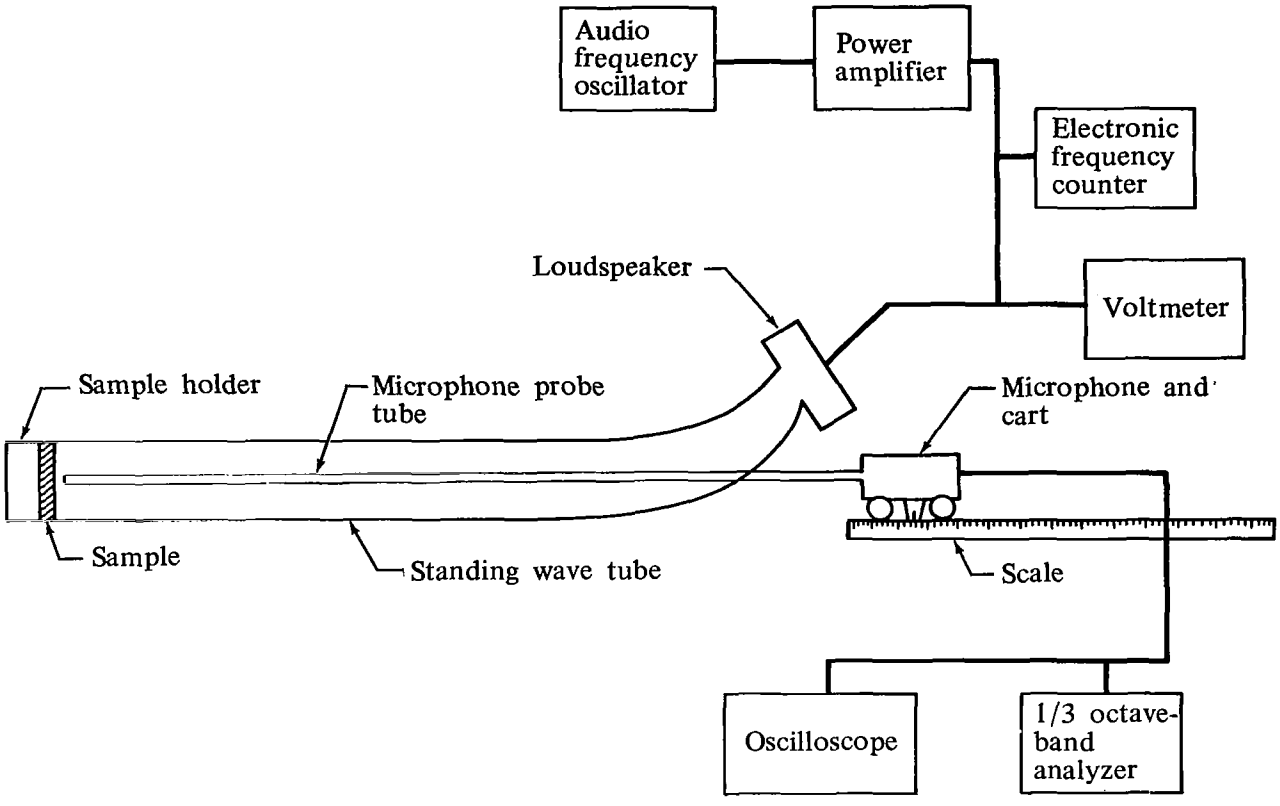

Figure 15. – Diagram of the standing-wave tube apparatus.

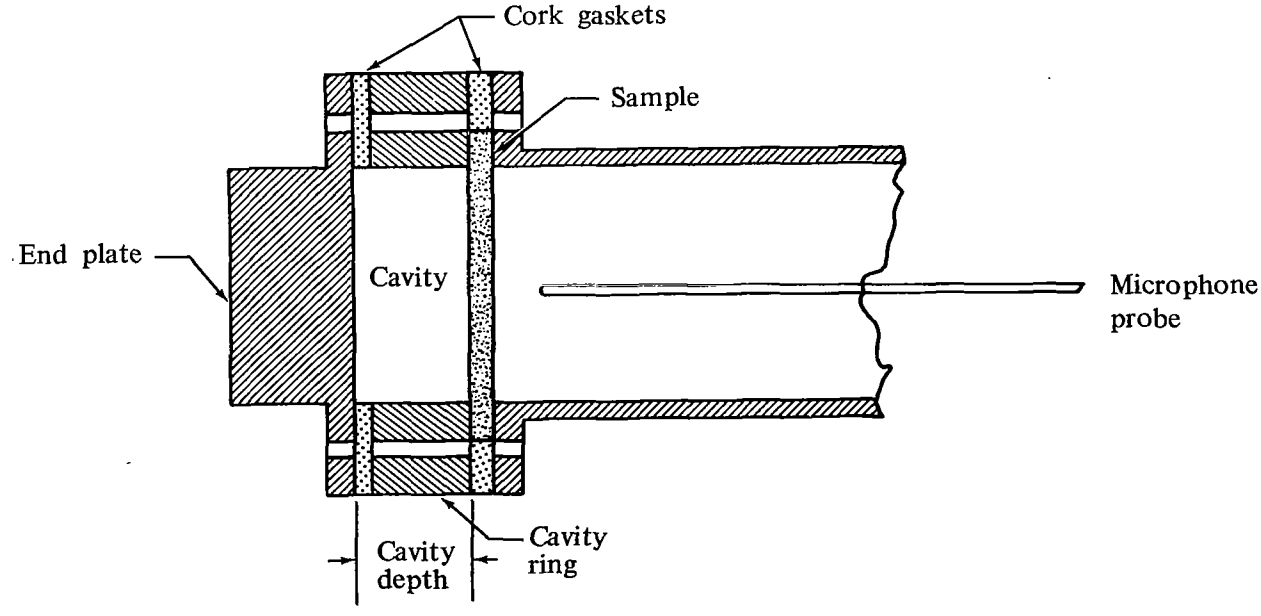

Figure 16. – Sample holder showing cavity spacing ring.

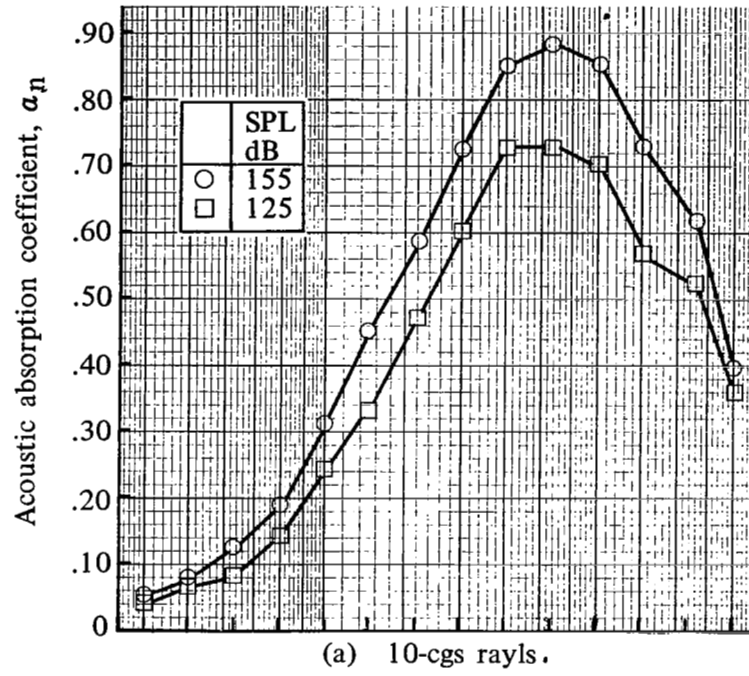

(a) 10-cgs rayls.

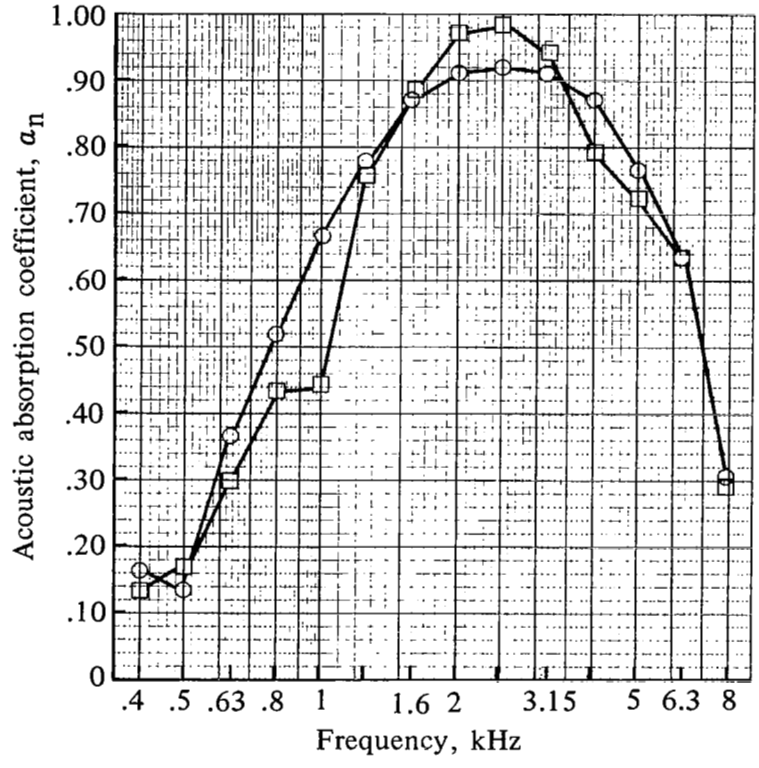

(b) 40-cgs rayls.

Figure 17. – Acoustic absorption coefficients of 10 and 40-cgs rayl fibermetal over 0.75-in.-deep cavities.

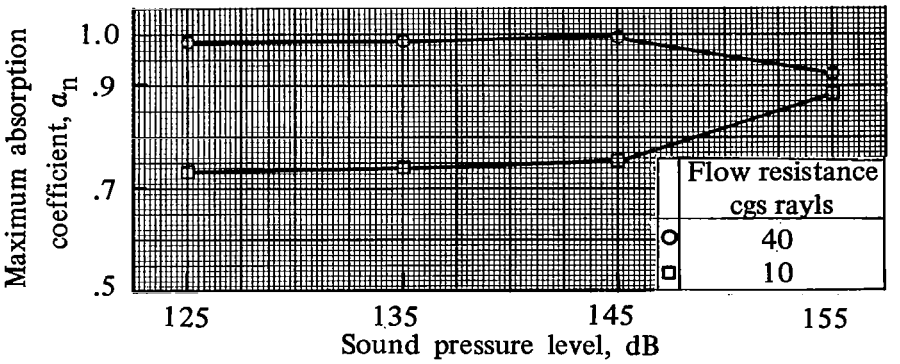

Figure 18. – Effect of SPL on the maximum absorption coefficient of 10 and 40-cgs rayl samples backed by 0.75-in.-deep cavities.

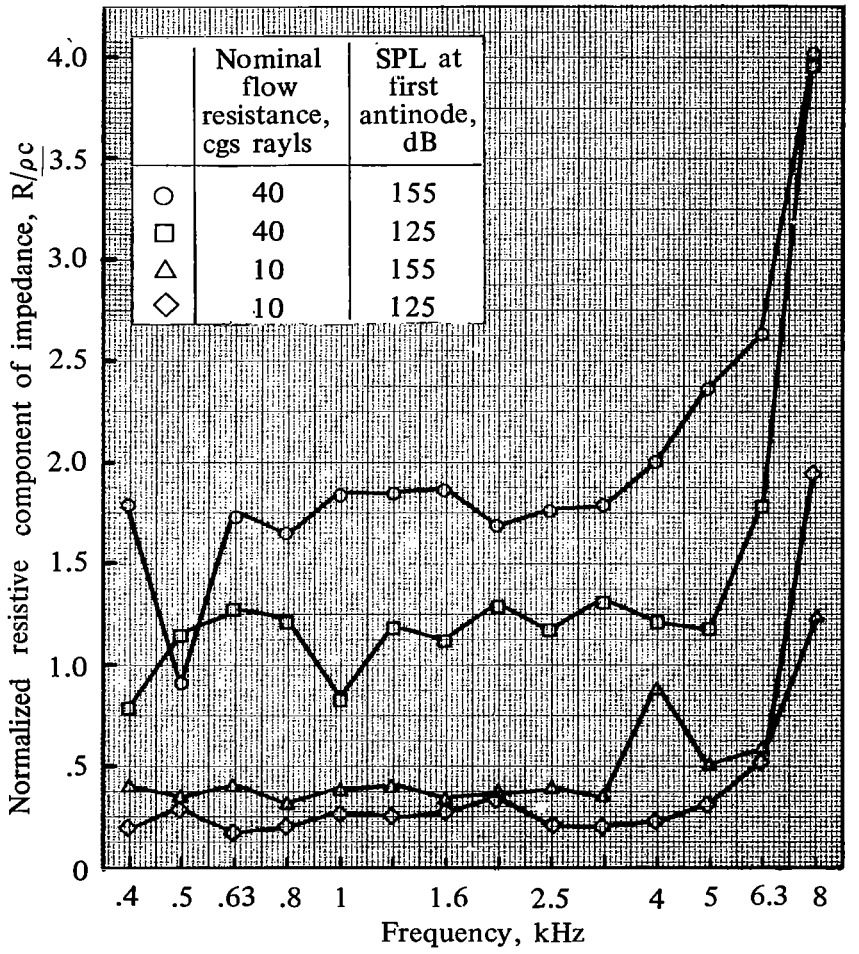

Figure 19. – Effect of SPL on the resistive component of the impedance for 10 and 40-cgs rayl samples backed by a 0.75-in.-deep cavity.

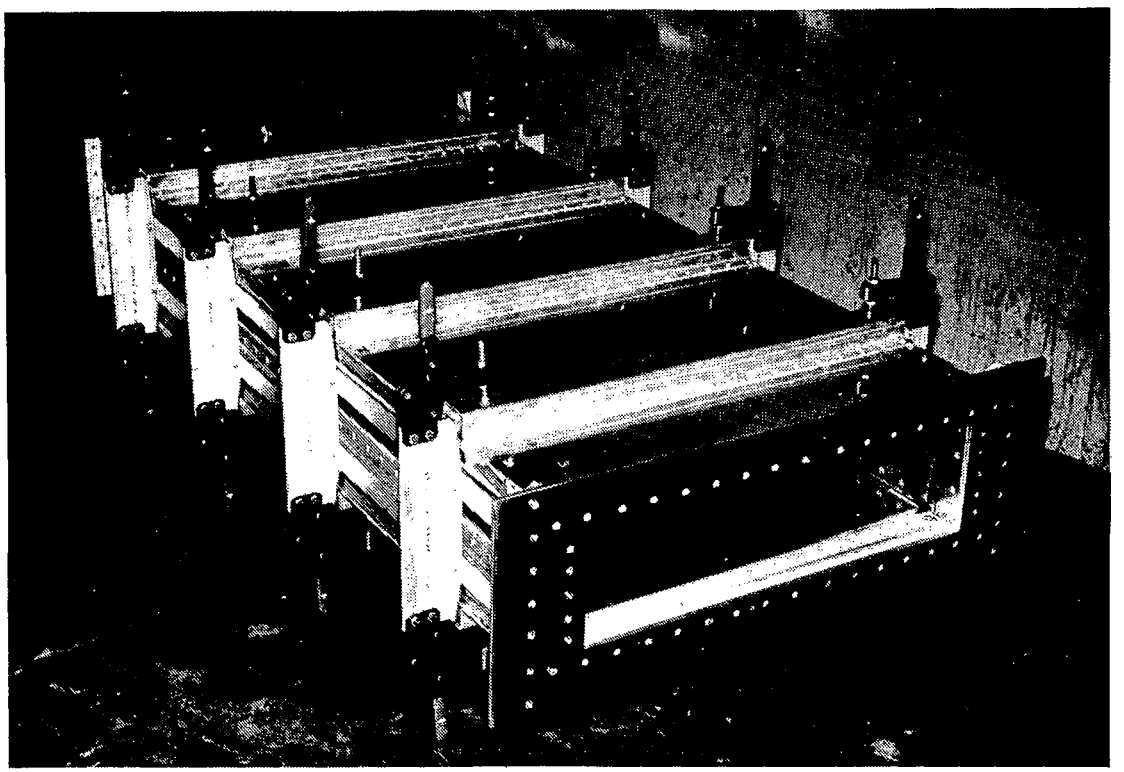

Figure 20. – 5 x 20 x 45-inch test duct showing outer surface of typical test panel.

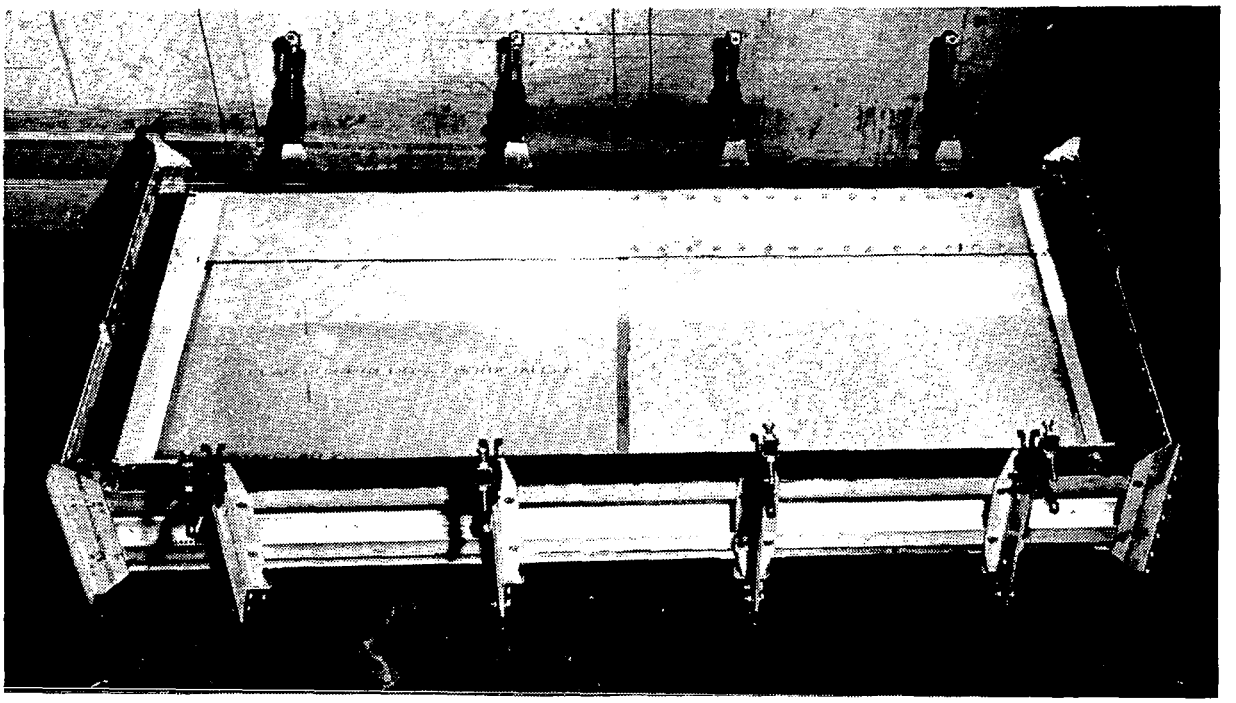

(a) Inner surface of panel showing fibermetal and aluminum surfaces.

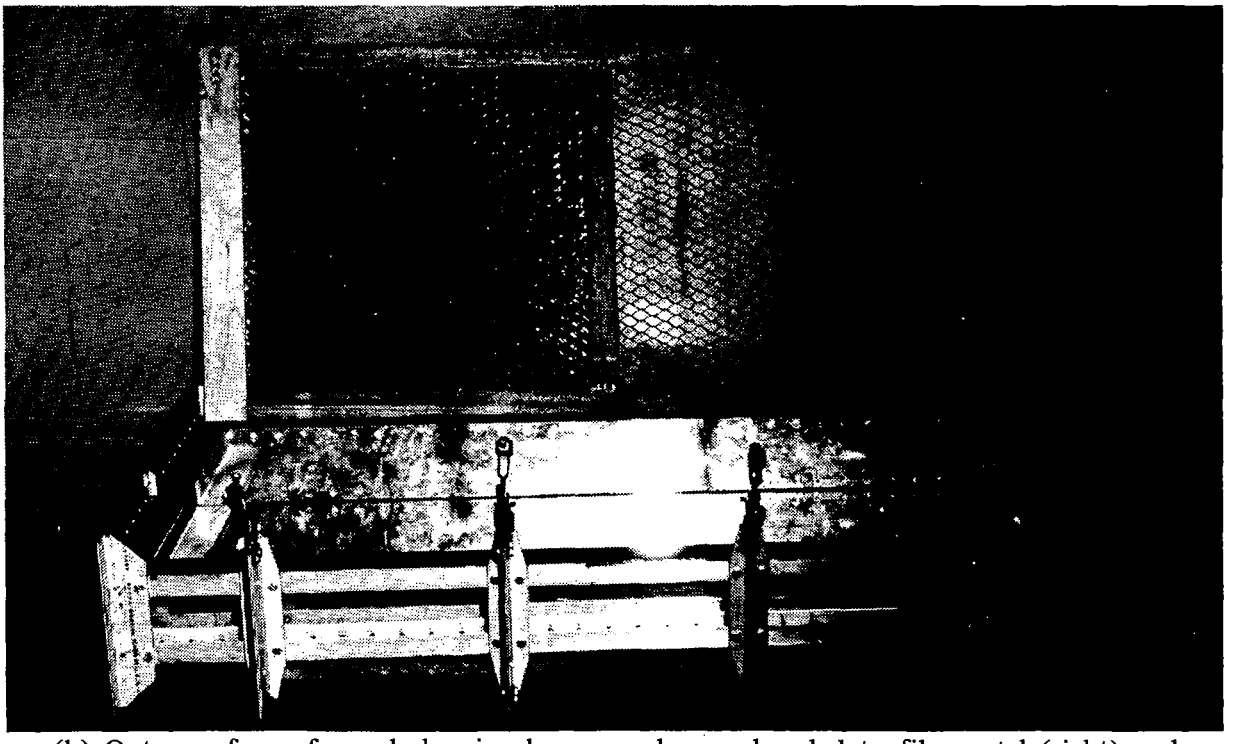

(b) Outer surface of panel showing honeycomb core bonded to fibermetal (right) and aluminum (left).

Figure 21. – Typical test panel installation.

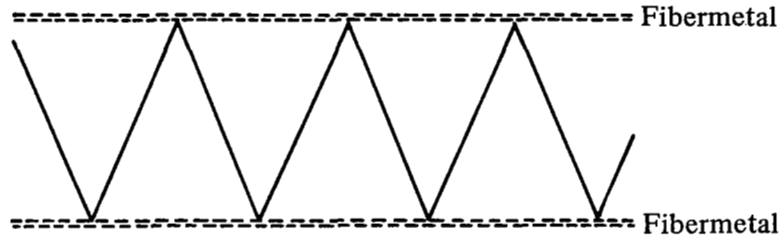

(a) Corrugated (two sides)

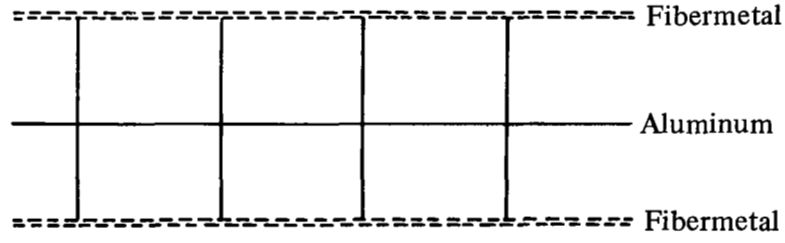

(b) .5-in. deep cavities (two sides)

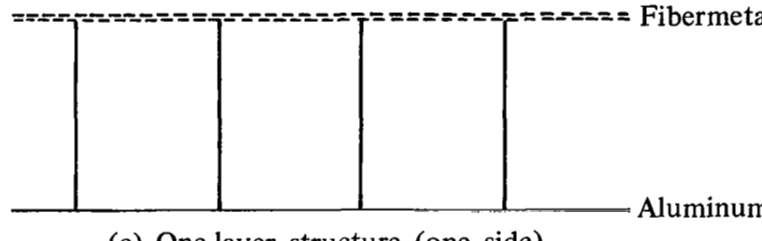

(c) One-layer structure (one side)

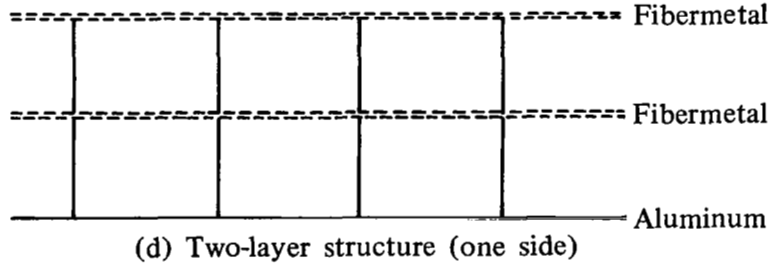

(d) Two-layer structure (one side)

Figure 22. – Cross section of 1-in.-thick acoustically treated splitters.

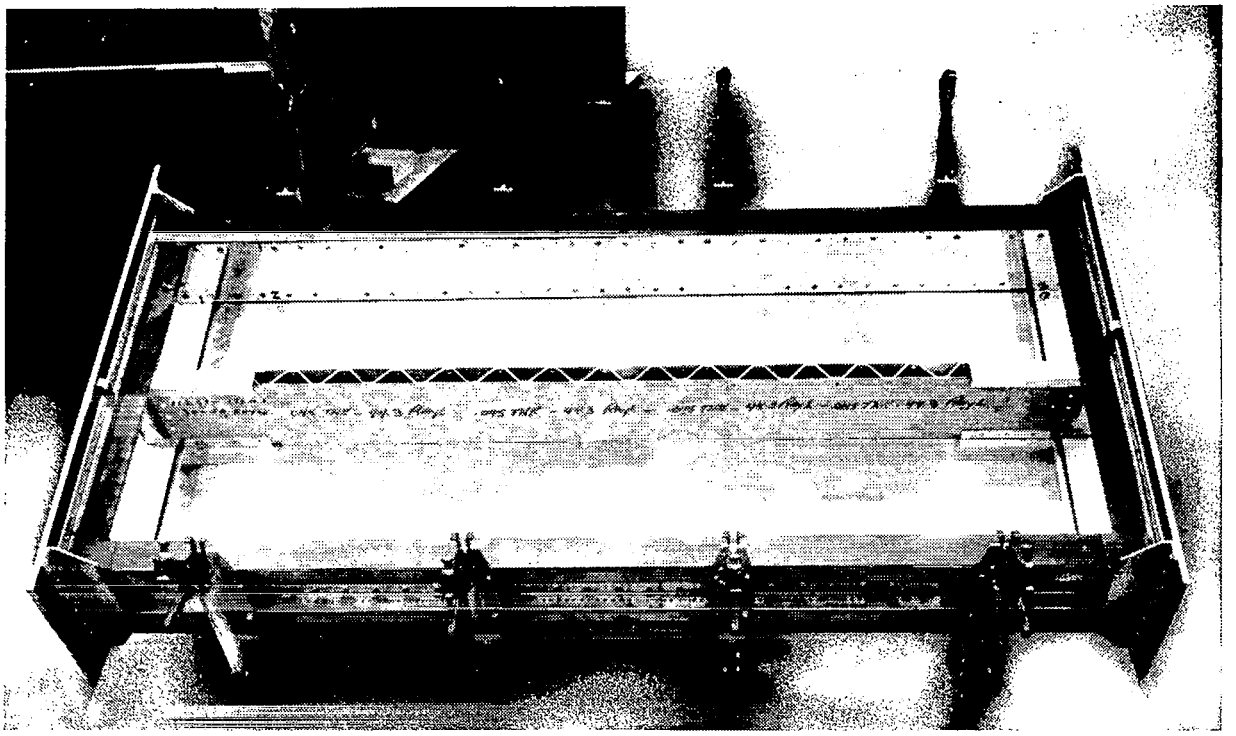

Figure 23. — Corrugated splitter installed in test duct.

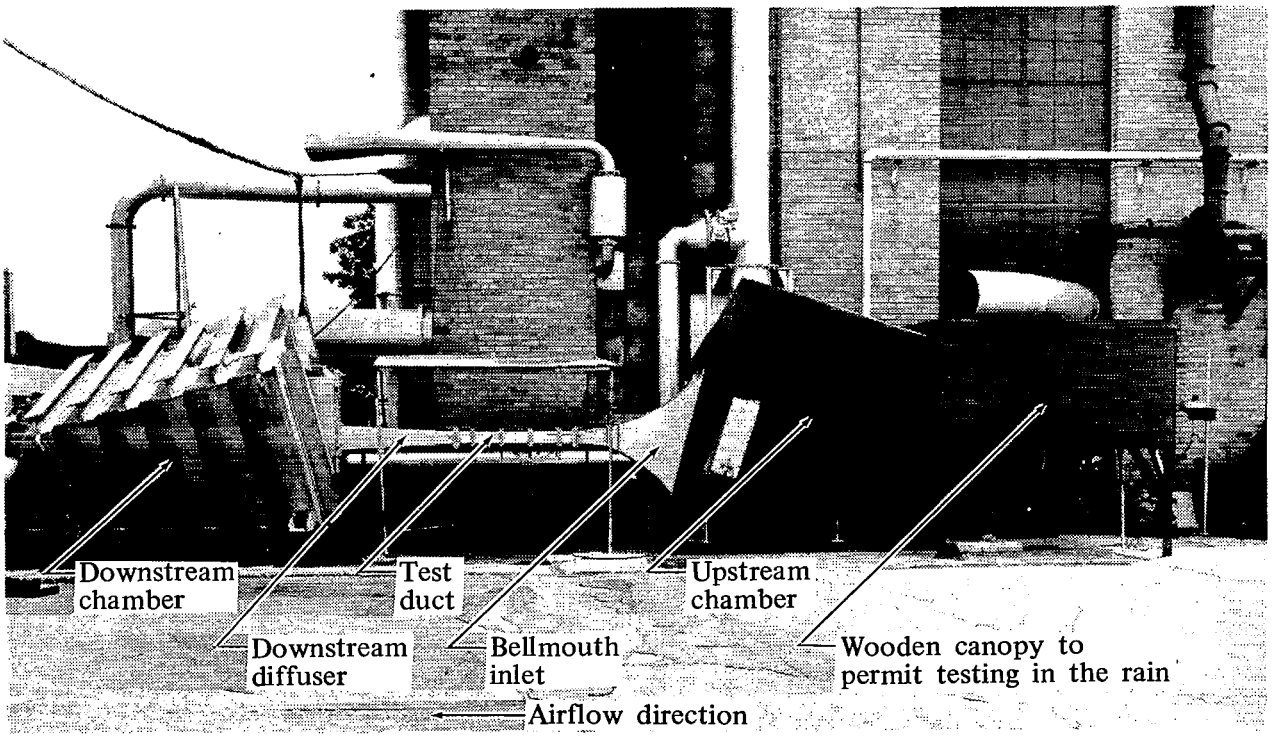

Figure 24. — Duct transmission-loss test facility.

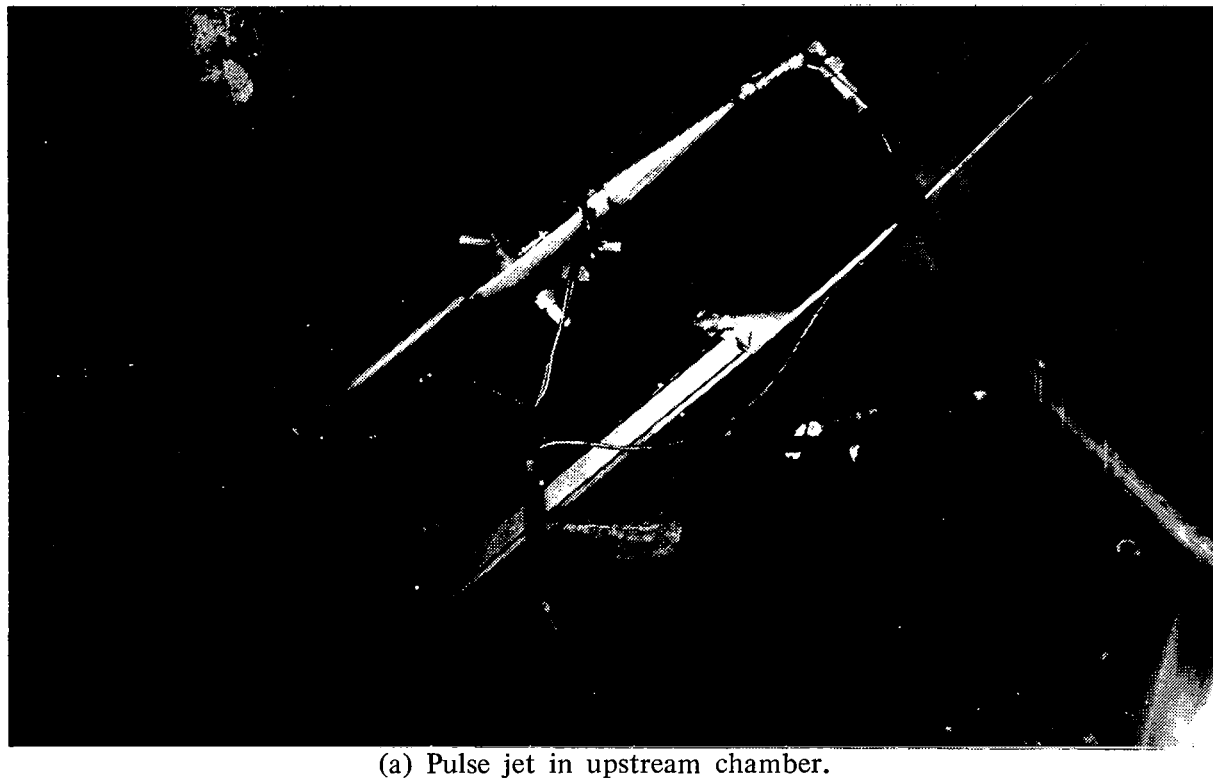

(a) Pulse jet in upstream chamber.

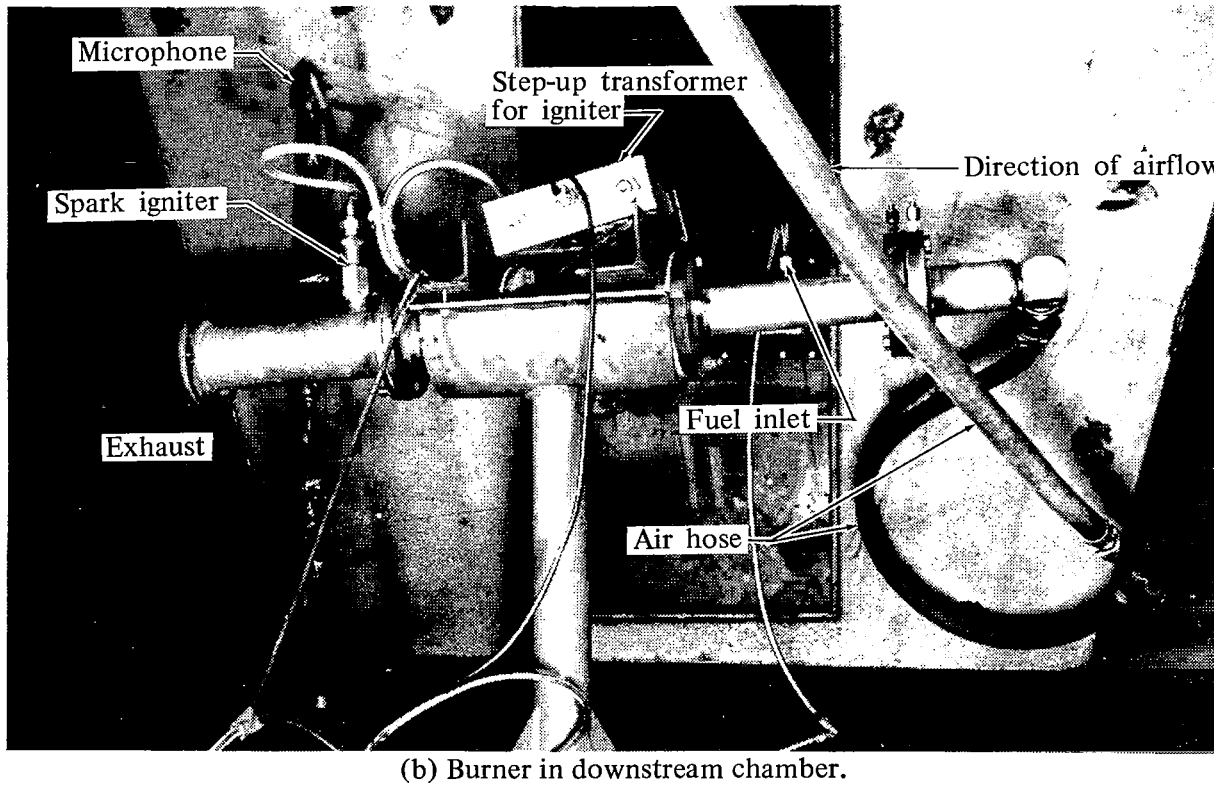

(b) Burner in downstream chamber.

Figure 25.– Sound sources in reverberant chambers.

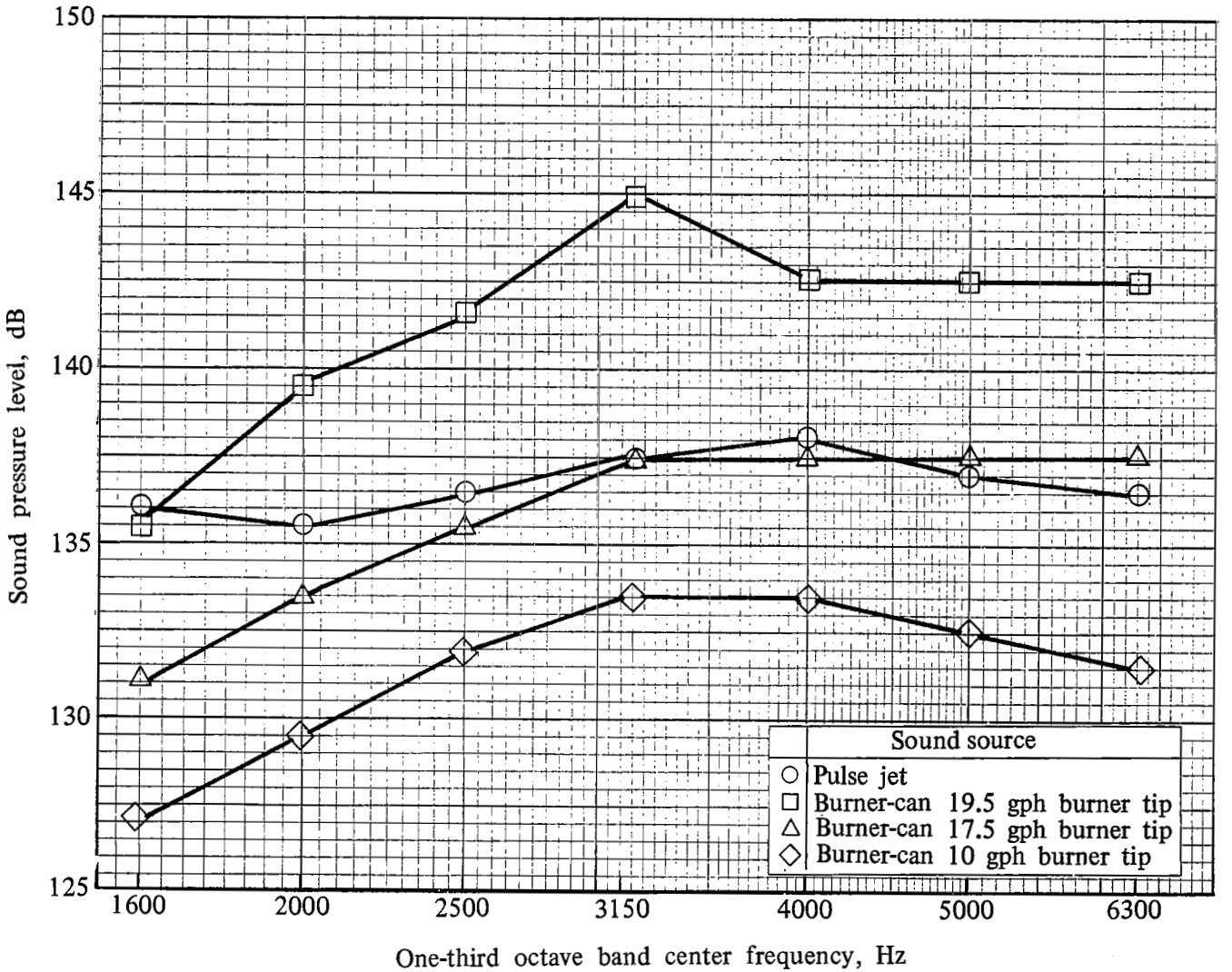

Figure 26. – Source-room sound pressure levels in downstream chamber at a duct velocity of 500 ft/sec.

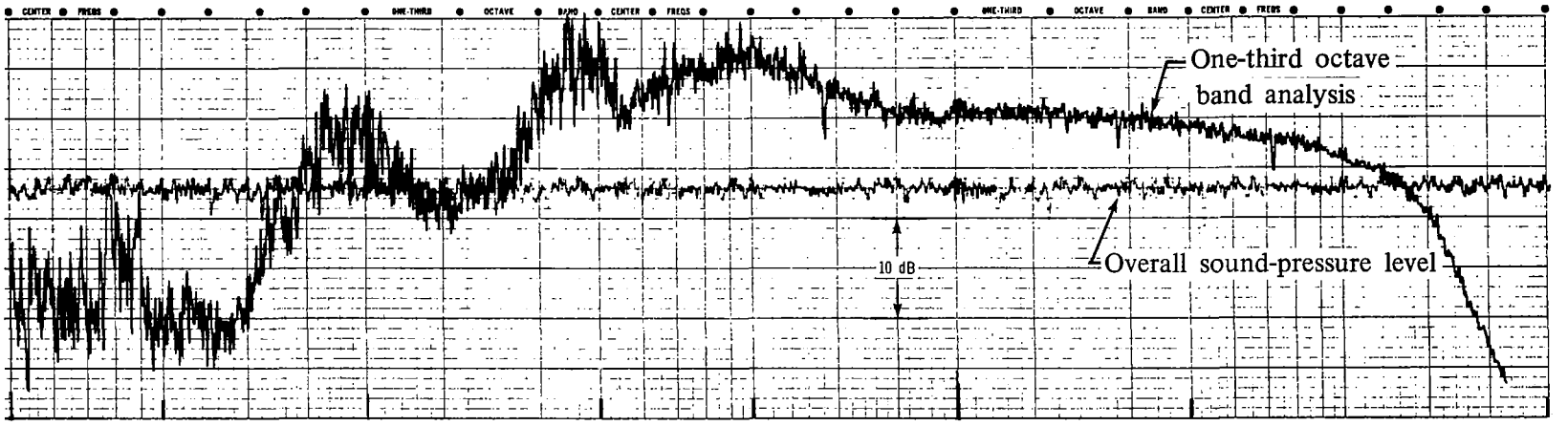

(a) Pulse jet.

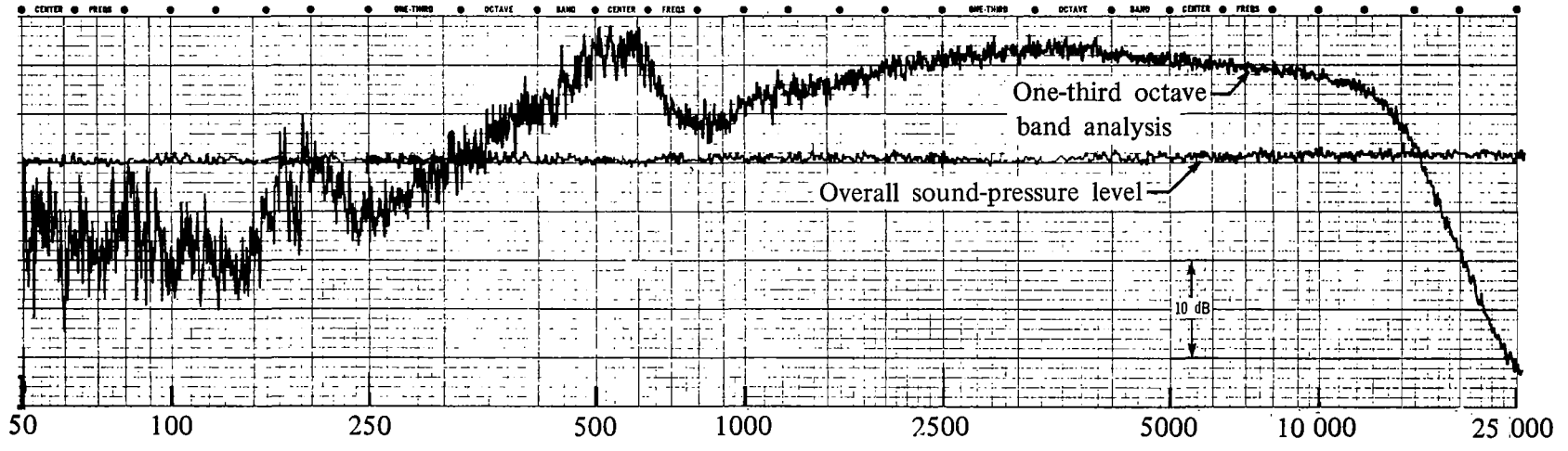

(b) Burner can, 17.5-gph burner tip, 38 psig air pressure.

Figure 27. Source-room sound spectra in downstream chamber at a duct velocity of 500 ft/sec

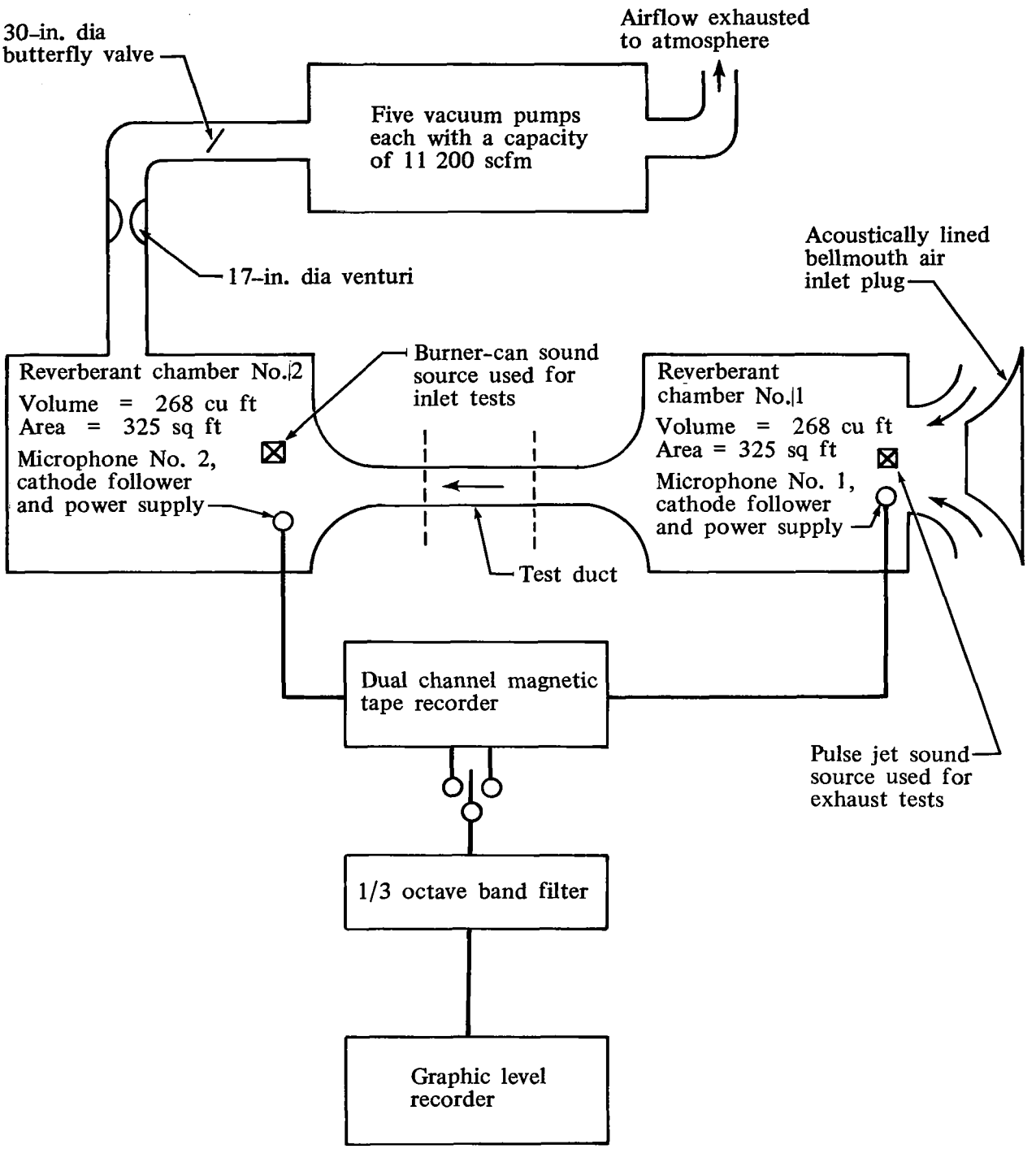

Figure 28. – Diagram of instrumentation and equipment for duct transmission-loss testing.

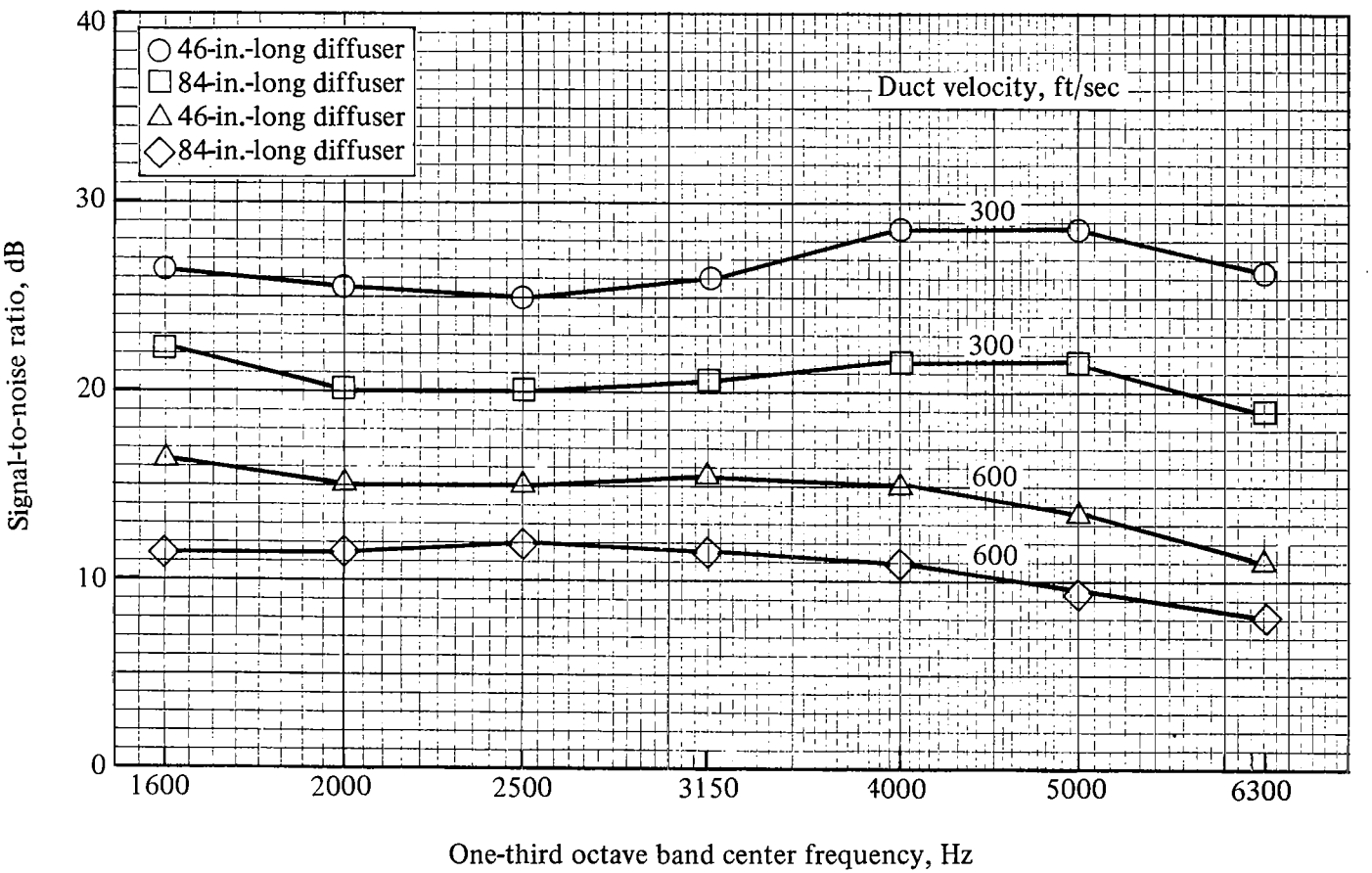

Figure 29. – Signal-to-noise ratios for 46-in. and 84-in. downstream diffusers for exhaust mode tests.

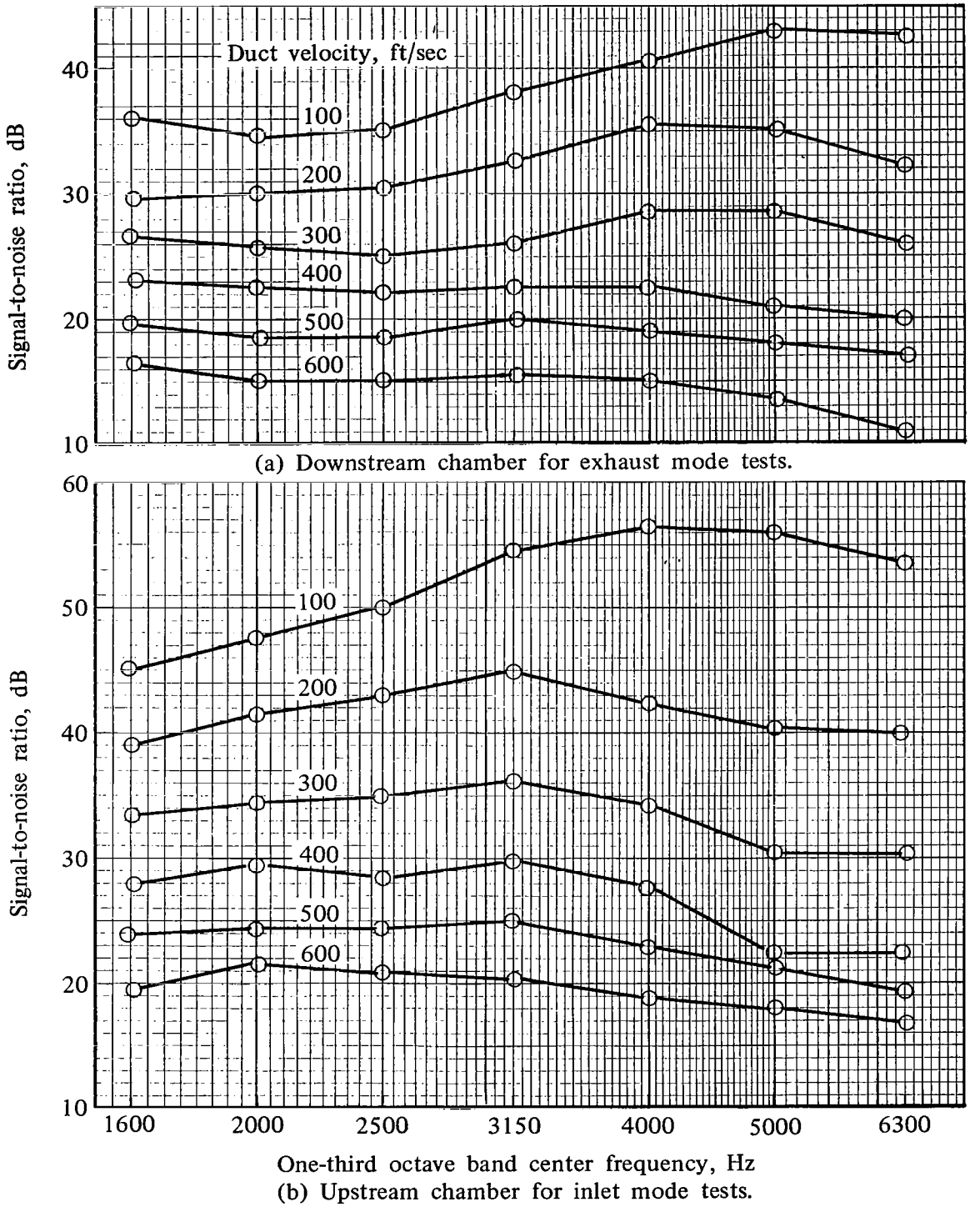

Figure 30. – Signal-to-noise ratios in the inlet and exhaust mode with the 46 in. downstream diffuser.

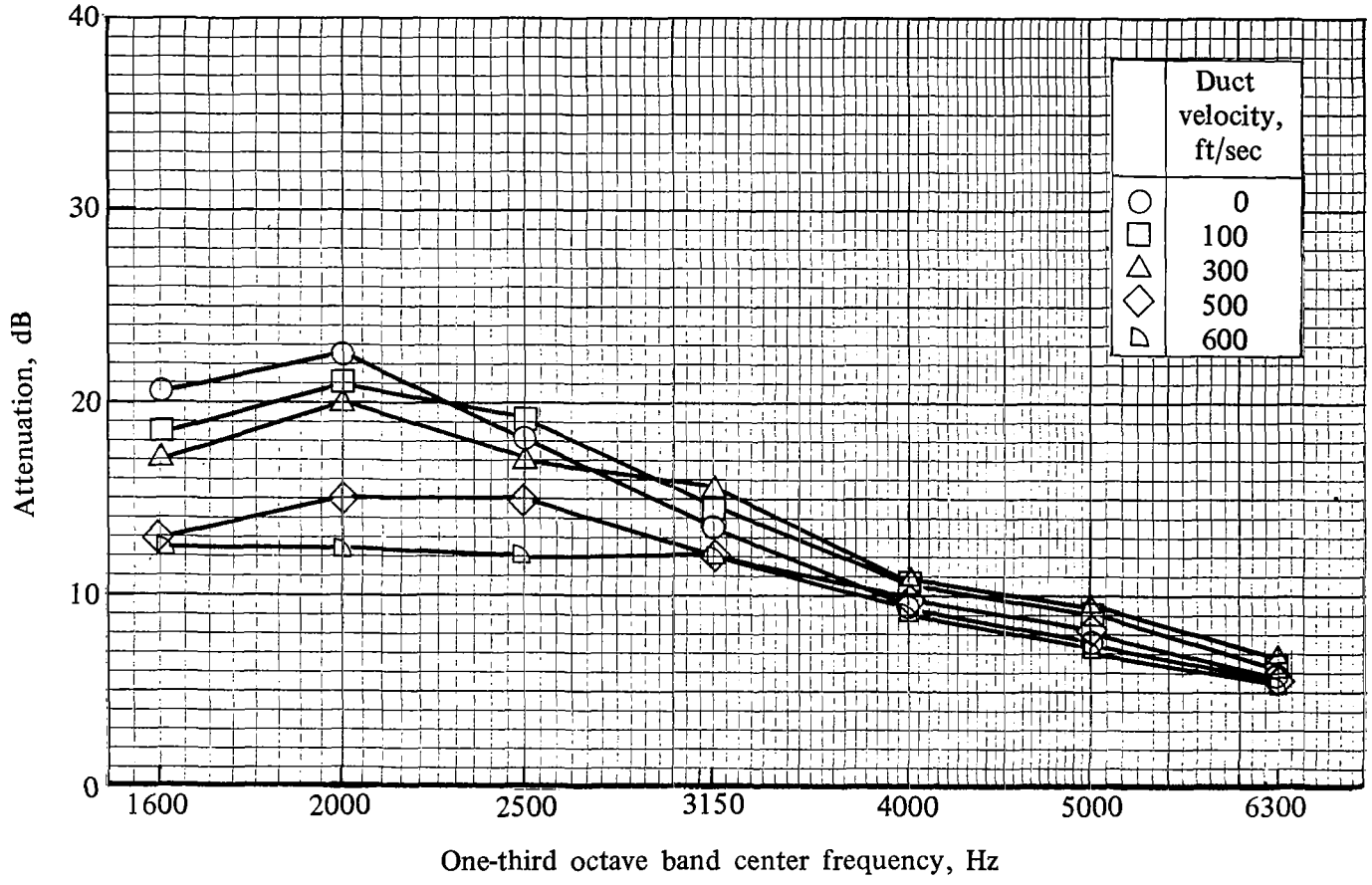

Figure 31. – Effect of velocity on attenuation in exhaust mode. Treatment was nominal 40-rayl fibermetal over 1-in.-deep cavities. Area of treatment was 900 sq in.

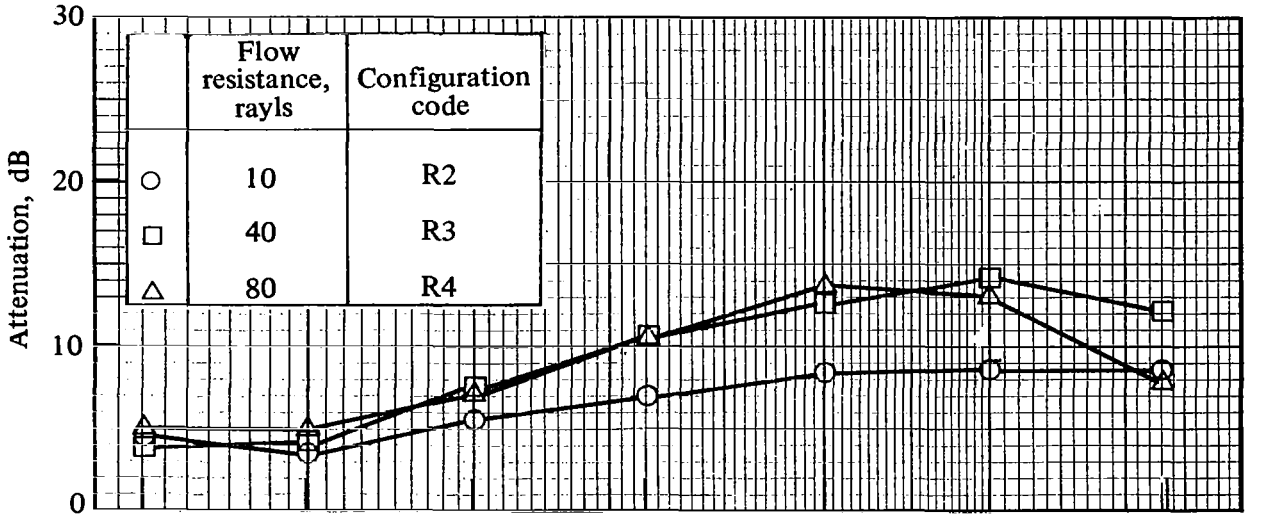

(a) .25 in. cavity depth.

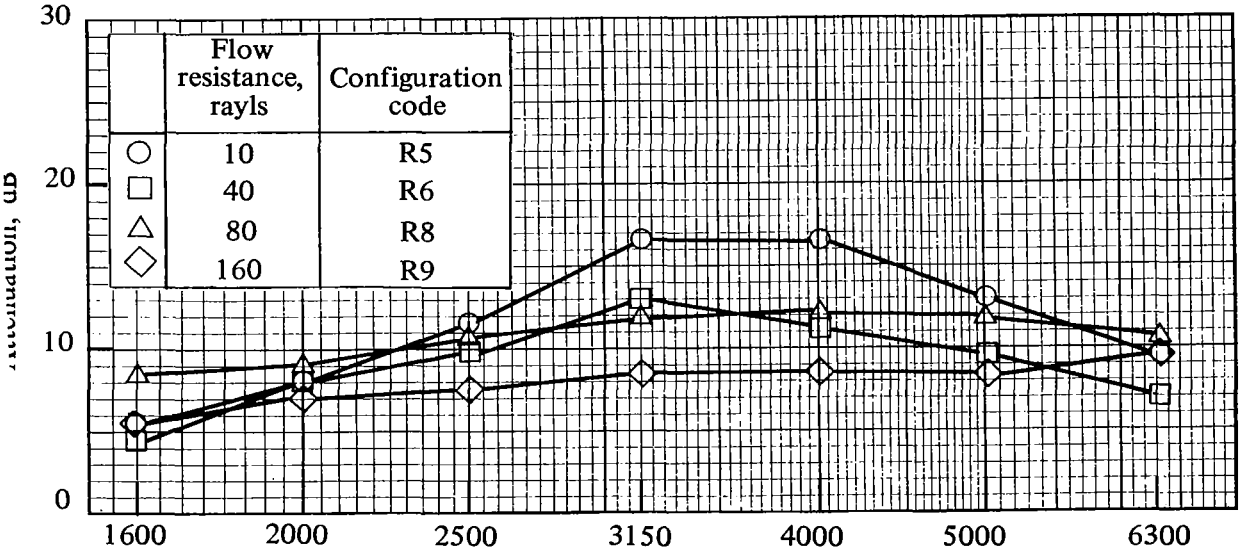

(b) .5 in. cavity depth.

Figure 32. — Effect of nominal flow resistance on attenuation in exhaust mode.

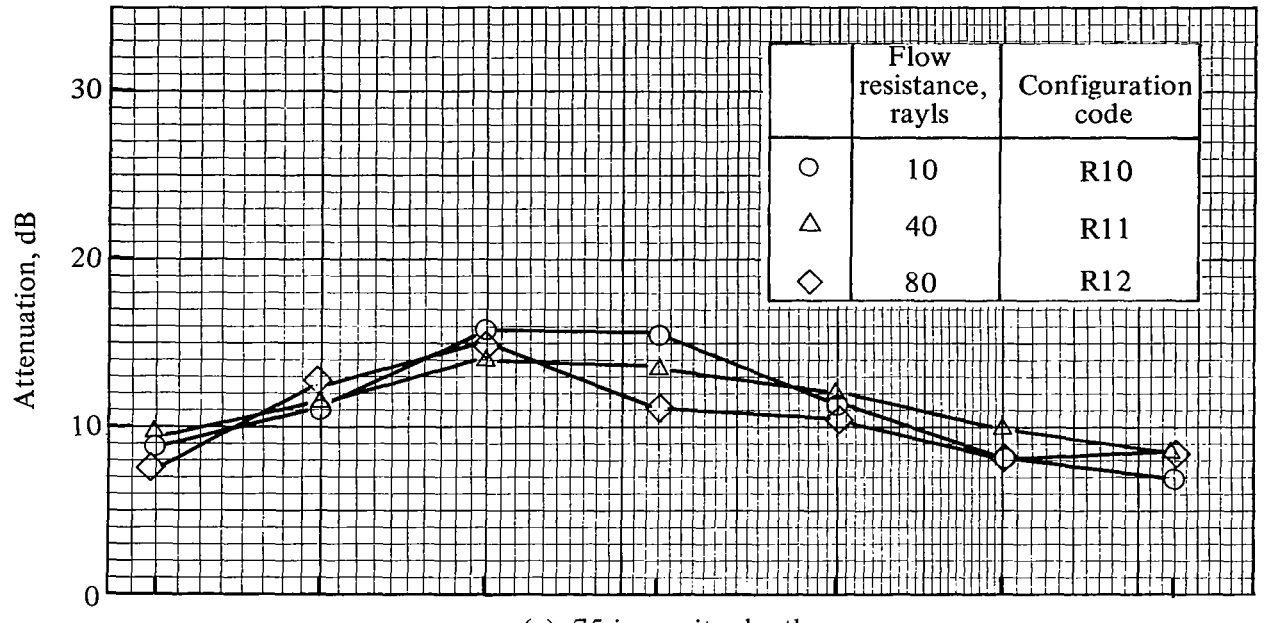

(c) .75-in. cavity depth.

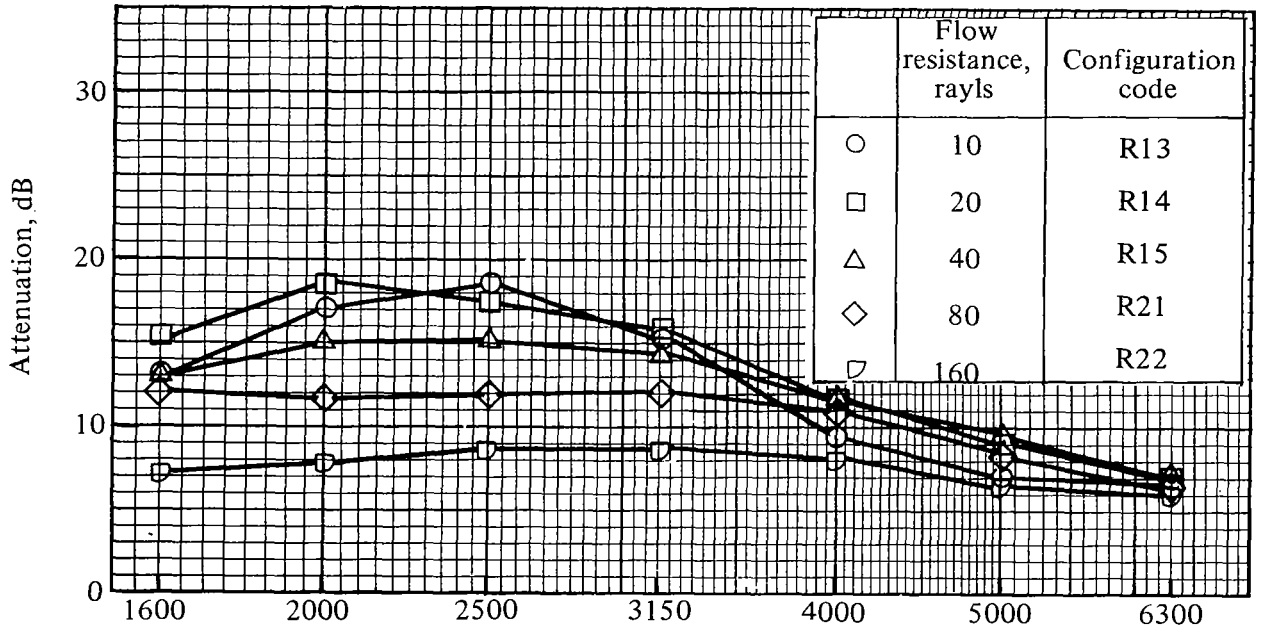

(d) 1-in. cavity depth.

Figure 32. – Concluded.

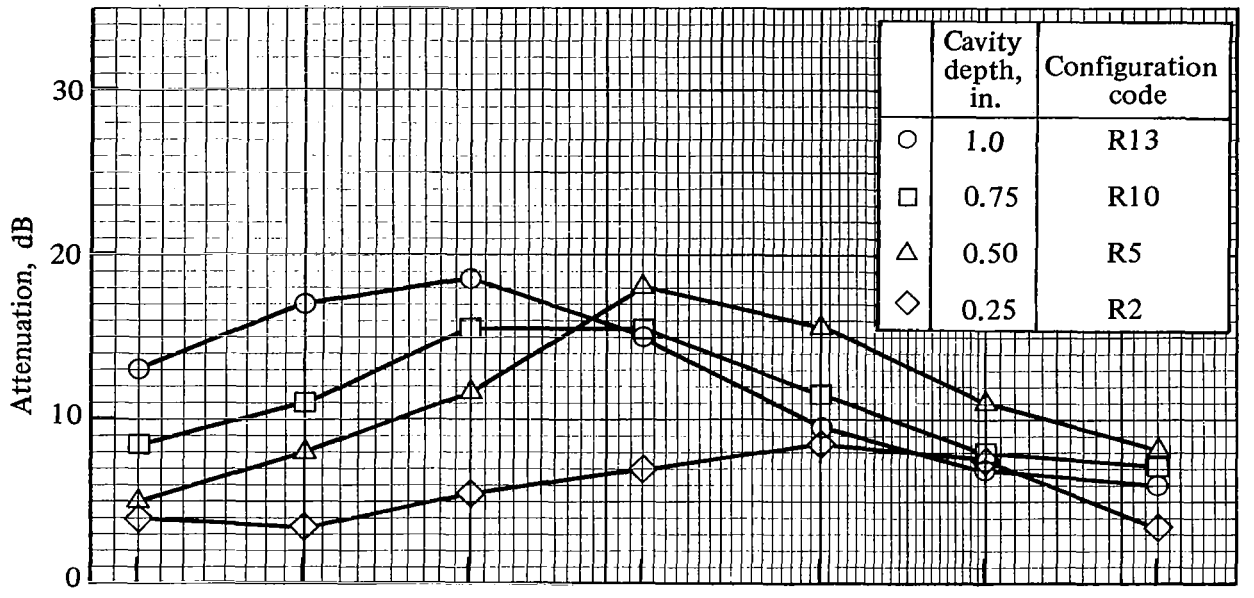

(a) Nominal flow resistance 10 cgs rayls.

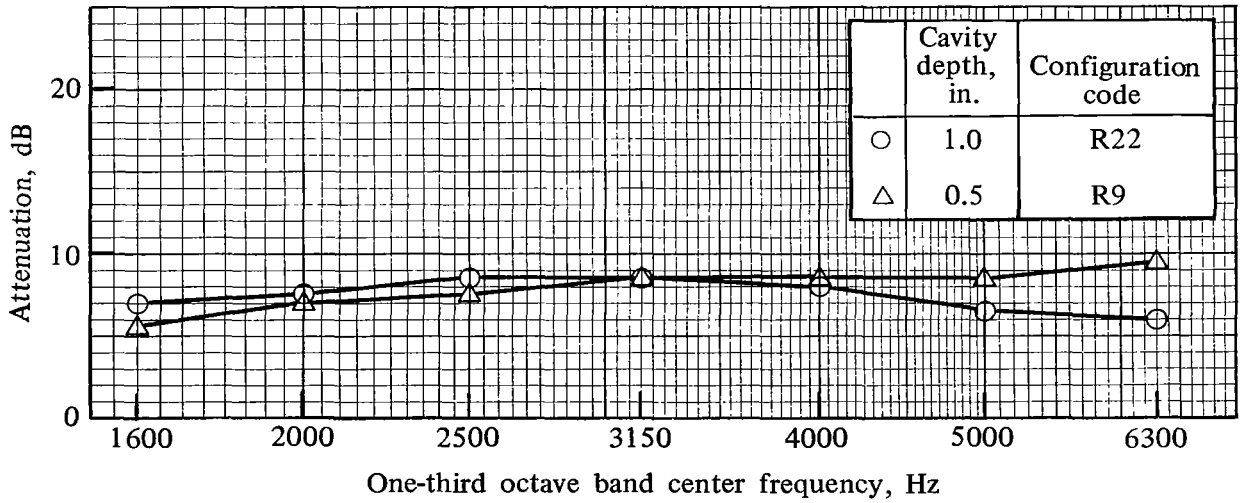

(b) Nominal flow resistance 160 cgs rayls.

Figure 33. — Effect of cavity depth on attenuation in exhaust mode.

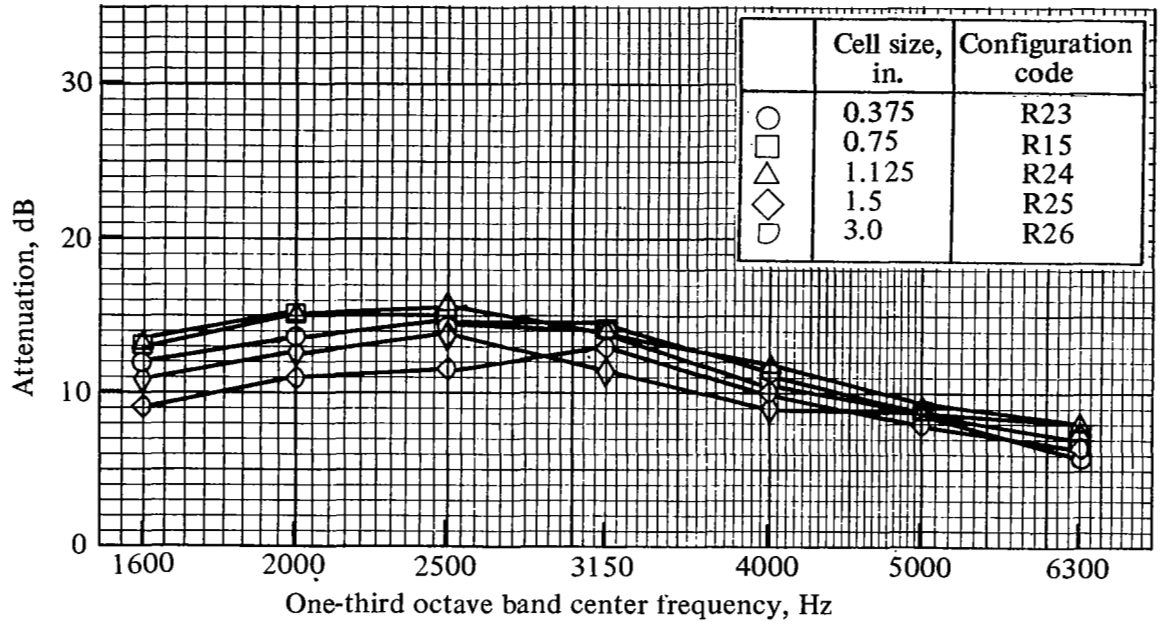

Figure 34. – Effect of honeycomb cell size on attenuation in exhaust mode.

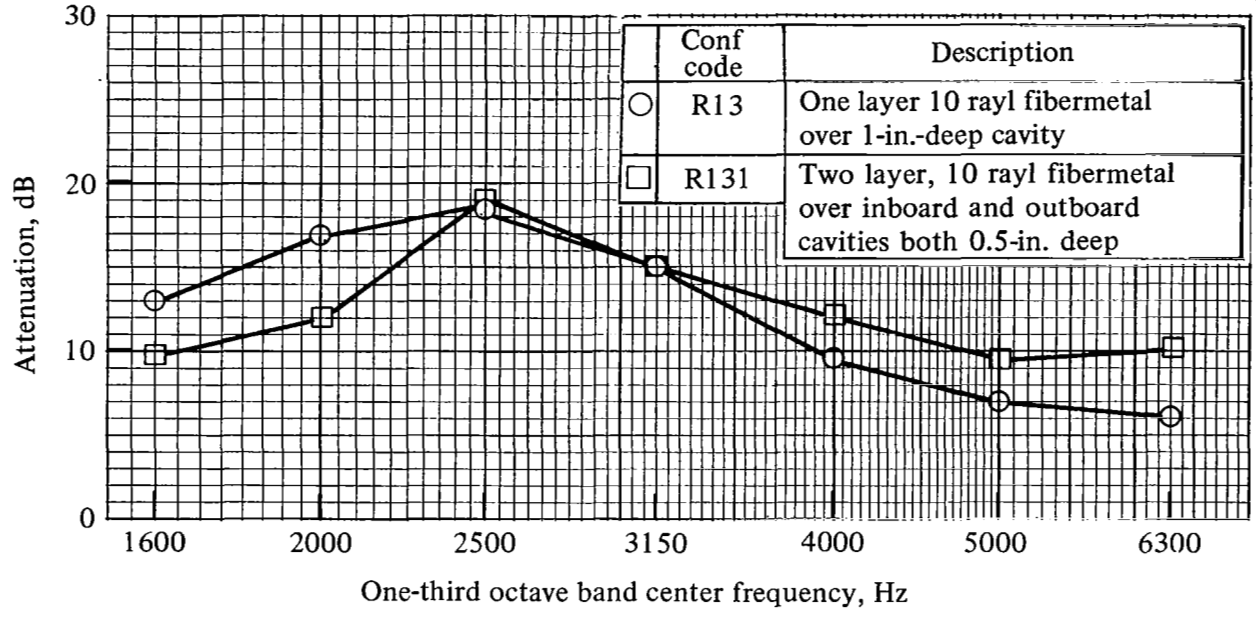

Figure 35. – Comparison of attenuation produced in exhaust mode by one-layer design to that produced by two-layer design.

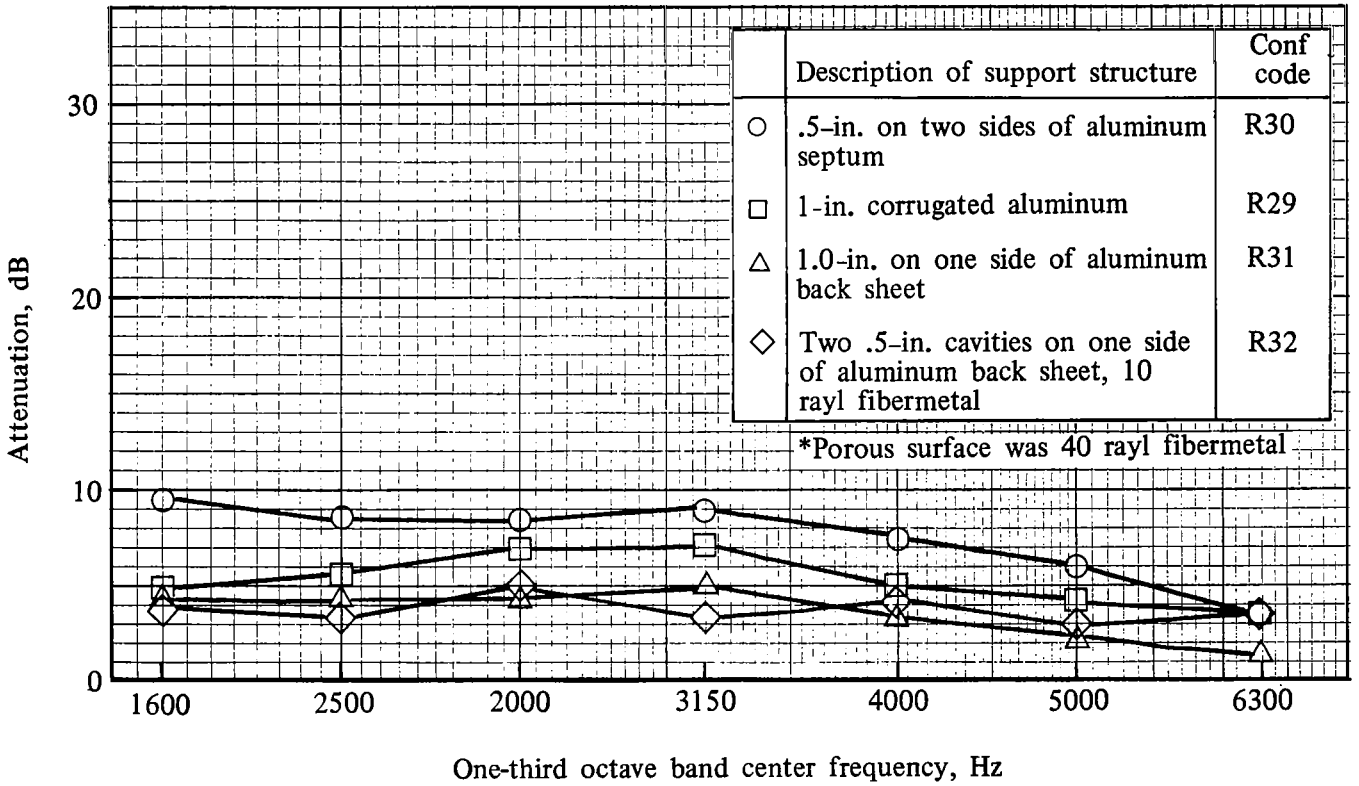

Figure 36. – Effect of acoustical design of various splitters on attenuation in exhaust mode. The duct walls remained hard.

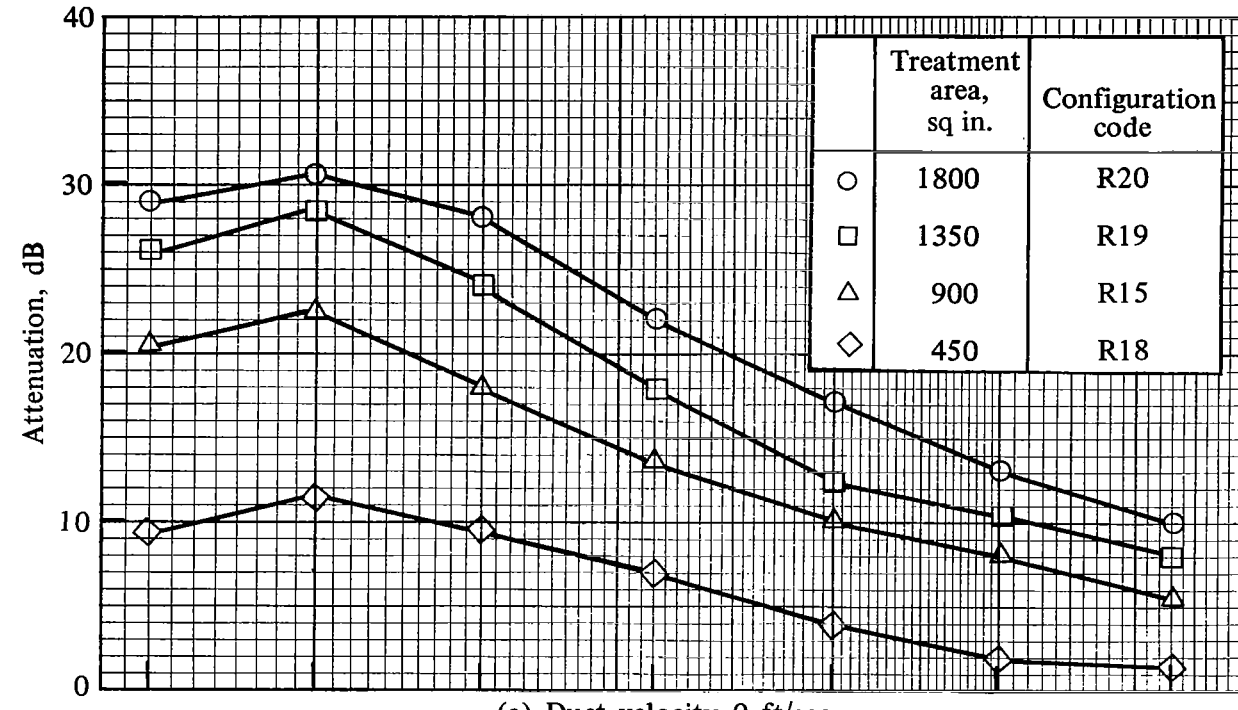

(a) Duct velocity 0 ft/sec.

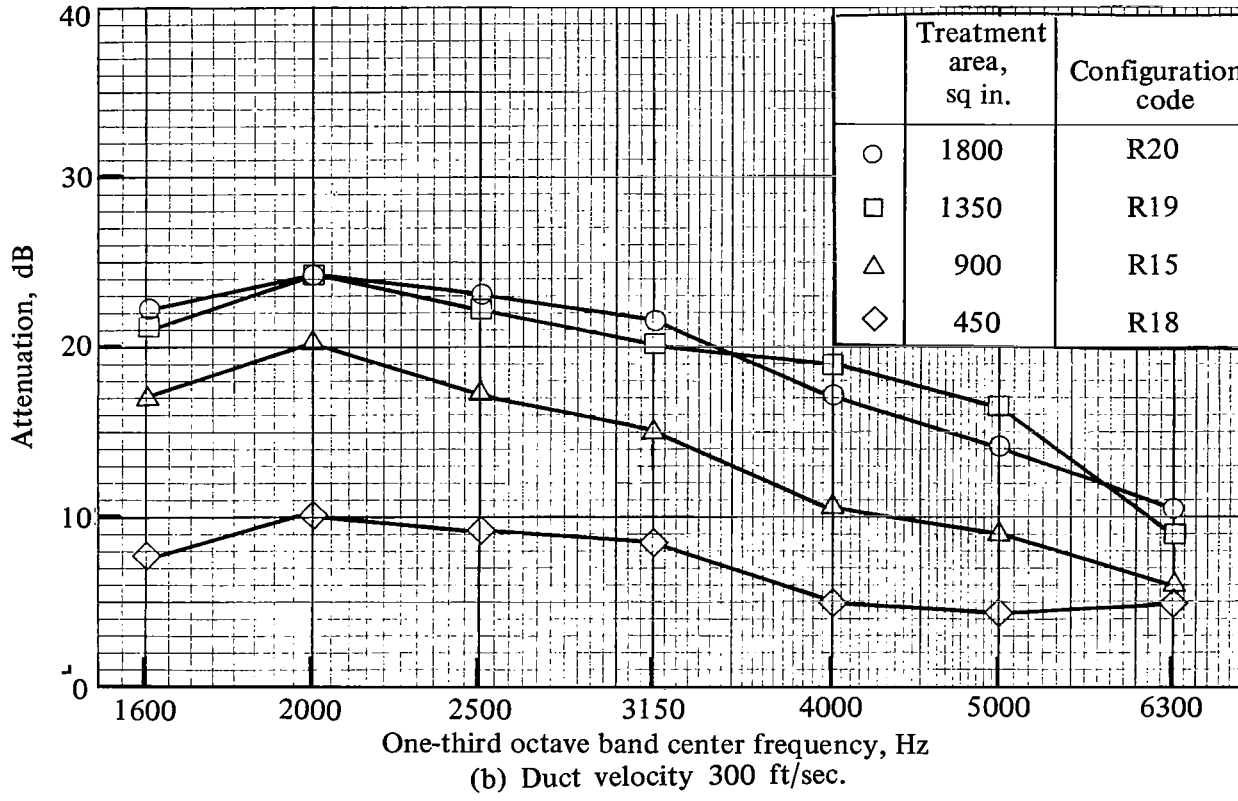

(b) Duct velocity 300 ft/sec.

Figure 37. — Effect of treated area on attenuation in exhaust mode. Treatment was 40-rayl fibermetal over 1-in.-deep cavities.

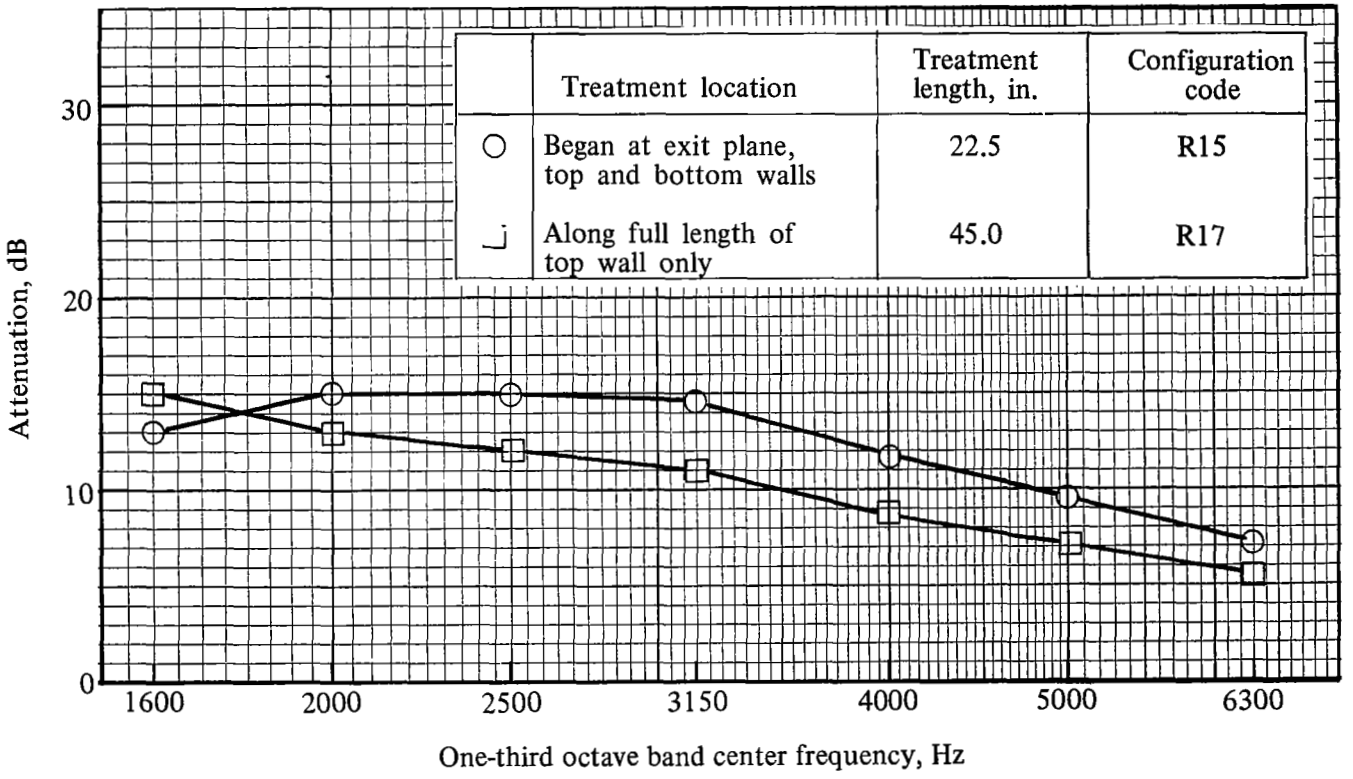

Figure 38. Effect of treatment location on attenuation in exhaust mode. Treatment was 40–rayl fibermetal over 1–in.–deep cavities.

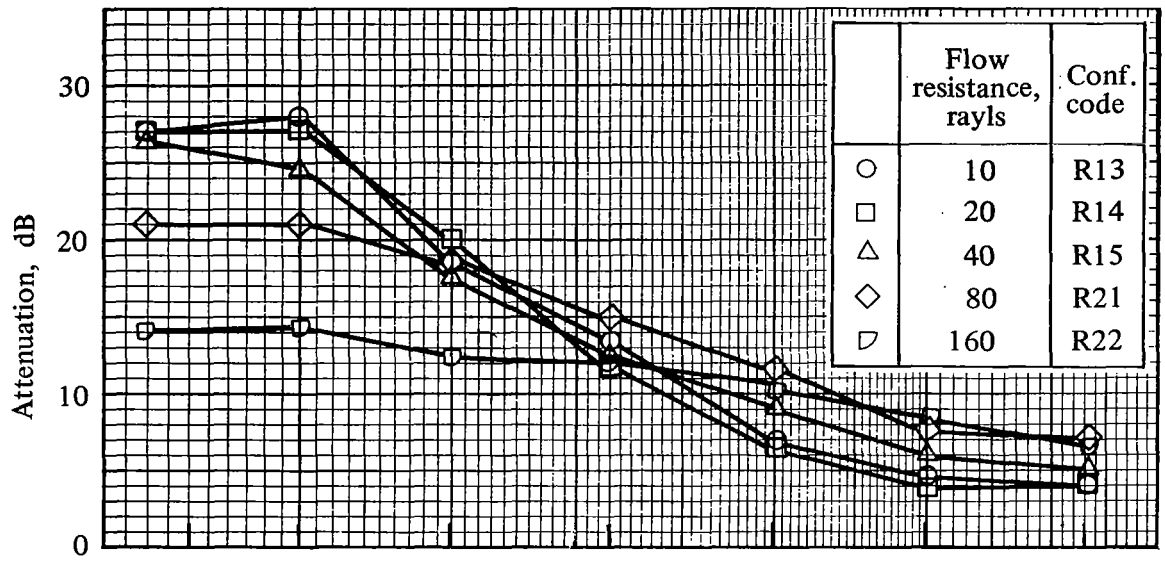

(a) Duct velocity 0 ft/sec.

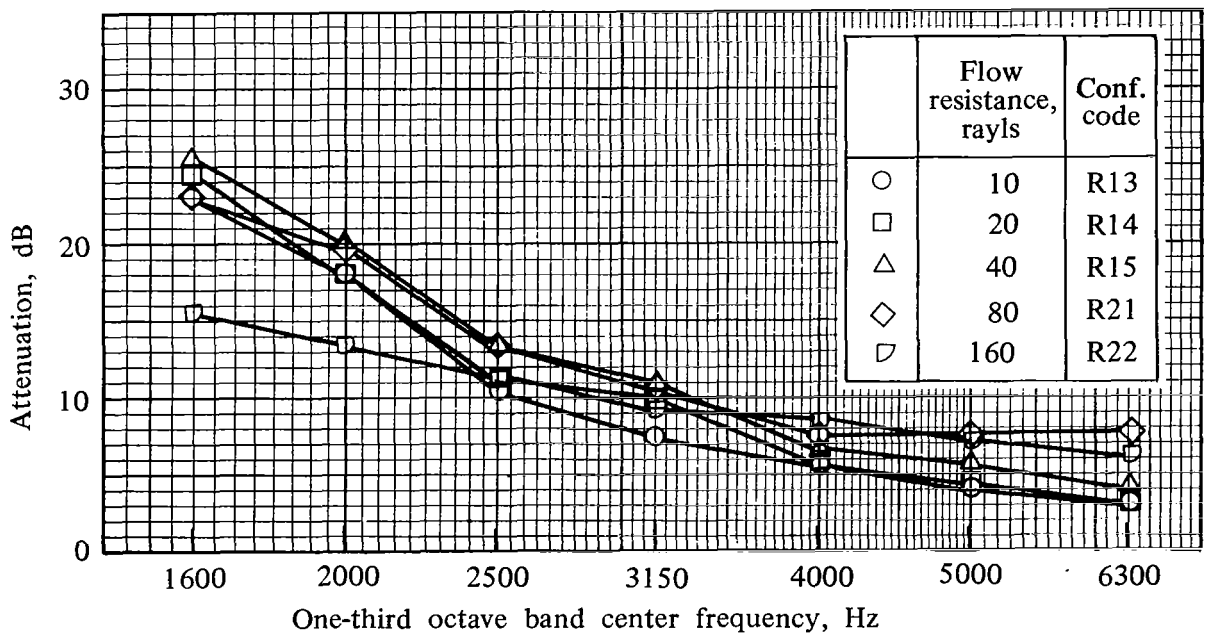

(b) Duct velocity 500 ft/sec.

Figure 39. – Effect of nominal flow resistance on attenuation in inlet mode. Cavity depth was 1 in.

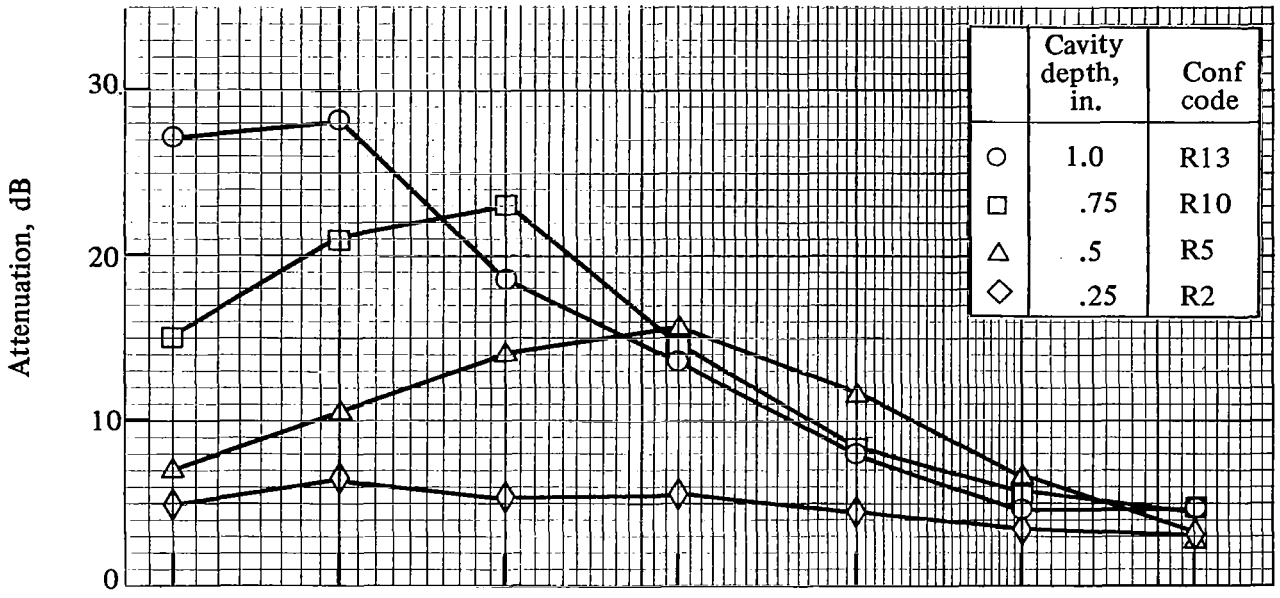

(a) Nominal flow resistance 10 cgs rayls and duct velocity 0 ft/sec.

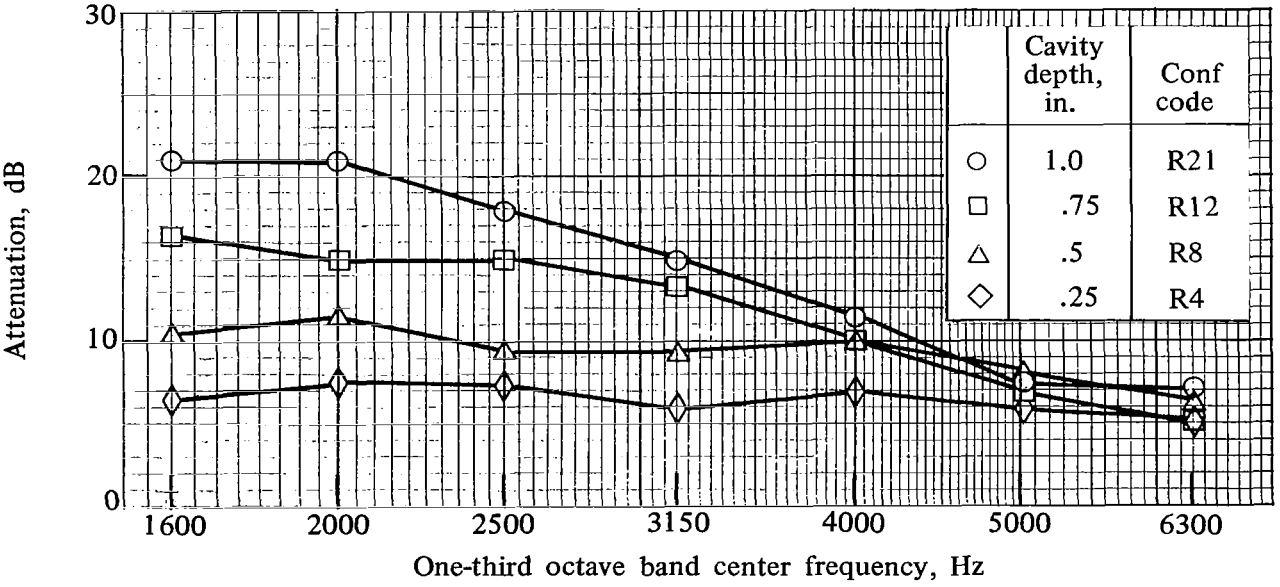

(b) Nominal flow resistance 80 cgs rayls and duct velocity 500 ft/sec.

Figure 40. – Effect of cavity depth on attenuation in inlet mode.

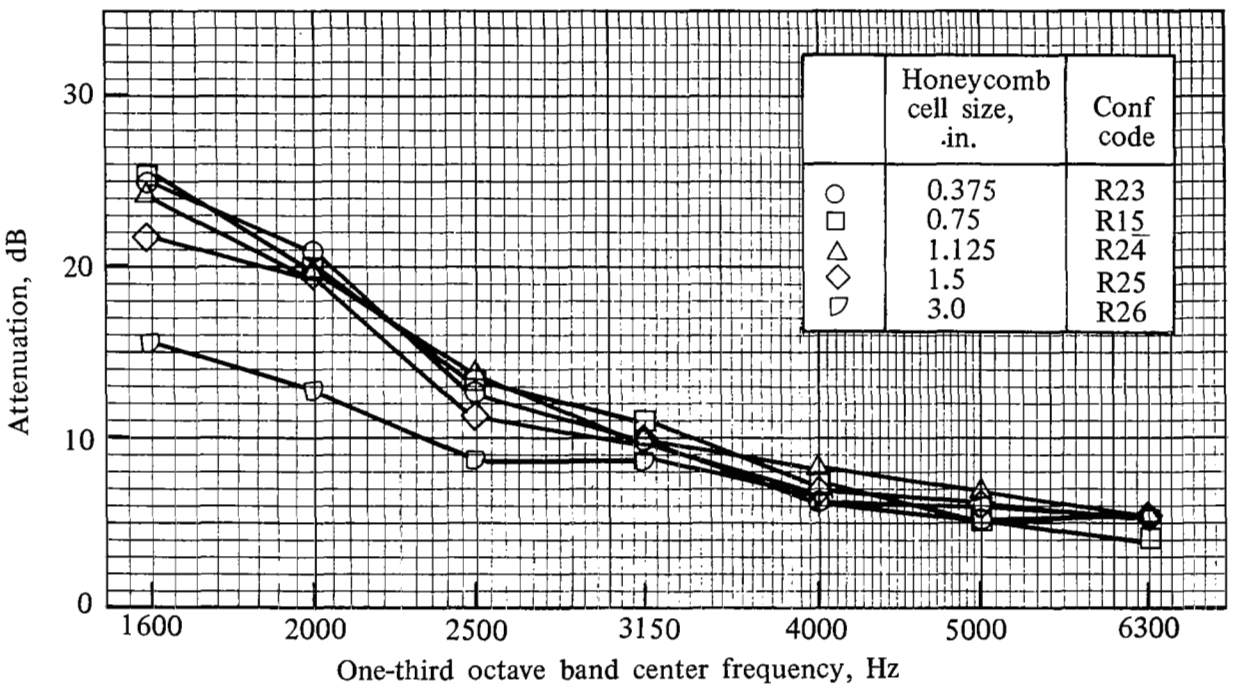

Figure 41. – Effect of honeycomb cell size on attenuation in inlet mode. Treatment was 40-rayl fibermetal over 1-in.-deep cavities.

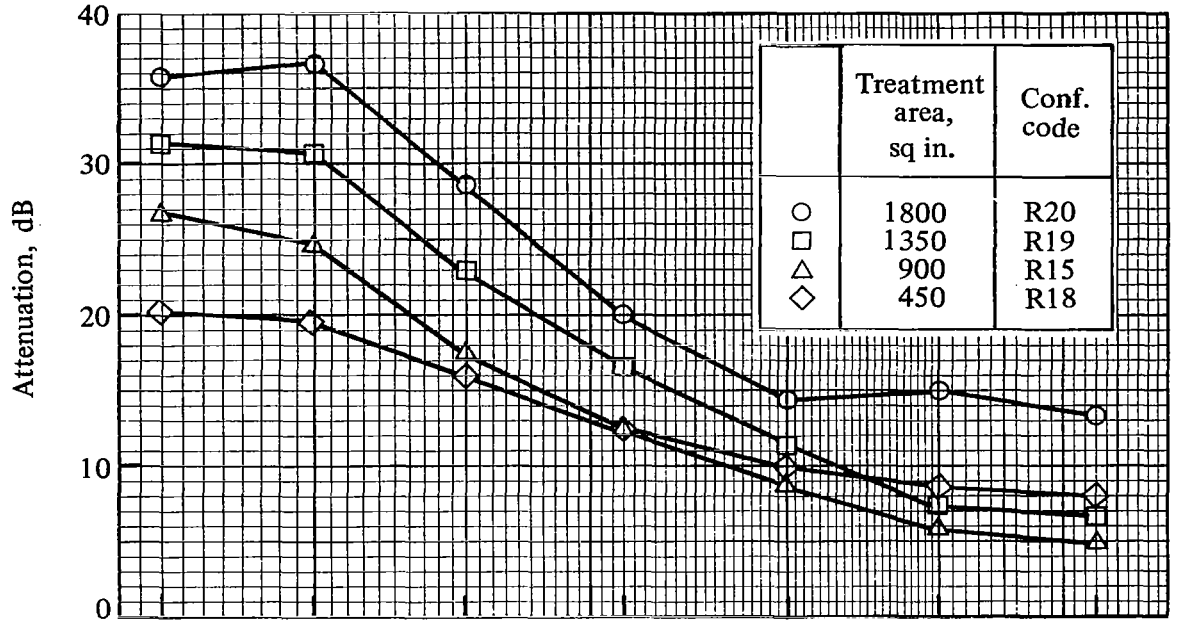

(a) Duct velocity 0 ft/sec.

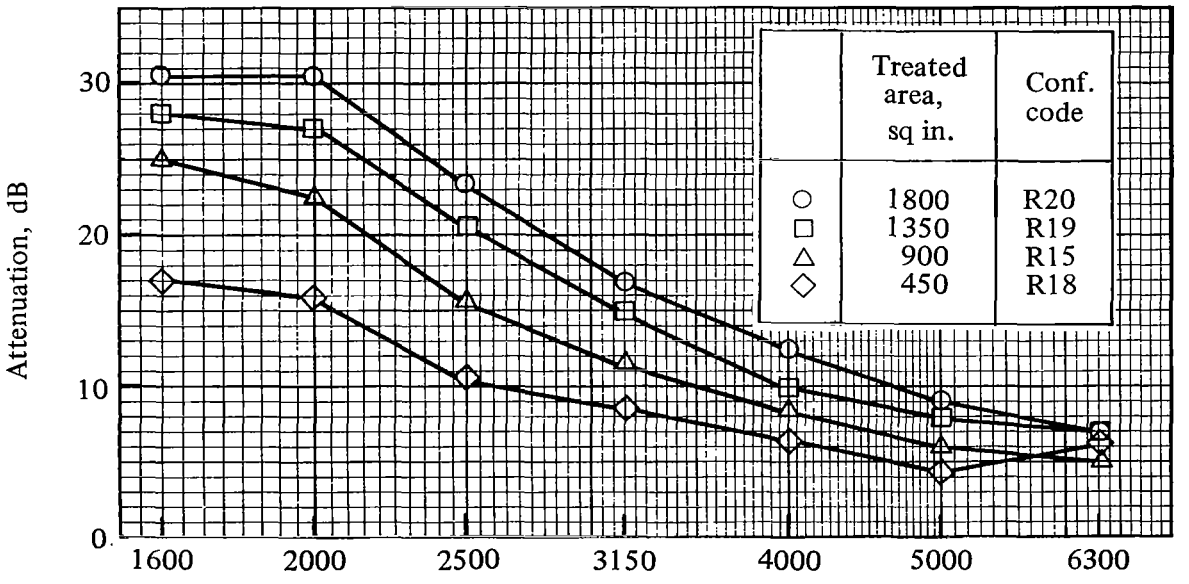

One-third octave band center frequency, Hz

(b) Duct velocity 300 ft/sec.

Figure 42. – Effect of treated area on attenuation in inlet mode. Treatment was 40-rayl fibermetal over 1-in.-deep cavities.

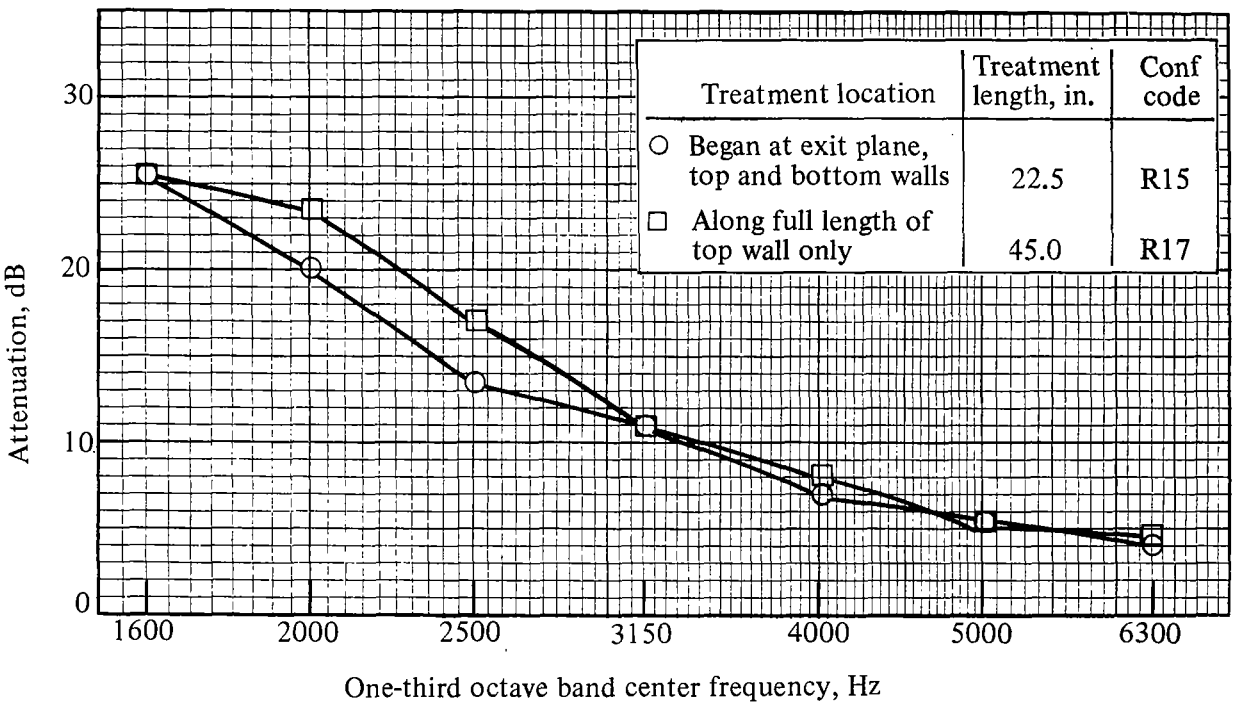

Figure 43. – Effect of treatment location on attenuation in inlet mode. Treatment was 40-rayl fibermetal over 1-in.-deep cavities.

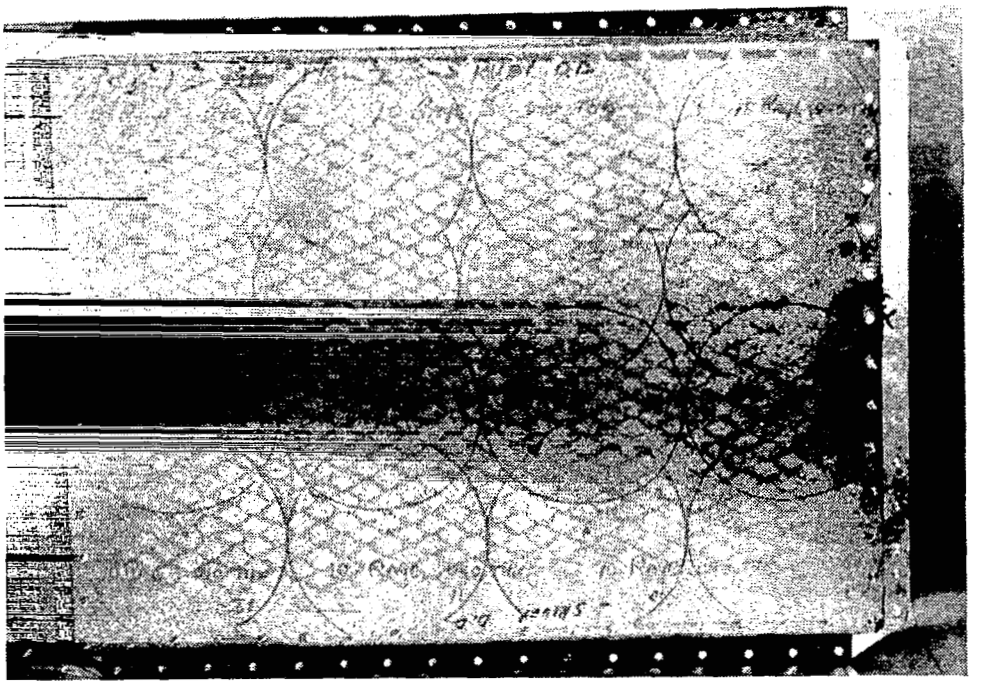

(a) Front side.

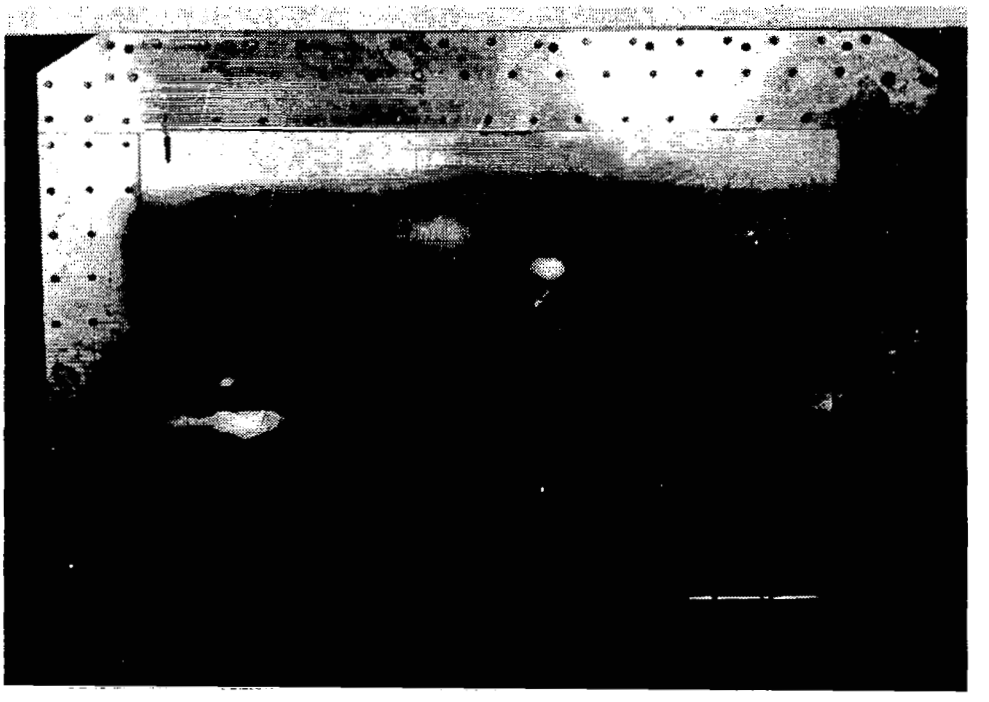

(b) Back side.

Figure 44. – Treated honeycomb-sandwich panel (test panel no. I).

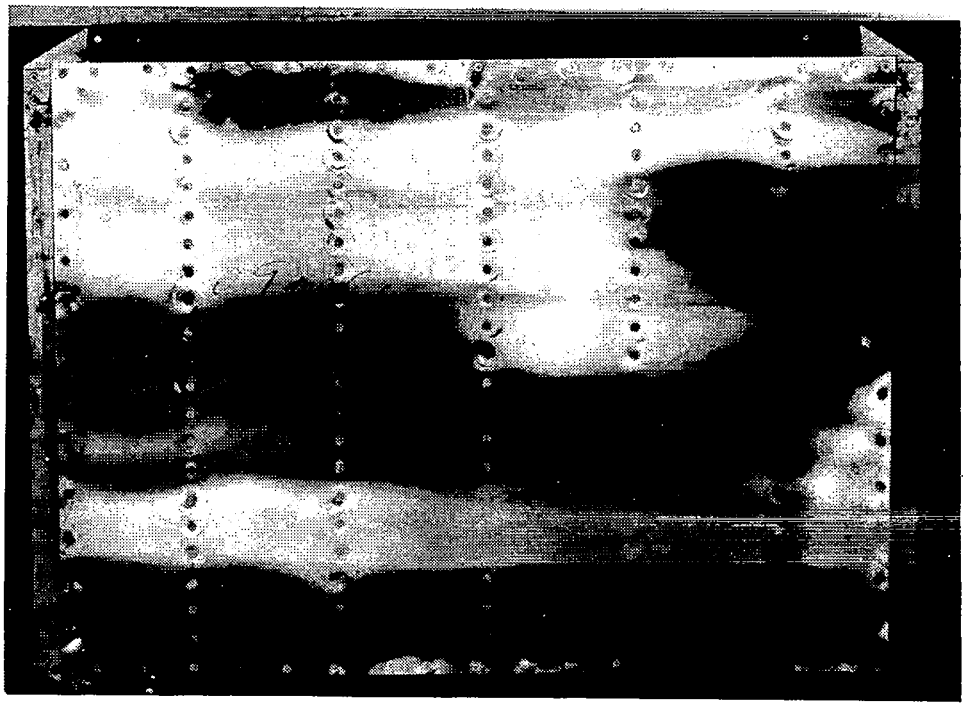

(a) Front side.

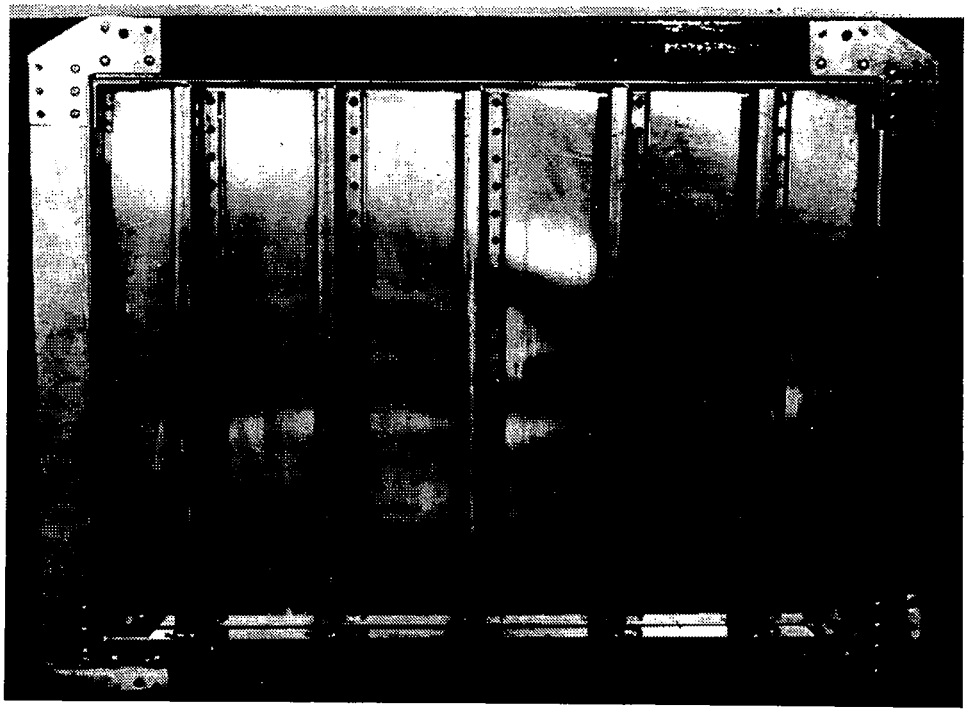

(b) Back side.

Figure 45. – Baseline skin-and-rib panel

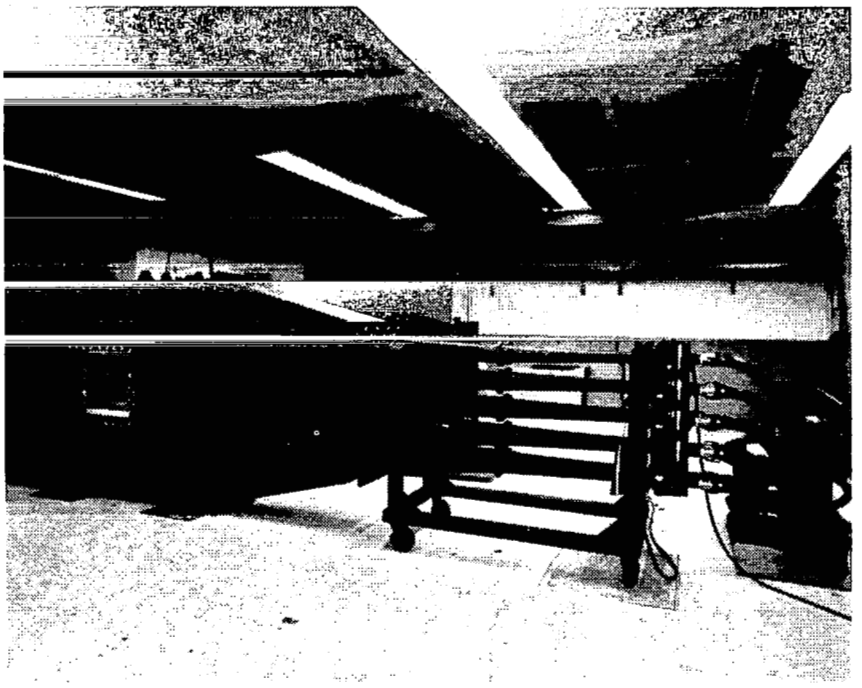

Figure 46. – Overall view of 6 x 60-in. progressive-wave tube showing electropneumatic transducers and exponential horns.

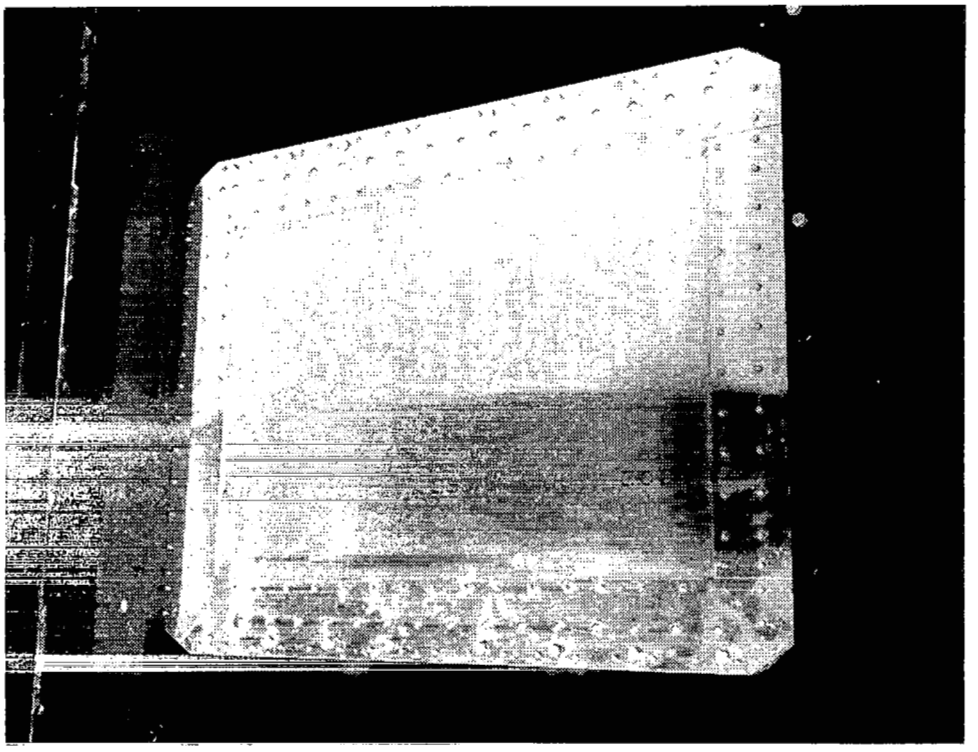

Figure 47. – Back side of test panel no. I mounted in progressive-wave tube.

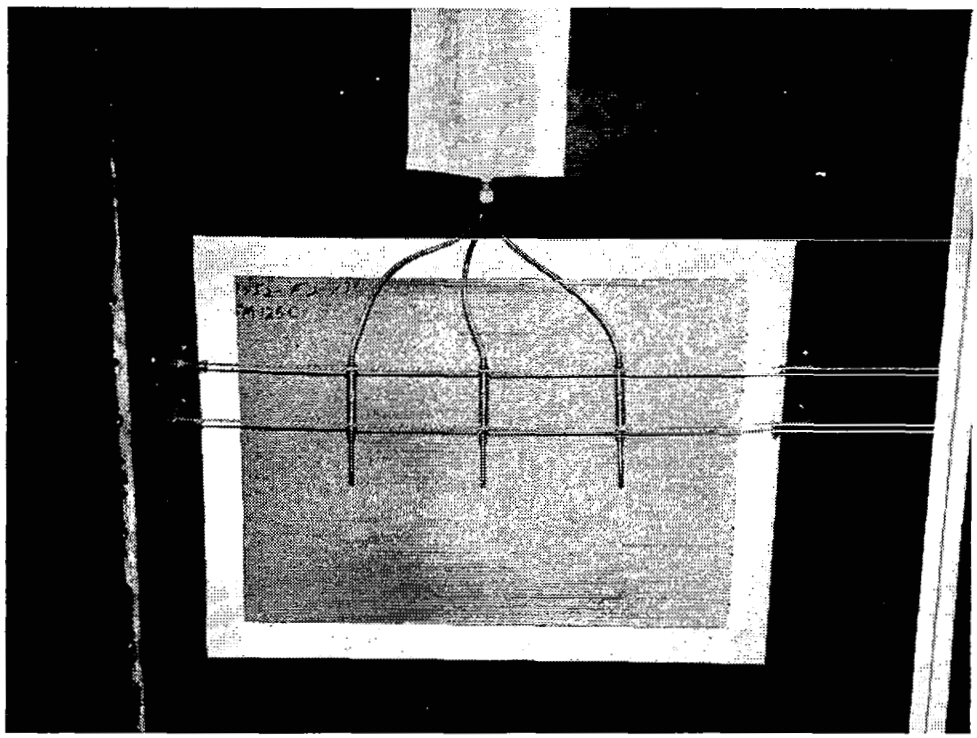

Figure 48. – Treated honeycomb-sandwich panel installed in progressive-wave tube showing locations of microphones over fibermetal surface.

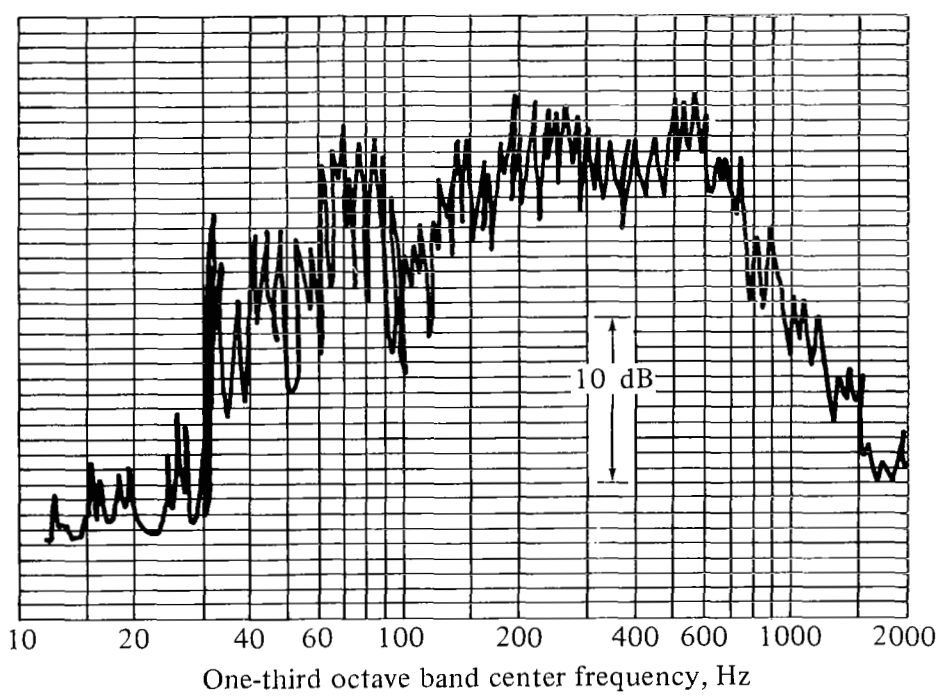

Figure 49. – Typical 1/3-octave band sound spectrum at front side of test panel.

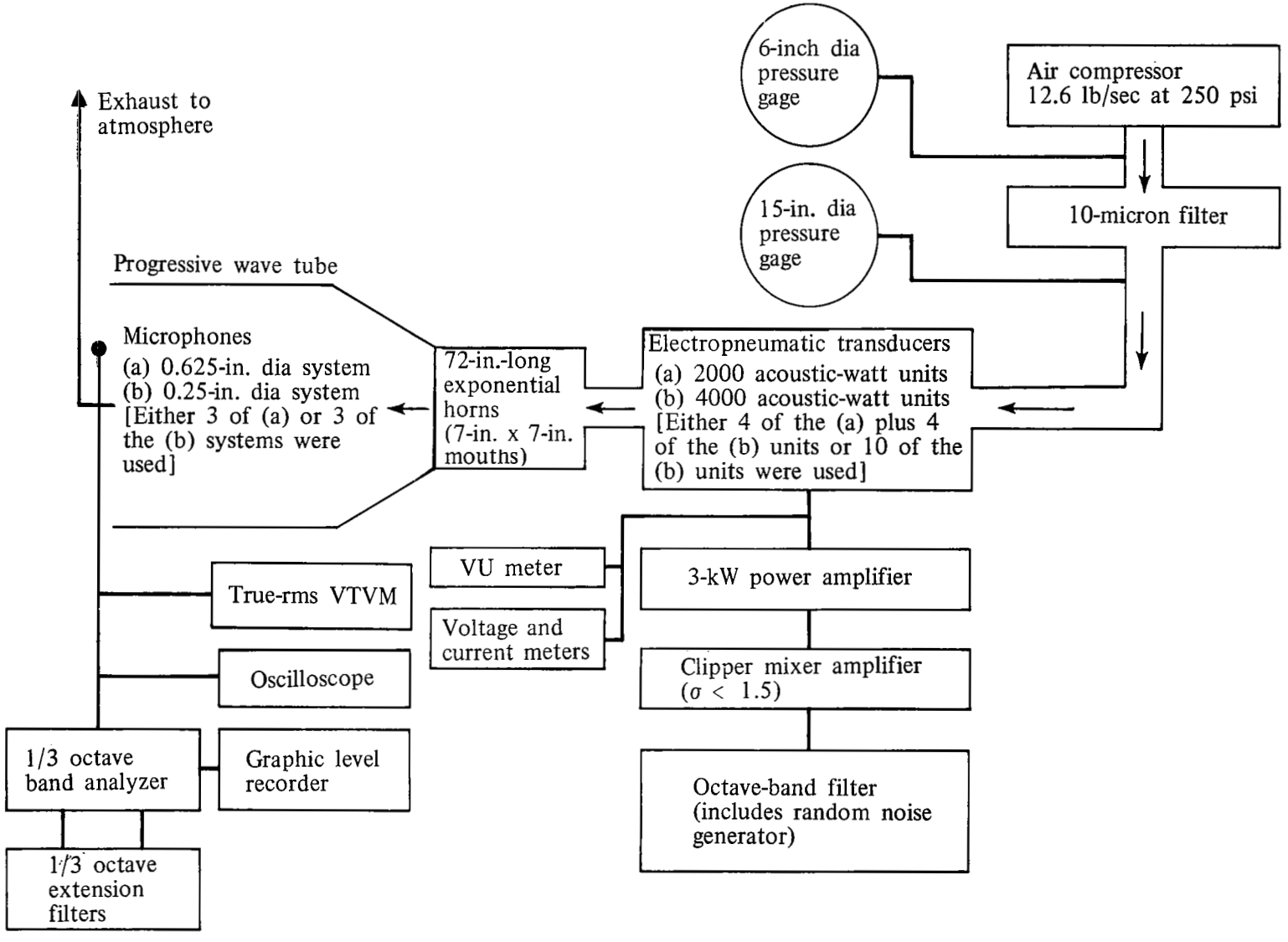

Figure 50. – Diagram of instrumentation and equipment for noise generation and measurement.

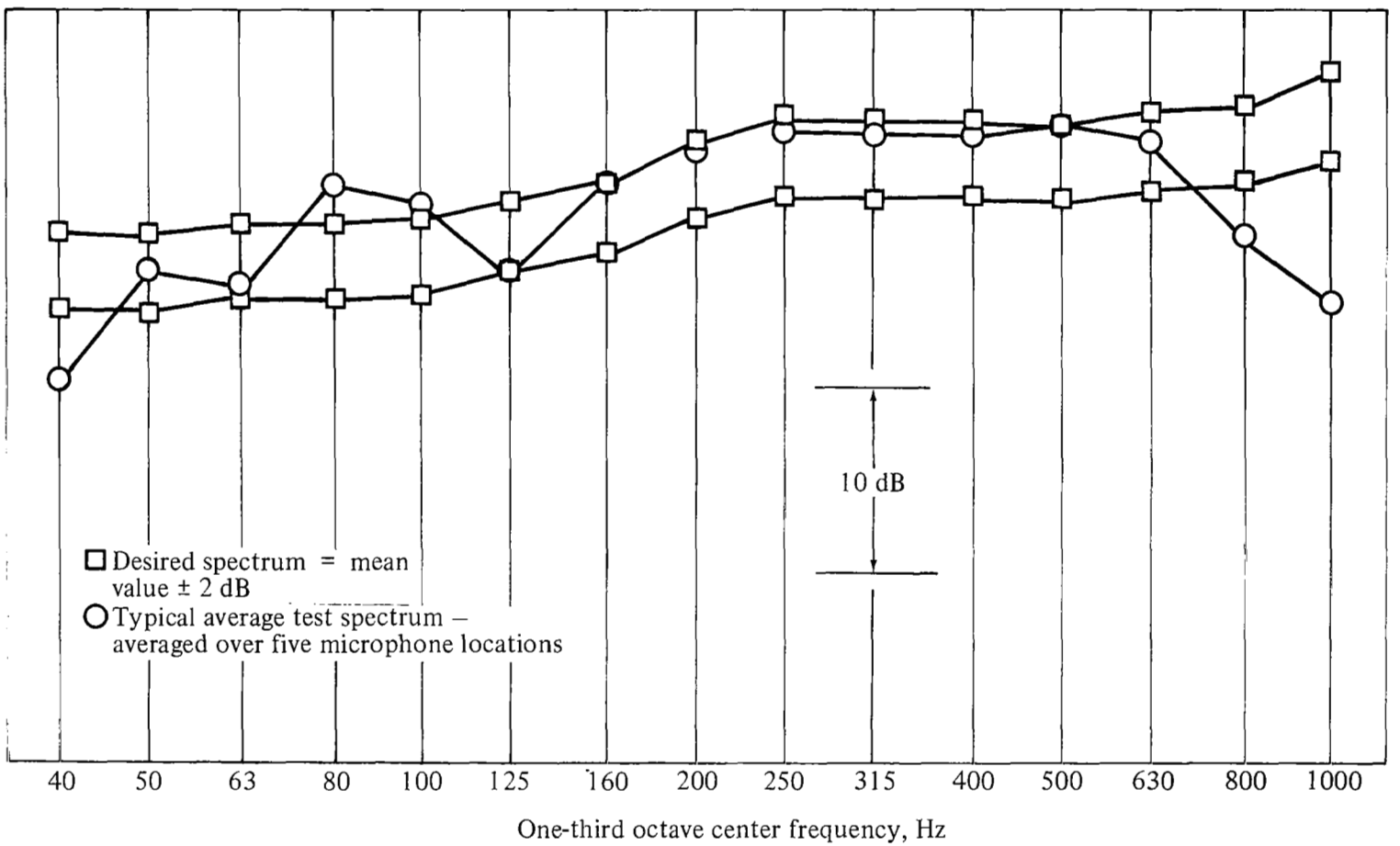

Figure 51. – Comparison of desired and measured test spectra.

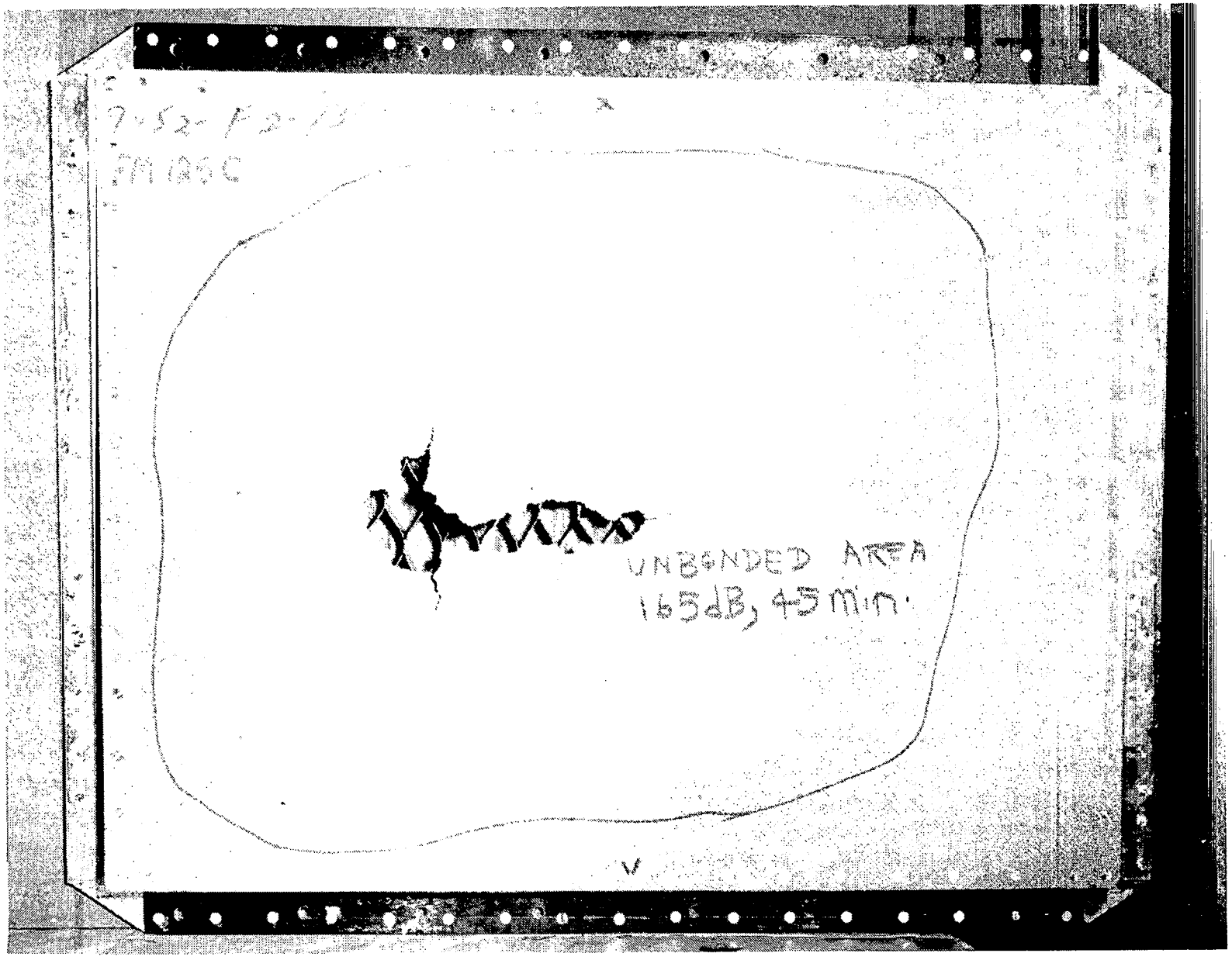

Figure 52. – Extended failure of test panel no. I after exposure to an overall SPL of 165 dB for 49.5 min.

(b) Downstream doubler.

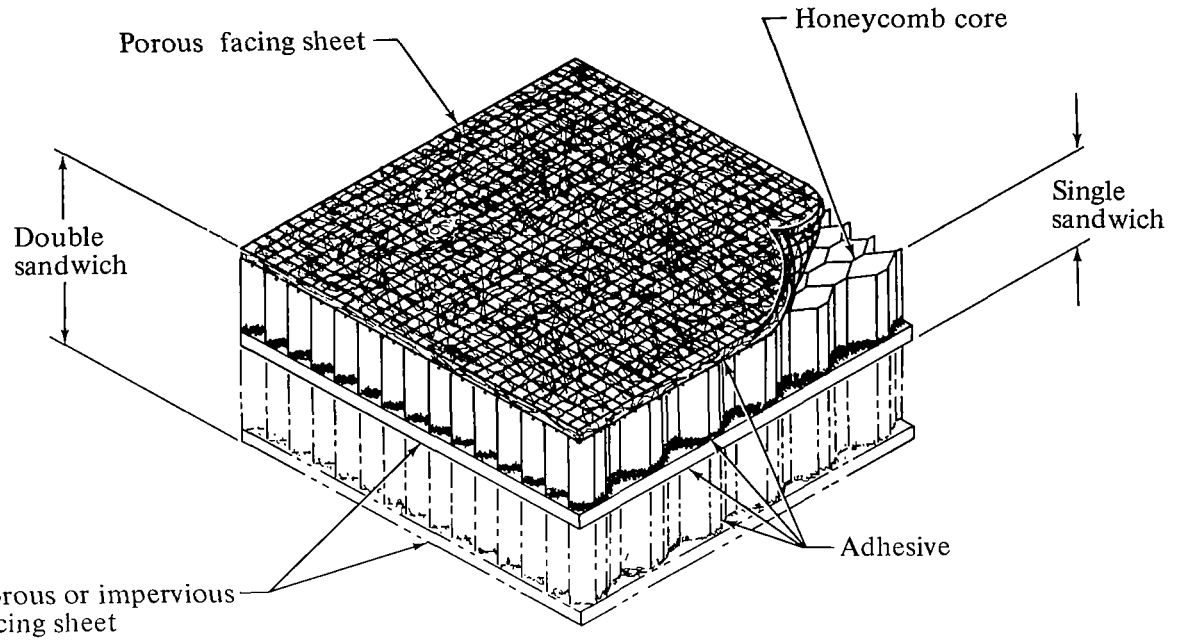

Figure 54. – Multiple-layer acoustical sandwich components.

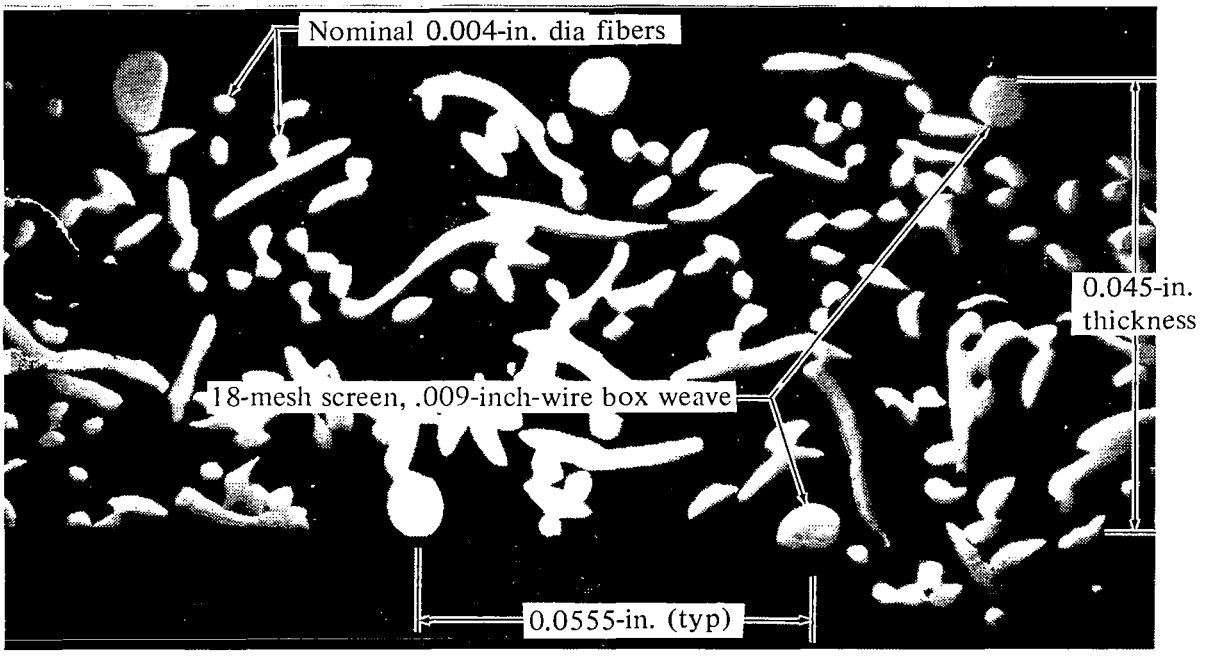

Figure 55. – Micrographic cross section of nominal 10-cgs rayl fibermetal.

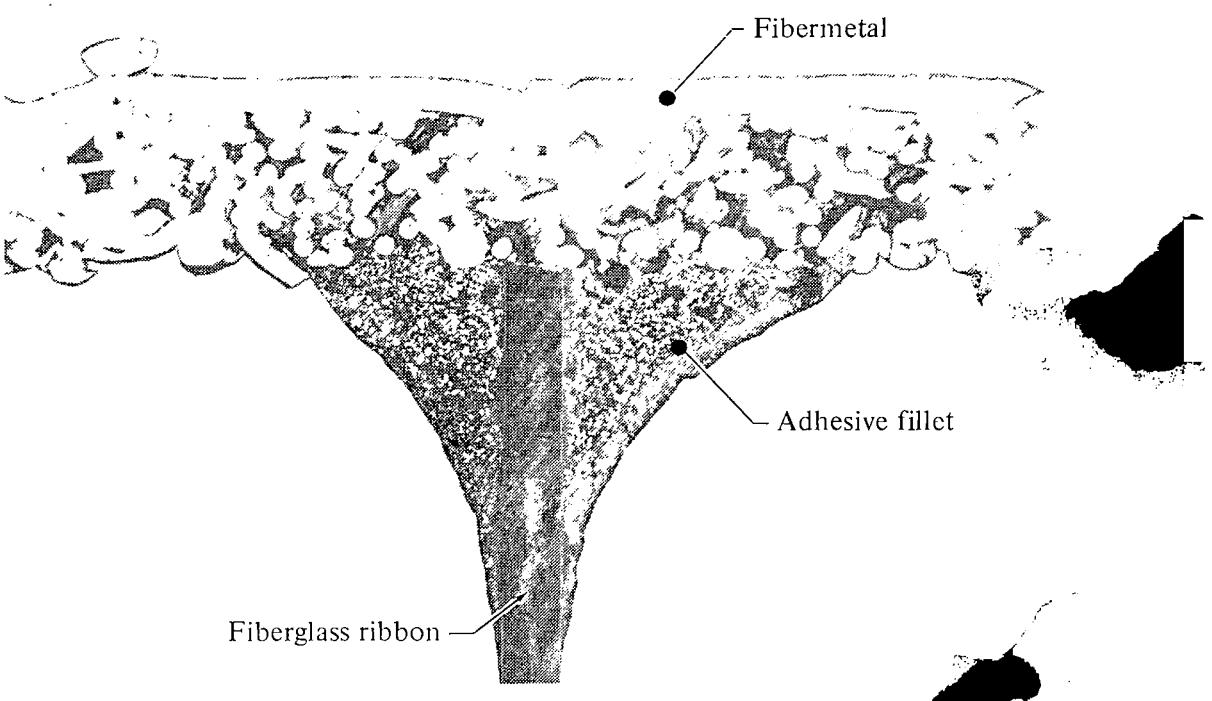

Figure 56. – Micrographic study of bonded interface betwe
fibermetal facing sheet and honeycomb core.

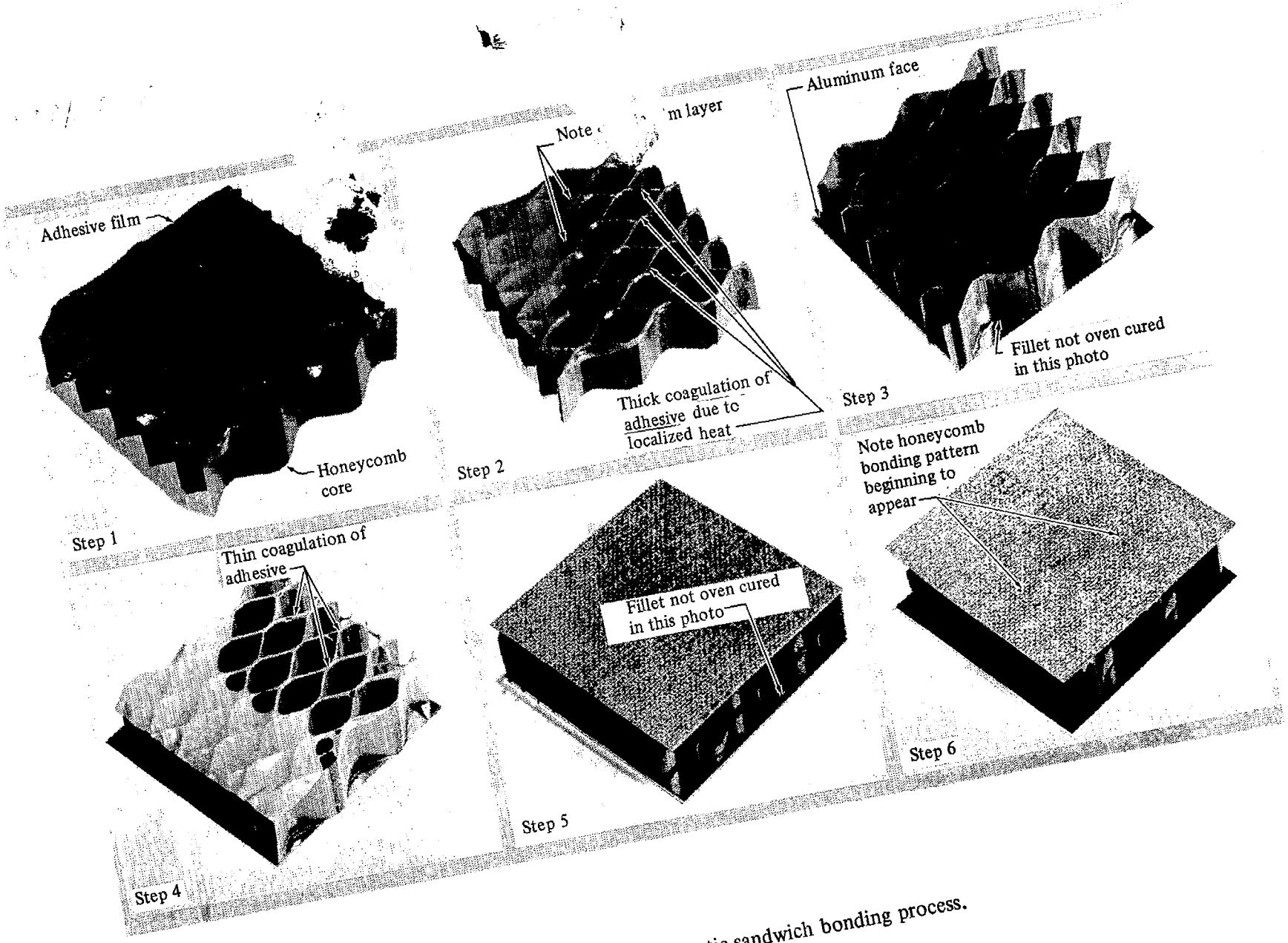

Acoustic-sandwich bonding process.

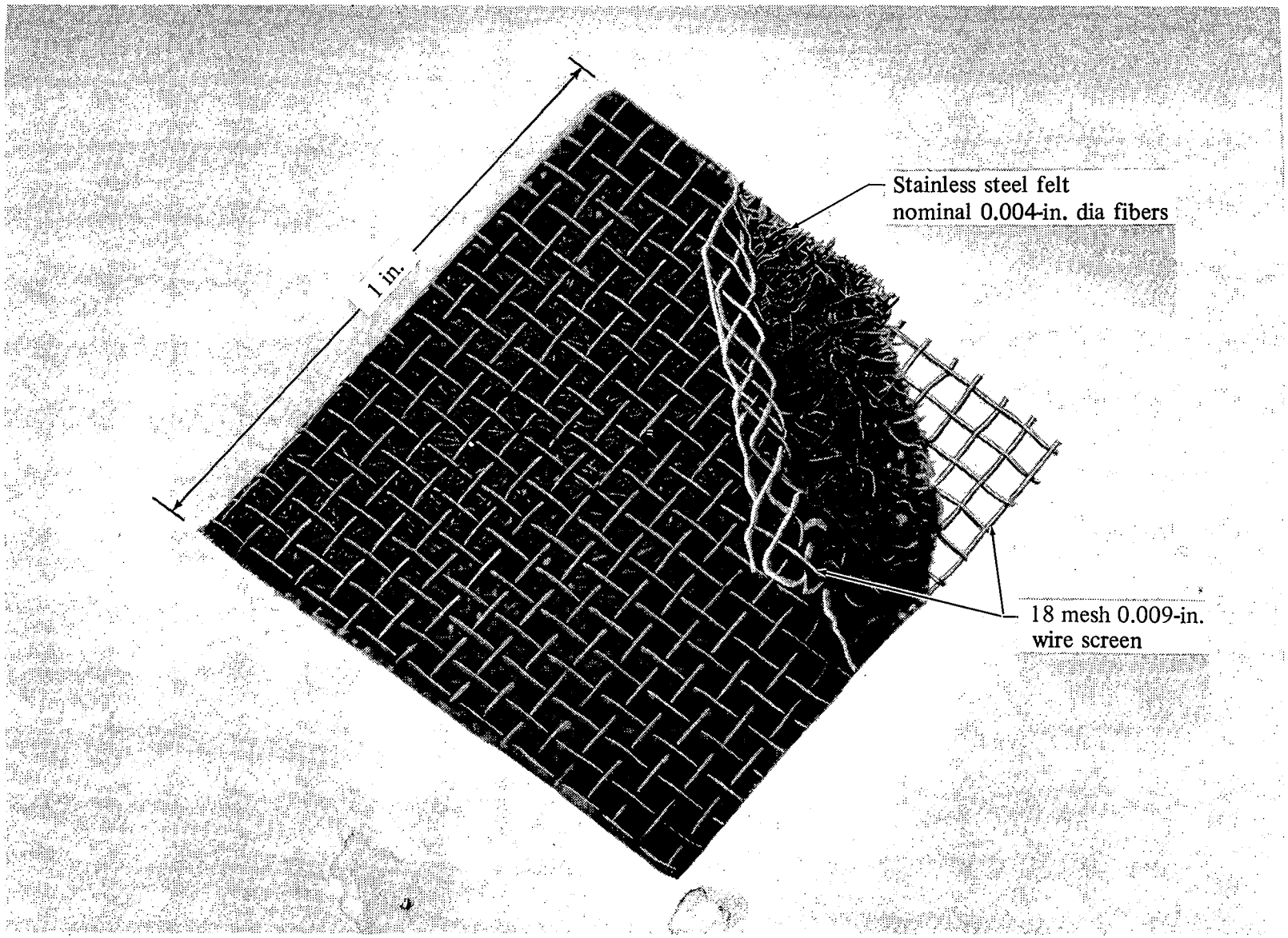

Figure 58. – Sintered fibermetal with reinforcing screens.

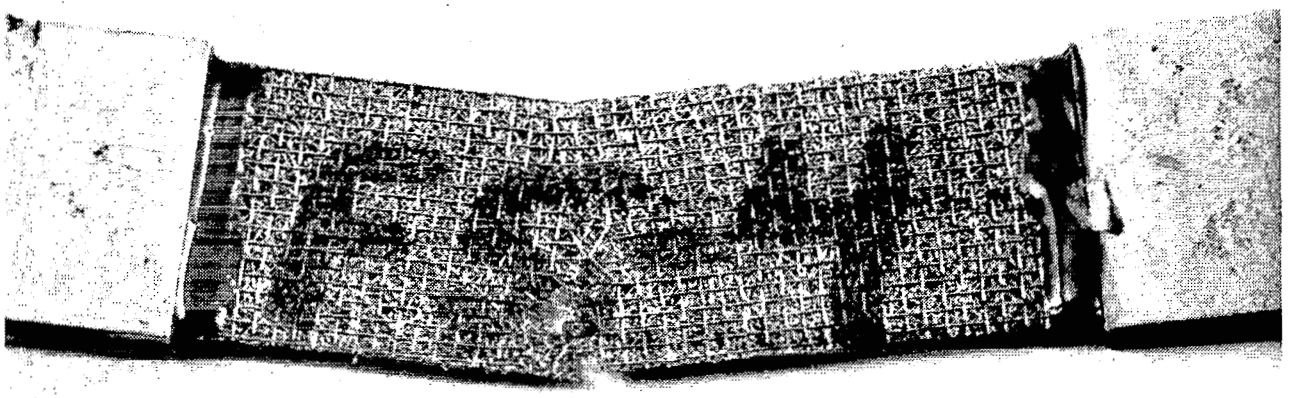

Figure 59. – Closeup view of failure of 10-cgs rayl fibermetal tensile specimen.

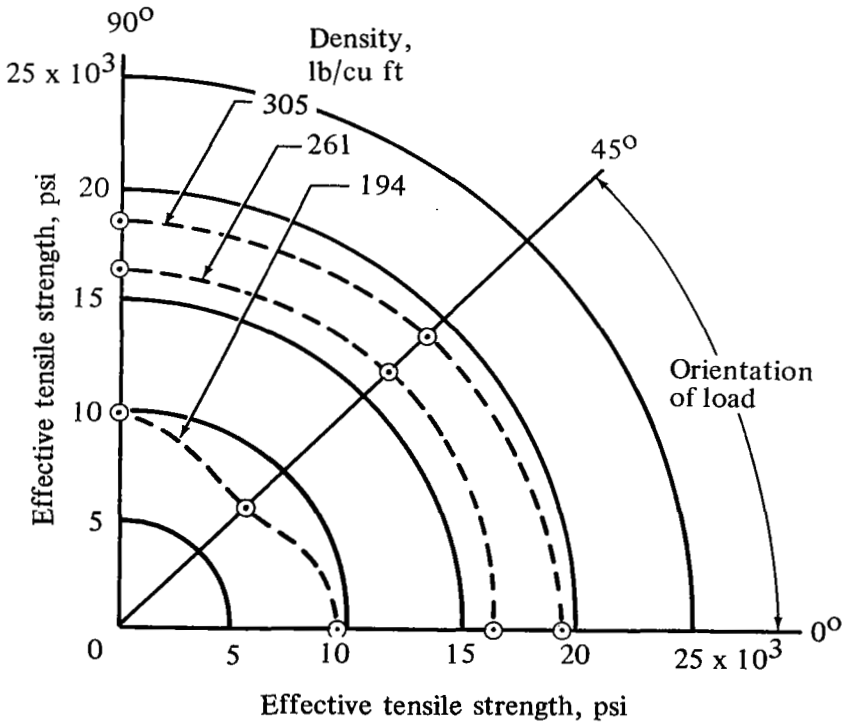

Figure 60. – Polar orientation of effective tensile strength of fibermetal made from nominal 0.003-in. diameter wire fibers.

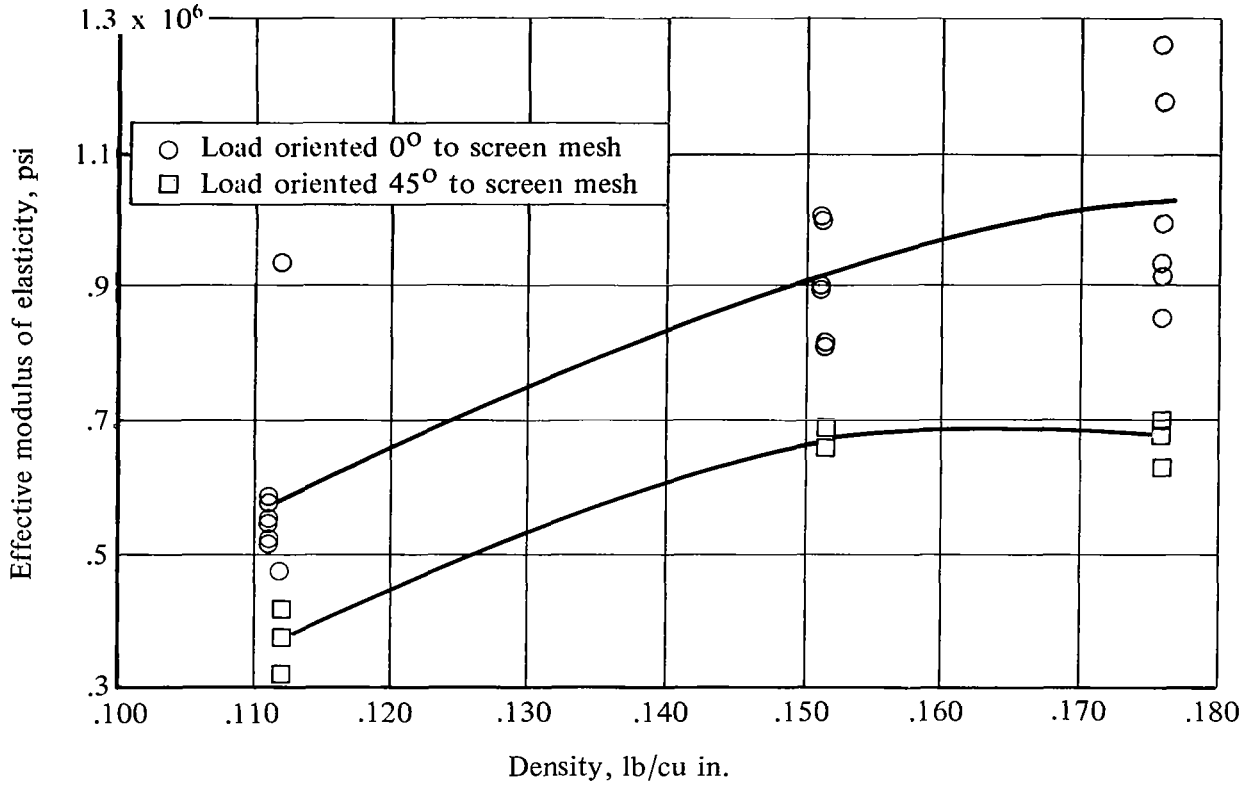

Figure 61. – Effective modulus of elasticity for fibermetal specimens made from nominal 0.003-in. diameter wire fibers. Average thickness of specimen was 0.048 inch.

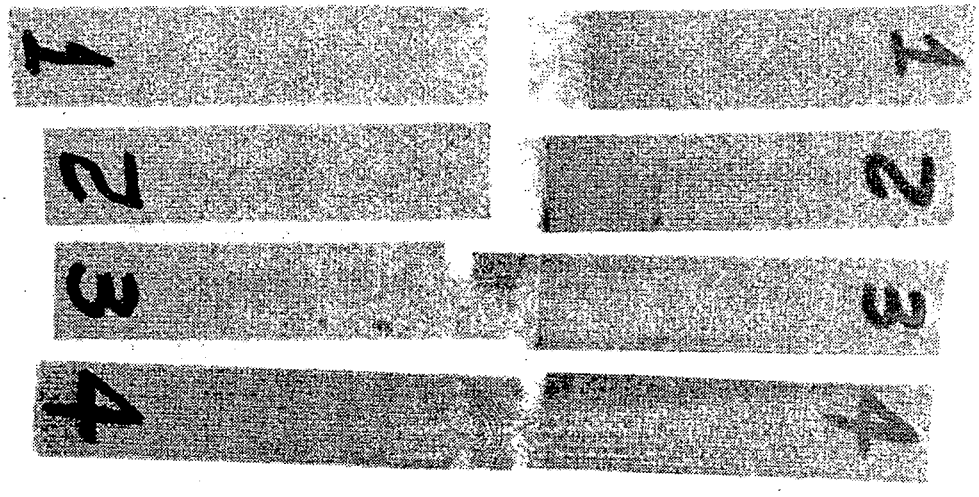

Figure 62. – Failures of interlaminar-shear test specimens.

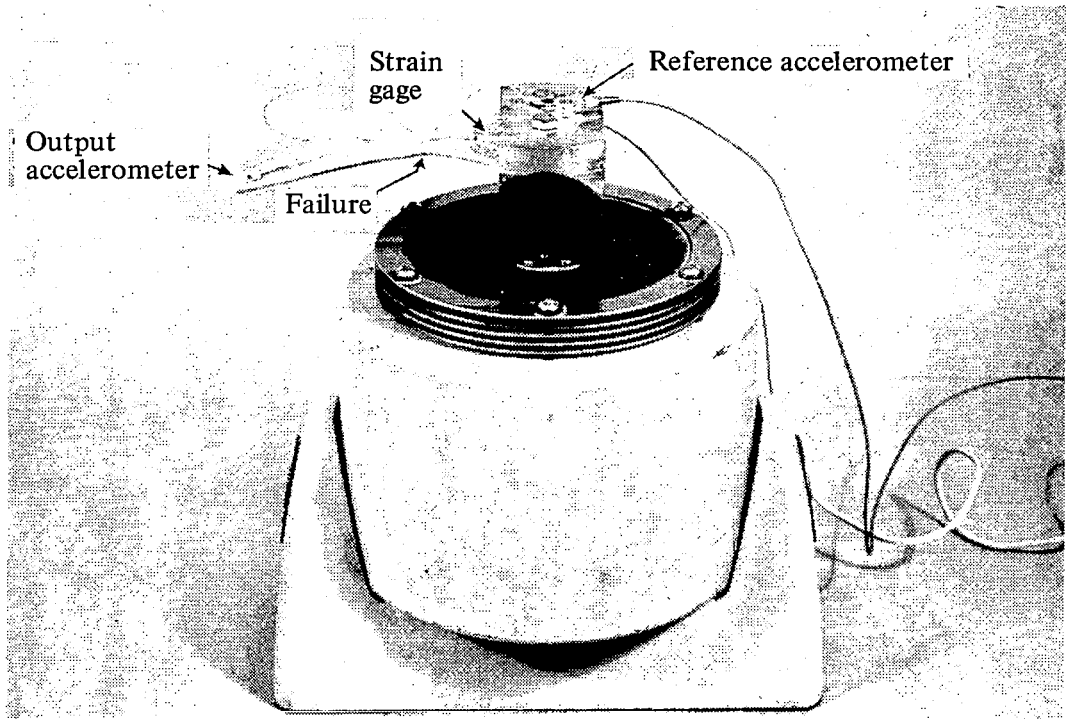

Figure 63. – Fibermetal flexural-fatigue-specimen and electrodynamic-shaker.

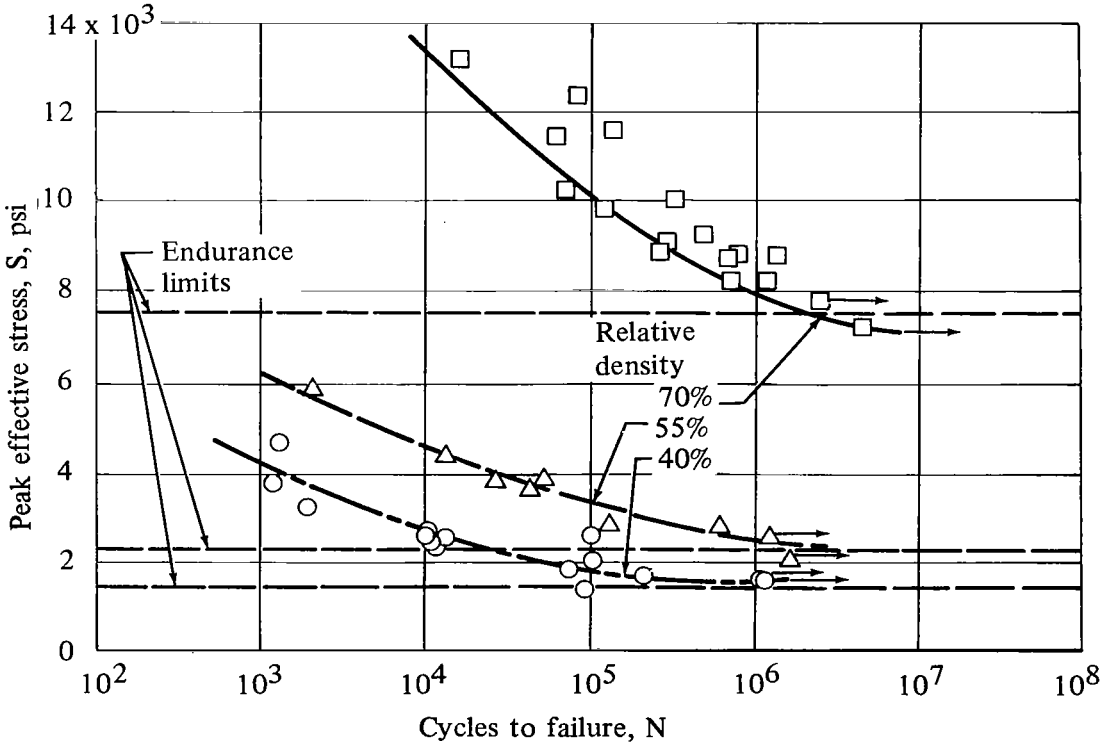

Figure 64. – Effective S-N curves of fibermetal in flexural fatigue.

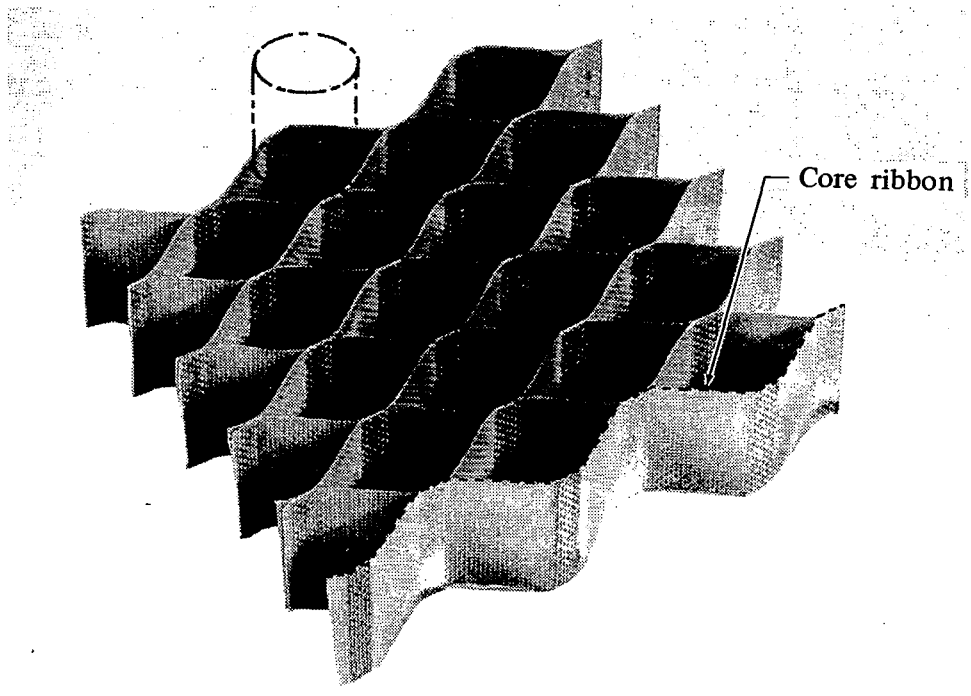

Figure 65. – Sine-wave fiberglass honeycomb core with inscribed cylinder to define cell size.

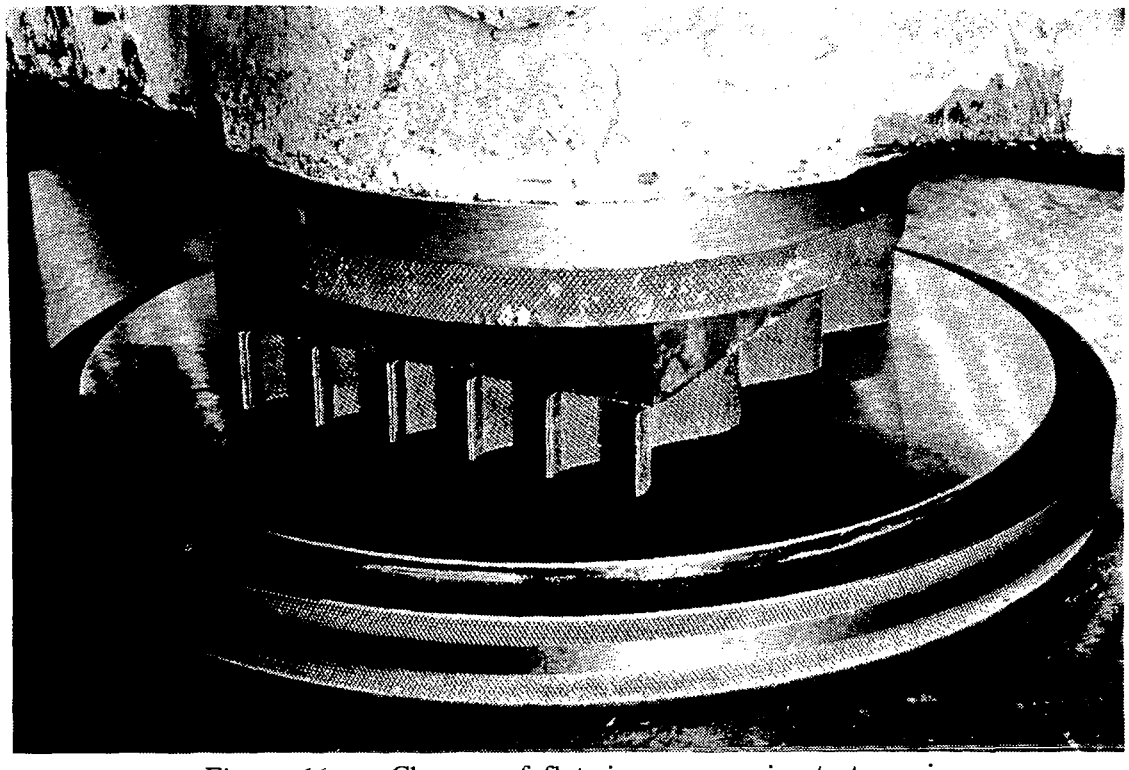

Figure 66. – Closeup of flatwise compression-test specimen.

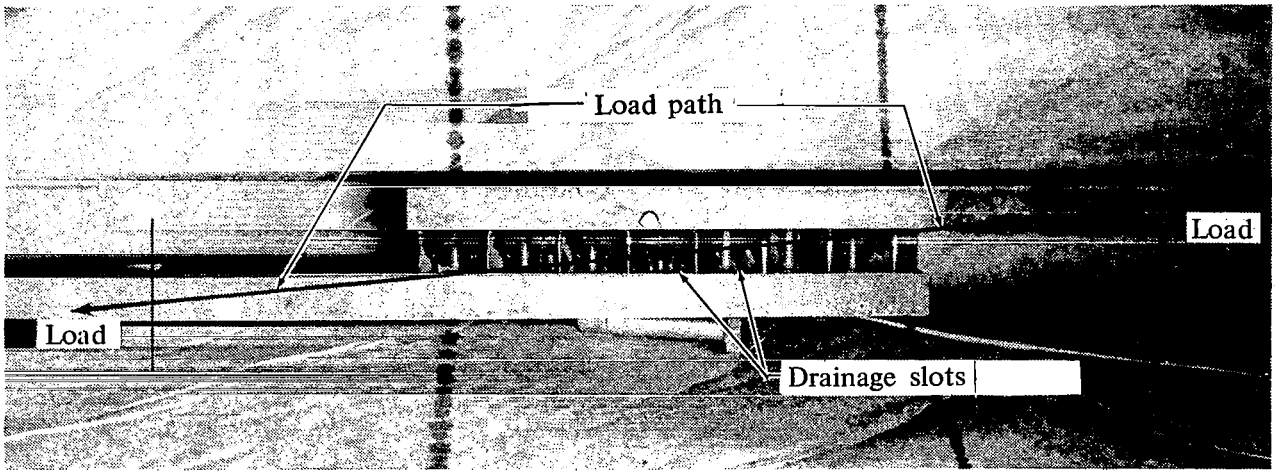

Figure 67. — Core-shear test specimen.

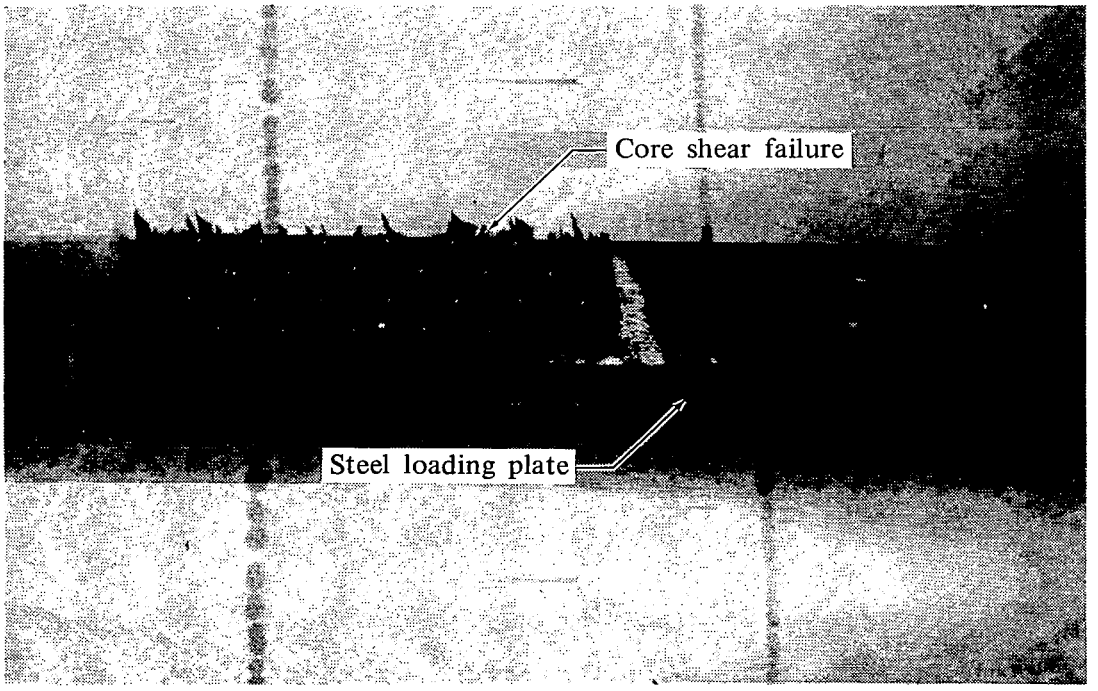

Figure 68. — Typical failure of honeycomb-core-shear test specimen.

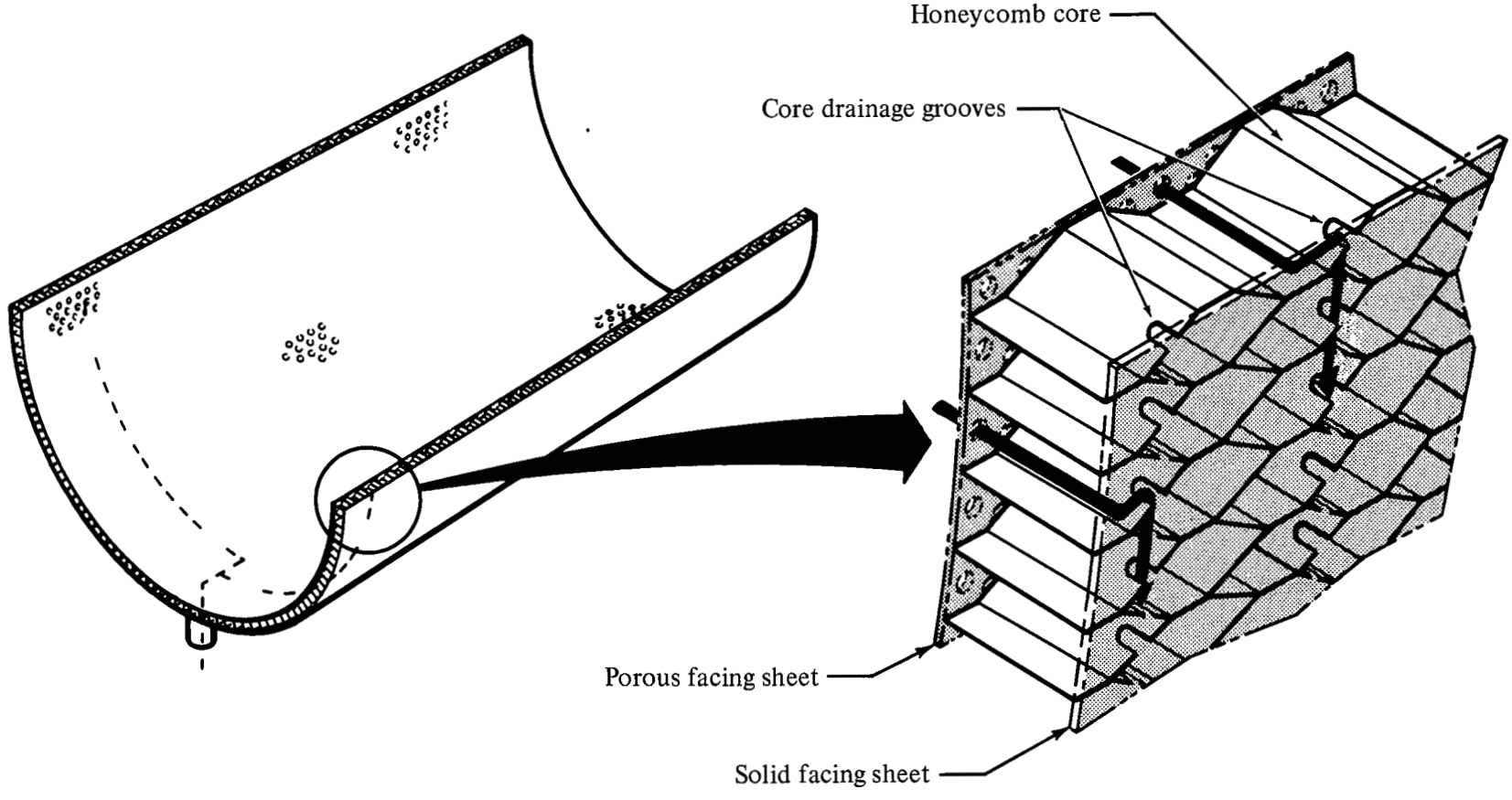

Figure 69. – Drainage test fixture.

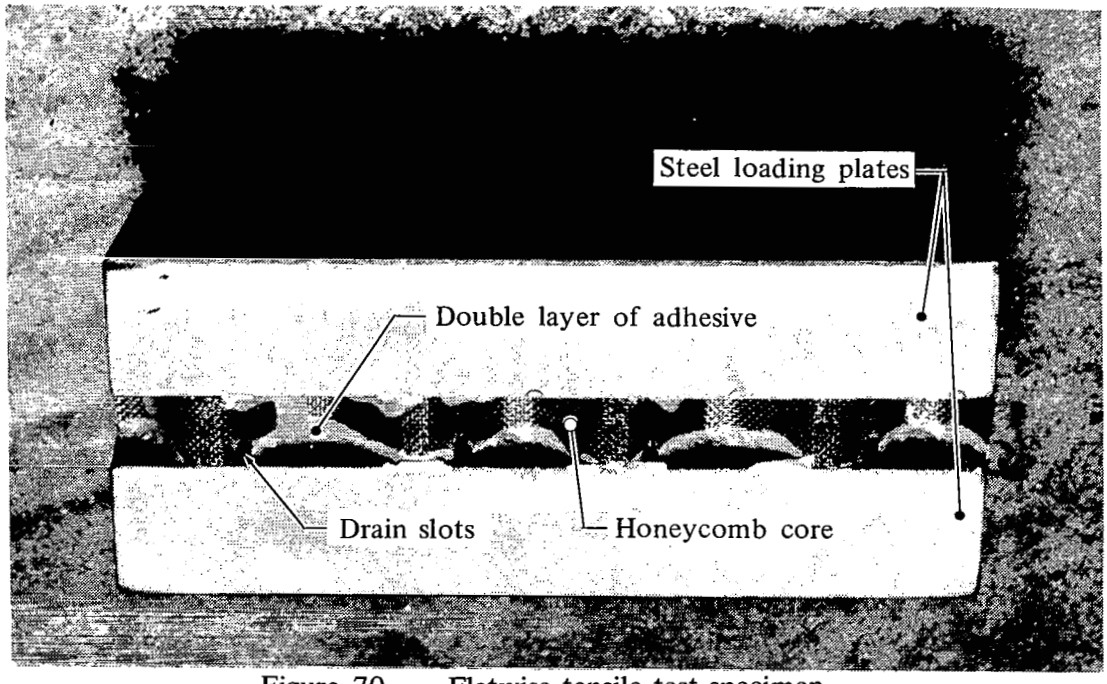

Figure 70. — Flatwise tensile test specimen.

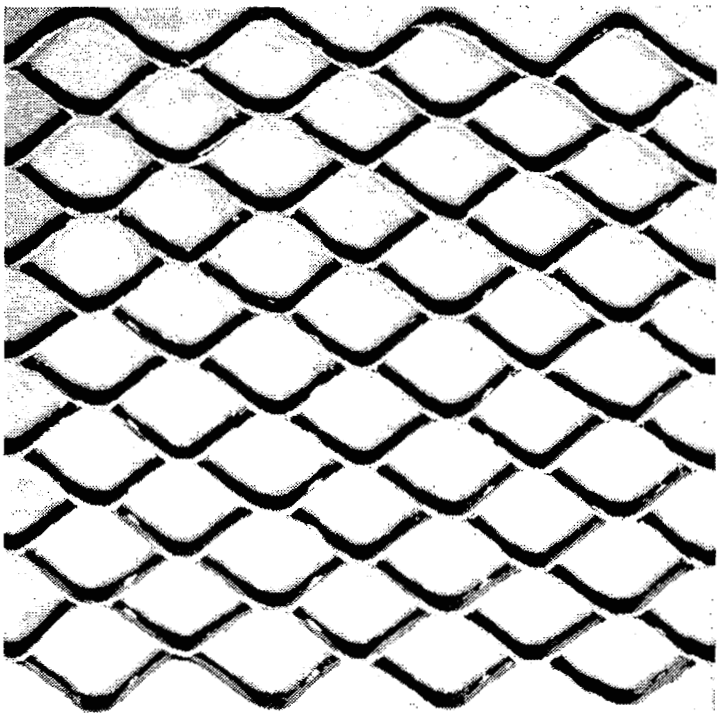

(a) Tensile block with core attached.

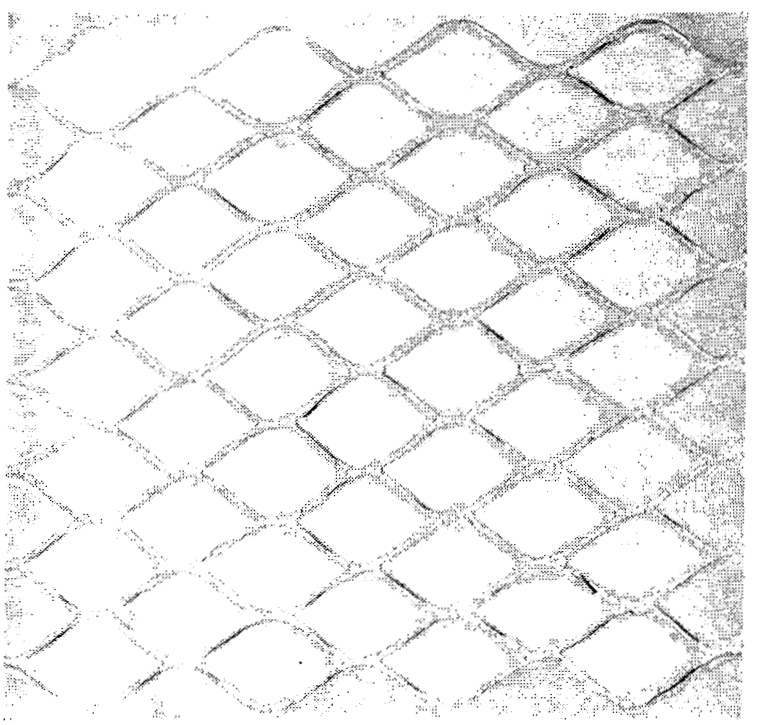

(b) Opposite block with core imprint.

Figure 71. – Typical failure of flatwise tensile-test specimen.

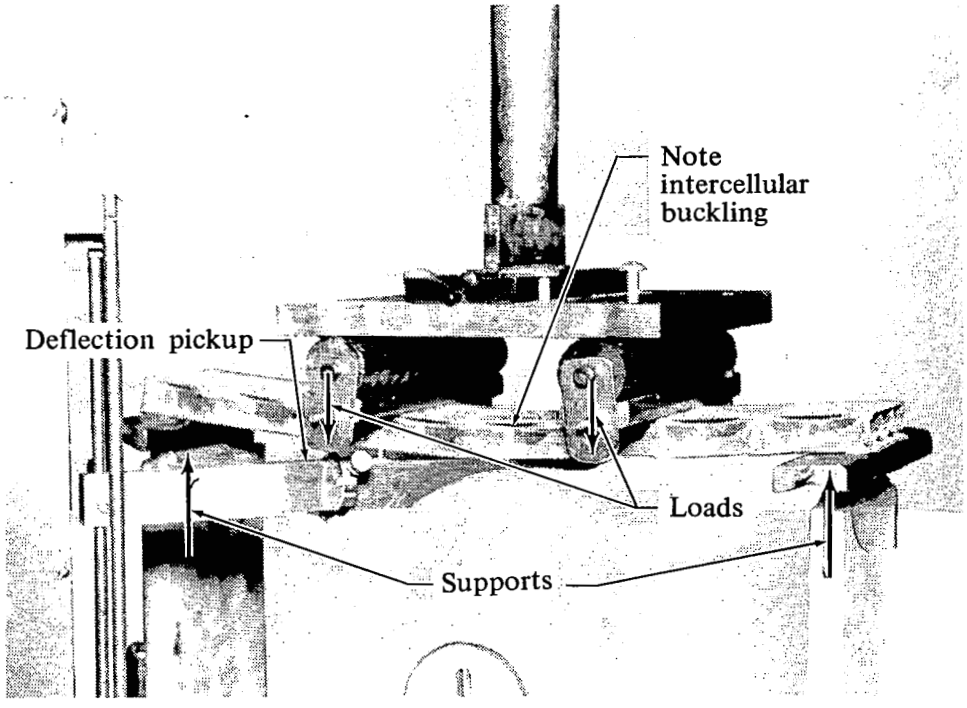

Figure 72. – Closeup of bending-beam test specimen and load fixture.

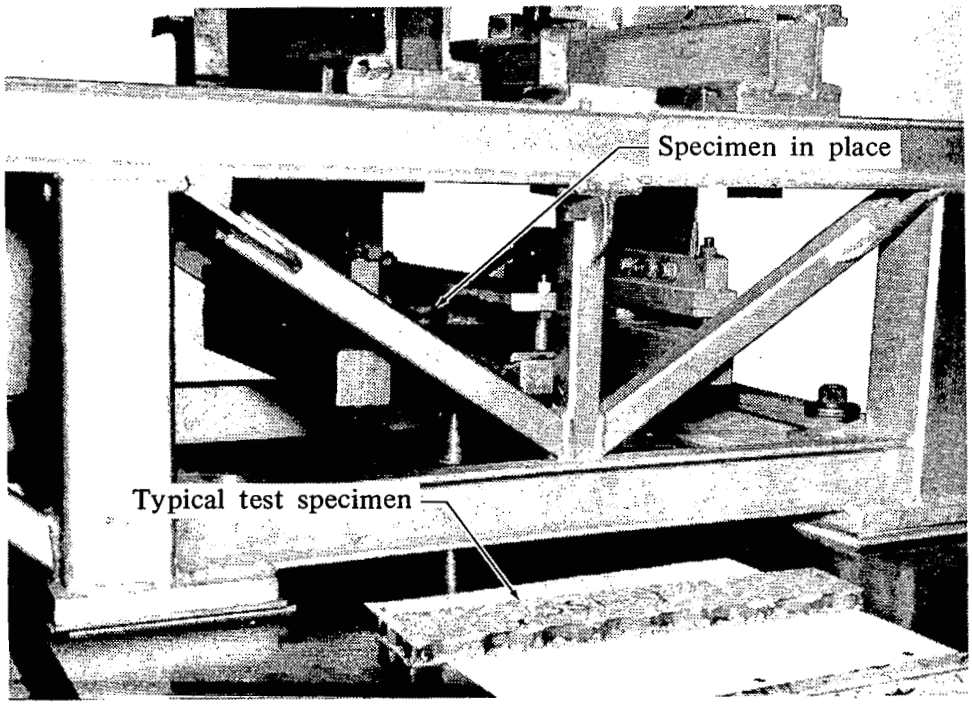

Figure 73. – Flexural-fatigue test fixture.

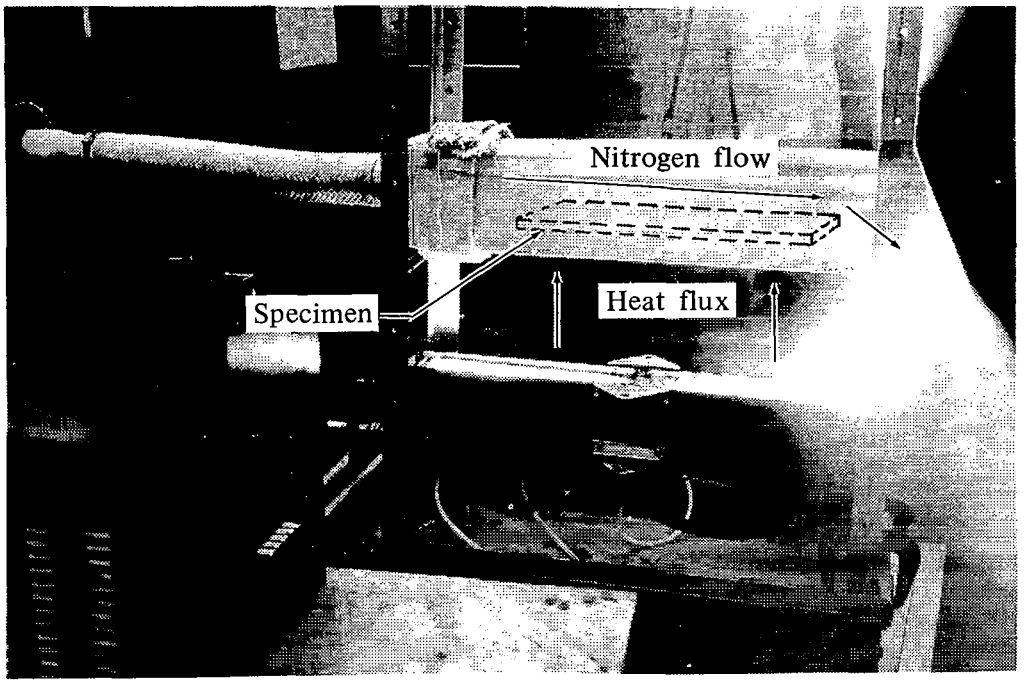

Figure 74. – Thermal-shock-test in progress.

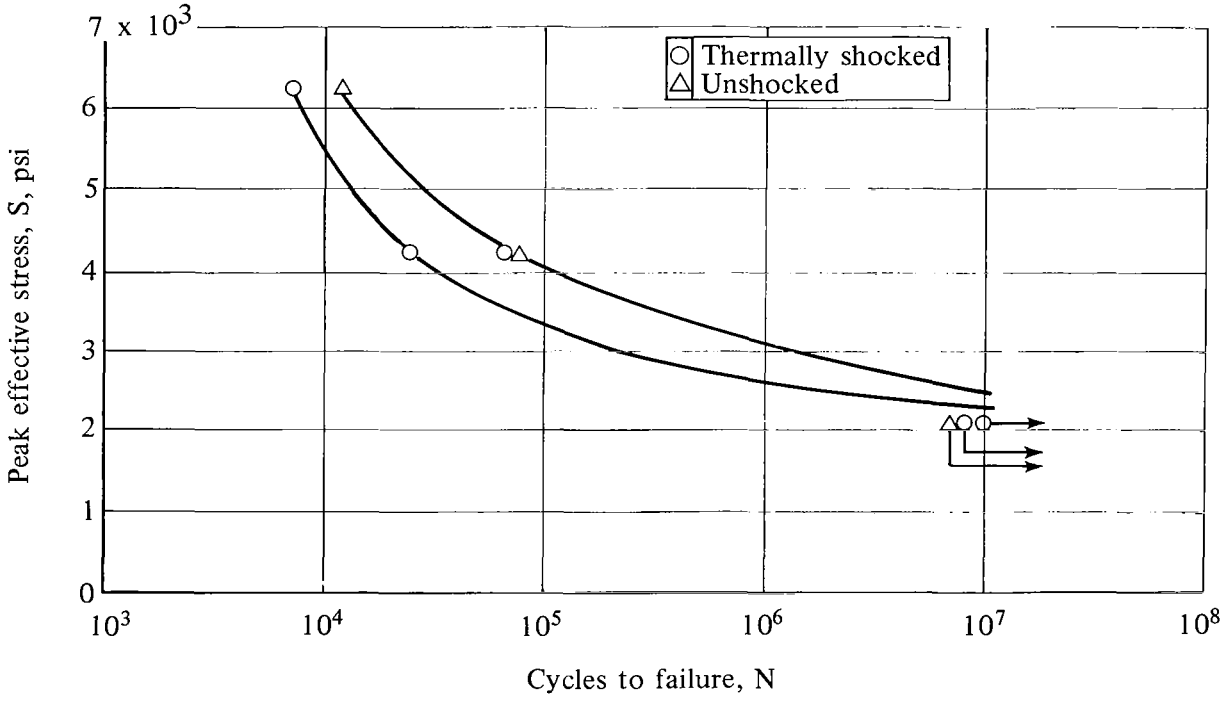

Figure 75. – Effective S-N curves of flexural-fatigue tests of fibermetal-honeycomb sandwich specimens.

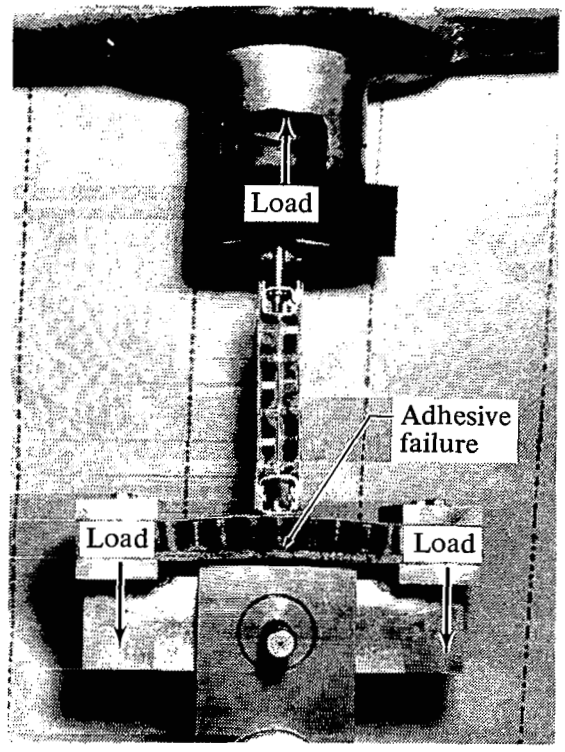

Figure 76. – Splitter-to-fan-duct-wall attachment-test-specimen.

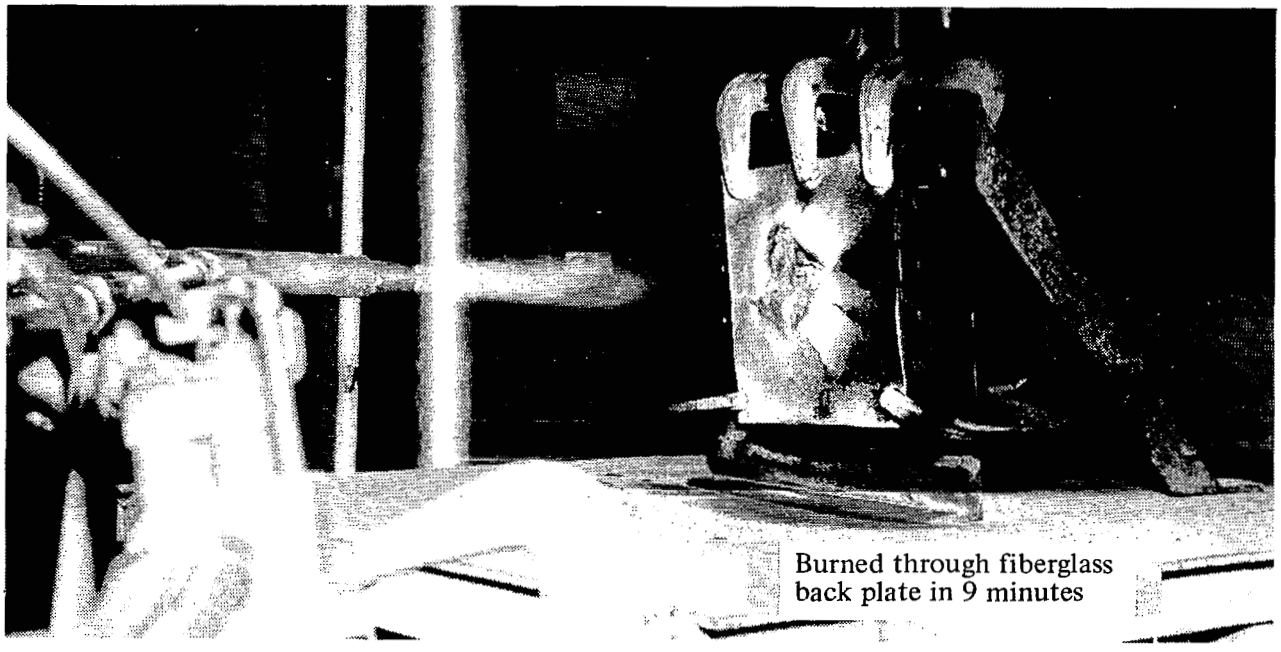

Figure 77. – Burn-through test using 2000°F flame.

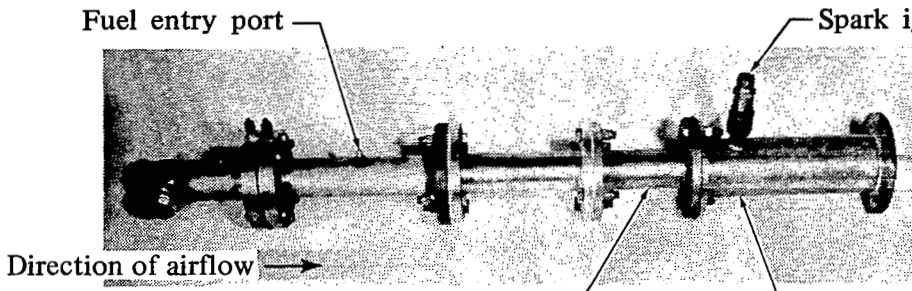

(a) Assembled.

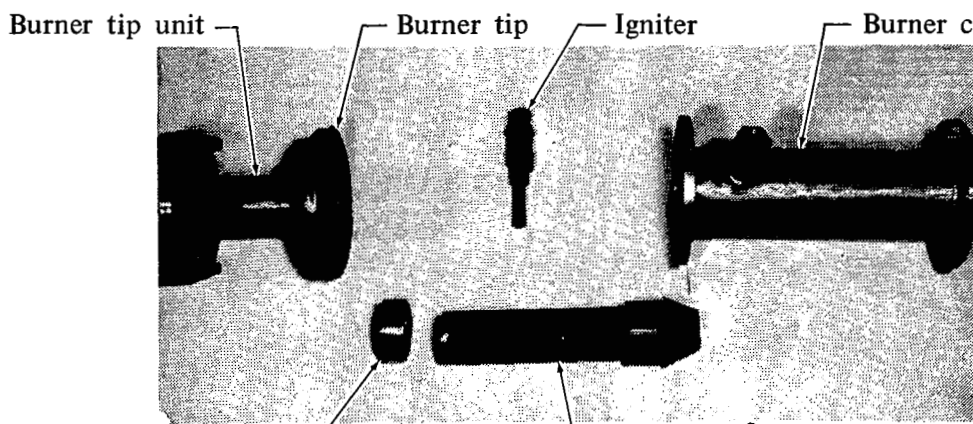

(b) Combustor components.

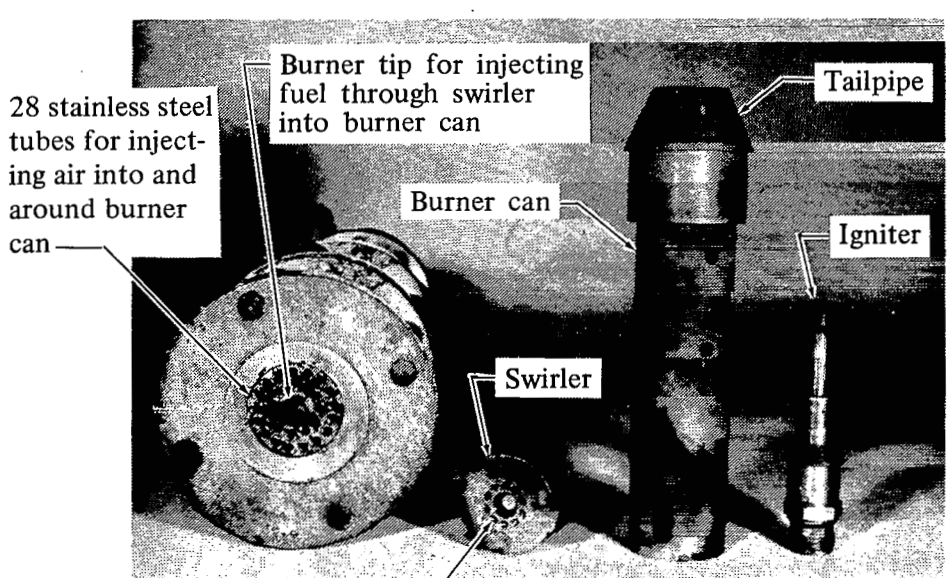

(c) Details of combustor components.

Figure 78. – Burner sound-source.

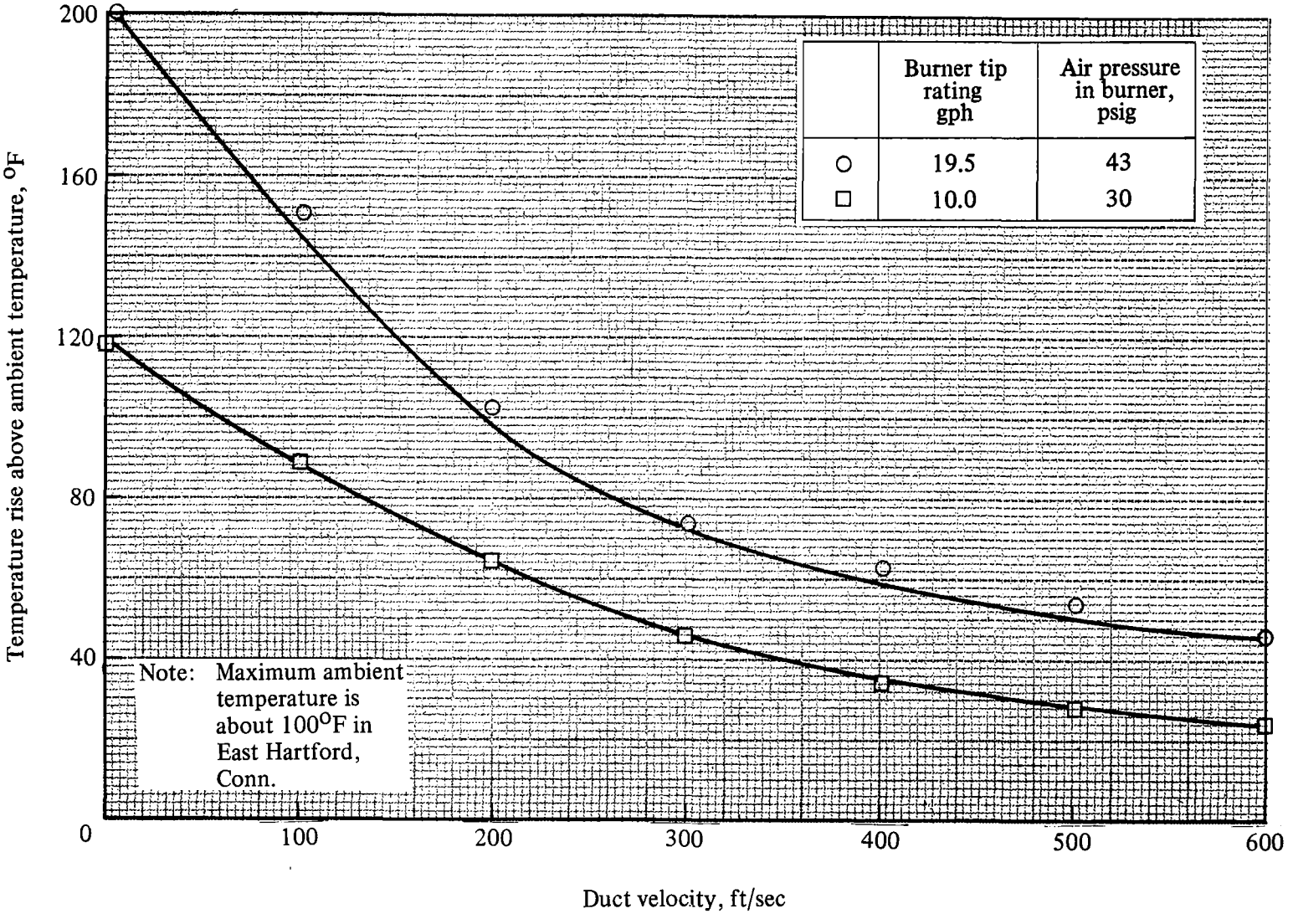

Figure 79. – Effect of duct velocity on temperature in downstream chamber.